AD-A134 068 RESEARCH ON INTENSE ELECTRON BEAMS AND APPLICATIONS(U) 1/2
BERKELEY RESEARCH ASSOCIATES INC CA D CHERNIN ET AL.
AUG 83 PD-BRA-83-302R N00014-81-C-2371

UNCLASSIFIED F/G 20/7 NL

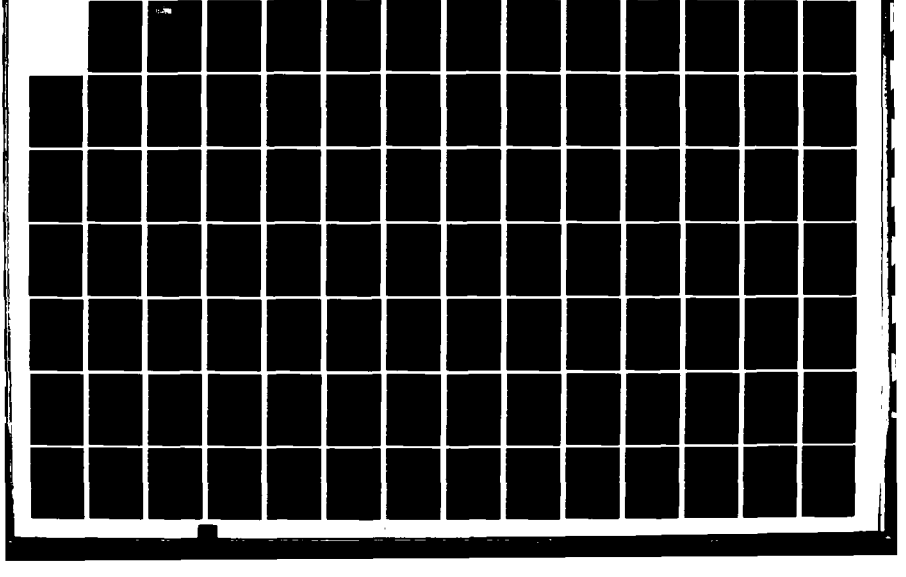

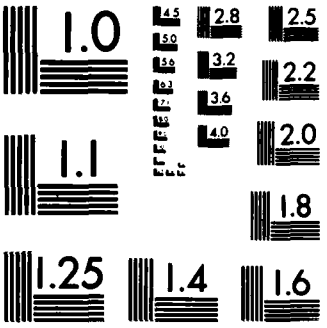

(1)

BERKELEY RESEARCH ASSOCIATES

PD INC. A SUBSIDIARY OF physical dynamics, inc.

PD-BRA-83-302R
August 1983

RESEARCH ON INTENSE
ELECTRON BEAMS
AND APPLICATIONS

558.471
(3)

FINAL REPORT
Contract N00014-81-C-2371

for
Plasma Physics Division
Naval Research Laboratory
Washington, D.C. 20375

by
Berkeley Research Associates
P.O. Box 241
Berkeley, California 94701

PD-BRA-83-302R
August 1983

RESEARCH ON INTENSE ELECTRON BEAMS AND APPLICATIONS

FINAL REPORT

Contract N00014-81-C-2371

for
Plasma Physics Division
Naval Research Laboratory
Washington, D.C. 20375

by
Berkeley Research Associates
P.O. Box 241
Berkeley, California 94701

Authors

D. Chernin	BRA
P. Sprangle	NRL
A. Mondelli	SAI
C. Roberson	ONR

CONTENTS

I. INTRODUCTION AND OVERVIEW

This report describes research performed by Berkeley Research Associates under Contract #N00014-81-C-2371 with the Plasma Physics Division, Naval Research Laboratory. ~~The~~ This report covers the period June 1981 to June 1983, during which time investigations were conducted into several major topics concerning the behavior of an intense (multi-kiloampere) electron beam in the modified betatron electron accelerator. The work described here was performed in support of and in close association with the staff of the NRL special focus program, "Advanced Accelerators."

The modified betatron has been selected by NRL for experimental evaluation as a high-current electron accelerator. Theoretical support has been directed at identifying those phenomena which will most directly affect accelerator performance. To this end, research has been carried out in the following areas: (1) Transverse linear beam dynamics in time varying, azimuthally symmetric fields, (2) Effects of grad B_θ induced drifts, (3) Orbital resonance effects due to small field errors, (4) Nonlinear effects, especially those due to non constant betatron field index, (5) Collective effects, especially the negative mass instability, and (6) Strongly focused systems. These studies were undertaken with a view toward assisting in the choice of parameters for an experimental device to be constructed at NRL. The results

of this work have served as intended, to focus the experimental design effort in that region of parameter space most likely to produce a beam of the required characteristics.

This report is divided into eight sections. Following the introduction, in Section II, we describe, in outline, the assumptions, analysis, and conclusions of our study of the dynamics of an intense, azimuthally symmetric beam. The beam is studied in the paraxial approximation wherein all fields, both self and externally applied, are taken to vary linearly with displacement from the nominal design orbit (assumed to be planar). This approximation allows us, by performing an average over an ensemble of initial conditions, to obtain equations for the motion of the beam centroid about the center of the vacuum chamber, as well as for the motion of individual particles about the center of the beam. A WKB solution to these equations allows several conclusions to be drawn about the stability of the betatron oscillations and the adiabatic behavior of these oscillations, both during acceleration and the subsequent removal of the toroidal magnetic field.

Section III outlines our analysis of the effect of the radial gradient of the toroidal field on beam motion--a nonlinear effect. We find grad-B drift to be canceled by the weak focusing forces, the net effect being a slight shift in the equilibrium beam position, unless it happens that the

focusing forces are just canceled by wall image forces. The avoidance of this transition point, where betatron focusing and wall image defocusing forces balance, leads to an important limit on beam current which is independent of the toroidal field. This limit is given in Section III.

Sections IV and V deal with resonance effects. In Section IV we describe the effect on the beam centroid of small azimuthal variations in the applied fields. We obtain an important bound on the allowable azimuthal field perturbation in order that certain so-called integer resonances will not disrupt the beam. The approach again employs the paraxial equations of motion and the averaging technique developed in our study of the dynamics of the symmetric beam. The analysis of Section V presents certain results on nonlinear resonance effects caused by the transverse variation of the field index n.

Next, in Section VI, some results on collective instabilities are given, building on work by Sprangle and Vomvoridis. A novel result--a double valuedness in the current vs energy spread stability curve--is predicted as a result of competition between growth and stabilization mechanisms. A strongly stabilizing effect of the toroidal field is evident.

In the final technical section, Section VII, a discussion is given of the sensitivity of a weakly-focused system to average beam momentum-vertical field mismatch.

Consideration of this problem has led to a proposal for the use of a type of strong-focusing coil arrangement in which orbits have been studied in the linear approximation.

In all technical sections, calculations are only summarized or outlined. Details are relegated to Appendices. Additionally, computer codes developed in the course of this work are documented in Appendices.

A final section, Section VIII, briefly summarizes the work, states our conclusions, and suggests directions for further study.

II. TRANSVERSE BEAM DYNAMICS IN THE MODIFIED BETATRON

The modified betatron electron accelerator field configuration consists of a conventional weak focusing betatron field upon which is superimposed a toroidal magnetic field. It has been shown[1,2] that this toroidal field greatly increases the amount of charge that can be confined in a device of given size. Acceleration is accomplished as in a conventional betatron, that is, by changing the flux through the electrons' orbit.

The orbit of any particular electron depends, however, not only on the external fields as in a conventional (low ν/γ) device, but also on the non negligible fields produced by all other particles in the system. These fields are found by solving Maxwell's equations with the correct sources. Since we do not attempt here to calculate the particle dynamics self-consistently, we are forced to make some approximation for these sources which we do by taking the number and current densities as constants across the beam cross-section. This approximation appears to agree fairly well with the number and current distributions found in numerical simulations and our final results are quite insensitive to the exact distributions which affect only a certain coefficient in the argument of a logarithm. Maxwell's equations are solved through first order in the inverse aspect ratio of the torus. It is very important to include these "toroidal

corrections" to the self-fields for intense beams ($\nu/\gamma \gtrsim .02$). They affect both the value of the required vertical field needed to hold the beam at its equilibrium radius as well as the values of the betatron frequencies. These corrections were not included in previous treatments[1,2].

The resulting fields, when substituted in the equations of motion, yield a paraxial equation description of the beam. When solved, the equations illustrate several interesting phenomena involving the beam. First, two basic modes of oscillation exist, a "fast" mode corresponding roughly to cyclotron motion about the toroidal field, and a "slow" mode corresponding to an $\vec{F} \times \vec{B}$ drift motion where here the force $\vec{F}$ is due to a combination of the ordinary weak focusing fields, image currents and charges in the wall, and hoop stresses on the ring. It may be arranged, by judicious choice of parameters, that the fast mode will always be stable, throught the injection-acceleration-ejection cycle. The slow (drift) mode, however, is more complicated. Under certain conditions the net radial focusing force ($\vec{F}$) may vanish, leading to a transition to unstable behavior followed by a subsequent reversal in sign of the drift motion that is described in detail in Appendix A. This transition may be shown to occur at a boundary in parameter space on one side of which the toroidal field is <u>essential</u> for beam stability, while on the other side the toroidal field is

superfluous for stability. This "instability gap" may not be so serious for single particle motion since it may be shown that a small expansion of the beam restabilizes the motion. For motion of the beam centroid, however, it is much more serious. In fact, we have concluded, on the basis both of this work and other numerical studies, that the beam must be launched and accelerated so as to avoid passage through the instability gap for beam center motion[3]. Fortunately, this does appear possible to do, though it does place a limit on the current that may be accelerated in a device of given aspect ratio. That limit is given by

$$\frac{r_b^2}{a^2} n_s \equiv 2\frac{\nu}{\gamma^3}(r_o/a)^2 < 1/2 \qquad \text{(II-1)}$$

where r_o and a are the major and minor radii of the toroidal chamber, r_b is the beam radius, and n_s is the so-called self-field index. It is interesting to note that this limit is independent of the value of the toroidal field and may in fact represent a more stringent requirement than the basic stability criterion for the fast mode, which can always in principle be satisfied by choosing a large enough toroidal field. For example, according to the above constraint, a 10 kA beam must be injected such that its in situ energy (i.e., that energy retained as kinetic energy by the beam after the beam has given up some fraction of its energy to

the fields within the chamber, after leaving the diode) corresponds to a value of γ in excess of 6.2 for a chamber with $r_o/a = 10$. (Toroidal corrections modify this number somewhat; these are described in Appendix A.)

This constraint (II-1) also affects the workability of certain injection schemes which are based on drifting the beam away from the injector structure during one major transit of the machine. Since the drift frequency is proportional to the quantity $(1/2 - r_b^2 n_s/a^2)$ (B_z/B_θ), one does not want to work too close to transition since a minimum value of B is required to stabilize the fast mode and one requires that the drift frequency ω_B be at least as large as

$$\omega_B > 2\frac{r_b}{\Delta}\frac{1}{T} \qquad \text{(II-2)}$$

where Δ is the distance from the injector port to the beam equilibrium orbit and T is the orbital (major) period. (Constraint (II-2) comes from requiring the beam center to drift two beam radii during one transit around the machine--a minimal requirement for achieving low levels of loss due to scattering by the injector structure.) Both constraints (II-1) and (II-2) favor a large value for γ at injection time.

The instability gaps for particle and whole beam motion have no analog in a conventional betatron. They occur, roughly speaking, when self-fields become comparable to applied fields, which is never the case in a conventional, low current

device. The modified betatron, if it operates as projected, will be the first cyclic particle accelerator in which beam self-fields play a significant role in the particle dynamics.

Another phenomenon occuring in the modified betatron does have an analog in a conventional betatron. This is the adiabatic change in amplitude of the betatron oscillations, as external parameters (B_z, B_θ, field index, flux, ...) are slowly changed[4]. The solution to the linearized equations of motion allows us to obtain explicit expressions for the ratio of the beam radius at the end of the acceleration to that at the beginning. The result is that the beam undergoes a slight compression, as in a conventional accelerator. The beam remains well-behaved during all slow changes in parameters as long as one avoids the instability gap, the boundaries of which appear mathematically as two turning points in the WKB solution.

Unlike the case in a conventional betatron, however, this adiabatic decrease in the betatron oscillation amplitude does not help very much in the basic injection problem; that is, ensuring that the beam misses the injector after one turn. In a conventional betatron one has at least a few turns to accelerate the beam before a particle returns to the vicinity of the injector, since the betatron wavelength is somewhat greater than the machine circumference. With a strong toroidal field in place, however, particles in the

modified betatron tend to follow the toroidal field lines and one must depend on the slow drift to carry the beam away from the injection port in only one turn. The beam, if successful in missing the injector on the first turn, may be subsequently trapped by changing external parameters.

In the course of these investigations on transverse beam dynamics in azimuthally symmetric fields, two computer programs were developed to assist in our understanding of the electron orbits. First, a code LBE (for "Linearized Betatron Equations") was written which integrates the linearized equations of motion for either an individual particle or the beam centroid in arbitrarily time-varying external fields, $E_\theta(t)$, $B_z(t)$, $B_\theta(t)$. The code includes toroidal corrections to the self-fields, assuming a given fixed beam radius. It was used to generate Figs. 4-6 of Appendix A. The code itself is documented by I/O description in Appendix AA, where a listing is also given.

A second code, a single-particle integrator, was also written for the purpose of studying nonlinear dynamics at high energies, where self-field effects are less important. This program, named BTRAK, was eventually modified to include azimuthally varying fields for our study of resonance effects. (See Sections IV, V, and VII.) Its documentation, including listing, appears in Appendix BB.

REFERENCES (For Section II)

1. P. Sprangle and C.A. Kapetanakos, J. Appl. Phys. 49, 1 (1978).
2. N. Rostoker, Comments on Plasma Physics 6, 91 (1980).
3. There is another reason this beam motion instability gap should be avoided. "Below" the gap, where the toroidal field is essential for the stability of whole beam motion, the so-called drag instability, due to finite wall resistivity, becomes operative. See P. Sprangle and C.A. Kapetanakos, NRL Memorandum Report 4950 (1983).
4. D. Kerst, Handbuch der Physik, XLIV, 13 (1959).

III. GRAD-B_θ DRIFT IN THE MODIFIED BETATRON

The effect of nonlinearities in the self- and applied fields will modify the results of Section II; in general, however, these corrections are expected to be small, and in any event are hard to calculate. If the toroidal field B_θ is strong, however, an important nonlinearity to consider is the radial gradient in B_θ.

In general, an electron streaming along a field line executing small gyro orbits will experience a drift in the direction $\vec{\nabla}B \times \vec{B}$ which, in the modified betatron, is vertical. In the betatron however, the situation is complicated by the presence of the vertical field gradient which gives a vertical restoring force; motion in the vertical field clearly cannot be treated in the drift approximation, since the orbit size is of the same order as the scale length of $\vec{\nabla}B_z$. To find the true behavior in the combination of vertical and toroidal fields, we must solve the betatron equations of motion, including the $\partial B_\theta/\partial r$ term. Such a calculation has been carried out; the details appear in Appendix B, part V.

The conclusion reached in the Appendix is that, except for the exceptional case in which the net radial focusing force (due to the betatron field and image fields) vanishes, the $\partial B_\theta/\partial r$ term affects the motion only slightly, giving a radial shift in the position of the equilibrium orbit and a resulting slight change in the betatron frequencies (which

remain real). The radial shift in equilibrium may be interpreted as the result of a balance between the outward "diamagnetic" force, which tends to expel the beam from the high field region and the inward radial restoring force. When the radial restoring force vanishes, the grad-B drift is free to operate. Since the resulting drift is extremely fast, the only reasonable experimental alternative is to avoid the vanishing point for the restoring force. The condition for this has been given in Section II, Eq. (II-1), which provides a bound on the accelerator current which is independent of the toroidal field.

IV. INTEGER RESONANCES IN THE MODIFIED BETATRON

Throughout the analysis of the previous sections it was assumed that all applied fields were perfectly azimuthally symmetric. In practice, of course, any actual accelerator will have slight field imperfections in the toroidal direction, which will be encountered periodically by each electron. In the general case these small periodically applied perturbations to the electron's orbit cause only a small response. However, if it happens that the frequency of the betatron oscillations matches the circulation frequency (or an integer multiple thereof) a constant phase relationship is maintained over many circulation times between the particle motion and a Fourier component of the field imperfection. The resulting "integer resonance" can cause an enormous buildup of betatron oscillations and loss of beam confinement.

In a conventional betatron integer resonances do not occur (neglecting the marginally stable cases n = 0 or 1) because the betatron frequencies, both radial and axial, are necessarily always lower than the particle circulation frequency. In the modified betatron, however, the fast mode can be resonant. For motion of the beam center the ℓ-th resonance occurs when the ratio of the toroidal to vertical fields is

$$B_\theta/B_z = \frac{1}{\ell}(\ell^2 - \frac{1}{2} + \frac{r_b^2}{a^2} n_s), \qquad \text{(IV-1)}$$

where ℓ is the Fourier harmonic number of the field error. Since both B_θ and B_z will in general be changing in time during an experiment, some of these resonances may have to be passed through. This will necessarily be the case if one anticipates removing the toroidal field prior to beam ejection. The question then arises as to how fast the ℓ-th resonance must be passed through in order to avoid beam disruption.

To answer this question the equations of motion in the presence of a field error were formulated and solved, assuming that the fields varied slowly over a circulation time. The result, derived in Appendix C, gives a bound on the magnitude of the field error that may be tolerated. The bound, expressed in terms of the acceleration rate ($\dot{\gamma}$), is rather restrictive, in a practical example that is worked out in the Appendix, leading us to speculate on ways that the resonant effect might be minimized.

One possibility which immediately suggests itself is the use of short acceleration times, thereby limiting the time during which the resonance effect may operate. Very short times may be needed, however, since the required acceleration time for a given final oscillation amplitude scales as the (field error)$^{-2}$. (See Appendix C, Eq. [14].)

A second possibility for stabilization investigated in the Appendix is thermal spread. Though thermal spread

in the beam introduces a spread in resonant frequencies and subsequent reduction of the response of the beam center motion when passing through resonance, individual particle motion may still be such that an unacceptably large beam expansion occurs.

Yet another possibility, which may be practical for certain devices, involves maintaining the ratio B_z/B_θ constant throughout the acceleration. This technique will keep the tunes constant (save for the tune shift due to space charge, which is small for large B_θ) during the experiment. If the application involves use of the beam in situ, then the presence of a strong toroidal field within the device at the end of the acceleration should not be a problem. It would probably complicate an ejection scheme, however.

A final possibility that was investigated for stabilization is the frequency shifting effect of nonlinearities. Specifically, both the toroidal field and the betatron field index will generally vary with radial position. Since the betatron frequencies depend on the values of these quantities, it is possible that the frequencies will be shifted sufficiently by a small (tolerable) radial displacement so as to detune the resonance. A rather strong radial gradient in n may be required to produce the desired effect, however. Results of an investigation into this question are presented in the next section.

In order to be able to predict when certain resonances will be crossed for a given time history of vertical and toroidal fields, a computer program named TUNES was written. This program searches for a specified set of resonances of the form

$$n_f \nu_f + n_s \nu_s = p \qquad \text{(IV-2)}$$

where ν_f and ν_s are the numbers of betatron wavelengths of the fast and slow oscillation modes within the machine circumference, and n_f, n_s, and p are integers. The search is restricted to $|n_f| + |n_s| \leq 3$ and $p < p_{max}$ where p_{max} is specified by the user. Output includes the resonance label (n_f, n_s, p), the time of crossing, and the values of various parameters at crossing. TUNES is documented in Appendix CC. Its use may be helpful in identifying experimentally observed resonance effects.

V. EFFECT OF TRANSVERSELY VARYING FIELD INDEX ON SINGLE PARTICLE DYNAMICS

As discussed in the last section, one possibility considered for controlling resonant response is the intentional introduction of strong nonlinearities (large values of $r\partial n/\partial r$ where n is the betatron field index) which would result in an amplitude-dependent betatron frequency. If this effect were sufficiently strong, the resonant response of a particle could be limited to small values if its finite amplitude oscillations lead to a detuning of the resonance. We have examined the effect of quadratic nonlinearities, limiting ourselves to single-particle motion for simplicity. Though this does not allow us to study the general case (since cubic terms also contribute to frequency shifts), there is a special circumstance in which the contribution of the quadratic terms dominate. This occurs when a coupling resonance (defined below) ccincides with an integer resonance. In this special circumstance, certain progress may be made analytically in studying the effect of resonance detuning. Both a coupling resonance by itself and this "coincidence resonance" have been examined. Details are given in Appendix D. Here we describe the results of this investigation.

The equations of motion of a particle in azimuthally symmetric fields are

$$x'' + (1-n)x = by' + (2n-1-\frac{n_2}{2})x^2 - (\frac{n-n_2}{2})y^2 + \frac{1}{2}(x'^2-y'^2) \quad \text{(V-1a)}$$

$$y'' + ny = -bx' - (2n-n_2)xy + x'y', \qquad \text{(V-1b)}$$

correct to second order where $x = (r-r_o)/r_o$, r_o is the major radius, $b = B_{\theta o}/B_{zo}$, n is the linear field index, n_2 is the second order field index, and a prime indicates $\partial/\partial\theta$. These equations are solved perturbatively to second order in Appendix D. To linear order one obtains the usual betatron oscillations with frequencies (Appendix D, Eq. [11].):

$$\nu_{f,s} = \left[\frac{b^2+1\pm[(b^2+1)^2-4n(1-n)]^{\frac{1}{2}}}{2}\right]^{\frac{1}{2}} \qquad \text{(V-2)}$$

where the subscripts f and s refer to the fast (+) and slow (-) modes respectively. These single-particle oscillations are always stable if $n(1-n)>0$.

By inserting the linear solutions into the equations of motion, we find that the second order correction remains small unless it happens that the following resonance condition is satisfied:

$$\nu_f = 2\nu_s. \qquad \text{(V-3)}$$

This condition turns out to be a generalization of the so-called Walkinshaw resonance condition occuring for $n = 0.2$ or 0.8 in conventional accelerators at which energy is exchanged between radial and vertical oscillation modes. This phenomenon has been observed in early cyclotron experiments[1] where, due to small vertical aperture size, it has led to loss of the beam. In the modified betatron the resonance is shown

in Appendix D to lead to energy exchange between fast and slow modes, with no noticeable growth in beam size under typical experimental conditions. Thus the resonance (V-3) is fairly inconsequential in the modified betatron.

This picture changes somewhat when departures from azimuthal symmetry are taken into account. It turns out that when $n=\frac{1}{2}$ the generalized Walkinshaw resonance coincides with both ordinary integer ($\ell=1$) and half-integer orbital resonances. By including field error terms we may derive equations governing the evolution of the mode amplitudes for this "triple coincidence" resonance and use their solution to study the effect of frequency shifts on resonance detuning in this special case. This program is described in detail and carried through in Appendix D where particle orbits under resonance conditions are illustrated and discussed. The basic result from this analysis is that even fairly strong gradients in n (i.e., large values of n_2) do not adequately control the resonant response of a single particle, that is, the frequency shifting effect is too small to be helpful in the case we have studied.

Our conclusion from this and the preceding section seems clear: It appears to be important to avoid machine operation near low order integer resonances, the condition for which being (IV-1).

REFERENCE

1. D.C. Sewell, L. Henrich, and J Vale, Phys. Rev. 72, 739 (1947).

VI. BEAM INSTABILITIES IN THE MODIFIED BETATRON

The question of what limits the current a particular accelerator can carry in a stable manner is a complicated one. In the case of the modified betatron, the first analyses (Section II, Refs. 1 and 2) suggested, based on examination of individual particle betatron oscillations in the self-fields of the beam, that particle motion could be stable for large currents if the toroidal field were made sufficiently strong. Later work (Section II, Ref. 3 and Appendix B), which considered motion of the beam centroid, led to the discovery that the total beam current must satisfy the constraint given by (II-1), which is independent of the strength of the toroidal field. These analyses, however, treated the beam as smooth and azimuthally symmetric. It is known that under certain conditions small azimuthally varying density perturbations can grow exponentially in time leading to either bunched or kinked beams. Such longitudinal and transverse beam instabilities in general become more destructive (faster growing) the higher the current and so it becomes important to consider their current limiting effect in the modified betatron.

A dispersion relation for longitudinal and transverse modes for a beam in the modified betatron has been derived by Sprangle and Vomvoridis[1], where a stability condition is also given. Building on this work, Sprangle and Chernin[2]

(Appendix E) have considered a slightly more general case, taking into account short wavelength contributions to the wave impedances and the stabilizing effect of finite amplitude betatron oscillations. In Appendix E it is shown that the presence of the toroidal field greatly enhances beam stability to both longitudinal and transverse modes, thereby greatly increasing the current limit over that of a conventional betatron; this stabilizing effect was noticed in Reference [1] where several numerical examples are worked out. The growth rate of the negative mass/kink mode, for example, scales as B_θ^{-1}, a fact attributed to the inhibiting effect the toroidal field has on transverse motion. Stabilization of both longitudinal and transverse modes, for toroidal mode number $\ell \neq 0$, is due to energy spread, or, more precisely, angular frequency spread in the beam; if two particles, initially traveling together, separate by a wavelength or more in a (cold beam) growth time, clearly the coherence of the instability will be lost and growth will stop. If we call the spread in angular frequency in the steady state beam $\Delta\Omega$ and the growth rate in the absence of frequency spread, Γ, then we expect, on the above grounds, the stability condition to be given by

$$\Gamma \leq \ell |\Delta\Omega| \qquad \text{(VI-1)}$$

to within a numerical factor. In fact, it may be rigorously shown[1] that for a beam with a Lorentzian distribution of

canonical angular momentum (VI-1), is the exact stability condition.

The frequency spread $\Delta\Omega$ of the equilibrium beam is related to the energy spread via the single particle momentum compaction factor; the relation is

$$|\Delta\Omega| = \frac{1}{2}\omega_c|\alpha|(\Delta E/E) \qquad \text{(VI-2)}$$

where $\alpha = (\frac{1}{2} - n_s)^{-1} - \gamma^{-2}$, ω_c is the cyclotron frequency, and $\Delta E/E$ is the full width of the energy distribution. We note the importance here of including self-field effects, represented by the self-field index n_s, in the definition of α. It is the appearance of n_s in α, which leads to a novel effect, predicted in Appendix E on the basis of (VI-1,2): For low currents ($n_s << \frac{1}{2}$), α is effectively independent of current and so, since the cold beam growth rate increases with current, the beam energy spread required for stability also increases. As one continues to increase the current, however, α begins to increase significantly, eventually overcoming the increasing growth rate beyond which point increasing the current still further results in stabilization! In fact, for $n_s \approx \frac{1}{2}$, virtually no energy spread is required. There results therefore, from this competition between growth and stabilization mechanisms, a double valuedness in the current vs energy spread stability curve, illustrated and discussed in Appendix E. The prediction of a second stable operating regime for accelerators is the main new result of

this investigation. Our conclusion is that the toroidal field makes possible operation at high currents by (1) reducing cold beam growth rates and, (2) giving access to stable, high-current sectors of the current vs energy spread diagram.

REFERENCES

1. P. Sprangle and J Vomvoridis, NRL Memorandum Report (1982).

2. P. Sprangle and D. Chernin, to be published (Appendix E).

VII. STRONG-FOCUSING SYSTEMS

Conventional betatrons are weak-focusing accelerators, meaning that the wavelengths of the betatron oscillations are of the order of the machine circumference. A second consequence of weak-focusing is that the momentum compaction factor, defined as the fractional radial shift in a mismatched beam divided by its fractional momentum mismatch:

$$\alpha \equiv (\Delta r/r_o)/(\Delta p/p_o) \qquad \text{(VII-1)}$$

is typically of order unity. For a conventional betatron it may be shown, for instance, that $\alpha = (1-n)^{-1}$. As a result, for weak-focusing systems one can typically tolerate only a few percent momentum mismatch before a beam is lost to the chamber wells. Strong-focusing systems, on the other hand, have small values for the momentum compaction factor and betatron wavelengths are much smaller than the machine circumference. A strong-focusing accelerator, consequently, can tolerate a relatively large momentum mismatch. It was the discovery over 30 years ago of the strong-focusing principle which has allowed the construction of the large radius research accelerators in use today.

A modified betatron is a strong-focusing system with respect to particle orbits about the center of the beam, but is a weak-focusing system with respect to motion of the beam centroid about the center of the vacuum chamber. As a

result, it is necessary that the average beam energy be matched to the vertical field to within a few percent. This may be done with careful injector and magnetic field design but design tolerances tend to be tight.

It was the realization of this tolerance problem which led to the consideration of ways to implement strong-focusing in a modified betatron in a way consistent with its design. As a result of a study, it was proposed to add so-called $\ell=2$ stellarator windings to the betatron in order to obtain the beneficial effects of strong-focusing on the beam centroid motion. This extra winding is basically a continuously twisted quadrupole, the limiting case of conventional, closely-spaced discrete quadrupoles which we used in alternating gradient focusing. Beam dynamics in the resulting configuration, consisting of a conventional weak-focusing betatron field, a strong-toroidal field, and an $\ell=2$ stellarator winding have been analyzed in the linear approximation including the effects of self-fields. The results are given and discussed in Appendix F where expressions for the betatron frequencies and momentum compaction factor are derived. We find the results to be encouraging in the sense that the addition of the stellarator winding allows large beam currents to be confined and a large beam momentum mismatch (~50% is not unreasonable) to be tolerated.

The addition of the stellarator winding is not without some drawbacks. As with any strong-focusing system, the effects of orbital resonances must be carefully considered. As discussed above in Section IV, resonances are present and may be a problem already in the modified betatron without the stellarator field. Addition of the $\ell=2$ winding introduces new sets of resonances which must be examined. This work is presently in progress and should lead to important guides for design.

From a practical point of view, the stellarator winding introduces some other possible complications. Injection may become difficult due to the presence of the separatrix, though one possible way to avoid this problem is to introduce straight sections along which to inject. Construction, support, and power supply questions for the stellarator winding also need to be examined. Some preliminary study of the injection and coil design questions in fact have led to consideration of an $\ell=0$ system which may be preferable from the point of view of some of these problems. The $\ell=0$ stellatron, or "bumpy torus accelerator" may have some practical advantages over the $\ell=2$ system. It is described and analyzed in Appendix G.

Despite possible drawbacks, we conclude that strong-focusing systems show significant promise as high-current accelerators. Basic issues in orbital stability and

momentum bandwidth have been addressed. Resonance effects, beam instabilities, injection, and detailed coil design issues remain to be studied further.

VIII. CONCLUSIONS

The analysis of beam behavior in the modified betatron carried out by Berkeley Research Associates over the past two years has led to a detailed understanding of how such an accelerator should operate, its advantages compared to conventional betatrons, and its limitations. Among the advantages must be listed its ability to hold large currents stably during acceleration. We have found that the toroidal field greatly enhances the equilibrium current that may be carried and also enhances the stability of the beam to the longitudinal (negative mass) and transverse collective beam instabilities which may affect the beam. We have found nonlinear effects, including grad-B drifts and effects of transversely varying field index to be negligible as long as the net radial beam-focusing forces remain finite (II-1). Orbital resonances may be a problem in the device unless thay are passed through very rapidly or avoided altogether; avoidance of the low ℓ-number resonances, at least, is probably essential and possible to do in some acceleration scenarios which have been discussed.

Among the limiting features of the modified betatron must be mentioned the sensitivity of the position of the beam equilibrium orbit with respect to its momentum mismatch. This feature, a consequence of the weak-focusing betatron fields, may be overcome by the addition of stellarator fields,

the effect of which is to allow beams with a large momentum mismatch to be confined.

Studies of beam dynamics under this contract have contributed in an important way to the selection of parameters for the high-current injection experiment now being constructed. This experiment will challenge and refine our understanding of the properties of high-current electron beams in toroidal devices. Once completed, the experiment should lead to an operational high-current accelerator.

Theoretical issues which remain to be addressed include: verification of the double-valuedness in the stability curve discussed in Section VI, in a simple but rigorous (Vlasov-Maxwell) model; analysis of the expected radiation spectrum (for diagnostic purposes or for radiation source development); and investigation of resonance effects, injection methods, and coil design in the stellatron. Work in these areas is presently being pursued in association with NRL personnel. Combined with the efforts of the past two years, this continuing research will assist in a significant way in meeting the goals of the NRL Special Focus Program on advanced high-current electron accelerators.

APPENDIX A

Transverse Beam Dynamics in the Modified Betatron

Particle Accelerators
1982 Vol. 12 pp. 85–100
0031-2460/82/1202-0085$06.50/0

TRANSVERSE BEAM DYNAMICS IN THE MODIFIED BETATRON*

D. CHERNIN

Berkeley Research Associates, P.O. Box 852 Springfield, Virginia 22150 U.S.A.

and

P. SPRANGLE

Plasma Theory Branch, Plasma Physics Division, Naval Research Laboratory, Washington, D.C. 20375 U.S.A.

(Received December 16, 1981; in final form April 5, 1982)

The linearized equations governing the motion of the center of a beam about its equilibrium position in a modified betatron, as well as equations governing the motion of an individual particle about the beam center, are presented and solved. Self field effects, including toroidal hoop stresses and wall image forces, are included in the analysis. All fields, both self and applied, are assumed to be azimuthally symmetric but are allowed to have arbitrary time dependences. The solutions to the equations of motion are analyzed for stability and conditions for stability are obtained. Further study of the solutions illustrates two phenomena of experimental interest: (1) the unavoidable traversal of a finite "instability gap" in parameter space during acceleration and (2) the adiabatic increase in the amplitude of the betatron oscillations during removal of the toroidal magnetic field, prior to beam ejection. By careful design, the effects of these phenomena can be reduced to insignificant levels in an actual accelerator.

I. INTRODUCTION

It has been suggested[1,2] that the current carrying capacity of a conventional betatron accelerator might be improved dramatically by the addition of a strong toroidal magnetic field. Such a field acts to confine the beam during injection and early stages of acceleration when γ, the usual relativistic factor, is small and space charge effects which tend to expand the beam are large. After acceleration is complete, γ is large, space charge effects are small, and the usual weak focussing betatron fields are sufficient to confine the beam; the toroidal field may then be removed to facilitate beam ejection. In general both vertical and toroidal magnetic fields may be changing simultaneously during beam injection and ejection. It is the purpose of this paper to examine the behavior of the beam in such time-varying fields.

Some early, though unsuccessful experiments using this modified betatron field configuration were carried out in England after World War II;[3] subsequent analysis[4] attributed the poor results to the injection method used at the time whereby significant numbers of electrons intersected the back of the injector structure after a few trips around the device. Recently other, more promising injection schemes have been proposed[2,5] to take full advantage of the focusing action of the toroidal field. The resulting prospect of constructing a very high current (~ 1–10 KA) betatron has prompted the analysis presented here.

We shall derive and solve equations governing the motion of the center of an electron beam confined in a modified betatron as well as equations governing the motion of an individual particle within the beam. Whole beam and single particle stability criteria will be presented; the stabilizing effect of the toroidal field for both beam and single particle motions, noted earlier,[1,2] will be apparent.

When the fields are allowed to vary in time two interesting phenomena occur. The first phenomenon, which occurs during acceleration, has no analogue in a conventional betatron: As the beam accelerates (γ increases) the betatron makes a transition from a region in parameter space in which the toroidal field is *essential* to stability (modified betatron regime) to a region in which the toroidal field is *superfluous* to stability (conventional betetron regime). It turns out that, except under extraordinary circumstances, the system must pass through an "instability gap"—a region of parameter space, separating the modified and conventional betatron regimes, in which

* Supported by the Office of Naval Research

single particle motion is unstable, though beam center motion may not be, *irrespective* of the magnitude of the toroidal magnetic field. However, though the size of the instability gap is independent of the toroidal field, the instability growth rate within the gap is inversely proportional to this field. We find below that by judicious magnet design and sufficiently rapid acceleration, this gap may be successfully traversed with minimal beam disturbance.

The second phenomenon occuring in time varying fields does have an analogue in a conventional betatron; this is the adiabatic change in the amplitude of the betatron oscillations.[6] Since the frequency of these oscillations depends now on both the vertical and toroidal fields a slow change in either is expected to alter the amplitude of the betatron oscillations. During acceleration we find, as in a conventional accelerator,[6] that the oscillation amplitude decreases as the vertical field increases. If one now considers removal of the toroidal field prior to beam ejection, we find that, as long as the toroidal magnetic field is much larger than the vertical field, the beam motion will describe orbits of increasing amplitude as the toroidal field is decreased. Once the toroidal field becomes comparable to the vertical field, however, the motion becomes more complicated and the betatron oscillations no longer continue to increase in amplitude. We find that, by careful choice of field strengths, the ratio of the betatron oscillation amplitude before acceleration to the amplitude of oscillation following complete removal of the toroidal field can be adjusted to be near one.

In the following analysis we assume "perfect," i.e., azimuthally symmetric fields. By neglecting the possibility of azimuthal variation in the self fields (due to beam bunching or kinking) we omit here consideration of a variety of beam instabilities that may occur;[7] by neglecting similar azimuthal variation in the applied fields ("field errors") we neglect the effects of orbital resonances. These will be addressed in a separate report.[8]

II. EQUILIBRIUM RADIAL FORCE BALANCE

The geometry of the modified betatron is shown in Fig. 1. The field configuration is that of an ordinary betatron with the addition of a toroidal magnetic field, $B_{\theta 0}$, here taken to be positive and constant across the minor cross section of the torus. We consider an electron beam of circular cross section, as shown in Fig. 2, with center located at $(r_c, z_c) = (r_0 + \Delta r, \Delta z)$ where r_0 is the equilibrium radius for the center of the beam at which the electric, magnetic, and centrifugal forces on a particle at the center of the beam are in balance. We shall take r_0 to be the major radius of the accelerator chamber. In the absence of self field effects radial force balance requires the electron circulation frequency at $r = r_0$, $z = 0$ to be given by

$$\theta_0 = \Omega_{z0} \equiv eB_{z0}/m\gamma_0 c \quad \text{(no self field effects)}, \tag{1}$$

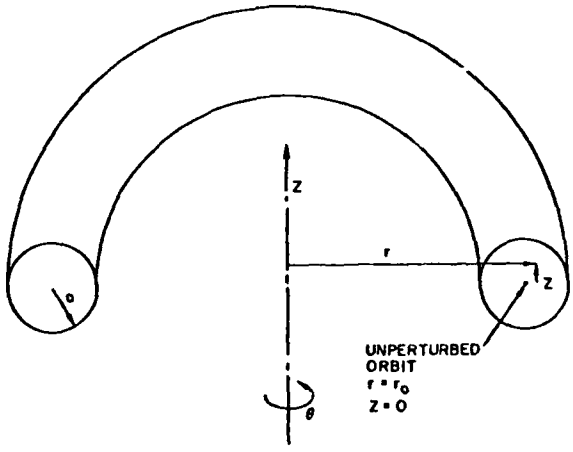

FIGURE 1 Cutaway view of modified betatron geometry

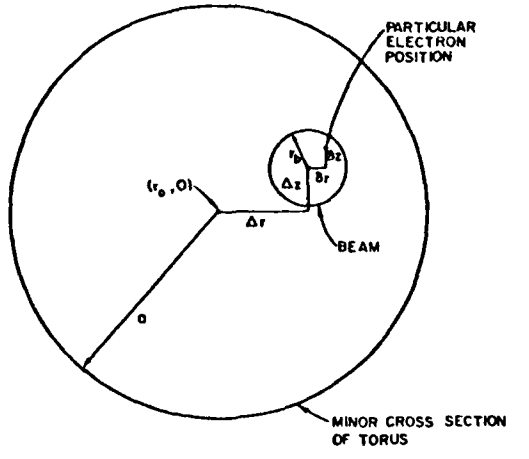

FIGURE 2 Coordinates of beam and particle in modified betatron. Center of beam is at $(r, z) = (r_0 + \Delta r, \Delta z)$. Electron is at $(r, z) = (r_0 + \Delta r + \delta r, \Delta z + \delta z)$.

where B_{z0} is the value of the applied vertical betatron field at the location of the orbit, γ_0 is the usual relativistic factor, $e(>0)$ is the magnitude of the electron charge, m is the electron rest mass, and c is the speed of light.

Self field effects will modify Eq. (1) however.[9] A nonneutral current ring produces both a zero order vertical magnetic field and a radial electric field. In general, for a reference particle at $r = r_0$, $z = 0$, radial force balance requires

$$-\gamma_0 r_0 \dot{\theta}_0^2 = \frac{-e}{m}\left[E_r^{(0)} + \frac{1}{c} r_0 \dot{\theta}_0 B_z^{(0)}\right] \quad (2)$$

where $E_r^{(0)}$ and $B_z^{(0)}$ are the zero order fields at $r = r_0$, $z = 0$. From Appendix A, Eqs. (A-25c, 26c, 26d)

$$B_z^{(0)} = B_{z0} - \pi n_0 e \beta_0 \frac{r_b^2}{r_0} l_B \quad (3)$$

$$E_r^{(0)} = -\pi n_0 e \frac{r_b^2}{r_0} l_E \quad (4)$$

where the notation is defined in Appendix A.

The terms proportional to l_B in Eq. (3) and l_E in Eq. (4) are toroidal corrections to the self fields of a cylindrical beam. They represent "hoop stresses"—self forces on a nonneutral ring of current which act to expand the ring. Since we do not attempt here to construct a consistent equilibrium for the beam[10–12] we leave l_B and l_E arbitrary in the analysis below since their precise values depend upon the particular distributions of charge and current in the beam. Still, one expects the leading order logarithms in the expressions for l_B and l_E, Eqs. (A-27, 28) to be correct.

Using now the zero order fields, Eqs. (3, 4), in Eq. (2) we may write the condition for radial force balance as

$$\left[1 + \frac{\nu}{\gamma_0} l_B\right]\dot{\theta}_0^2 - \Omega_{z0}\dot{\theta}_0 + \frac{\nu}{\gamma_0}\frac{c^2}{r_0^2} l_E = 0 \quad (5)$$

where

$$\nu/\gamma_0 = \frac{1}{\gamma_0}\left[\pi r_b^2 n_0 \frac{e^2}{mc^2}\right] = \frac{1}{4}\frac{\omega_b^2 r_b^2}{c^2} \quad (6)$$

and where ω_b is the beam plasma frequency, $(4\pi n_0 e^2/m\gamma_0)^{1/2}$. Here and below Ω_{z0} retains the definition assigned to it in Eq. (1).

Equation (5) is a quadratic equation for the circulation frequency, $\dot{\theta}_0$. The solution which approaches Ω_{z0} as $\nu/\gamma_0 \to 0$ is, to first order in ν/γ_0

$$\dot{\theta}_0 \approx \Omega_{z0}\left[1 - \frac{\nu}{\gamma_0}\left(\frac{1}{\alpha^2} l_E + l_B\right)\right], \quad (7)$$

where $\alpha = \Omega_{z0} r_0/c$. Self field effects, represented by the ν/γ_0 term, are seen to *reduce* the single particle circulation frequency below that expected for zero density; the correction term can be significant (20–30%) in presently contemplated devices. The general result, Eq. (7), will be needed below in the derivation of the first order equations of motion.

III. FIRST ORDER EQUATIONS OF MOTION

In this section the equations governing the motion of a beam and motion of an electron within the beam are obtained and discussed. We shall consider in detail only motion transverse to the toroidal magnetic field, assuming that all fields, both self and applied, are independent of θ.

The equations of motion for a particle in the fields of (A-25, 26) to first order in the displacements from the reference orbit $(r_0, 0)$, are derived in Appendix B. They are

$$\ddot{r}_1 + \frac{\dot{\gamma}_0}{\gamma_0}\dot{r}_1 + \Omega_{z0}^2\left[1 - n^* - \frac{\nu}{\gamma_0}\left(\frac{3}{\alpha^2} l_E + 2 l_B\right)\right] r_1 - n_s \Omega_{z0}^2\left(\delta r + \frac{r_b^2}{a^2}\Delta r\right) - \frac{\nu}{\gamma_0} l_B \Omega_{z0}^2 \Delta r = \frac{e\dot{B}_{\theta 0}}{2m\gamma_0 c} z_1 + \Omega_{\theta 0}\dot{z}_1 + \Omega_{z0}\frac{P_{\theta 1}}{\gamma_0 m r_0} \times \left[1 - \frac{\nu}{\gamma_0}\left(\frac{1 + \gamma_0^{-2}}{\alpha^2} l_E + l_B\right)\right] \quad (8a)$$

$$\ddot{z}_1 + \frac{\dot{\gamma}_0}{\gamma_0}\dot{z}_1 + \Omega_{z0}^2 n^* z_1 - n_s \Omega_{z0}^2\left(\delta z + \frac{r_b^2}{a^2}\Delta z\right) = -\frac{e\dot{B}_{\theta 0}}{2m\gamma_0 c} r_1 - \Omega_{\theta 0}\dot{r}_1, \quad (8b)$$

where

$$r_1 = r - r_0 = \Delta r + \delta r$$

$$z_1 = z = \Delta z + \delta z$$

$$n^* = n\left[1 - \frac{\nu}{\gamma_0}\left(\frac{1}{\alpha^2} l_E + l_B\right)\right]$$

$$n_s = \omega_b^2/(2\gamma_0^2\Omega_{z0}^2)$$

$$\Omega_{\theta 0} = eB_{\theta 0}/m\gamma_0 c$$

and where $P_{\theta 1}$ is equal to the canonical angular momentum of the particle at (r, z) minus the canonical angular momentum of the reference particle at $(r_0, 0)$, to first order in small quantities. It may be shown, using the definition of P_θ, $P_\theta \equiv r\left(m\gamma V_\theta - \frac{e}{c}A_\theta\right)$, that

$$P_{\theta 1} = m\gamma_0 r_0 \times \left[V_{\theta 1}\gamma_0^2 - \frac{\nu}{\gamma_0}\frac{1}{\alpha^2}\Omega_{z0} l_E r_1 - \frac{\nu}{\gamma_0}\Omega_{z0} l_B \Delta r\right], \quad (9)$$

where $V_{\theta 1} = V_\theta - V_{\theta 0}$.

As they stand Eqs. (8a) and (8b) are not easily solved since, before they can be solved for the coordinates of a particle (r_1, z_1) the beam position $(\Delta r, \Delta z)$ must somehow be known as a function of time. However, a set of consistent equations for beam and particle motion may be obtained by performing an ensemble average of Eqs. (8a, b) over initial particle coordinates and velocities. Denoting such an average by brackets it may be shown that, as long as the beam is assumed not to kink (Δr, Δz independent of θ), we will have

$$\langle r_1\rangle = \Delta r, \langle \delta r\rangle = \langle \dot{\delta} r\rangle = \langle \ddot{\delta} r\rangle = 0 \quad (10a)$$

$$\langle z_1\rangle = \Delta z, \langle \delta z\rangle = \langle \dot{\delta} z\rangle = \langle \ddot{\delta} z\rangle = 0. \quad (10b)$$

Upon performing this averaging procedure on Eqs. (8a, b) we will obtain equations governing the motion of the center of the beam. These may subsequently be subtracted from the original, unaveraged Eqs. (8a, b) to obtain equations governing the motion of a single particle within the beam. Both resulting sets of equations may be summarized by the following single set:

$$\ddot{x} + \omega_x^2 x = \Omega_{\theta 0}\dot{y} + \tfrac{1}{2}\dot{\Omega}_{\theta 0} y + F \quad (11a)$$

$$\ddot{y} + \omega_y^2 y = -\Omega_{\theta 0}\dot{x} - \tfrac{1}{2}\dot{\Omega}_{\theta 0} x \quad (11b)$$

where the various quantities appearing in Eqs. (11a, b) are defined in Table I.

Equations (11a, b) are our basic starting points for the analysis to be presented below. In the following sections we will derive and study the WKB solutions to Eqs. (11a, b). First we make a few remarks on the equations themselves.

The term proportional to x on the left hand side of Eq. (11a) and the term proportional to y on the left hand side of Eq. (11b) represent radial and vertical focussing forces respectively. In general the coefficients of x and y in these terms are not

TABLE I

Definition of Quantities Appearing in Equations of Motion, Eqs. (11a,b)

	Beam Equations	Particle Equations
(x, y)	$\gamma_0^{1/2}(\Delta r, \Delta z)$	$\gamma_0^{1/2}(\delta r, \delta z)$
ω_x^2	$\Omega_{z0}^2\left[1 - n^* - \frac{r_b^2}{a^2}n_s - \frac{3\nu}{\gamma_0}\left(\frac{1}{\alpha^2}l_E + l_B\right)\right] - \frac{1}{2}\frac{\ddot{\gamma}_0}{\gamma_0} + \frac{1}{4}\left(\frac{\dot{\gamma}_0}{\gamma_0}\right)^2$	$\Omega_{z0}^2\left[1 - n^* - n_s - \frac{\nu}{\gamma_0}\left(\frac{3}{\alpha^2}l_E + 2l_B\right)\right] - \frac{1}{2}\frac{\ddot{\gamma}_0}{\gamma_0} + \frac{1}{4}\left(\frac{\dot{\gamma}_0}{\gamma_0}\right)^2$
ω_y^2	$\Omega_{z0}^2\left[n^* - \frac{r_b^2}{a^2}n_s\right] - \frac{1}{2}\frac{\ddot{\gamma}_0}{\gamma_0} + \frac{1}{4}\left(\frac{\dot{\gamma}_0}{\gamma_0}\right)^2$	$\Omega_{z0}^2[n^* - n_s] - \frac{1}{2}\frac{\ddot{\gamma}_0}{\gamma_0} + \frac{1}{4}\left(\frac{\dot{\gamma}_0}{\gamma_0}\right)^2$
F	$\Omega_{z0}\frac{\langle P_{\theta 1}\rangle}{m\gamma_0 r_0} \times \left[1 - \frac{\nu}{\gamma_0}\left(\frac{1 + \gamma_0^{-2}}{\alpha^2}l_E + l_B\right)\right]$	$\Omega_{z0}[P_{\theta 1} - \langle P_{\theta 1}\rangle]\frac{1}{m\gamma_0 r_0} \times \left[1 - \frac{\nu}{\gamma_0}\left(\frac{1 + \gamma_0^{-2}}{\alpha^2}l_E + l_B\right)\right]$

equal which suggests that an initially circular beam may not remain circular. The value of n which makes these terms equal (the value required to maintain a circular beam cross section) is

$$n_{cir} = \frac{1}{2}\left[1 - \frac{\nu}{\gamma_0}\left(\frac{2}{\alpha^2} l_E + l_B\right)\right] \qquad (12)$$

which depends on γ_0 and therefore on time. In what follows we will leave n arbitrary, though we shall assume implicitly that its value is close to n_{cir}. This is necessary for self consistency since we obtained the beam self fields Eqs. (A-26) assuming a circular beam cross section.

In the case of constant fields Eqs. (11a, b) are elementary. For this case we have

$$\begin{pmatrix} x \\ y \end{pmatrix} = \begin{pmatrix} F/\omega_x^2 \\ 0 \end{pmatrix} + \sum_{j=1}^{4} C_j \begin{pmatrix} \sqrt{\omega_y^2 - \omega_j^2} \\ \sqrt{\omega_j^2 - \omega_x^2} \end{pmatrix} e^{i\omega_j t} \qquad (13)$$

where the eigenfrequencies (frequencies of betatron oscillations) are given by

$$\omega_j = \pm \left[\frac{\omega_x^2 + \omega_y^2 + \Omega_{00}^2}{2} \pm \frac{[(\omega_x^2 + \omega_y^2 + \Omega_{00}^2)^2 - 4\omega_x^2\omega_y^2]^{1/2}}{2}\right]^{1/2} \qquad (14)$$

and where the C_j, $j = 1, 2, 3, 4$ are constants.

Stability conditions result in the usual way by requiring $\omega^2_j > 0$. We postpone examination of these conditions, however, until the following section. We note here only that for values of γ above a value dependent on geometry (r_b, a, r_0, n) but *not* on beam density, the self field contributions to ω_x^2 and ω_y^2 fall off as γ_0^{-1}, rather than γ_0^{-3}. For whole beam motion the value of γ at which the ν/γ_0 terms become comparable to the $r_b^2 n_s/a^2$ term can be modest ($\gamma \sim 10$) for typical laboratory parameters ($r_b = 1$ cm, $a = 10$ cm, $r_0 = 100$ cm, $n = 0.5$).

The particular solution in Eq. (13) represents physically for particle motion a first order radial shift of a particle which, while located initially at the reference orbit (r_0, 0) does not have the correct energy to be maintained there by the local vertical magnetic field. It therefore moves in or out slightly depending on the sign of the energy mismatch. If, however, the radial focussing forces, represented by ω_x^2, happen to vanish the behavior becomes secular (no equilibrium radius exists) and the particle moves vertically, up or down depending on the sign of the mismatch; this secular motion is just the so called "curvature" or "centrifugal" drift.

The solution to the homogeneous part of Eqs. (11a, b) also becomes secular when $\omega_x^2 = 0$. In fact, when $\omega_x^2 = 0$ and $\omega_y^2 \neq \omega_x^2$ ($n \neq n_{cir}$), the point $\omega_x^2 = 0$ corresponds to a turning point (transition from stable to unstable behavior) in the WKB solution presented in the next section. Since ω_x^2 for particle motion *will pass through zero* during acceleration, it becomes important to examine the behavior of the solutions to Eqs. (11a, b) for time dependent fields. In general, for slowly time varying fields, a numerical solution to Eqs. (11a, b) over the entire acceleration cycle is prohibitive since the numerical integration time step must be small compared to Ω_{00}^{-1} which in turn is extremely small compared to typical acceleration times. An explicit solution for this case is therefore essential.

IV. MOTION OF BEAM IN SLOWLY VARYING EXTERNAL FIELDS

A. *Stability Considerations*

If the coefficients of the derivatives of x and y in Eqs. (11a, b) are slowly varying during a period of a betatron oscillation, the equations may be solved by the WKB method. (See Appendix C.) To leading order the solution is

$$\begin{pmatrix} x \\ y \end{pmatrix} \sim \frac{1}{\omega_\Delta} \sum_{j=1}^{4} \frac{A_j}{\omega_j^{1/2}} \begin{pmatrix} (\omega_y^2 - \omega_j^2)^{1/2} \\ (\omega_j^2 - \omega_x^2)^{1/2} \end{pmatrix} \qquad (15)$$

$$\times \exp i \int^t \omega_j dt' + \int^t dt' \begin{bmatrix} K_x(t, t') \\ K_y(t, t') \end{bmatrix} F(t'),$$

where the eigenfrequencies are those given in (14) in which now all quantities may depend on time,

$$\omega_\Delta \equiv [(\omega_x^2 + \omega_y^2 + \Omega_{00}^2)^2 - 4\omega_x^2\omega_y^2]^{1/4}, \qquad (16)$$

and where the kernels $K_x(t, t')$ and $K_y(t, t')$ are

given in Appendix C. The A_j, $j = 1, 2, 3, 4$ are constants in this approximation.

This solution, Eq. (16), is valid far from any turning point, i.e. where any ω_j vanishes. Turning points will occur if $\omega_x^2\omega_y^2 = 0$ and if $\omega_x^2 \neq \omega_y^2$. (See below.) Initially we shall confine attention to a cold beam (no longitudinal momentum spread) for which the particular solution in (15) vanishes identically. Later we shall comment on the effect of temperature.

The solution is unstable (exponentially growing) in time for such times that $\mathrm{Im}(\omega_j) < 0$ for any j. Unstable behavior will occur therefore whenever either of the following conditions is violated:

$$\omega_x^2\omega_y^2 > 0 \tag{17a}$$

$$\omega_x^2 + \omega_y^2 + \Omega_{\theta 0}^2 > 2(\omega_x^2\omega_y^2)^{1/2}, \tag{17b}$$

For $n = n_{\mathrm{cir}}$ ($\omega_x^2 = \omega_y^2$) inequality (17a) is trivial and (17b) gives the simplified stability condition

$$\Omega_{\theta 0}^2 > \max(0, -4\omega_x^2). \tag{18}$$

If $n \neq n_{\mathrm{cir}}$ then both conditions (17a, b) must be simultaneously satisfied for stability. Condition (17a) in particular *cannot always be satisfied*. At injection n_s is typically quite large and both ω_x^2 and ω_y^2 for particle motion (and perhaps for beam motion) are negative. During acceleration, as γ_0 increases n_s decreases ($n_s \sim \gamma_0^{-3}$) and ω_x^2 and ω_y^2 change sign (for different values of γ_0, if $n \neq n_{\mathrm{cir}}$); an instability "gap" therefore exists while ω_x^2 and ω_y^2 have opposite signs.

It is important to point out that ω_x^2 and ω_y^2 for beam center motion (Re: Table I) may start out and remain positive throughout the injection-acceleration cycle while ω_x^2 and ω_y^2 for particle motion change sign. We recall from Table I that the small quantity $(r_b/a)^2$ multiplies n_s in the expressions for ω_x^2 and ω_y^2 for beam center motion but not for single particle motion. Therefore unless n_s is extremely large initially, beam center motion will remain stable.

The inequalities Eq. (17a-b) are illustrated graphically in Fig. 3. The stable regions of the $(\omega_y/\Omega_{\theta 0})^2$, $(\omega_x/\Omega_{\theta 0})^2$ plane are those shaded regions I and II in the figure. After injection but before acceleration both $(\omega_y/\Omega_{\theta 0})^2$ and $(\omega_x/\Omega_{\theta 0})^2$ for particle motion are negative and in region I. In this region the toroidal magnetic field is essential for stability (modified betatron regime). Following acceleration both $(\omega_y/\Omega_{\theta 0})^2$ and $(\omega_x/\Omega_{\theta 0})^2$ are positive, i.e., in region II in which the

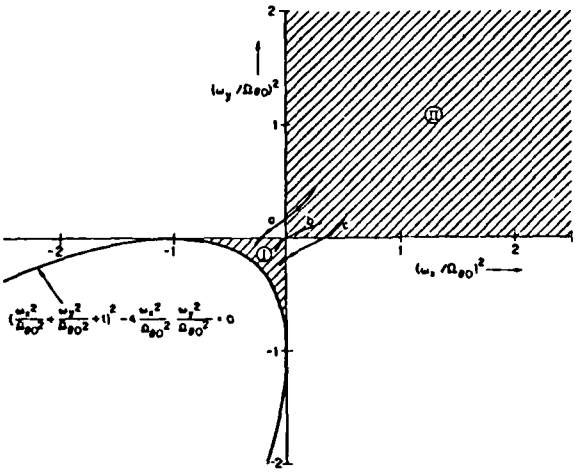

FIGURE 3 The $\left(\frac{\omega_y}{\Omega_{\theta 0}}\right)^2, \left(\frac{\omega_x}{\Omega_{\theta 0}}\right)^2$ plane. Shaded regions are stable. Trajectors *a* and *c* pass through unstable regions. Only trajectories, such as *b*, avoid all unstable behavior.

toroidal field is no longer required for stability (conventional betatron regime). Only by passing precisely through the origin (e.g., trajectory b in Fig. 3) can instability be avoided altogether. While the size of the instability gap does not depend on the magnitude of $B_{\theta 0}$ the value of $\mathrm{Im}(\omega_j)$ in the gap does and is inversely proportional to $B_{\theta 0}$. Therefore by choosing a sufficiently large toroidal field it should be possible to pass through the instability gap safely (within a few growth times, or less).

We may be quantitative for a case in which toroidal effects may be neglected: When Eq. (17a) is violated and if $\Omega_{\theta 0}^2 \gg |\omega_x^2|, |\omega_y^2|$ then for the unstable mode, from Eq. (14),

$$\mathrm{Im}\ \omega_j \approx \frac{\sqrt{-\omega_x^2\omega_y^2}}{\Omega_{\theta 0}} \tag{19}$$

which has a peak value, assuming only γ_0 and not $B_{\theta 0}$ is changing in time, of

$$\Omega_{z0}\left(\frac{B_{z0}}{B_{\theta 0}}\right)\left|n - \frac{1}{2}\right| \equiv \tau_g^{-1}. \tag{20}$$

If

$$\int_{t_1}^{t_2} dt\ \mathrm{Im}\ \omega_j \equiv \int_{\gamma_1}^{\gamma_2} \mathrm{Im}\ \omega_j \frac{d\gamma_0}{\dot{\gamma}_0} \ll 1, \tag{21}$$

where t_1 and t_2 are the times at which the insta-

bility gap is entered and exited, respectively, then one expects that the transit through the gap will not significantly disrupt the beam; Eq. (21) translates into a constraint on $\dot{\gamma}_0$

$$\frac{\dot{\gamma}_0}{\gamma_0} \gg \frac{\pi}{3}\,\Omega_{z0}\,\frac{B_{z0}}{B_{\theta 0}}\,(n - \tfrac{1}{2})^2. \qquad (22)$$

If the acceleration is fast enough to satisfy Eq. (22) particle motion will be essentially unaffected by passage through the gap. It should be possible to choose a machine design (i.e., a sufficiently large toroidal field and a field index close to $\frac{1}{2}$) so that Eq. (22) is well satisfied.

The instability which occurs while $\omega_x^2\omega_y^2 < 0$ has an interesting dynamical origin. Let us consider the equations of motion, Eqs. (11a, b), taking $F = 0$, and taking the external fields to be constant in time:

$$\ddot{x} + \omega_x^2 x = \Omega_{\theta 0}\dot{y} \qquad (23a)$$

$$\ddot{y} + \omega_y^2 y = -\Omega_{\theta 0}\dot{x}. \qquad (23b)$$

These equations are just those governing the motion of a particle in an effective electric field

$$E_x^{\text{eff}} = \frac{m}{e}\,\omega_x^2 x \qquad (24a)$$

$$E_y^{\text{eff}} = \frac{m}{e}\,\omega_y^2 y \qquad (24b)$$

and a magnetic field $B_{\theta 0}/\gamma_0$. Converting to polar coordinates ρ, ϕ we have

$$E_\rho^{\text{eff}} = \frac{m}{e}\,\rho[\omega_x^2\cos^2\phi + \omega_y^2\sin^2\phi] \qquad (25a)$$

$$E_\phi^{\text{eff}} = \frac{m}{e}\,\rho[\omega_y^2 - \omega_x^2]\sin\phi\cos\phi. \qquad (25b)$$

The particle behavior may be understood as follows. Let us assume that $n > \frac{1}{2}$, from which it follows that $\omega_y^2 > \omega_x^2$ always, and let us consider first the modified betatron regime ($\omega_x^2 < 0$, $\omega_y^2 < 0$). E_ρ^{eff} in this regime is everywhere negative thereby giving rise to a *clockwise* $\vec{E} \times \vec{B}$ drift, assuming $B_{\theta 0}$ is positive. E_ϕ^{eff}, which is much smaller in magnitude than E_ρ^{eff}, gives a radial drift of alternating sign as the particle moves from quadrant to quadrant, thereby producing an elliptical orbit. Stable motion is established by balancing the outward radial electrostatic + outward centrifugal forces against the $\vec{V} \times \vec{B}$ confining force.

In the conventional betatron regime $\omega_x^2 > 0$, $\omega_y^2 > 0$ and the sign of E_ρ^{eff} is reversed. Azimuthal particle drift is now *counter-clockwise* and the major axis of the elliptical orbit is rotated by 90°. Stable motion is achieved by balancing the inward radial electrostatic force against the centrifugal force; the toroidal field is no longer needed.

In the instability gap E_ρ^{eff} has zeroes at polar angles given by

$$\cos^2\phi_0 = \left(1 - \frac{\omega_x^2}{\omega_y^2}\right)^{-1} \qquad (26)$$

at which points the azimuthal drift velocity vanishes. The radial drift velocity, $cE_\phi^{\text{eff}}/B_\theta$, cannot also vanish at the same point. Consequently the particle drifts radially, with increasing velocity, since $E_\phi^{\text{eff}} \sim \rho$, at the angle ϕ_0, as long as $\omega_x^2\omega_y^2 < 0$. Increasing the toroidal B field, thereby reducing the radial drift velocity, reduces the growth rate of this instability, a fact reflected in Eq. (19).

Typical orbits during transit of the instability gap are illustrated for a simple case in Figs. 4 and 5 in which results of a numerical integration of

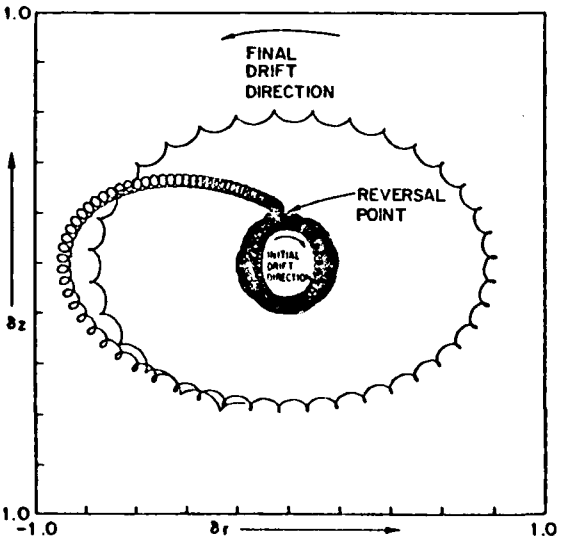

FIGURE 4 Particle trajectory (δz vs. δr) in the modified betatron during transit of the instability gap. γ varies linearly in time from 7.0 to 16.1 in 2.4 μs. B_θ = 600 gauss, r_0 = 100 cm, a = 10 cm, r_b = 1 cm, n = 0.53, $\nu/\gamma = 8.4 \times 10^{-3}$ at t = 0.

Eqs. (11a, b) are plotted. In Fig. 4 condition (21) is not well satisfied. The dramatic drift direction reversal and instability are evident. In Fig. 5 condition (21) is well satisfied (n is near $\frac{1}{2}$); particle motion is virtually unaffected, except for the reversal of drift direction, by passage through the gap. The two graphs, in Figs. 4 and 5 differ only by the value of n used; all other external parameters and total integration time are identical.

So far no mention has been made of the effect of temperature, the inhomogeneous term in Eqs. (11a, b), on particle orbit behavior in or near the instability gap. Particles having an energy mismatch—either too little or too much energy to be maintained at the reference orbit by the local vertical field—will seek out their new equilibrium orbits about which they will execute betatron oscillations. Secular behavior is expected, as discussed earlier, when ω_x^2 vanishes.

The effect of energy mismatch on a particle orbit is illustrated in Fig. 6 where the particle of Fig. 5 has been given an energy mismatch of

$$\frac{P_{\theta 1} - \langle P_{\theta 1}\rangle}{mr_0c} \approx \gamma_1 - \langle\gamma_1\rangle = 0.10.$$

The effect is twofold. The orbit center shifts slightly outward and the amplitude of betatron oscillations following passage through the instability gap has increased by a factor of ~35 over

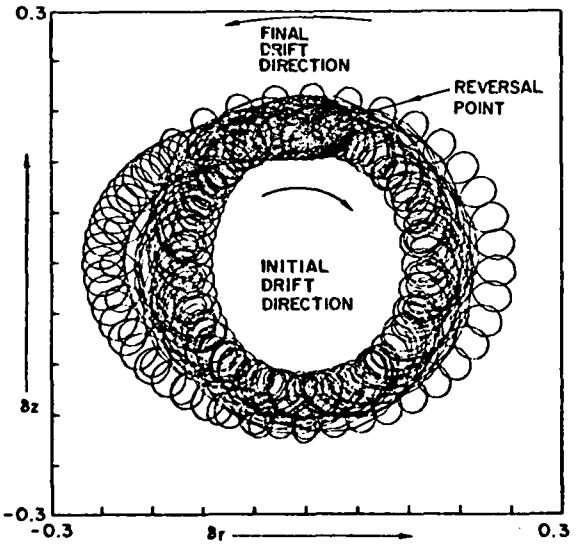

FIGURE 5 Particle trajectory (δz vs. δr) in the modified betatron during transit of the instability gap. All parameters are as in Fig. 4 except $n = 0.51$.

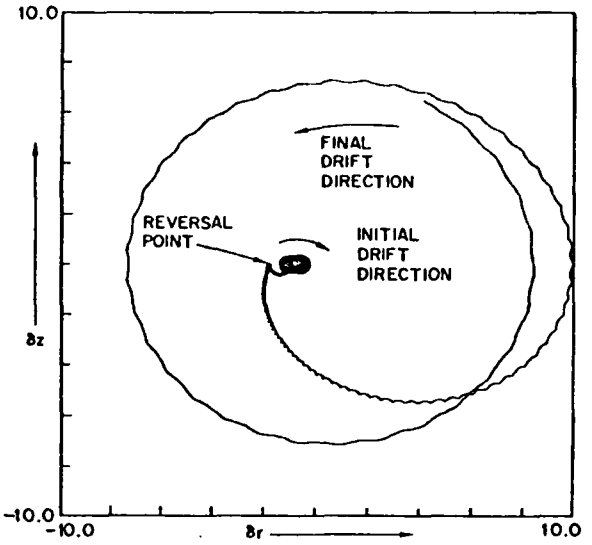

FIGURE 6 Particle trajectory (δz vs. δr) in the modified betatron during transit of the instability gap, including energy mismatch. All parameters are as in Fig. 5 except an energy mismatch of $(P_{\theta 1} - \langle P_{\theta 1}\rangle)/mr_0c = 0.10$ has been introduced.

the zero mismatch case. Such a large expansion of the particle orbits cannot, in fact, be reliably computed using the linearized Eqs. (11a, b) used here. One non-linear effect in particular, namely the reduction of beam density during the orbit expansion, will clearly speed the passage of a particle through the instability gap. (Recall that n_s is proportional to density.) Due to this density reduction the actual degree of orbit expansion to be anticipated in a real device is likely to be significantly less than that seen in Fig. 6. Still, these calculations suggest that a fairly cold beam will be required for successful acceleration through the instability gap. Poorly "matched" particles are likely to be lost as ω_x^2 goes through zero. It should be pointed out as well that a strong toroidal field greatly reduces the effects of energy mismatch. The computer runs necessarily employ a very modest toroidal field (600 gauss in the case of Figs. 4–6) due to time step considerations. A stronger field, by further restricting radial motion, is expected to improve the confinement properties of a warm beam.

B. Adiabatic Behavior

Let us next briefly consider, using the solutions to the equations of motion, Eq. (15), the effects on the particle orbits of the removal of the to-

roidal magnetic field. The toroidal field may need to be removed in order to facilitate beam extraction though this may not be essential. Let us assume that Eq. (15) is valid throughout the acceleration cycle, i.e., that ω_x^2 and ω_y^2 pass through zero simultaneously and that the solution to the homogeneous equation (the sum in Eq. (15)) dominates the solution. This is certainly true for matched particles ($P_\theta = \langle P_\theta \rangle = 0$) when $n = \frac{1}{2}$ and when toroidal effects may be neglected ($\nu/\gamma \ll 1$). One may show, using Eq. (15) for such a case, that for beam center motion in either the fast or slow oscillation mode

$$\frac{[(\Delta r)^2 + (\Delta z)^2]_f}{[(\Delta r)^2 + (\Delta z)^2]_i} = \left[\frac{\left[\left(\frac{1}{2} - \frac{r_b^2}{a^2} n_s\right) B_{z0}^2 + \frac{1}{4} B_{\theta 0}^2\right]_i}{\left[\left(\frac{1}{2} - \frac{r_b^2}{a^2} n_s\right) B_{z0}^2 + \frac{1}{4} B_{\theta 0}^2\right]_f}\right]^{1/2}, \tag{27}$$

while for particle motion about the beam center[13]

$$\frac{[(\delta r)^2 + (\delta z)^2]_f}{[(\delta r)^2 + (\delta z)^2]_i} = \left[\frac{[(\frac{1}{2} - n_s) B_{z0}^2 + \frac{1}{4} B_{\theta 0}^2]_i}{[(\frac{1}{2} - n_s) B_{z0}^2 + \frac{1}{4} B_{\theta 0}^2]_f}\right]^{1/2}, \tag{28}$$

where the subscripts i and f correspond to any initial and final states. The latter expression, Eq. (28), may be interpreted as the fractional change in beam cross sectional area. Note that for large B_θ the area of the orbits $\sim B_\theta^{-1}$, as expected.

Expressions for these ratios in the case that toroidal effects are not negligible and $n \neq \frac{1}{2}$ may be obtained from Eq. (15). The expressions are complicated, however, and will not be cited here.

As a numerical example we consider a 1 kA beam of 1 cm initial radius in an initial state corresponding to $\gamma_i = 7$, $B_{z0,i} = 120$ g, $B_{\theta 0,i} = 1.5$ kg and a final state with $\gamma_f = 100$, $B_{z0,f} = 1.7$ kg, and $B_{\theta 0,f} = 0$. In such a case Eq. (27) gives for the orbital area ratio a value of 0.63 while Eq. (28) gives for the ratio of beam cross sectional areas a value of 0.60.

We conclude that it should be possible both to accelerate the beam and to remove the toroidal field to facilitate beam ejection without causing either the beam orbit or individual particle orbits to expand without limit.

V. CONCLUSIONS

The beam in a modified betatron can be stably confined both during the acceleration phase and during the subsequent gradual removal of the toroidal magnetic field prior to beam ejection. As the beam is accelerated, however, unless very special conditions are satisfied, a region of instability will be passed through; however if the time of transit through this instability gap is small compared to the time specified in Eq. (20) the net effect should be small.

As the toroidal field is removed to facilitate beam extraction following acceleration no further instability gaps occur but the magnitude of the beam betatron oscillations will change adiabatically. By arranging that the ratios, Eqs. (27, 28), be near one, one expects the beam to be well behaved during the removal of the toroidal field.

It should be remarked however that changing the toroidal field changes the "tune" of the betatron which, in general, will necessitate the passage through orbital resonances as the toroidal field is removed. These resonances, due to the periodic encounter by a particle of a field error or "bump" are currently under investigation. It is anticipated that a condition governing the minimum speed with which B_θ must be removed, expressed as a function of the magnitude of the field error, will be obtained.[8]

Note added in proof: Due to a quirk in the publication process the work of reference 8, while completed and submitted for publication after the present work, actually appears in print earlier in this volume (Part. Acc. *12*, 329 (1982)).

ACKNOWLEDGMENTS

We have benefitted from discussions with J. L. Vomvoridis, C. A. Kapetanakos, and N. Rostoker. We wish to thank J. D. Lawson for bringing Ref. 4 to our attention.

APPENDIX A

Fields in the Modified Betatron

In this appendix we calculate the fields seen by a particle in a modified betatron. The particle is assumed to be close to the axis of the torus,

that is, the coordinates of the particle are taken to be (refer to Figs. 1 and 2 in the text)

$$(r, z) = (r_0 + \Delta r + \delta r, \Delta z + \delta z)$$

and all fields will be calculated to first order in Δr, δr, Δz, and δz. Fields will be given in the (r, θ, z) coordinate system of Fig. 1 and all will be assumed to be independent of θ. Superscripts a and s will be used below to denote applied and self fields, respectively.

Part I (Applied Fields)

Magnetic Field

The usual weak focussing betatron field has r and z components. The z component is taken to behave near r_0 as

$$B_z^a \approx B_{z0}(r_0/r)^n \approx B_{z0}\left(1 - n\frac{\Delta r + \delta r}{r_0}\right), \tag{A-1}$$

where B_{z0} depends only on time and n, taken as a constant to this order, is the so-called vacuum field index. The radial field is obtained by requiring $(\vec{\nabla} \times \vec{B})_\theta = 0$ and $B_r(z = 0) = 0$ (making the $z = 0$ plane a plane of symmetry). The result is

$$B_r^a \approx -nB_{z0}\left(\frac{\Delta z + \delta z}{r_0}\right) \tag{A-2}$$

The applied toroidal field generally falls off as r^{-1} across the minor cross section of the torus

$$B_\theta^a \approx B_{\theta 0}\left(1 - \frac{\Delta r + \delta r}{r_0}\right),$$

where $B_{\theta 0}$ depends only on time. However, in the equations of motion B_θ multiplies only $\dot{r}$ and $\dot{z}$ terms which are already first order. Therefore the gradient of B_θ does not enter the linearized equations of motion and we take only the zero order value,

$$B_\theta^a \simeq B_{\theta 0}. \tag{A-3}$$

Electric Field

All applied electric fields are inductive. The toroidal electric field is governed by the changing central flux and is taken to be a specified function of time

$$E_\theta^a = E_{\theta 0}(t). \tag{A-4}$$

E_θ is negative for electron acceleration with B_{z0} positive.

Changing the toroidal magnetic field, $B_{\theta 0}$, will induce a poloidal electric field, the r and z components of which are easily found

$$E_r^a = -\frac{1}{2c}\dot{B}_{\theta 0}(\Delta z + \delta z) \tag{A-5}$$

$$E_z^a = \frac{1}{2c}\dot{B}_{\theta 0}(\Delta r + \delta r), \tag{A-6}$$

where a dot indicates a time derivative.

Part II (Self Fields)

Since we neglect beam diamagnetism and the possibility of a change in self flux due to time varying beam current we take $B_\theta^s = E_\theta^s = 0$. It remains to calculate the r and z components of the beam self electric and magnetic fields.

Consider a beam circulating inside a perfectly conducting toroidal chamber of circular cross section as shown in Fig. A-1. (The beam dis-

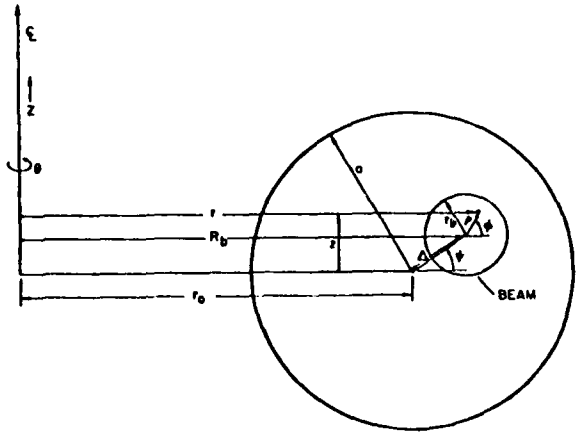

FIGURE A-1 Geometry for self field calculation

placement is exaggerated for clarity; we will assume $\Delta \ll a$). The chamber major and minor radii are r_0 and a respectively. The beam major and minor radii are R_b and r_b respectively. We must calculate the fields *inside* the beam ($\rho < r_b$), assuming the chamber is a perfect conductor. To proceed we define a scalar potential $\Phi(\rho, \phi)$ and a magnetic flux or stream function $\Psi(\rho, \phi) \equiv rA_\theta$ where A_θ is the usual vector potential. The equations for Φ and Ψ are

$$\frac{1}{\rho}\frac{\partial}{\partial\rho}\left(\rho\frac{\partial\Phi}{\partial\rho}\right) + \frac{1}{\rho^2}\frac{\partial^2\Phi}{\partial\phi^2} = 4\pi e n_0(\rho,\phi) - \frac{\left[\cos\phi\frac{\partial\Phi}{\partial\rho} - \frac{1}{\rho}\sin\phi\frac{\partial\Phi}{\partial\phi}\right]}{R_b + \rho\cos\phi} \tag{A-7}$$

$$\frac{1}{\rho}\frac{\partial}{\partial\rho}\left(\rho\frac{\partial\Psi}{\partial\rho}\right) + \frac{1}{\rho^2}\frac{\partial^2\Psi}{\partial\phi^2} = -\frac{4\pi}{c}(R_b + \rho\cos\phi)J_\theta(\rho,\phi) + \frac{\left[\cos\phi\frac{\partial\Psi}{\partial\rho} - \frac{1}{\rho}\sin\phi\frac{\partial\Psi}{\partial\phi}\right]}{R_b + \rho\cos\phi}, \tag{A-8}$$

where n_0, the beam number density and J_θ, the beam current density, are assumed to have been specified. Here we shall take both n_0 and J_θ constant, independent of ρ and ϕ.

The boundary conditions on Φ and Ψ are the same; they both must vanish at the surface of the chamber, specified by

$$\rho \approx a - \Delta\cos(\psi - \phi), \tag{A-9}$$

correct to first order in Δ/a.

Scalar Potential and Electric Field

The general solution for Φ, including the first toroidal correction, is

$$\Phi = \begin{cases} \Phi_0 + q(1 - \rho^2/r_b^2) + \dfrac{q\rho^3}{4R_b r_b^2}\cos\phi \\ \quad + A\dfrac{\rho}{r_b}\sin\phi + B\dfrac{\rho}{r_b}\cos\phi \quad \rho < r_b \\ \Phi_0 - 2q\ln\rho/r_b + \dfrac{q\rho}{R_b}\ln\rho/r_b\cos\phi \\ \quad + \left(A'\dfrac{\rho}{r_b} + C'\dfrac{r_b}{\rho}\right)\sin\phi \\ \quad + \left(B'\dfrac{\rho}{r_b} + D'\dfrac{r_b}{\rho}\right)\cos\phi \quad \rho > r_b \end{cases} \tag{A-10}$$

where $q \equiv -en_0\pi r_b^2$ and Φ_0, A, B, A', B', C', and D' are constants.

Applying now the correct boundary conditions both at the beam surface and the wall determines all of the constants:

$$\Phi_0 = 2q\ln a/r_b \tag{A-11a}$$

$$A = A' = -2q\frac{\Delta}{a}\frac{r_b}{a}\sin\psi \tag{A-11b}$$

$$B = B' = -q\frac{r_b}{R_b}\ln a/r_b - \frac{qr_b^3}{4R_b a^2} - 2q\frac{\Delta}{a}\frac{r_b}{a}\cos\psi \tag{A-11c}$$

$$C' = 0 \tag{A-11d}$$

$$D' = \frac{q}{4}\frac{r_b}{R_b}. \tag{A-11e}$$

Using this result in Eq. (A-10) we may calculate the r and z components of $\vec{E}^s$ inside the beam, to first order:

$$E_r^s = -\frac{\partial\Phi}{\partial\rho}\cos\phi + \frac{1}{\rho}\frac{\partial\Phi}{\partial\phi}\sin\phi = \frac{2q}{r_b^2}\left[\delta r + \frac{r_b^2}{a^2}\Delta r\right] + \frac{q}{R_b}\ln\frac{a}{r_b} \tag{A-12}$$

$$E_z^s = -\frac{\partial\Phi}{\partial\rho}\sin\phi - \frac{1}{\rho}\frac{\partial\Phi}{\partial\phi}\cos\phi = \frac{2q}{r_b^2}\left[\delta z + \frac{r_b^2}{a^2}\Delta z\right], \tag{A-13}$$

where $(\delta r, \delta z) \equiv \rho\,(\cos\phi, \sin\phi)$ and $(\Delta r, \Delta z) \equiv \Delta\,(\cos\psi, \sin\psi)$.

Magnetic Flux (or Stream) Function and Magnetic Field

The general solution for Ψ, including the first toroidal correction, is

$$\Psi = \begin{cases} \Psi_0 + Q(1 - \rho^2/r_b^2) - \dfrac{3}{4}\dfrac{Q}{R_b}\dfrac{\rho^3}{r_b^2}\cos\phi \\ \quad + \bar{A}\dfrac{\rho}{r_b}\sin\phi + \bar{B}\dfrac{\rho}{r_b}\cos\phi \quad \rho < r_b \\ \Psi_0 - 2Q\ln\rho/r_b - \dfrac{Q\rho}{R_b}\ln\rho/r_b\cos\phi \\ \quad + \left(\bar{A}'\dfrac{\rho}{r_b} + \bar{C}'\dfrac{r_b}{\rho}\right)\sin\phi \\ \quad + \left(\bar{B}'\dfrac{\rho}{r_b} + \bar{D}'\dfrac{r_b}{\rho}\right)\cos\phi \quad \rho > r_b \end{cases} \tag{A-14}$$

where $Q \equiv \pi r_b^2 J_\theta R_b/c = -\pi r_b^2 e n_0 \beta_0 R_b$, $\beta_0 = V_{\theta 0}/c$, and Ψ_0, $\bar{A}$, $\bar{B}$, $\bar{A}'$, $\bar{B}'$, $\bar{C}'$, and $\bar{D}'$ are constants.

Applying the boundary conditions gives

$$\Psi_0 = 2Q\ln\frac{a}{r_b} \tag{A-15a}$$

$$\bar{A} = \bar{A}' = -2Q\frac{\Delta}{a}\frac{r_b}{a}\sin\psi \tag{A-15b}$$

$$\bar{B} = \bar{B}' + Q\frac{r_b}{R_b} = -2Q\frac{\Delta}{a}\frac{r_b}{a}\cos\psi + Q\frac{r_b}{R_b}\ln\frac{a}{r_b} + Q\frac{r_b}{R_b} - \frac{1}{4}\frac{Q}{R_b}\frac{r_b^3}{a^2} \tag{A-15c}$$

$$\bar{C}' = 0 \tag{A-15d}$$

$$\bar{D}' = \frac{1}{4}Q\frac{r_b}{R_b}. \tag{A-15e}$$

The resulting magnetic field, to first order, is

$$B_r^s = -\frac{1}{r}\left(\frac{\partial\Psi}{\partial\rho}\sin\phi + \frac{\partial\Psi}{\partial\phi}\frac{\cos\phi}{\rho}\right) = -2\pi e n_0\beta_0\left(\delta z + \frac{r_b^2}{a^2}\Delta z\right) \tag{A-16}$$

$$B_z^s = \frac{1}{r}\left(\frac{\partial\Psi}{\partial\rho}\cos\phi - \frac{\partial\Psi}{\partial\phi}\frac{\sin\phi}{\rho}\right) = 2\pi e n_0\beta_0 \times \left[\delta r + \frac{r_b^2}{a^2}\Delta r - \frac{r_b^2}{2R_b}\left(\ln\frac{a}{r_b} + 1\right)\right]. \tag{A-17}$$

In the circulation frequency, $\dot{\theta}_0$, rather than the current itself, is taken to be constant across the beam (current $\sim r$) then it is straightforward to show that $\ln\frac{a}{r_b} + 1$ in Eq. (A-17) is replaced by $\ln\frac{a}{r_b} + 2$.

If the magnetic field of the beam has diffused completely through the wall then the field surrounding the beam is most directly calculated using the free space Green's function

$$\vec{A}(\vec{r}) = \frac{1}{c}\int d\vec{r}'\,\frac{\vec{J}(\vec{r}')}{|\vec{r} - \vec{r}'|}. \tag{A-18}$$

If $\vec{J} = J_\theta\hat{\theta}$ is constant across the beam and J_θ is independent of θ then $\vec{A} = A_\theta\hat{\theta}$ where

$$A_\theta(r, z) = \frac{J_\theta}{c}\int_{R_b - r_b}^{R_b + r_b} r'dr' \int_0^{2\pi} d\theta' \int_{-z_b(r')}^{z_b(r')} dz' \times \frac{\cos\theta'}{[r^2 + r'^2 - 2rr'\cos\theta' + (z - z')^2]^{1/2}}$$

$$z_b(r') = [r_b^2 - (r' - R_b)^2]^{1/2}. \tag{A-19}$$

The integral over θ' may be expressed in terms of the complete elliptic integrals[1]

$$A_\theta = \frac{4J_\theta}{c}\int_{R_b - r_b}^{R_b + r_b} r'dr' \int_{-z_b(r')}^{z_b(r')} dz' \times \frac{1}{[(r - r')^2 + (z - z')^2]^{1/2}} \times \left[\left(1 + \frac{2}{m}\right)K(-m) - \frac{2}{m}E(-m)\right], \tag{A-20}$$

[1] Handbook of Mathematical Functions, M. Abramowitz and I. Stegun, eds. Dover Publications, ch 17.

where

$$m = \frac{4rr'}{(r - r')^2 + (z - z')^2}.$$

In the beam interior m is large. Using the asymptotic expansions for K and E one may show that

$$\left(1 + \frac{2}{m}\right)K(-m) - \frac{2}{m}E(-m) \sim \tfrac{1}{2}m^{-1/2}(\ln m + 4\ln 2 - 4). \tag{A-21}$$

Using Eq. (A-21) in Eq. (A-20) the resulting integrals are elementary. The result, for the vector potential inside the beam is

$$A_\theta{}^s = \frac{I}{c}\left[2\ln\left(\frac{8R_b}{e^2 r_b}\right) + 1 - \rho^2/r_b{}^2 + \frac{\rho}{R_b}\cos\phi\left(-\ln\frac{8R_b}{r_b} + 3\right)\right], \tag{A-22}$$

where $I = \pi r_b{}^2 J_\theta$, from which it follows that the fields inside the beam, to first order in ρ, are

$$B_r{}^s = \frac{2I}{c}\frac{\rho}{r_b{}^2}\sin\phi \tag{A-23}$$

$$B_z{}^s = \frac{I}{cr_b}\left[\frac{r_b}{R_b}\ln\frac{8R_b}{r_b} - 2\frac{\rho\cos\phi}{r_b}\right]. \tag{A-24}$$

We may summarize all of the foregoing results as follows:

The applied fields are,

$$B_r{}^a = -nB_{z0}\frac{\Delta z + \delta z}{r_0} \tag{A-25a}$$

$$B_\theta{}^a = B_{\theta 0} \tag{A-25b}$$

$$B_z{}^a = B_{z0}\left[1 - n\left(\frac{\Delta r + \delta r}{r_0}\right)\right] \tag{A-25c}$$

$$E_r{}^a = -\frac{1}{2c}\dot{B}_{00}(\Delta z + \delta z) \tag{A-25d}$$

$$E_\theta{}^a = E_{\theta 0} \tag{A-25e}$$

$$E_z{}^a = \frac{1}{2c}\dot{B}_{\theta 0}(\Delta r + \delta r) \tag{A-25f}$$

where B_{z0}, $B_{\theta 0}$, and $E_{\theta 0}$ are taken to be prescribed functions of time.

The self fields are

$$B_r{}^s = -2\pi n_0 e\beta_0\left(\delta z - \frac{r_b{}^2}{a^2}\Delta z\right) \tag{A-26a}$$

$$B_\theta{}^s = 0 \tag{A-26b}$$

$$B_z{}^s = 2\pi n_0 e\beta_0\left(\delta r + \frac{r_b{}^2}{a^2}\Delta r - \frac{r_b{}^2}{2r_0}l_B\right) \tag{A-26c}$$

$$E_r{}^s = -2\pi n_0 e\left(\delta r + \frac{r_b{}^2}{a^2}\Delta r + \frac{r_b{}^2}{2r_0}l_E\right) \tag{A-26d}$$

$$E_\theta{}^s = 0 \tag{A-26e}$$

$$E_z{}^s = -2\pi n_0 e\left(\delta z + \frac{r_b{}^2}{a^2}\Delta z\right) \tag{A-26f}$$

where

$$l_B = \begin{cases} \ln\dfrac{a}{r_b} + 2 \text{ if circulation frequency, } \dot{\theta}, \\ \quad \text{is constant across the beam} \\ \ln\dfrac{a}{r_b} + 1 \text{ if current density is constant} \\ \quad \text{across the beam} \end{cases} \tag{A-27}$$

$$l_E = \ln\frac{a}{r_b} \text{ if density is constant across the beam.} \tag{A-28}$$

For times long compared to the time it takes the magnetic field to diffuse through the chamber wall the result (A-24) shows that one must replace a in the logarithm in the definition of l_B by $(8\ r_0/e) \approx 2.9r_0$. This suggests that fields in an actual device may have to be programmed in time to compensate for this extra change (reduction) in B_z, in order to hold the beam in place.

APPENDIX B

Linearized Equations of Motion for a Particle in the Modified Betatron

In this appendix the equations of motion for a particle in the fields (A-25) and (A-26) are obtained, correct to first order in small quantities.

The complete equations of motion are

$$\frac{d}{dt}(\gamma\dot{r}) - \gamma r\dot{\theta}^2 = -\frac{e}{m}\left[E_r + \frac{1}{c}(r\dot{\theta}B_z - \dot{z}B_\theta)\right] \tag{B-1}$$

$$\frac{1}{r}\frac{d}{dt}(\gamma r^2\dot{\theta}) = -\frac{e}{m}\left[E_\theta + \frac{1}{c}(\dot{z}B_r - \dot{r}B_z)\right] \tag{B-2}$$

$$\frac{d}{dt}(\gamma\dot{z}) = -\frac{e}{m}\left[E_z + \frac{1}{c}(\dot{r}B_\theta - r\dot{\theta}B_r)\right]. \tag{B-3}$$

We consider first the linearization of Eq. (B-2). This equation has an exact first integral, assuming the fields do not depend on θ; it is the canonical angular momentum

$$P_\theta \equiv r\left[m\gamma r\dot{\theta} - \frac{e}{c}A_\theta\right]. \tag{B-4}$$

We now write all quantities Q as $Q = Q_0 + Q_1$ where $Q_1 \ll Q_0$ and Q_0 refers to quantities evaluated at the reference orbit $(r, z) = (r_0, 0)$. Defining $V_\theta = r\dot{\theta}$ it is straightforward to show from Eq. (B-4) using (A-14) for $(rA_\theta^s)_1$ that

$$V_{\theta 1} = \frac{P_{\theta 1}}{m\gamma_0^3 r_0} - \frac{r_1}{\gamma_0^2}\left[\dot{\theta}_0 - \frac{eB_{z0}^{(0)}}{m\gamma_0 c}\right] + \frac{\Delta r}{\gamma_0^2}\Omega_{z0}\frac{\nu}{\gamma_0}l_B, \tag{B-5}$$

where

$$B_{z0}^{(0)} = B_{z0} - \pi n_0 e\beta_0 \frac{r_b^2}{r_0} l_B$$

$$\frac{\nu}{\gamma_0} = \frac{1}{\gamma_0}\left(\pi r_b^2 n_0 \frac{e^2}{mc^2}\right) = \frac{1}{4}\frac{\omega_b^2 r_b^2}{c^2}$$

$$\omega_b^2 = 4\pi n_0 e^2/m\gamma_0$$

and where we have used $\gamma_1 = V_{\theta 0}\gamma_0^3 V_{\theta 1}/c^2$. Now, using the expression for $\dot{\theta}_0$ in Eq. (7), one obtains

$$V_{\theta 1} = \frac{P_{\theta 1}}{m\gamma_0^3 r_0} + \frac{r_1}{\gamma_0^2}\frac{\nu}{\gamma_0}\frac{1}{\alpha^2}\Omega_{z0}l_E + \frac{\Delta r}{\gamma_0^2}\Omega_{z0}\frac{\nu}{\gamma_0}l_B \tag{B-6}$$

where $\alpha = \Omega_{z0}r_0/c$.

The expression Eq. (B-6) will be needed next in the linearization of the radial equation, (B-1). Carrying out a straightforward linearization of Eq. (B-1), using the zero order fields from Eqs. (A-25b, c) and Eqs. (A-26c, d) gives

$$\ddot{r}_1 = -\frac{e}{m\gamma_0}\left[E_{r1} + \frac{V_{\theta 0}}{c}B_{z1}\right] + \Omega_{\theta 0}\dot{z}_1 - \frac{\dot{\gamma}_0}{\gamma_0}\dot{r}_1 - \dot{\theta}_0^2 r_1 + V_{\theta 1}\Omega_{z0}\gamma_0^2 \times\left[1 - \frac{\nu}{\gamma_0}\left(\frac{1+\gamma_0^{-2}}{\alpha^2}l_E + l_B\right)\right] \tag{B-7}$$

where

$$\Omega_{\theta 0} = eB_{\theta 0}/m\gamma_0 c.$$

Using now Eq. (B-6) and keeping terms only to first order in ν/γ_0 and using Eqs. (A-25c, d) and Eqs. (A-26c, d) to write

$$-\frac{e}{m\gamma_0}\left[E_{r1} + \frac{V_{\theta 0}}{c}B_{z1}\right] = \frac{e\dot{B}_{\theta 0}}{2m\gamma_0 c}z_1 + \frac{\omega_b^2}{2\gamma_0^2}\left(\delta r + \frac{r_b^2}{a^2}\Delta r\right) + n\dot{\theta}_0\Omega_{z0}r_1 \tag{B-8}$$

we obtain our final result for the radial equation:

$$\ddot{r}_1 + \frac{\dot{\gamma}_0}{\gamma_0}\dot{r}_1 + \Omega_{z0}^2\left[1 - n - \frac{\nu}{\gamma_0} \times\left((3-n)\frac{1}{\alpha^2}l_E + (2-n)l_B\right)\right]r_1$$

$$= \frac{e\dot{B}_{\theta 0}}{2m\gamma_0 c} z_1 + \Omega_{\theta 0}\dot{z}_1 + n_s\Omega_{z0}^2$$

$$\times \left(\delta r + \frac{r_b^2}{a^2}\Delta r\right) + \frac{\nu}{\gamma_0}\Omega_{z0}^2 l_B \Delta r \qquad \text{(B-9)}$$

$$+ \Omega_{z0}\frac{P_{\theta 1}}{\gamma_0 m r_0}\left[1 - \frac{\nu}{\gamma_0}\left(\frac{1+\gamma_0^{-2}}{\alpha^2} l_E + l_B\right)\right],$$

where $n_s \equiv \omega_b^2/2\gamma_0^2\Omega_{z0}^2$ is the "self field index."

The analogous linearization of the z equation [Eq. (B-3)] is completely straightforward, using the fields (A-25a, b, f) and (A-26a, b, f). The result is

$$\ddot{z}_1 + \frac{\dot{\gamma}_0}{\gamma_0}\dot{z}_1 + n\Omega_{z0}^2$$

$$\times \left[1 - \frac{\nu}{\gamma_0}\left(\frac{1}{\alpha^2} l_E + l_B\right)\right] z_1 \qquad \text{(B-10)}$$

$$= -\frac{e\dot{B}_{\theta 0}}{2m\gamma_0 c} r_1 - \Omega_{\theta 0}\dot{r}_1$$

$$+ n_s\Omega_{z0}^2\left(\delta r + \frac{r_b^2}{a^2}\Delta r\right).$$

APPENDIX C

WKB Solution of Equations of Motion

The linearized equations of motion are given in the text, Eqs. (11a, b). Below we shall obtain first, an approximate solution to the homogeneous version of Eqs. (11a, b), assuming that all coefficients are slowly varying. We will then give the solution to the full, inhomogeneous equations.

The homogeneous equations are

$$\ddot{x} + \omega_x^2 x = \Omega_{\theta 0}\dot{y} + \tfrac{1}{2}\dot{\Omega}_{\theta 0} y \qquad \text{(C-1a)}$$

$$\ddot{y} + \omega_y^2 y = -\Omega_{\theta 0}\dot{x} - \tfrac{1}{2}\dot{\Omega}_{\theta 0} x \qquad \text{(C-1b)}$$

All coefficients, ω_x^2, ω_y^2, and $\Omega_{\theta 0}$ will be assumed to vary significantly only over a slow time scale. To carry out a formal asymptotic expansion then we define

$$\tau = t/\lambda,$$

where λ is a large dimensionless parameter. Denoting $\frac{d}{d\tau}$ by a prime ($'$), Eqs. (C-1a, b) become

$$x'' + \lambda^2\omega_x^2 x = \lambda\Omega_{\theta 0} y' + \frac{\lambda}{2}\Omega_{\theta 0}' y \qquad \text{(C-2a)}$$

$$y'' + \lambda^2\omega_y^2 y = -\lambda\Omega_{\theta 0} x' - \frac{\lambda}{2}\Omega_{\theta 0}' x. \qquad \text{(C-2b)}$$

Now writing

$$x = a_1(\tau;\lambda)e^{i\lambda\int\omega(\tau')d\tau'} \qquad \text{(C-3a)}$$

$$y = a_2(\tau;\lambda)e^{i\lambda\int\omega(\tau')d\tau'} \qquad \text{(C-3b)}$$

we proceed to express a_1 and a_2 in formal asymptotic series

$$a_1(\tau;\lambda) \sim \sum_{n=0}^{\infty}\frac{a_{1n}(\tau)}{\lambda^n} \qquad \text{(C-4a)}$$

$$a_2(\tau;\lambda) \sim \sum_{n=0}^{\infty}\frac{a_{2n}(\tau)}{\lambda^n}. \qquad \text{(C-4b)}$$

We must now find the a_{1n}, a_{2n}, and ω.

Substituting Eqs. (C-4a, b) in Eqs. (C-2a, b) one finds the leading order (λ^2) result

$$(\omega_x^2 - \omega^2)a_{10} - i\omega\Omega_{\theta 0}a_{20} = 0 \qquad \text{(C-5a)}$$

$$i\omega\Omega_{\theta 0}a_{10} + (\omega_y^2 - \omega^2)a_{20} = 0 \qquad \text{(C-5b)}$$

from which it follows that ω must be one of the four quantities

$$\omega = \pm\left[\frac{\pm\langle(\omega_x^2 + \omega_y^2 + \Omega_{\theta 0}^2)^2 - 4\omega_x^2\omega_y^2\rangle^{1/2}}{2}\right]^{1/2} \qquad \text{(C-6)}$$

The next order (λ^1) relation may be written, after some manipulation, as

$$i\left[2\omega - \frac{\omega^2 - \omega_y^2}{\omega}\right]a_{20}'$$

$$+ i\left[\omega' - \frac{1}{2}\frac{\omega^2 - \omega_y^2}{\omega}\frac{\Omega_{\theta 0}'}{\Omega_{\theta 0}}\right]a_{20} \qquad \text{(C-7)}$$

$$= \left[-\Omega_{\theta 0} + \frac{2}{\Omega_{\theta 0}}(\omega^2 - \omega_y^2)\right]a_{10}'$$

$$+ \left[-\frac{1}{2}\Omega_{\theta 0}' + \frac{\omega'}{\omega}\frac{(\omega^2 - \omega_y^2)}{\Omega_{\theta 0}}\right]a_{10}.$$

Using Eq. (C-5a) or Eq. (C-5b) and Eq. (C-7) an equation for just a_{10} (or just a_{20}) may be obtained. The solutions are

$$a_{10} = A\omega^{-1/2}(\omega_y^2 - \omega^2)^{1/2} (\omega_x^2 + \omega_y^2 + \Omega_{\theta 0}^2 - 2\omega^2)^{-1/2} \quad \text{(C-8a)}$$

$$a_{20} = A\omega^{-1/2}(\omega^2 - \omega_x^2)^{1/2} (\omega_x^2 + \omega_y^2 + \Omega_{\theta 0}^2 - 2\omega^2)^{-1/2} \quad \text{(C-8b)}$$

where A is an arbitrary complex constant.

Using Eq. (C-8a, b) and the definition of ω we may write the leading order WKB solution to Eqs. (C-1a, b) as

$$\begin{pmatrix} x \\ y \end{pmatrix} \sim [(\omega_x^2 + \omega_y^2 + \Omega_{\theta 0}^2)^2 - 4\omega_x^2\omega_y^2]^{-1/4} \times \sum_{j=1}^{4} \frac{A_j}{\omega_j^{1/2}} \begin{pmatrix} (\omega_y^2 - \omega_j^2)^{1/2} \\ (\omega_j^2 - \omega_x^2)^{1/2} \end{pmatrix} e^{i\int \omega_j dt}, \quad \text{(C-9)}$$

where the sum extends over the four values of ω in Eq. (C-6) and where the A_j are constants.

This solution is expected to be valid as long as ω_x, ω_y, and $\Omega_{\theta 0}$ are slowly varying compared to any ω_j, i.e.,

$$\left| \frac{\bar{d}}{dt} \ln \bar{\omega} \right| \ll |\omega_j|, \quad j = 1, 2, 3, 4,$$

where $\bar{\omega}$ is ω_x, ω_y, or $\Omega_{\theta 0}$. The solution is therefore expected to fail when $\omega_j \approx 0$, that is, near a turning point. From Eq. (C-6) this can happen when

$$\omega_x^2\omega_y^2 = 0. \quad \text{(C-10)}$$

Equation (C-9) is bounded, however, if in addition $\omega_x^2 = \omega_y^2 = 0$. Breakdown of Eq. (C-9) (and a transition to unstable behavior) occurs only if $\omega_x^2\omega_y^2 = 0$ and $\omega_x^2 \neq \omega_y^2$.

Once the solution to the homogeneous equations have been found the solution to the inhomogeneous equations follows by the usual variation of parameters or some similar method. Writing four independent solutions to the homogeneous equations as

$$\begin{pmatrix} x^{(j)} \\ y^{(j)} \end{pmatrix} j = 1, 2, 3, 4 \quad \text{(C-11)}$$

one finds in a straightforward way that a particular solution to Eqs. (11a, b) in the text is given by

$$\begin{pmatrix} x \\ y \end{pmatrix} = \int^t dt' \begin{pmatrix} K_x(t, t') \\ K_y(t, t') \end{pmatrix} F(t'), \quad \text{(C-12)}$$

where

$$K_x(t, t') = -\frac{1}{W} \epsilon_{jklm} x^{(j)}(t) x^{(k)}(t') y^{(l)}(t') \dot{y}^{(m)}(t')$$

$$K_y(t, t') = -\frac{1}{W} \epsilon_{jklm} y^{(j)}(t) x^{(k)}(t') y^{(l)}(t') \dot{y}^{(m)}(t')$$

$$W = \epsilon_{jklm} x^{(j)}(t) \dot{x}^{(k)}(t) y^{(l)}(t) \dot{y}^{(m)}(t),$$

and where the summation convention is understood. The Wronskian W is a constant, independent of time; its value is determined once a choice is made for the $x^{(j)}$, $y^{(j)}$.

REFERENCES

1. P. Sprangle and C. A. Kapetanakos, J. Appl. Phys. 49, 1 (1978).
2. N. Rostoker, Bull. APS, 25, B54 (1980). N. Rostoker, Comments on Plasma Physics 6, 91 (1980).
3. J. D. Lawson, private communication.
4. W. Walkinshaw and K. Wyllie, "The Effect of an Orbital Magnetic Field on Betatron Output," TRE (Malvern) Maths Group Memo 58/WW (1948) (Unpublished).
5. P. Sprangle, C. A. Kapetanakos, and S. J. Marsh in "Proceedings of the Fourth International Topical Conference on High Power Electron and Ion Beam Research and Technology," Palaiseau, France (1981).
6. D. Kerst, Handbuch der Physik, XLIV, 13 (1959).
7. P. Sprangle and J. L. Vomvoridis, NRL Memorandum Report 4688 (to be published).
8. D. Chernin and P. Sprangle, to be published in Particle Accelerators.
9. J. D. Lawson, Phys. Lett 29A, 344 (1969).
10. R. C. Davidson and J. D. Lawson, Particle Accelerators 4, 1 (1972).
11. N. Rostoker, Particle Accelerators, 5, 93 (1973).
12. R. C. Davidson, "Theory of Nonneutral Plasmas," (Benjamin, Reading Mass., 1974) Section 3.5.
13. A similar result has been obtained by N. Rostoker for the case $n = \frac{1}{4}$. (G. Barak, et al. IEEE Trans. Nucl. Sci. NS-28, 3340 (1981).)

APPENDIX B

Equilibrium of a High-Current Electron Ring in a Modified-Betatron Accelerator

Equilibrium of a high-current electron ring in a modified-betatron accelerator

C. A. Kapetanakos, P. Sprangle, D. P. Chernin,[a] S. J. Marsh,[b] and I. Haber
Naval Research Laboratory, Washington, D.C. 20375

(Received 17 September 1982; accepted 10 February 1983)

The dynamics of an ultrahigh-current electron ring in a modified-betatron configuration is addressed. This study includes analytical and numerical results for both "cold" and "hot" rings. It has been found that the walls surrounding the ring and toroidal effects play a very important role in the dynamics of the ring, even when the wall conductivity is infinite. For finite wall conductivity, the diffusion of the ring's self-magnetic field profoundly impacts its dynamics and in general the equilibrium could be lost if means are not provided to compensate for this effect. In addition, it has been found that the toroidal-field grad B drift is not important, except when the bounce frequency is very small. The general conclusion of these studies is that equilibrium states of ultrahigh-current rings in modified-betatron configuration exist over a wide range of parameters. These states are accessible and within the reach of existing pulsed power technology.

I. INTRODUCTION

Over the last few years, several laboratories[1-7] have been engaged in studies that are intended to assess the feasibility of developing ultrahigh-current accelerators. These studies are mainly motivated by the potential application of high-energy, high-current electron beams in nuclear physics research, medical radiography, and the fusion program.

In general, the effort is not directed toward developing novel accelerating schemes but rather toward modifying or improving the existing accelerator technology. Among the various proposed modifications, the addition of a strong toroidal magnetic field to a conventional betatron[8,9] has attracted considerable attention,[4-7] and the configuration has been named the modified betatron.

In this paper we analyze and discuss the dynamics of a high-current electron ring confined in a modified-betatron configuration. When the intense electron ring is surrounded by a finite conductivity wall, its dynamics can be divided, rather naturally, into three distinct phases: The pre-acceleration phase follows the injection and trapping of the electron beam. The duration of this phase is short, typically a few microseconds and the conducting wall surrounding the ring can be treated as a perfect conductor. The pre-acceleration phase is followed by the diffusion phase, which lasts for a time that is of the order of the magnetic field diffusion time. During the diffusion phase the self-magnetic field of the beam diffuses out of the metal torus. As a result the electron energy is reduced and the net radial force on the ring increases, but at a different rate. Therefore, the equilibrium will be lost if means are not provided to balance these two effects. The last phase, i.e., the main acceleration, starts after the self-magnetic field diffuses out of the torus and has a duration that is comparable with the acceleration time. For most of the third phase the energy of the ring has increased substantially and thus the effect of the self-fields is appreciably diminished.

The present work addresses the dynamics of the high-current ring in a modified-betatron configuration. It includes both analytical and computational studies for "cold" as well as "hot" electron rings. The main conclusions are: First, if the energy of the injected electrons is not exactly equal to the energy corresponding to the equilibrium orbit, which is assumed to coincide with the minor axis of the torus, the center of the orbit is displaced from the center of the minor cross section of the torus. The displacement is proportional to the energy mismatch. This imposes very stringent constraints on the injector. Second, during the diffusion of the self-magnetic field of the ring out of the chamber, the equilibrium can be lost if means are not provided to balance the change of the ring equilibrium radius. This change is due to the reduction of the relativistic factor γ_0 and the increased forces acting on the center of the ring. Third, the modification in the flux rule for high-current rings can be ignored, provided that ν/γ_0^3 (ν = Budker parameter) is very small. Fourth, with the exception of the expansion of the minor cross section of the ring, finite emittance does not have any other noticeable effect on the equilibrium, and fifth, considerably higher axial energy spread can be tolerated in high- than in low-current rings.

The general and most important conclusion of these studies is that equilibrium states of high-current rings in a modified-betatron configuration exist over a wide range of parameters. These equilibria are realistic and accessible with existing technology.

II. ORBIT STABILITY OF A COLD RING WITHOUT SURROUNDING WALLS AND TOROIDAL CORRECTIONS

The stability of a single particle orbit, when thermal effects, wall effects, and toroidal corrections are neglected, has been considered previously.[4] Using the coordinate system shown in Fig. 1 and assuming that the external-field components vary as

$$B_z(r,t) \simeq B_{0z}(t)[1 - n(r - r_0)/r_0], \qquad (1a)$$

[a] Permanent address: Berkeley Research Associates, Springfield, Virginia 22150.
[b] Permanent address: Sachs/Freeman Associates, Bowie, Maryland 20715.

 0031-9171/83/061634-15$01.90

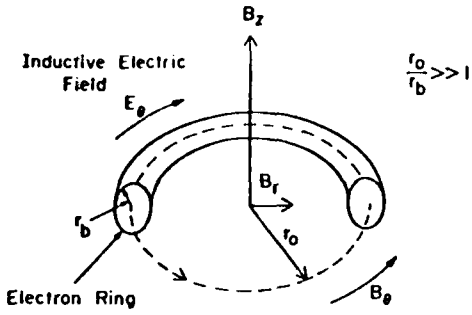

FIG. 1. Schematic of the modified-betatron configuration and system of coordinates used in the analysis.

$$B_r(r,t) \cong -B_{0z}(t)nz/r_0, \tag{1b}$$

$$E_\theta(r,t) = -\frac{1}{rc}\int_0^r r'\,dr'\,\frac{\partial B_z}{\partial t}(r',t), \tag{1c}$$

and

$$B_\theta(r) \cong B_{0\theta}[1-(r-r_0)/r_0], \tag{1d}$$

it has been determined that for $B_\theta \gg B_z$ and $\nu/\gamma_0 \ll 1$ the orbits are stable, provided that the following condition is satisfied:

$$n_s < (B_{0\theta}/2B_{0z})^2. \tag{2}$$

In the above equations $B_z(r,t)$ is the axial and $B_r(r,t)$ is the radial component of the betatron field, $B_\theta(r)$ is the toroidal magnetic field, $E_\theta(r,t)$ is the induced electric field, n is the external-field index, $(r_0,0)$ are the coordinates of the center of the electron ring, and n_s is the self-field index. The self-field index is defined as

$$n_s = \omega_b^2/(2\gamma_0\Omega_{0z}^2) = 2(\nu/\gamma_0)(c/\Omega_{0z}r_b)^2, \tag{3}$$

where $\omega_b^2 (= 4\pi e^2 n_0/m)$ is the beam plasma frequency squared, γ_0 is the relativistic factor, $\Omega_{0z} (= eB_{0z}/mc)$ is the cyclotron frequency corresponding to the axial component of the betatron field, r_b is the minor radius of the beam, and ν is Budker's parameter, i.e., the product of the number of electrons per unit length times the electron classical radius.

The electron-beam current that can be stably confined in a modified betatron can be obtained by substituting Eq. (3) into Eq. (2) and is

$$I_{mb} < 2.1(r_b/r_0)^2\gamma_0^3\beta_0^3(B_{0\theta}/B_{0z})^2 \ \text{(kA)} \tag{4}$$

where $\beta_0 = v_0/c$. If $\gamma_0 \gg 1$, then $r_0\Omega_{0z}/\gamma_0 \approx c$ and Eq. (4) becomes

$$I_{mb} < 7.22\times 10^{-7}\, r_b^2\gamma_0 B_{0\theta}^2 \ \text{(kA)},$$

with r_b in cm and $B_{0\theta}$ in G.

In addition, it has been shown under the same conditions, but with $B_\theta = 0$ (conventional betatron), the beam is stable provided

$$n_s < \tfrac{1}{2}, \quad \text{conventional betatron } (B_\theta = 0). \tag{5}$$

The electron-beam current that can be stably confined in a conventional betatron can be obtained by substituting Eq. (3) into Eq. (5) and is

$$I_{cb} < 4.2(r_b/r_0)^2\gamma_0^3\beta_0^3 \ \text{(kA)}, \tag{6}$$

or

$$I_{cb} < 14.44\times 10^{-7}\, r_b^2\gamma_0 B_{0z}^2 \ \text{(kA)},$$

when $\gamma_0 \gg 1$. The ratio of I_{mb} to I_{cb} obtained from Eqs. (4) and (6) is

$$I_{mb}/I_{cb} = \tfrac{1}{2}(B_{0\theta}/B_{0z})^2.$$

The above relation indicates that for $B_{0\theta} \gg B_{0z}$, the electron-beam current that can be stably confined in a modified betatron substantially exceeds the current that can be confined in a conventional betatron.

The modified-betatron stability condition given in Eq. (2) can be easily obtained from the well-known confined equilibrium condition[10]

$$2(\omega_b^2/\Omega_c^2) < 1 \quad \text{(nonrelativistic)}, \tag{7}$$

where ω_b is the beam plasma frequency and Ω_c is the cyclotron frequency. For relativistic energies, and taking into account the self-magnetic field of the beam, ω_b^2 becomes

$$\omega_b^2 \rightarrow (\omega_b^2/\gamma_0)(1/\gamma_0^2), \tag{8}$$

where $(1/\gamma_0^2)$ accounts for the self-magnetic field of the beam, and

$$\Omega_c^2 \rightarrow \Omega_\theta^2/\gamma_0^2. \tag{9}$$

Substituting Eqs. (8) and (9) into Eq. (7) we obtain the stability condition of Eq. (2). The equality sign in Eq. (2) gives the maximum electron density that can be supported at a specific value of $B_{0\theta}/B_{0z}$ and the corresponding equilibrium is known as Brillouin flow.[10]

III. WALL EFFECTS ON THE MACROSCOPIC MOTION OF A COLD BEAM

In this section we analyze the effects of surrounding walls on the motion of the center of the beam. In the Sec. IIIA, it is assumed that the perfect conductor that surrounds the beam is a straight cyclindrical pipe of circular cross section and thus toroidal effects (hoop forces) associated with the fields are omitted. These forces act to expand the ring and are reduced with increasing ring major radius. The toroidal effects are discussed in Sec. IIIB.

A. Without toroidal corrections

Consider a pencil-like electron beam inside a straight, perfectly conducting cylindrical pipe of circular cross section as shown in Fig. 2. The center of the beam is located at a

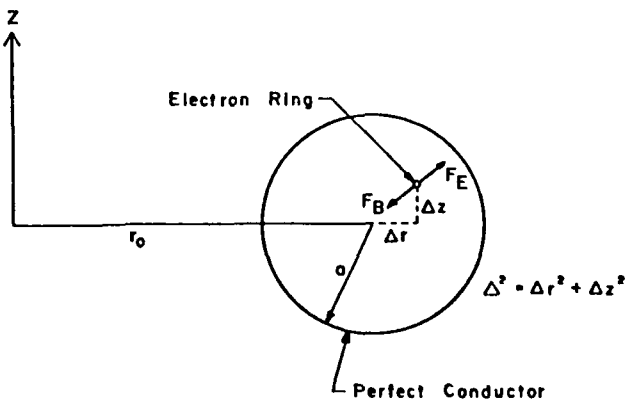

FIG. 2. Wall (images) forces acting on a pencil-like electron beam, situated inside a perfectly conducting cylindrical pipe.

distance Δr, Δz from the center of the minor cross section of the pipe. As a result of the induced charges on the wall, the center of the beam will experience a radial, outward-directed force, which for small displacements, i.e., Δr, $\Delta z \ll a$ is given by

$$\mathbf{F}_E = 2\pi e^2 n_0 (r_b/a)^2 (\Delta r \hat{e}_r + \Delta z \hat{e}_z), \tag{10}$$

where a is the cylinder radius and n_0 the uniform beam density.

Similarly, as a result of the induced current on the wall, the center of the beam will experience a radial force that is directed toward the opposite direction than $\mathbf{F}_E$ and is given by

$$\mathbf{F}_B = -\beta_0^2 \mathbf{F}_E. \tag{11}$$

Using the external fields of Eq. (1) and the induced fields of Eqs. (10) and (11), the equations describing the temporal linear evolution of the beam's center, for time-independent applied fields, are

$$\Delta\ddot{r} + \tilde{\omega}_r^2 \Delta r = \frac{\Omega_{0\theta}}{\gamma_0} \Delta\dot{z} + \left(\frac{\Omega_{0z}}{\gamma_0}\right) \frac{\langle \delta P_\theta \rangle}{\gamma_0 m r_0}, \tag{12}$$

and

$$\Delta\ddot{z} + \tilde{\omega}_z^2 \Delta z = -(\Omega_{0\theta}/\gamma_0)\Delta\dot{r}, \tag{13}$$

where

$$\tilde{\omega}_r^2 = (\Omega_{0z}/\gamma_0)^2 (1 - n - n_s r_b^2/a^2),$$
$$\tilde{\omega}_z^2 = (\Omega_{0z}/\gamma_0)^2 (n - n_s r_b^2/a^2),$$
$$\Omega_{0\theta} = eB_{0\theta}/mc, \quad \Omega_{0z} = eB_{0z}/mc,$$
$$\delta\gamma_0/\gamma_0 = \beta_0 \langle \delta P_\theta \rangle / \gamma_0 m r_0 c,$$

and δP_θ is the difference between the canonical angular momentum of an electron at (r,z) and its corresponding value at the equilibrium orbit $(r_0,0)$. The average is over initial coordinates and velocities. Equations (12) and (13) do not include the self-electric and self-magnetic fields, because both these fields are zero at the center of a straight beam. In addition, the nonlinear terms $(\Delta r/r_0)(\Omega_{0\theta}/\gamma_0)\Delta\dot{z}$ and $(\Delta r/r_0)(\Omega_{0\theta}/\gamma_0)\Delta\dot{r}$ have been omitted from Eqs. (12) and (13). These two terms have their origin in the gradient of the toroidal magnetic field and are considered in Sec. V. In general these terms are not significant except in the limit $\tilde{\omega}_r \to 0$.

In Eq. (12), $\delta\gamma_0 = \beta_0 \langle \delta P_\theta \rangle / m r_0 c$ indicates the energy mismatch, i.e., the difference between the energy of the reference electron (moving along the axis of the beam) and the energy required for the same electron to move on the equilibrium orbit $(r_0,0)$. The solution of Eqs. (12) and (13), for time-independent fields, is

$$\Delta r = \frac{\Omega_{0z} \langle \delta P_\theta \rangle}{\gamma_0^2 \tilde{\omega}_r^2 r_0 m} + \sum_{j=1}^{4} c_j (\tilde{\omega}_z^2 - \omega_j^2)^{1/2} e^{i\omega_j t}, \tag{14}$$

and

$$\Delta z = \sum_{j=1}^{4} c_j (\omega_j^2 - \tilde{\omega}_r^2)^{1/2} e^{i\omega_j t}, \tag{15}$$

where c_j is a constant and

$$\omega_j^2 = \tfrac{1}{2}\{\tilde{\omega}_r^2 + \tilde{\omega}_z^2 + (\Omega_{0\theta}/\gamma_0)^2 \pm \{[\tilde{\omega}_r^2 + \tilde{\omega}_z^2 + (\Omega_{0\theta}/\gamma_0)^2]^2 - 4\tilde{\omega}_r^2 \tilde{\omega}_z^2\}^{1/2}\}. \tag{16}$$

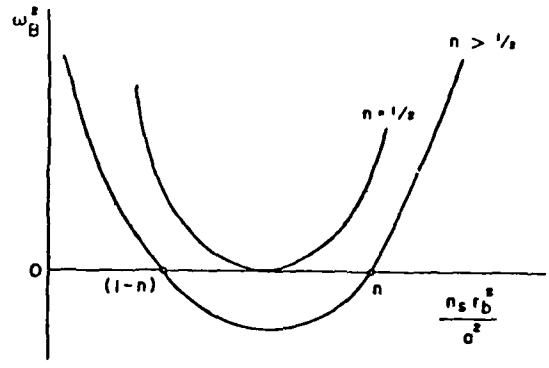

FIG. 3. Bounce frequency squared as a function of $n_s r_b^2/a^2$, with the field index n as a parameter. The orbits are open when $\omega_B^2 < 0$ and closed when $\omega_B^2 > 0$.

The first term on the right-hand side (RHS) of Eq. (14) gives the displacement of the center of the orbit from the center of the surrounding cylindrical pipe and can be written as

$$\Delta r_0 = \frac{\langle \delta P_\theta \rangle / \gamma_0}{(\Omega_{0z}/\gamma_0)(1 - n - n_s r_b^2/a^2) m r_0}. \tag{17}$$

Equation (16) has four roots. Two of them are fast (plus sign) and two are slow (minus sign). When $B_\theta \gg B_z$, the slow modes become

$$\omega_j^2 = \omega_B^2 = \left(\frac{\tilde{\omega}_r \tilde{\omega}_z}{\Omega_{0\theta}/\gamma_0}\right)^2 = \left(\frac{B_{0z}}{B_{0\theta}}\right)^2 \left(\frac{\Omega_{0z}}{\gamma_0}\right)^2 \left(1 - n - n_s \frac{r_b^2}{a^2}\right)\left(n - n_s \frac{r_b^2}{a^2}\right), \tag{18}$$

and the fast modes are $\approx \pm(\Omega_{0\theta}/\gamma_0)$. Equation (18) is plotted in Fig. 3 for two values of the external-field index. For $n > \frac{1}{2}$, ω_B^2 is negative when $1 - n < n_s r_b^2/a^2 < n$ and for $n < \frac{1}{2}$, ω_B^2 is negative when $n < n_s r_b^2/a^2 < 1 - n$. Negative values of ω_B^2 indicate that the beam motion is unstable and the orbit in the r,z plane is open. Since the parameter $n_s r_b^2/a^2$ scale as γ_0^{-3}, during acceleration $n_s r_b^2/a^2$ decreases rapidly. Therefore, in order to avoid the instability, it is necessary that before the commencement of the acceleration the parameter $n_s r_b^2/a^2 < 1 - n$ when $n > \frac{1}{2}$ and $< n$ when $n < \frac{1}{2}$. This implies that the injected beam current should be limited to

$$I < 8.5(1 - n)\beta_0^2 \gamma_0^3 a^2/r_0^2 \ \text{(kA)} \quad \text{for } n > \tfrac{1}{2},$$

and

$$I < 8.5 n \beta_0^2 \gamma_0^3 a^2/r_0^2 \ \text{(kA)} \quad \text{for } n < \tfrac{1}{2}.$$

The orbit of the ring's center is described by

$$\Delta r(t) = [\Delta r(0) - \Delta r_0] \cos \omega_B t + [\Delta\dot{r}(0)/\omega_B] \sin \omega_B t + \Delta r_0,$$
$$\Delta z(t) = \Delta z(0) \cos(\omega_B t) + [\Delta\dot{z}(0)/\omega_B] \sin(\omega_B t),$$

where the initial velocities and displacements are related by

$$\Delta\dot{r}(0) = -[\tilde{\omega}_z^2/(\Omega_{0\theta}/\gamma_0)]\Delta z(0),$$
$$\Delta\dot{z}(0) = \frac{\tilde{\omega}_r^2}{(\Omega_{0\theta}/\gamma_0)} \Delta r(0) - \left(\frac{\Omega_{0z}}{\Omega_{0\theta}}\right) \frac{\langle \delta P_\theta \rangle}{\gamma_0 m r_0} = \frac{\tilde{\omega}_r^2}{(\Omega_{0\theta}/\gamma_0)} [\Delta r(0) - \Delta r_0],$$

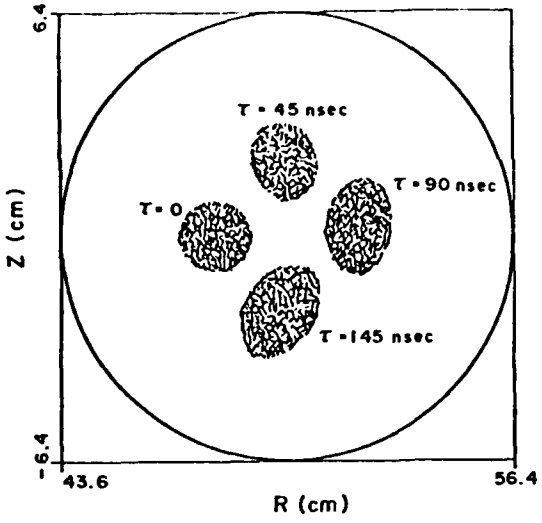

FIG. 4. Snapshots of the electron-ring minor cross section at four different times. The values of the various parameters are listed in Table I. The center of the ring's minor cross section describes a circle.

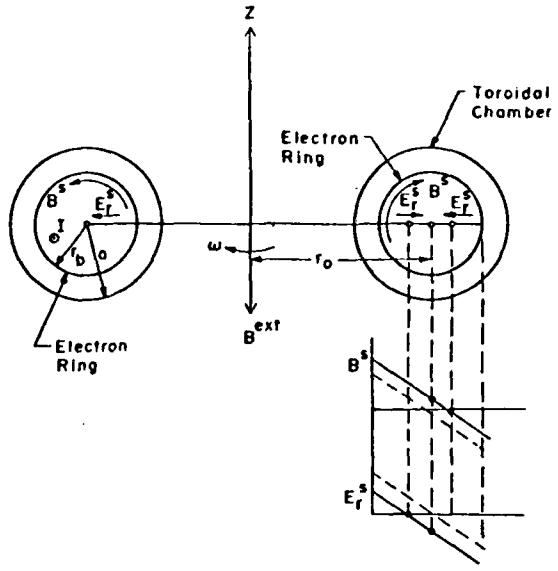

FIG. 5. An electron ring inside a conducting toroidal chamber. Because of the toroidal effects, neither the self-electric nor the self-magnetic field is zero at the geometric center of the ring.

and

$$\langle \delta P_\theta \rangle = \gamma_0 m r_0 (v_\theta - r_0 \Omega_{0z}/\gamma_0).$$

The predictions of Eq. (18) are in good agreement with the results of computer simulation shown in Fig. 4. This figure shows four snapshots of the beam in the r,z plane. At $t = 0$ the circular electron beam is injected near the center of the pipe. The values of the various parameters are listed in Table I. The electron-beam current is kept low (1 kA) in order to minimize the toroidal effects. As can be seen from Fig. 4, the center of the electron beam describes a circle in the r,z plane with a period of about 188 nsec. For the same parameters Eq. (18) predicts a period $\tau_B = 2\pi/\omega_B \simeq 180$ nsec. These numerical results are discussed further in the Sec. IIIB.

The displacement of the orbit's center because of the energy mismatch [Eq. (17)], imposes very stringent constraints on the injector. This becomes apparent when we consider some limiting cases. For example, when $n = \frac{1}{2}$ and $n_s r_b^2/a^2 \ll 1$, Eq. (17) is reduced to

$$\Delta r_0/r_0 \simeq 2(\delta\gamma_0/\gamma_0). \tag{19}$$

Equation (19) predicts that for a major radius $r_0 = 100$ cm, the ratio $\delta\gamma_0/\gamma_0$ should be less than 1% in order that the displacement of the orbit will be less than 2 cm. The condition $\delta\gamma_0/\gamma_0 < 1\%$ requires that the uncertainty in energy should be less than 35 keV, when the energy of the injected beam is 3 MeV. Although such a small energy uncertainty can be attained with sophisticated injectors, there are other factors, such as space charge and inductive effects, which contribute substantially to the uncertainty of energy. Although the displacement cannot be eliminated, its negative impact can be alleviated by elongating the minor cross section of the torus along the r direction.

TABLE I. Electron-ring parameters for the results of Fig. 4.

Beam energy (MeV)	3
Beam current (kA)	1
Beam minor radius (cm)	1
Beam major radius (cm)	50
Torus minor radius (cm)	6.4
Vertical magnetic field (G)	240
Toroidal magnetic field (kG)	2
External-field index	0.47
Self-field index	0.88

B. Toroidal corrections[5,11]

The cause of these effects is the finite curvature of the electron-beam orbit. For relatively large aspect ratio ($r_0/r_b \gg 1$) beams, the toroidal effects become important when v/γ_0 exceeds a few percent. Previous work[12] on toroidal effects was limited to "bare" rings, i.e., without surrounding conducting walls. In this subsection we briefly analyze the toroidal corrections for the more realistic geometry shown in Fig. 5, i.e., including the effect of conducting wall around the beam. Since different physics issues are involved in the case of a "bare" and a "shielded" ring, it is appropriate to start our discussion with a bare ring.

Consider an intense electron ring as shown in Fig. 5, but without the toroidal chamber. At the inner edge of the RHS cross section of the ring the self-magnetic field is greater than that of a straight beam with the same parameters, because of the contribution from the left-hand side (LHS) of the ring. At the outer edge of the cross section, the self-magnetic field is reduced because the contribution from the LHS of the ring has different polarity than the local field. Thus, the total self-magnetic field is shifted upwards, as shown schematically in Fig. 5. In contrast, the self-electric field decreases at the inner radius and its magnitude increases at the outer radius of the ring. Thus the self-electric field shifts downwards. As a result of these shifts neither the magnetic nor the electric field are zero at the geometric center of the ring.

When the electron ring is surrounded by a perfect conductor, the shift in the fields discussed above is reduced but

additional field components appear as a result of induced charge and current on the conducting wall. For small ring displacements from the center of the minor cross section of the torus, the induced fields vary linearly with the displacement and are identical to those given in Eqs. (10) and (11), for a cylindrical pipe. Quantitative extension of the previous qualitative considerations has shown that the fields at the center of a uniform-density electron ring inside a perfectly conducting toroidal chamber of circular cross section are[5,11]

$$\mathbf{E}_{\rm ind} = -2\pi|e|n_0 r_0\left\{\left[\frac{r_b^2}{a^2}\frac{\Delta r}{r_0} + \frac{1}{2}\frac{r_b^2}{r_0^2}\ln\left(\frac{a}{r_b}\right)\right]\hat{e}_r + \frac{r_b^2}{a^2}\frac{\Delta z}{r_0}\hat{e}_z\right\}, \tag{20}$$

and

$$\mathbf{B}_{\rm ind} = -2\pi|e|n_0\beta_0 r_0\left\{\frac{r_b^2}{a^2}\frac{\Delta z}{r_0}\hat{e}_r - \left[\frac{r_b^2}{a^2}\frac{\Delta r}{r_0} - \frac{r_b^2}{r_0^2}\left(1+\frac{1}{2}\ln\frac{a}{r_b}\right)\right]\hat{e}_z\right\}, \tag{21}$$

where n_0 is the ambient density, $\beta_0 = v_0/c$, v_0 is the azimuthal velocity defined by

$$v_0 = \frac{r_0\Omega_{0z}/\gamma_0}{1+2(\nu/\gamma_0)[1+\ln(a/r_b)]}, \tag{22}$$

and the displacement $\Delta r, \Delta z$ of the ring from the center of the torus has been assumed to be much less than a. In addition, the fields given by Eqs. (20) and (21) have been derived under the assumption that the angular frequency of the electrons is constant and therefore the electron current density varies proportionally to r.

Using Eqs. (20)–(22), it can be shown that the center of the beam is described by Eqs. (12) and (13) with $\tilde{\omega}_r^2$ and $\tilde{\omega}_z^2$ replaced by

$$\tilde{\omega}_r^2 \to (\Omega_{0z}^2/\gamma_0^2)(\alpha - n^* - n_s r_b^2/a^2), \tag{23}$$

$$\tilde{\omega}_z^2 \to (\Omega_{0z}^2/\gamma_0^2)(n^* - n_s r_b^2/a^2), \tag{24}$$

and

$$\delta P_\theta \to \xi\delta P_\theta,$$

where

$$\alpha = \xi^2 = \{1+(2\nu/\gamma_0)[1+\ln(a/r_b)]\}^{-2}, \tag{25}$$

and

$$n^* = n\xi.$$

The bounce frequency can be found by substituting Eqs. (23) and (24) into Eq. (18) and is

$$\omega_B^2 = \left(\frac{B_{0z}}{B_{0\theta}}\right)^2\left(\frac{\Omega_{0z}}{\gamma_0}\right)^2\left(\alpha - n^* - \frac{n_s r_b^2}{a^2}\right)\left(n^* - n_s\frac{r_b^2}{a^2}\right). \tag{26}$$

When $n^* = \alpha/2$, for the reasons stated in the paragraphs following Eq. (18), the orbits are closed (stable) as γ_0 increases, provided

$$n_s r_b^2/a^2 < \alpha/2$$

or,

$$I \lesssim 4.25\left(\frac{a}{r_0}\right)^2\left(1 - \frac{\nu}{\gamma_0}\ln\frac{a}{r_b}\right)\gamma_0^3 \ \text{(kA)} \quad \text{for } \gamma_0 \gg 1. \tag{27}$$

The limiting current given by Eq. (27) is considerably lower than that of Eq. (4) when $B_{0\theta} \gg B_{0z}$. In addition, in contrast to the current given by Eq. (4), the current of Eq. (27) is independent of the toroidal magnetic field $B_{0\theta}$. Toroidal effects shift the curves of Fig. 3 to the left and the critical current given by Eq. (27) is lower than the corresponding critical current when toroidal effects are omitted.

At this point, it is appropriate to return and discuss further the computer simulation results of Fig. 4. For the 1 kA, 3 MeV beam the $\nu/\gamma_0 = 0.0084$. Even at this small value of ν/γ_0 toroidal effects are noticeable. The value of ξ computed from Eq. (25) using the above value of ν/γ_0 and 6.4 for the ratio a/r_b is 0.95. According to Eqs. (23) and (24) the center of the beam will describe a circle when $\alpha - n^* = n^*$ or for $n = \frac{1}{2}[1-(\nu/\gamma_0)\ln(a/r_b)]\xi = 0.467$, which is in excellent agreement with the simulation. In addition, Eq. (26) predicts a period of 188 nsec, which also is in excellent agreement with the simulation.

The most striking manifestation of toroidal effects is in the value of the betatron magnetic field required to confine the rotating beam at a specific radius. When the axis of the beam lies along the axis of the torus, i.e., when $\Delta r = \Delta z = 0$, it can be shown from Eqs. (20) and (21) that the external magnetic field required for the beam to rotate with a radius r_0 is

$$B_{0z} = B_0\{1+(2\nu/\gamma_0)[1+\ln(a/r_b)]\},$$

where B_0 is the magnetic field necessary for a single particle of the same energy to rotate with a radius r_0.

The above expression for the magnetic field is based on the assumption that all the electrons rotate with a constant angular frequency, i.e., the current density increases linearly across the beam. If the current density is constant across the beam, the above expression is slightly modified and becomes

$$B_{0z} = B_0\{1+(2\nu/\gamma_0)[0.5+\ln(a/r_b)]\}.$$

For a 10 kA, 2 MeV uniform current density beam with a ratio $a/r_b = 6.4$, the correction is 55%, i.e., $B_{0z}/B_0 = 1.55$. This effect is demonstrated clearly by the results of computer simulation shown in Fig. 6. The three snapshots of the electron-ring minor cross section in a modified-betatron field correspond to $t \approx 0$, 20, and 40 nsec. For all practical purposes, the minor radius of the beam remains constant. The external betatron magnetic field is 127 G, i.e., approxi-

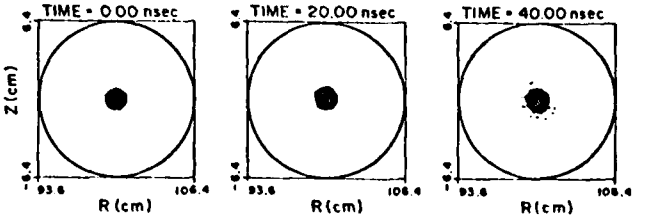

FIG. 6. Three snapshots of the electron-ring minor cross section in a modified-betatron field. The external magnetic field required to confine the ring is 50% higher than the single-particle field. The values of the various parameters in this run are listed in Table II.

TABLE II. Parameters of the uniform current density ring for the results shown in Fig. 6.

Beam energy (MeV)	2
Beam current (kA)	10
Beam minor radius (cm)	1
Beam major radius (cm)	100
Torus minor radius (cm)	6.4
Vertical magnetic field (G)	127
Toroidal magnetic field (kG)	1.7
External-field index	0.25

mately 50% higher than the single particle field. The remaining parameters are summarized in Table II.

Another consequence of the toroidal effects is the increase in the radial displacement of the orbit for fixed energy mismatch and major radius. For $n_s r_b^2/a^2 \ll 1$, the orbit displacement becomes

$$\Delta r_0/r_0 \approx \gamma_0[\delta\gamma_0/(\gamma_0^2-1)]/(1-n/\xi).$$

In addition, the ω_β^2 vs $n_s r_b^2/a^2$ curves of Fig. 3 are shifted to the left and thus the maximum permissible current that can be accelerated is reduced, as may be seen from Eq. (27).

IV. ACCELERATION

After injection and trapping the beam is accelerated to high energy by the inductive electric field generated by the time varying betatron magnetic field. As shown in Fig. 7, the acceleration may be divided into three phases:(1) pre-acceleration, (2) diffusion, and (3) main acceleration.

The pre-acceleration phase occurs for times much shorter than the field-diffusion time, i.e., $t \ll t_D = (4\pi/c^2)\sigma\delta a \ln(r_0/a)$, where σ is the conductivity, δ is the thickness, a is the minor radius, and r_0 is the major radius of the torus. During the pre-acceleration phase the self-magnetic field of the beam does not have time to diffuse out of the conducting torus. In the example shown in Fig. 7 the total acceleration time was chosen to be 1 msec and the diffusion time 10 μsec. The ratio of the temporal extent of each phase to the total acceleration time t/t_a is also given in the figure. It is apparent that the beam spends most of its time in the main acceleration phase.

During the pre-acceleration phase the metal wall surrounding the beam can be treated as a perfect conductor. As a result, for small displacement of the beam, the self-flux

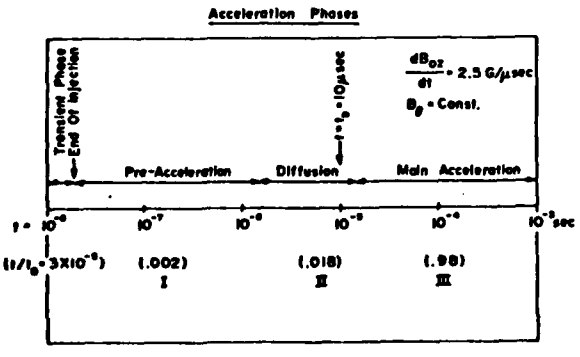

FIG. 7. The three phases of acceleration. In the example shown the acceleration time is 1 msec and the diffusion time is 10 μsec.

linking the axis of the electron ring remains constant to lowest order. This point is discussed further later.

The condition for the major radius of the electron ring to remain constant can be derived from the conservation of canonical angular momentum

$$P_\theta = m\gamma_0 v_{0\theta} - (e/c)r(A_\theta^{ext} + A_\theta^s), \tag{28}$$

where $v_{0\theta}$ is the toroidal velocity, A_θ^{ext} is the vector potential that describes the external-magnetic (betatron) field, A_θ^s is the vector potential that describes the self-magnetic field of the beam and r is the instantaneous radius of the beam.

The self-flux linking the axis of the ring Φ^s is

$$\Phi^s = 2\pi r A_\theta^s, \tag{29}$$

and to lowest order is independent of the beam displacement and thus of time [see Eq. (35)]. Substituting Eq. (29) into Eq. (28) and using the expression for

$$v_{0\theta} = \frac{r\Omega_{0z}/\gamma_0}{1+2(\nu/\gamma_0)[1+\ln(a/r_b)]},$$

Eq. (28) predicts that r remains constant, provided

$$\frac{\partial}{\partial t}\left(\frac{B_{0z}(t)}{1+2(\nu/\gamma_0)[1+\ln(a/r_b)]}\right) = \frac{1}{2}\frac{\partial}{\partial t}\langle B^{ext}\rangle. \tag{30}$$

In Eq. (30), $B_{0z}(t)$ is the local magnetic field, ν is the Budker's parameter, a is the minor radius of the torus, r_b is the beam radius, and $\langle B^{ext}\rangle$ is the average applied magnetic field within the electron ring.

Using the equation

$$mc^2\frac{\partial\gamma_0}{\partial t} = -ev\cdot E, \tag{31a}$$

together with

$$E_\theta = -\frac{r}{2c}\frac{\partial}{\partial t}\langle B^{ext}\rangle, \tag{31b}$$

Eq. (30) becomes

$$\frac{\partial B_{0z}(t)}{\partial t} = \frac{1}{2}\left[1+\frac{2\nu}{\gamma_0^3}\left(1+\ln\frac{a}{r_B}\right)\right]\frac{\partial}{\partial t}\langle B^{ext}\rangle. \tag{32}$$

A similar condition has been derived previously.[13]

Equation (32) is the condition that must be satisfied in order for the radius of the accelerated electron ring to remain constant. For low-ν/γ_0 beams, Eq. (32) is reduced to the well-known flux rule, i.e.,

$$\frac{\partial B_{0z}(t)}{\partial t} = \frac{1}{2}\frac{\partial}{\partial t}\langle B^{ext}\rangle.$$

The correction term $(2\nu/\gamma_0^3)[1+\ln(a/r_b)]$ in Eq. (32) is very sensitive to the beam energy. For a 10 kA, 3 MeV beam injected into a 10 cm minor-radius torus with $r_b = 1$ cm, the correction is only 1% and therefore can be neglected. However, when the energy of the same beam is reduced to 0.5 MeV the correction is 48%, i.e., very substantial. The design of the accelerator is simplified considerably by choosing the beam parameters such that the correction term is negligible.

The instantaneous value of $\gamma_0(t)$ may be determined from Eqs. (30) and (31) and for $\gamma_0^2(t) \gg 1$ is

$$\frac{\gamma_0(t)}{\gamma_0(0)} = \frac{\{1+2[\nu/\gamma_0(0)][1+\ln(a/r_b)]\}}{\{1+2[\nu/\gamma_0(t)][1+\ln(a/r_b)]\}}\frac{B_{0z}(t)}{B_{0z}(0)}.$$

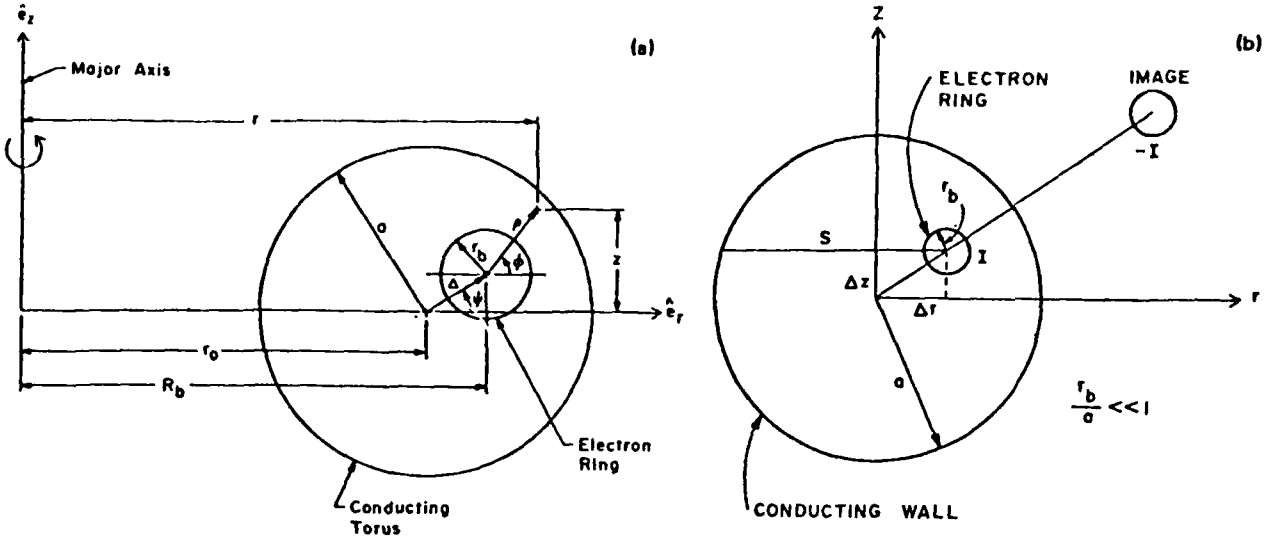

FIG. 8. System of coordinates: (a) depicts the various parameters appearing in Eq. (34); and (b) depicts a displaced straight electron beam inside a perfectly conducting pipe. The image curren: is located at a distance $a^2/(\Delta r^2 + \Delta z^2)^{1/2}$ from the center of the pipe.

In contrast to the low-current beams, in which $\gamma_0(t)/B_{0z}(t)$ remains approximately constant during acceleration, for high-current beams with toroidal corrections the quantity that remains constant during acceleration is

$$\frac{\gamma_0(t)}{B_{0z}(t)}\left\{1+2\frac{\nu}{\gamma_0(t)}\left[1+\ln\left(\frac{a}{r_b}\right)\right]\right\}=\text{const.} \tag{33}$$

As $\gamma_0(t)$ increases with time, the correction term decreases and Eq. (33) is reduced to $\gamma_0(t)/B_{0z}(t)=\text{const}$.

Now, we return to discuss the self-flux linking the axis of the ring. In the notation of the toroidal geometry shown in Fig. 8(a), the magnetic stream function $\Psi = rA^s_\theta$ for $\rho < r_b$ is given, to lowest order, by[11]

$$\frac{\Psi}{Q}=2\ln\left(\frac{a}{r_b}\right)+1-\frac{\rho^2}{r_b^2}-2\frac{\rho}{a}\frac{\Delta}{a}\cos(\psi-\phi)+\frac{\rho}{R_b}\left[\ln\left(\frac{a}{r_b}\right)-\frac{3}{4}\frac{r_b^2}{a^2}+2-\frac{5}{4}\frac{\rho^2}{r_b^2}\right]\cos\phi, \tag{34}$$

where $Q=-|e|n_0\pi r_b^2\Omega R_b^2/c$, $\Omega=v_\theta/r$, $\Delta^2=\Delta r^2+\Delta z^2$, n_0 is the uniform density, and it has been assumed that $a \ll r_0$, $r_b \ll a$, and $\Delta r, \Delta z \ll a$.

The self-flux through the axis of the ring ($\rho = 0$) is

$$\Phi' = 2\pi\Psi. \tag{35}$$

Substituting Eq. (34) into Eq. (35), we get

$$\Phi' = 2\pi Q[1+2\ln(a/r_b)], \tag{36}$$

which does not depend on the displacement Δr, Δz of the beam. This is a rather unusual result and deserves further discussion.

To gain some insight into the problem, we have computed the flux linking a horizontal surface s extended from the axis of a straight beam to the inner wall of a perfectly conducting cylinder of circular cross section as shown in Fig. 8(b). The beam displacement is arbitrary but the ratio $r_b/a \ll 1$. It is straightforward to show that the flux through such a surface of length l is

$$\Phi' = \frac{2Il}{c}\left[\frac{1}{2}+\ln\left(\frac{a}{r_b}\right)+\ln\left(1-\frac{(\Delta r^2+\Delta z^2)}{a^2}\right)\right], \tag{37}$$

where I is the beam current.

For $(\Delta r^2+\Delta z^2)^{1/2}/a \ll 1$, Eq. (37) indicates that the flux Φ' has a quadratic dependence on the beam displacement. Therefore, since only the linear terms on beam displacement were kept in the derivation of Eq. (34), it is not surprising that the flux given by Eq. (36) is independent of the displacement of the beam.

When the time approaches the magnetic-field-penetration time t_D, the self-magnetic field of the electron beam starts to diffuse out of the finite conductivity metal torus. Using the geometry shown in Fig. 9, it is shown in Appendix A, that for a very thin conductor, i.e., $a \approx b$, to lowest order, the self-magnetic field of the beam at time t is

$$\begin{aligned} B_\phi(r,t) &\approx (2I/cr)(1-e^{-t/t_D}), \quad r > b, \\ B_\phi(r,t) &\approx 2I/cr, \quad r_b < r < a, \end{aligned} \tag{38}$$

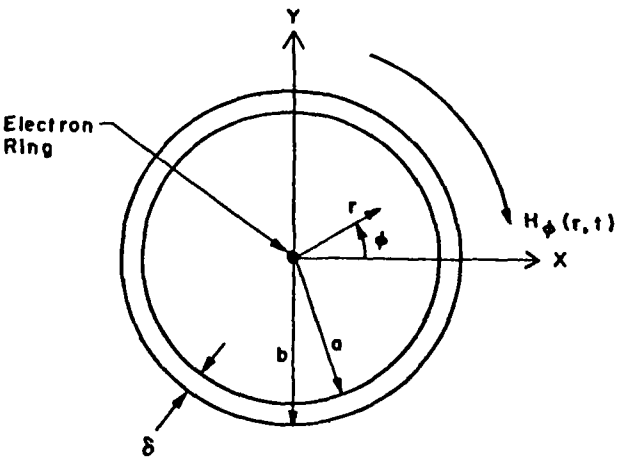

FIG. 9. System of coordinates used to compute the magnetic field during diffusion.

where

$$t_D \equiv (4\pi\sigma\delta a/c^2)\ln(r_0/a).$$

These equations are based on the assumptions that $\delta/a \ll 1$, $[(\delta/b)\ln(r_0/b)]^{1/2} \ll 1$, and the inductive electric field varies as $E_z(r,t) = (b/c)[\partial B_\phi(b,t)/\partial t]\ln(r/r_0)$, i.e., goes to zero at $r = r_0$ (pseudotoroidal geometry).

The self-magnetic flux in the three regions is given by

$$\Phi^s \approx \begin{cases} (4\pi r_0/c)I\ln(a/r_b), & r<a, \\ 0, & a<r<b, \\ (4\pi r_0/c)I(1-e^{-t/t_D})\ln(r_0/b), & r>b, \end{cases}$$

and it diffuses out at the rate

$$\frac{d\Phi^s}{dt} = \frac{4\pi r_0 I}{t_D c} e^{-t/t_D} \ln\left(\frac{r_0}{b}\right). \tag{39}$$

The inductive electric field generated by the changing flux given in Eq. (39) acts to slow down the beam. In addition, for a constant current density ring, the hoop forces increase by the ratio $[1 + \ln(8r_0/r_b)]/[1 + \ln(a/r_b)]$, and the induced magnetic-field components go to zero at the end of the diffusion. However, the electric-field components remain the same. As a result, for an electron ring that is situated along the minor axis of the torus, the decrease in its equilibrium radius associated with the reduction of γ_0 is greater than the corresponding increase of the equilibrium radius associated with the enhanced hoop forces and thus equilibrium can be lost. This difficulty can be avoided by placing a set of external conductors along the minor cross section of the torus having a poloidal distribution that closely resembles the distribution of wall currents in a perfect conductor, i.e.,

$$I_w = -(I_b/2\pi a)[1 - (a/2r_0)\cos\phi],$$

where I_w is the wall current per unit length and I_b the ring current.

This compensation is satisfactory even when the beam is displaced off center and rotates around the equilibrium position with ω_B, provided that $\omega_B\tau_D \gg 1$. The reason is that the correction term in the fields at the center of the ring,[14] when the skin depth is much greater than the thickness of the conductor, is

$$(-2e^{-t/\tau_D}/\omega_B\tau_D)\sin\omega_B t,$$

and therefore, it can be neglected. Similarly, when the skin depth is much smaller than the thickness, the correction term is also small and is given by

$$\left(\frac{2(b-a)/a}{\omega_B\tau_D}\right)^{1/2} + \frac{2e^{-t/\tau_D}}{\omega_B\tau_D}\sin\omega_B t.$$

In addition, we have shown that the components of the magnetic field that are proportional to the displacement of the beam do not diffuse out of the chamber when $\omega_B\tau_D \gg \gamma_0^2$. As a consequence $n_s r_b^2/a^2$ does not increase during diffusion and ω_B does not change polarity. Therefore, the drag instability[14] can be avoided by choosing the various parameters to give $\omega_B > 0$ at the commencement of the diffusion process.

During the main acceleration phase the significance of toroidal effects is reduced because $\nu/\gamma_0 \to 0$. When B_θ remains approximately constant (as shown in Fig. 10) or increases with time, the accelerated beam moves closer to the center of the minor cross section of the torus. This may be seen from the beam equations, which, for $B_{0\theta} = \text{const}$, are

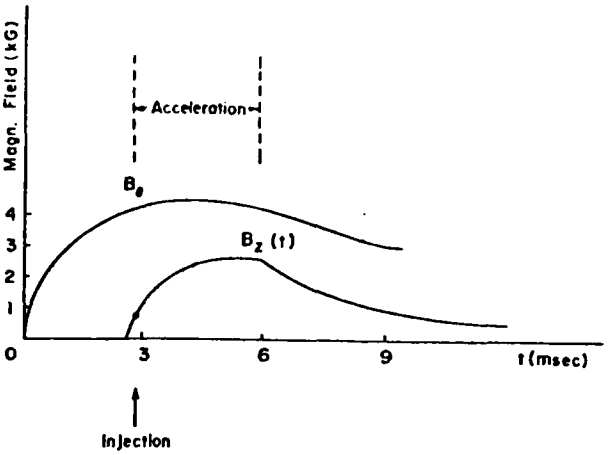

FIG. 10. This figure illustrates a possible time dependence of the toroidal and betatron fields. From the stability point of view other time variations are more appropriate.

$$\Delta\ddot{r} + \frac{\dot\gamma}{\gamma}\Delta\dot r + \bar\omega_r^2\Delta r = \frac{\Omega_{0\theta}}{\gamma}\Delta\dot z + \frac{\Omega_{0z}}{\gamma}\frac{\langle\delta P_\theta\rangle}{\gamma m r_0}, \tag{40}$$

$$\Delta\ddot z + (\dot\gamma/\gamma)\Delta\dot z + \bar\omega_z^2\Delta z = -(\Omega_{0\theta}/\gamma)\Delta\dot r. \tag{41}$$

With the exception of the second term $(\dot\gamma/\gamma)\Delta\dot r$, Eqs. (40) and (41) are identical to Eqs. (12) and (13). For $n = \frac{1}{2}$, Eqs. (40) and (41) can be readily solved. Introducing a new variable $\psi = \Delta r + i\Delta z$, these two equations can be combined into a single equation

$$\ddot\psi + \frac{1}{\gamma}(\dot\gamma + i\Omega_{0\theta})\dot\psi + \omega_0^2\psi = \frac{\Omega_{0\theta}}{\gamma}\frac{\langle\delta P_\theta\rangle}{\gamma m r_0}, \tag{42}$$

where $\omega_0^2 = \bar\omega_r^2 = \bar\omega_z^2$. The general solution of Eq. (42) is

$$\psi = \psi_1 + \psi_2 + \psi_p,$$

where

$$\psi_1 = \frac{a_1\exp(-i\int_0^t \omega_+^{(0)}\,dt')}{\gamma^{1/2}[(\Omega_{0\theta}/\gamma)^2 + 4\omega_0^2]^{1/4}},$$

$$\psi_2 = \frac{a_2\exp(-i\int_0^t \omega_-^{(0)}\,dt')}{\gamma^{1/2}[(\Omega_{0\theta}/\gamma)^2 + 4\omega_0^2]^{1/4}},$$

and

$$\psi_p = \psi_1\int_0^t \frac{[-(\Omega_{0\theta}/\gamma)(\langle\delta P_\theta\rangle/\gamma m r_0)\psi_2]\,dt'}{w(\psi_1,\psi_2)} + \psi_2\int_0^t \frac{[(\Omega_{0\theta}/\gamma)(\langle\delta P_\theta\rangle/\gamma m r_0)]\psi_1\,dt'}{w(\psi_1,\psi_2)}.$$

In the above equations $\omega_\pm^{(0)} = (\Omega_{0\theta}/2\gamma) \pm [(\Omega_{0\theta}/2\gamma)^2 + \omega_0^2]^{1/2}$ and $w(\psi_1,\psi_2)$ is the Wronskian of the two independent solutions ψ_1 and ψ_2 of the homogeneous equation.

Since the denominators of ψ_1 and ψ_2 increase when the betatron field increases in time, the center of the beam moves toward the center of the minor cross section of the torus during the acceleration.

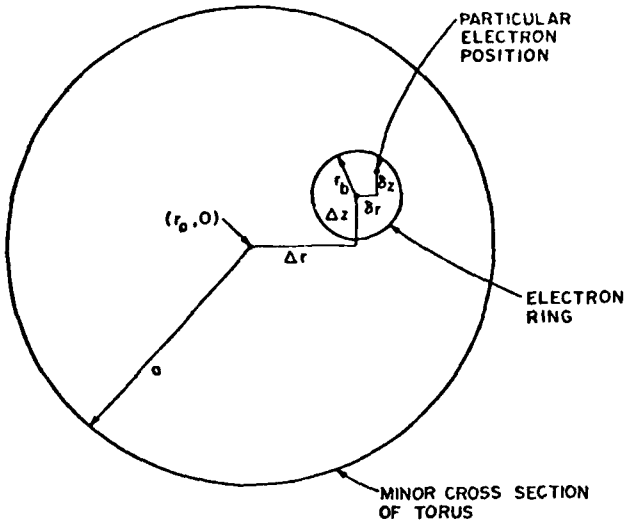

FIG. 11. System of coordinates used to analyze the drift resulting from the gradient in the toroidal magnetic field.

V. GRAD B DRIFT IN THE MODIFIED BETATRON

Until now we have neglected in our analysis the radial gradient in the toroidal magnetic field B_θ. In this section we consider carefully the effect of this nonlinearity on particle motion, assuming that it is the dominant nonlinear effect.

The linearized equations of motion of a particle located at $r = r_0 + \Delta r + \delta r$, $z = \Delta z + \delta z$, where Δr and Δz define the beam position with respect to the center of the torus (see Fig. 11), are

$$\ddot{r}_1 + (1-n)\tilde{\Omega}_{x0}^2 r_1 - n_s\tilde{\Omega}_{x0}^2\left(\delta r + \frac{r_b^2}{a^2}\Delta r\right) = \tilde{\Omega}_{\theta 0}\left(1 - \frac{r_1}{r_0}\right)\dot{z}_1 + \tilde{\Omega}_{z0}\frac{\delta P_\theta}{\gamma_0 m r_0},$$

$$\ddot{z}_1 + n\tilde{\Omega}_{x0}^2 z_1 - n_s\tilde{\Omega}_{x0}^2\left(\delta z + \frac{r_b^2}{a^2}\Delta z\right) = -\tilde{\Omega}_{\theta 0}\left(1 - \frac{r_1}{r_0}\right)\dot{r}_1,$$

where

$$r_1 = \Delta r + \delta r, \quad z_1 = \Delta z + \delta z, \tag{43}$$

$$\tilde{\Omega}_{z0} = \Omega_{0z}/\gamma_0, \quad \tilde{\Omega}_{\theta 0} = \Omega_{0\theta}/\gamma_0.$$

Choosing $n = \frac{1}{2}$ simplifies the subsequent analysis. Making this choice and defining $\psi = r + iz$ gives

$$\ddot{\psi}_1 + \tfrac{1}{2}\tilde{\Omega}_{x0}^2\psi_1 - n_s\tilde{\Omega}_{x0}^2[\delta\psi + (r_b^2/a^2)\Delta\psi] = -i\tilde{\Omega}_{0\theta}[1 - (\mathrm{Re}\,\psi_1/r_0)]\dot{\psi}_1 + \tilde{\Omega}_{z0}(\delta P_\theta/\gamma_0 m r_0). \tag{44}$$

We proceed to solve (44) perturbatively, assuming $\mathrm{Re}\,\psi_1 \ll r_0$.

The zero-order equation, neglecting the nonlinearity, is easily solved. First an averaged is performed over initial positions and velocities of the particles to obtain a single equation governing the motion of the beam center $\Delta\psi$. Denoting this average by brackets we will have $\langle\delta\psi\rangle = 0$ by definition and, as long as no kinks develop in the beam, it may be shown that $\langle\delta\dot{\psi}\rangle = 0 = \langle\delta\ddot{\psi}\rangle$. Once the average equation is obtained it may be subtracted from (44) to obtain an equation for $\delta\psi$. Carrying out this program, we find for the zero-order solution:

$$\Delta\psi^{(0)} = \frac{\langle\delta P_\theta\rangle}{\tilde{\Omega}_{z0}\gamma_0 m r_0[\frac{1}{2} - (r_b^2/a^2)n_s]} + Ae^{-i\omega_1 t} + Be^{-i\omega_2 t},$$

$$\delta\psi^{(0)} = \frac{\delta P_\theta - \langle\delta P_\theta\rangle}{\tilde{\Omega}_{z0}\gamma_0 m r_0(\frac{1}{2} - n_s)} + Ce^{-i\omega_3 t} + De^{-i\omega_4 t}, \tag{45}$$

where A, B, C, and D are complex constants dependent on initial coordinates and where the frequencies $\omega_1 \cdots \omega_4$ are given by

$$\omega_{1,2} = \tfrac{1}{2}\{\tilde{\Omega}_{\theta 0} \pm [\tilde{\Omega}_{\theta 0}^2 + 4\tilde{\Omega}_{x0}^2[\tfrac{1}{2} - (r_b^2/a^2)n_s]\}^{1/2}),$$

$$\omega_{3,4} = \tfrac{1}{2}\{\tilde{\Omega}_{\theta 0} \pm [\tilde{\Omega}_{\theta 0}^2 + 4\tilde{\Omega}_{x0}^2(\tfrac{1}{2} - n_s)]^{1/2}\}. \tag{46}$$

We shall take subscripts 1 and 3 to correspond to the + signs.

In writing (45) we have assumed that neither $[\frac{1}{2} - (r_b^2/a^2)n_s]$ nor $(\frac{1}{2} - n_s)$ is zero. If either of these quantities does vanish (corresponding physically to the vanishing of net radial restoring forces) the corresponding solutions to (44) grow secularly, indicating a curvature or centrifugal drift in the vertical direction. Below we assume that the radial restoring forces do not vanish for either beam or particle motion. In addition we shall make the assumption that $\langle\delta P_\theta\rangle = 0$. This is the same as the requirement that the equilibrium position of the beam be at the center of the minor cross section of the torus. This assumption has no effect whatsoever on the basic physical results and conclusions but does simplify the mathematics somewhat.

We may return to (44) and calculate the first-order correction to the beam position $\Delta\psi^{(1)}$. The equation to be solved is

$$\Delta\ddot{\psi}^{(1)} + i\tilde{\Omega}_{\theta 0}\Delta\dot{\psi}^{(1)} + \tilde{\Omega}_{x0}^2[\tfrac{1}{2} - (r_b^2/a^2)n_s]\Delta\psi^{(1)} = i\frac{\tilde{\Omega}_{\theta 0}}{r_0}\langle(\mathrm{Re}\,\psi_1^{(0)})\dot{\psi}_1^{(0)}\rangle. \tag{47}$$

Substituting from (45) we find the right-hand side of (47) is

$$\langle(\mathrm{Re}\,\psi_1^{(0)})\dot{\psi}_1^{(0)}\rangle = -i\sum_{j=1}^{2}\sum_{k=1}^{2}\omega_j\rho_j\rho_k e^{-i(\omega_j t - \alpha_j)} \times\cos(\omega_k t - \alpha_k) - \frac{i}{2}\sum_{j=3}^{4}\omega_j\langle\rho_j^2\rangle, \tag{48}$$

where we have defined

$$A,B,C,D \equiv \rho_j e^{i\alpha_j}, \quad j = 1,2,3,4,$$

and where we have assumed that

$$\langle C\rangle = \langle D\rangle = 0,$$

with the average taken over the initial positions and velocities of a particle.

From (47) and (48) we can see that apart from the oscillating terms the net effect of the radial gradient in B_θ is to cause an outward shift in the equilibrium position of the beam:

$$\Delta\psi_1^{(1)} = \frac{(\tilde{\Omega}_{\theta 0}/2r_0)\langle\Sigma_{j=1}^{4}\omega_j\rho_j^2\rangle}{\tilde{\Omega}_{x0}^2[\frac{1}{2} - (r_b^2/a^2)n_s]} + \text{oscillating terms}. \tag{49}$$

This result is simply understood as the result of a balance between the outward, "diamagnetic" force (which tends to expel the beam from the high field region) and the inward radial restoring force.

Since the ρ_j values in (49) depend on the details of the injection process, it is difficult to draw practical, quantitative conclusions from this result. However it is probably safe to conclude quite generally that any device should be designed so that $\frac{1}{2} > (r_b^2/a^2)n_s$ for all times, or

$$\nu/\gamma_0 < \tfrac{1}{4}[\gamma_0 \tilde{\Omega}_{z0} a/c)]^2, \tag{50}$$

for the case of a perfectly conducting wall. The γ_0 should be omitted in the parentheses on the right-hand side of (50) in the case of a poorly conducting wall (diffusion time short compared to a beam oscillation period). We note that the constraint in (50) is independent of the strength of the toroidal magnetic field.

Two-dimensional computer simulations bear out our claim that self-consistent beam equilibria exist in the presence of a gradient in B_θ, as long as the net radial focusing forces [proportional, basically, to the denominator in (49) but generalized to include the case $n \neq \frac{1}{2}$, and to include toroidal corrections to the self-fields] do not vanish. In Fig. 12 we show a succession of "snapshots" of a beam cross section, which remains in its equilibrium position for significant times compared to r_b/V_D, where V_D is the single-particle drift velocity,

$$V_D = \Omega_{\theta 0}\rho^2/2r_0,$$

and where ρ is a particle gyradius. No drift is observed. (This is not just a visual observation but is obtained from a plot of average particle position versus time.)

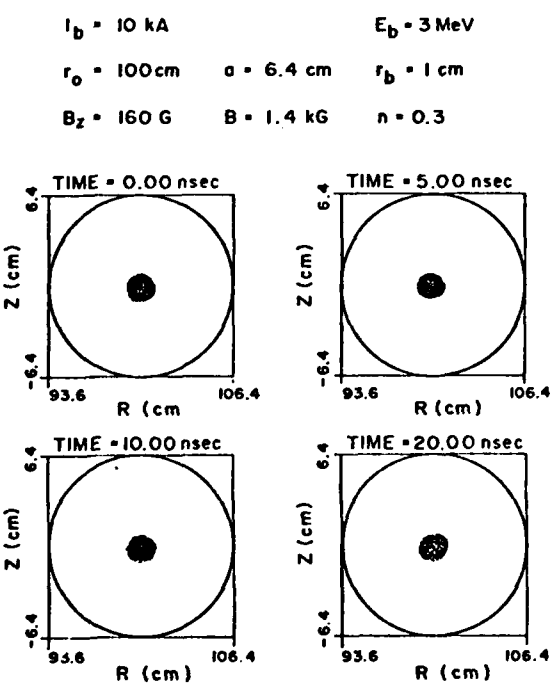

FIG. 12. Four snapshots of the electron-ring minor cross section. The values of the various parameters used in this computer simulation run are shown at the top of the figure.

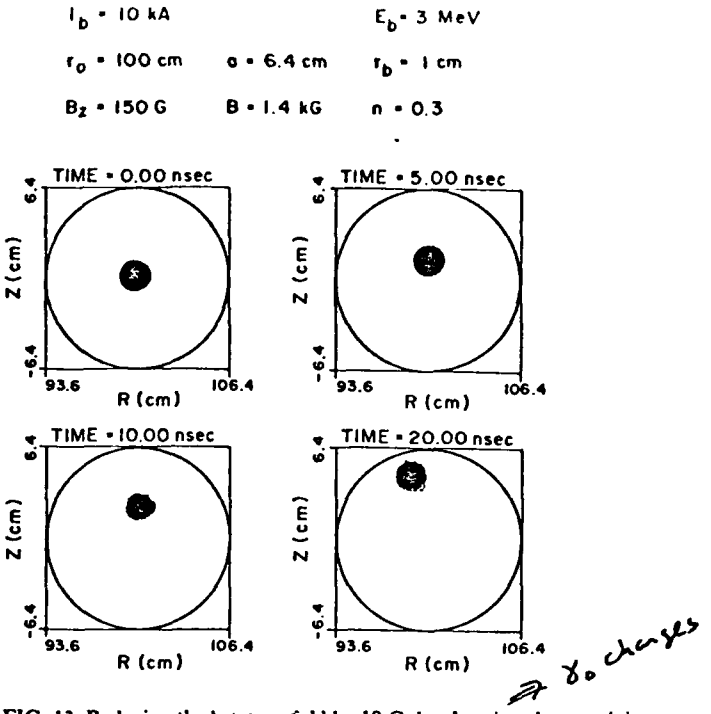

FIG. 13. Reducing the betatron field by 10 G, but keeping the remaining parameters fixed, as in the run of Fig. 12, the electron ring drifts rapidly in the vertical direction.

In Fig. 13, on the other hand, we present a case in which net radial focusing does nearly vanish. Loss of confinement is extremely rapid under such conditions. The ring drifts vertically with an average speed of 0.25 cm/nsec.

VI. THE EFFECT OF EMITTANCE

Up to this point, we have dealt with the equations describing the motion of the center of an electron ring in a modified-betatron configuration. In this section, we discuss the effect of the finite emittance on the equilibrium of the gyrating electron ring using the beam envelope equation. When the major beam radius r_0 is large, $n = \frac{1}{2}$, $\gamma_0 = \text{const}$, $\nu/\gamma < 1$, the thermal energy spread $\Delta\gamma_0 = 0$, and the effect of surrounding walls is neglected, the beam envelope equation in the paraxial approximation for $B_{0\theta} \gg B_{0z}$ becomes,[13] in the Larmor frame of reference,

$$r_b''(s) + \frac{1}{r_0^2}\left(\frac{B_{0\theta}}{2B_{0z}}\right)^2 r_b(s) - \frac{2\nu/\gamma_0^3}{\beta_0^2 r_b(s)} - \frac{\epsilon^2}{r_b^3(s)} = 0, \tag{51}$$

where ϵ is the beam emittance (unnormalized), $s = \theta r_0$ is the length along the minor axis of the torus, and $r_b'(s) \equiv dr_b/ds$. For a zero-emittance beam the motion of the particles is laminar and the equilibrium is called either laminar flow or Brillouin flow. The equilibrium radius in this case is obtained from Eq. (51) by setting

$$r_b'' = \epsilon = 0,$$

and is

$$r_{b,eq}' \cong (2c/\Omega_{0\theta})(2\nu/\gamma_0)^{1/2}, \tag{52}$$

when $\gamma_0 \gg 1$. For a finite emittance beam, the equilibrium radius can be determined from Eq. (51) by taking $r_b''(s) = 0$ and is

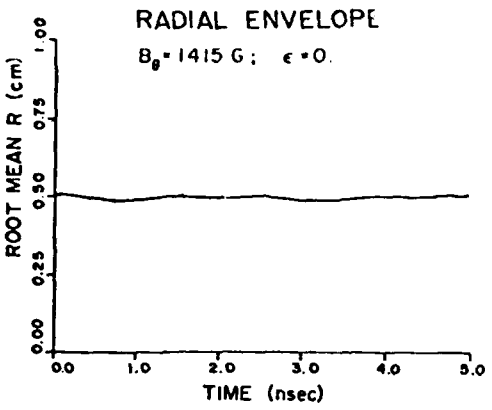

FIG. 14. Root-mean distance of the electrons from the center of the ring as a function of time, when the emittance ϵ is zero.

$$r_{b,eq} \approx \frac{2c}{\Omega_{0\theta}} \left\{ \frac{\nu}{\gamma_0} + \left[\left(\frac{\nu}{\gamma_0} \right)^2 + \epsilon^2 \left(\frac{\Omega_{0\theta}\gamma_0}{2c} \right)^2 \right]^{1/2} \right\}^{1/2}. \quad (53)$$

For small envelope oscillations $r_b = r_{b,eq} + \delta$, with $\delta / r_{b,eq} \ll 1$, and Eq. (51) gives

$$\delta'' + 2[(\Omega_{0\theta}/2\gamma_0 c)^2 + \epsilon^2 / r_{b,eq}^4]\delta = 0,$$

which has a period

$$T = \frac{2\pi/c}{2[(\Omega_{0\theta}/2\gamma_0 c)^2 + \epsilon^2 / r_{b,eq}^4]^{1/2}}. \quad (54)$$

The effect of emittance on the equilibrium of the ring has been studied extensively using a computer-simulation code. Numerical results from the computer simulation are given in Figs. 14–17. For a beam with $\gamma_0 = 7$, $I = 10$ kA, $r_0 = 100$ cm, $B_{0z} = 160$ G, and $B_{0\theta} = 1415$ G, Eq. (52) predicts that the equilibrium radius for the Brillouin flow is 1 cm. The numerical results of Fig. 14 also give a radius of 1 cm, that for all practical purposes remains constant in time. In this run the electron beam is injected into the torus with a rotational frequency that is half of the local cyclotron frequency. Figure 15 shows the envelope in time of a nonrotating beam. The various parameters in this run have the same values as those in Fig. 14, except now the emittance is nonzero in the Larmor frame. For the equivalent emittance of $\epsilon = 50$ mrad cm, Eq. (53) gives $r_{b,eq} = 1.21$ cm and the numerical results give an equilibrium radius approximately equal to 1.24 cm. Similarly, Eq. (54) gives a period of 2.13 nsec and the numerical results give 2.28 nsec. Snapshots of the beam cross section from the same run are given in Fig. 14. The oscillations observed in the run of Fig. 15 can be avoided by "matching" the beam, i.e., by raising the $B_{0\theta}$ magnetic field to 1830 G. This value of the magnetic field gives an $r_{b,eq} \approx 1$ cm, which is the radius of the beam for Brillouin flow. Numerical results from this run are shown in Fig. 17.

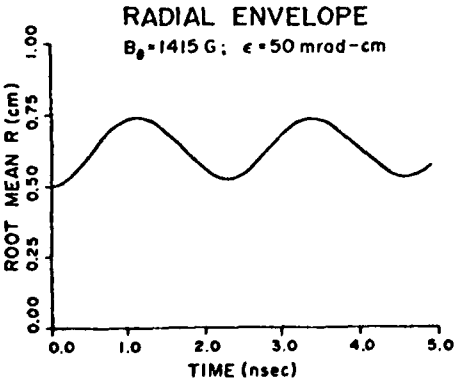

FIG. 15. Root-mean distance of the electron from the center of the ring as a function of time. In this run $\epsilon = 50$ mrad cm.

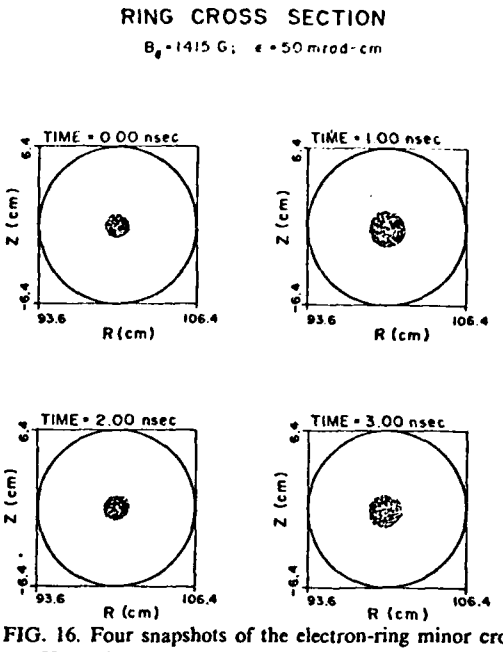

FIG. 16. Four snapshots of the electron-ring minor cross section when $\epsilon = 50$ mrad cm.

The electron beams discussed so far in this section were monoenergetic with finite emittance. Such beams have an axial velocity spread equivalent to that of a cold beam with energy spread $\Delta\gamma$ that is given by[15]

$$(\Delta\gamma/\gamma)_\epsilon = \tfrac{1}{2}(\gamma\beta\epsilon/r_b)^2.$$

Hot beams have an additional energy spread. This thermal energy spread in the direction of beam propagation has an important effect on the dynamics of electrons as may be seen as follows. The equations describing the motion of individual electrons in cylindrical geometry are identical with those

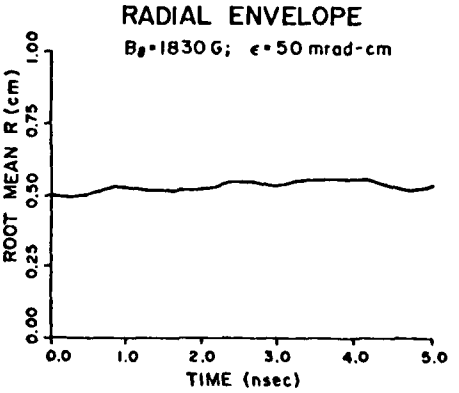

FIG. 17. Root-mean distance of the electrons from the center of the ring. The envelope oscillations are drastically reduced when the toroidal magnetic field is increased from 1415 G to 1830 G.

describing the motion of the center of the beam, provided that $\tilde{\omega}_r^2$ and $\tilde{\omega}_z^2$ are replaced by

$$\tilde{\omega}_r^2 = (\Omega_{0z}/\gamma_0)^2(1 - n - n_s),$$

$$\tilde{\omega}_z^2 = (\Omega_{0z}/\gamma_0)^2(n - n_s),$$

and

$$\frac{\langle \delta P_\theta \rangle}{\gamma_0 m r_0} = \frac{c^2}{r_0 \Omega_{0z}} \frac{\Delta\gamma}{\gamma_0}.$$

The above set of equations are based on the assumption that toroidal effects can be neglected. In addition, it should be emphasized that $\Delta\gamma$ is the thermal energy spread and not the energy mismatch $\delta\gamma_0$ discussed in Sec. III.

For $n = \frac{1}{2}$, the solution of the individual-particle equations are

$$r - r_0 = \delta r_0 \cos\omega_B t - \delta z_0 \sin\omega_B t + r_0 \frac{\Delta\gamma}{\gamma_0} \times \frac{(1 - \cos\omega_B t)}{\frac{1}{2} - n_s}, \quad (55)$$

$$\delta z = \delta z_0 \cos\omega_B t + \delta r_0 \sin\omega_B t - r_0 \frac{\Delta\gamma}{\gamma_0} \frac{\sin\omega_B t}{\frac{1}{2} - n_s}, \quad (56)$$

where

$$\omega_B = (\Omega_{0z}/\gamma_0)(B_z/B_\theta)(\tfrac{1}{2} - n_s).$$

According to Eq. (55), when $n_s \ll 1$, i.e., for low-current beams, thermal effects substantially increase the minor radius of the beam. In such beams the minor radius varies as $2r_0\Delta\gamma/\gamma_0$.

In contrast, when $n_s \gg 1$, i.e., for high-current beams, thermal effects do not change significantly the minor radius of the beam, which varies as $(r_0/n_s)(\Delta\gamma/\gamma_0)$.

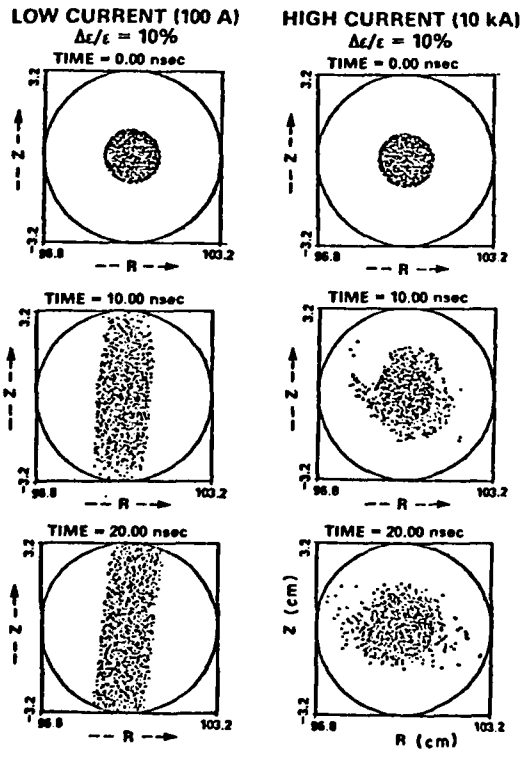

FIG. 18. Snapshots of the electron-ring minor cross section for low and high current. The values of the various parameters for this run are listed in Table II. The energy spread in both cases is 10%.

TABLE III. Electron-ring parameters for the two computer runs shown in Fig. 18.

Parameters	Low current	High current
Beam current (kA)	0.1	10
Beam energy (MeV)	3	3
Energy spread (%)	10	10
Major radius (cm)	100	100
Beam minor radius (cm)	1	1
Initial betatron field (G)	116	146
Toroidal field (kG)	1.4	1.4
External-field index	0.5	0.35
Self-field index (n_s)	0.37	23.4
Torus minor radius (cm)	3.2	3.2

The effect of the axial energy spread on the minor cross section of the beam in a modified-betatron geometry has been studied numerically. Results from both the high- and low-current beams are given in Fig. 18. In these two runs the various parameters have the values listed in Table III. In the high-current-beam case the minor radius expands by approximately a factor of two. However, in the low-current-beam run the beam expands significantly and strikes the wall. Therefore, a substantial energy spread can be tolerated in high-current beams without a catastrophic expansion of the minor radius of the beam. Such energy spread may be required to stabilize the various disruptive instabilities.[16-18]

VII. SUMMARY

In this paper we review the dynamics of ultrahigh-current electron rings in the modified-betatron configuration. Our discussion mainly addresses the evolution of the electron ring after injection. The formation of the ring during injection has been analyzed and reported previously.[19]

Our work includes both analytical and numerical results for "cold" and "hot" rings. The conclusion of these studies is that equilibrium states of ultrahigh-current rings in a modified betatron exist over a wide range of parameters. These equilibra are realistic and accessible with state-of-the-art injectors.

The results presented in this paper are based on several simplified assumptions. Among them, we have assumed that the various fields are free of errors, the conducting wall that surrounds the electron ring was assumed to be smooth (i.e., without ports and gaps), and the external-field index was assumed to be constant in time and space. The consequences of these assumptions are presently under investigation.

ACKNOWLEDGMENTS

The authors are grateful to Professor D. Kerst as well as to the members of the Special Focus "Advanced Accelerator" and in particular to Dr. J. Golden, Dr. J. Pasour, and Dr. F. Mako for many illuminating discussions.

APPENDIX A: DIFFUSION OF THE SELF-MAGNETIC FIELD OF THE BEAM THROUGH A CONDUCTING LINER

The purpose of this appendix is to briefly outline the calculation of the diffusion of the self-magnetic field of the

beam through a conducting liner. To simplify the analysis, it is assumed that the electron beam is located along the axis of a straight, circular cylinder of inner radius a, outer radius b, and thickness $\delta = b - a$, as shown in Fig. 9. In addition, it is assumed that the current of the electron beam is a step function that is turned on at $t = 0$. Since the problem of interest is that of an electron ring inside a torus, it is further assumed that the axial inductive electric field goes to zero at $r = r_0$, where r_0 is the major radius of the torus.

Neglecting the displacement current (quasistatic approximation), the fields inside the cylindrical conducting shell ($a<r<b$) are given in mks units by

$$\nabla\times\mathbf{H} = \mathbf{J}, \tag{A1}$$

$$\nabla\cdot\mathbf{B} = 0, \tag{A2}$$

$$\nabla\times\mathbf{E} = -\frac{\partial\mathbf{B}}{\partial t}, \tag{A3}$$

and

$$\mathbf{J} = \sigma\mathbf{E}, \tag{A4}$$

where $\mathbf{J}$ is the current density, $\mathbf{H}$ is the magnetic field, $\mathbf{B}$ is the magnetic induction, and σ is the conductivity of the conductor.

Assuming that all quantities are independent of z and ϕ, Eqs. (A1) to (A4) can be combined to give a diffusion equation for the azimuthal component of the magnetic field

$$\frac{\partial}{\partial r}\left(\frac{1}{r}\frac{\partial}{\partial r}[rH_\phi(r,t)]\right) = \sigma\mu\frac{\partial H_\phi}{\partial t}(r,t). \tag{A5}$$

For $r<a$ and $r>b$, the conductivity is equal to zero and Eq. (A5) becomes

$$\frac{\partial}{\partial r}\left(\frac{1}{r}\frac{\partial}{\partial r}[rH_\phi(r,t)]\right) = 0, \tag{A6}$$

with the only acceptable solutions

$$H_\phi(r,t) = (I/2\pi r)\Theta(t), \quad r_b<r<a, \tag{A7}$$

$$H_\phi(r,t) = H_\phi(b,t)b/r, \quad r>b, \tag{A8}$$

where $\Theta(t)$ is the step function and r_b is the beam radius.

To complete the specification of the problem we have to introduce boundary conditions. From Eqs. (A3) and (A8), we get

$$\frac{\partial E_z}{\partial r} = \mu\frac{\partial H_\phi(b,t)}{\partial t}\frac{b}{r},$$

which after integration yields

$$E_z(r,t) = \mu\frac{\partial H_\phi(b,t)}{\partial t}\, b\ln\left(\frac{r}{r_0}\right), \tag{A9}$$

where we have assumed that $E_z(r,t)$ is zero at $r = r_0$.

Combining Eqs. (A1), (A4), and (A9) at $r = b$, we obtain the first boundary condition, namely

$$\left(\frac{1}{r}\frac{\partial}{\partial r}(rH_\phi)\right)_{r=b} = \mu\frac{\partial H_\phi}{\partial t}(b,t)b\ln\left(\frac{b}{r_0}\right). \tag{A10}$$

The second boundary condition is furnished from the continuity of the magnetic field at $r = a$, i.e.,

$$(I/2\pi a)\Theta(t) = H_\phi(a,t). \tag{A11}$$

Since the magnetic field is zero at $t = 0$, Eqs. (A5), (A9), and (A10) take the following forms in their transformed state

$$\frac{\partial^2\hat{H}_\phi}{\partial r^2} + \frac{1}{r}\frac{\partial\hat{H}_\phi}{\partial r} - \left(\frac{1}{r^2} + \sigma\mu p\right)\hat{H}_\phi = 0, \tag{A12}$$

$$\left(\frac{\partial}{\partial r}(r\hat{H}_\phi)\right)_{r=b} = \sigma\mu p\hat{H}_\phi(b,t)b^2\ln\left(\frac{b}{r_0}\right), \tag{A13}$$

and

$$(I/2\pi a p) = [\hat{H}_\phi(r,t)]_{r=a}, \tag{A14}$$

where, the Laplace transform of H_ϕ is defined by

$$\hat{H}_\phi(r,p) = \int_0^\infty e^{-pt}H_\phi(r,t)\,dt, \quad \mathrm{Re}(p)>\tau.$$

Equation (A12) is the modified Bessel equation and its solution is

$$\hat{H}_\phi(r,p) = AI_1(\lambda r) + BK_1(\lambda r),$$

where A and B are constants and $\lambda^2 = \sigma\mu p$.

The two constant coefficients A and B, determined from Eqs. (A13) and (A14), are

$$A = (I/2\pi a p)[K_0(\lambda b) + \lambda b\ln(b/r_0)K_1(\lambda b)]/\Delta,$$

$$B = (I/2\pi a p)[I_0(\lambda b) - \lambda b\ln(b/r_0)I_1(\lambda b)]/\Delta,$$

where

$$\Delta = K_0(\lambda b)I_1(\lambda a) + I_0(\lambda b)K_1(\lambda a) + \lambda b\ln(b/r_0) \times[K_1(\lambda b)I_1(\lambda a) - K_1(\lambda b)I_1(\lambda b)]. \tag{A15}$$

The magnetic field in the region $a<r<b$ as a function of space and time can be obtained by inverting the Laplace transform, i.e.,

$$H_\phi(r,t) = \frac{I}{2\pi i}\int_{c-i\infty}^{c+i\infty}\frac{dp e^{pt}}{2\pi a p} \times\frac{1}{\Delta}\left\{\left[\left[K_0(\lambda b) + \lambda b\ln\left(\frac{b}{r_0}\right)K_1(\lambda b)\right]I_1(\lambda r) + \left[I_0(\lambda b) - \lambda b\ln\left(\frac{b}{r_0}\right)I_1(\lambda b)\right]K_1(\lambda r)\right\}, \tag{A16}$$

where the path of integration is a vertical line in the complex p plane to the right of all singularities of the integrand.

Equation (A16) has a simple pole at $p = 0$ of residue a/r and an infinite set of simple poles at $\Delta = 0$.

Contour integration of Eq. (A16) gives

$$H_\phi(r,t) = \frac{I}{2\pi a}\left\{\frac{a}{r} + \sum_{s=1}^{\infty}\exp\left(\frac{-\alpha_s^2 t}{\sigma\mu_0}\right) \times\left[Y_0(\alpha_s b)J_1(\alpha_s r) - Y_1(\alpha_s r)J_0(\alpha_s b) + \alpha_s b\ln\left(\frac{b}{r_0}\right)[Y_1(\alpha_s b)J_1(\alpha_s r) - Y_1(\alpha_s r)J_1(\alpha_s b)]\right]\right\}\left[\alpha_s\left(\frac{dD}{d\alpha}\right)_{\alpha=\alpha_s}\right]^{-1} \tag{A17}$$

where $\mu = \mu_0$, $\lambda = i\alpha$, Y and J are the Bessel functions, α_s are the roots of equation

$$Y_0(\alpha_s b)J_1(\alpha_s a) - Y_1(\alpha_s a)J_0(\alpha_s b) + \alpha_s b \ln(b/r_0)[Y_1(\alpha_s b)J_1(\alpha_s a) - Y_1(\alpha_s a)J_1(\alpha_s b)] = 0, \tag{A18}$$

and

$$\alpha_s\left(\frac{dD}{d\alpha}\right)_{\alpha=\alpha_s} = \alpha_s a[Y_0(\alpha_s b)J_0(\alpha_s a) - Y_0(\alpha_s a)J_0(\alpha_s b)] - \alpha_s b[Y_1(\alpha_s b)J_1(\alpha_s a) - Y_1(\alpha_s a)J_1(\alpha_s b)]$$
$$+ \alpha_s b \ln(b/r_0)\{b\alpha_s[Y_0(\alpha_s b)J_1(\alpha_s a) - Y_1(\alpha_s a)J_0(\alpha_s b)] + \alpha_s a[J_0(\alpha_s a)Y_1(\alpha_s b) - Y_0(\alpha_s a)J_1(\alpha_s b)]\}.$$

For $\alpha_s a \gg 1$, Eq. (A17) is reduced to

$$H_\phi(r,t) \approx \frac{I}{2\pi a}\left\{\frac{a}{r} - \left(\frac{a}{r}\right)^{1/2}\sum_{s=1}^{\infty}\exp\left(\frac{-\alpha_s^2 t}{\sigma\mu_0}\right)\left[\cos\alpha_s(b-r) + \alpha_s b\ln\left(\frac{b}{r_0}\right)\sin\alpha_s(b-r)\right]\right.$$
$$\left.\times\left[\alpha_s\delta\sin(\alpha_s\delta) - \alpha_s^2 b\ln\left(\frac{b}{r_0}\right)\cos\alpha_s\delta\right]^{-1}\right\}, \tag{A19}$$

where the α_s are now the roots of

$$\cos(\alpha_s\delta) + \alpha_s b\ln(b/r_0)\sin(\alpha_s\delta) = 0. \tag{A20}$$

Equations (A19) and (A20) are further simplified when $\alpha_s\delta \ll 1$. In this case

$$H_\phi(r,t) \approx \frac{I}{2\pi a}\left\{\frac{a}{r} - \left(\frac{a}{r}\right)^{1/2}\left[\cos\alpha_s(b-r)\right.\right.$$
$$\left.\left.+ \alpha_s b\ln\left(\frac{b}{r_0}\right)\sin\alpha_s(b-r)\right]\exp\left(\frac{-\alpha_s^2 t}{\sigma\mu_0}\right)\right\},$$

which at $r = b$, becomes

$$H_\phi(b,t) = (I/2\pi b)[1 - \exp(-\alpha_s^2 t/\sigma\mu_0)],$$

and

$$\alpha_s^2 = [\delta b\ln(r_0/b)]^{-1}. \tag{A21}$$

Therefore, to lowest order, the magnetic field in the region $r > b$ is

$$H_\phi(r,t) = \frac{I}{2\pi r}\left[1 - \exp\left(\frac{-\alpha_s^2 t}{\sigma\mu_0}\right)\right], \quad r > b \text{ (mks)}, \tag{A22}$$

or

$$H_\phi(r,t) = (2I/rc)[1 - \exp(-\alpha_s^2 tc^2/4\pi\sigma)] \text{ (cgs)}. \tag{A23}$$

Under the same approximations, the electric field of the inner edge ($r = a$) of the conducting shell is

$$E_z(a,t) = -\frac{I}{2\pi\sigma}\alpha_s^2\ln\left(\frac{r_0}{b}\right)\exp\left(\frac{-\alpha_s^2 t}{\sigma\mu_0}\right) \text{ (mks)}, \tag{A24}$$

Since the electric field is uniform in the region $r < a$, Eq. (A24) also gives the electric field that acts on the beam. Substituting Eq. (A24) into the energy-rate equation

$$mc^2\frac{d\gamma}{dt} = -e\mathbf{v}\cdot\mathbf{E},$$

we obtain for highly relativistic beams

$$\Delta\gamma/\gamma \approx -2(v/\gamma)\ln(r_0/b). \tag{A25}$$

For $r_0/b = 10$ and $v/\gamma = 0.1$, Eq. (A25) gives $\Delta\gamma/\gamma = 0.46$, i.e., a substantial reduction in the energy of the beam. However, for highly relativistic beams $v_z \simeq c$ and thus the current of the beam remains approximately constant.

APPENDIX B: DESCRIPTION OF THE PARTICLE-IN-CELL COMPUTER CODE

The Naval Research Laboratory (NRL) modified-betatron accelerator is designed for a maximum $v/\gamma_0 \approx 0.1$, i.e., the current is high enough so that the self-fields of the ring can exceed the externally applied fields. A realistic theoretical description must therefore self-consistently include the beam's self-fields as well as the effect of surrounding walls. Since this is difficult analytically, particularly if the ring is displaced substantially from the center of the minor cross section of the torus, numerical simulations are useful both in gaining insight into the important physical processes as well as to provide a method to check the applicability of specific assumptions in an analytic model.

The dynamics of the accelerated electron ring are determined by forces that vary on a number of different time scales which range from the electron cyclotron period, i.e., a few nanoseconds, to the beam acceleration time, which is of order of a millisecond. The code described here is tailored to simulate efficiently the various phenomena on the intermediate time scale. This time scale is characteristic of the drift (bounce) motion of the ring after equilibrium has been established, rather than the rapid evolution occurring at injection. Simulation of a single turn around the major axis that lasts about 20 nsec using 4000 particles on a 64×64 grid typically takes about one minute on the NRL Texas Instruments ASC (Advanced Scientific Computer).

The simulation code is $r - z$, spatially two-dimensional, i.e., $\partial/\partial\theta = 0$, but with three velocity components. Although B_θ is used in calculating the particle trajectories, it is not solved self-consistently, i.e., it is assumed to be generated from external coils only. This assumption is valid to first order in v/γ. The radiative term (displacement current) is also ignored, i.e., the code uses the Darwin model for Maxwell's equations.

The electrostatic potential is computed from Poisson's equation

$$\nabla^2\Phi = \rho/\epsilon_0, \tag{B1}$$

and the magnetic vector potential from

$$\nabla^2 A_\theta - A_\theta/r^2 = -\mu_0 J_\theta, \tag{B2}$$

with the boundary condition $\Phi = A_\theta = 0$ at the conducting wall.

Equations (B1) and (B2) are solved by Fourier decomposition in the z direction and then by Gaussian elimination of

the resultant tridiagonal matrix of equations obtained from a three-point differencing scheme for ∇_r^2. The inverse Fourier transform yields A_θ and Φ on the grid. Note that the θ-particle velocities are advanced using the conservation of canonical momentum in the θ direction, the equation for A_θ is therefore not properly time-centered since the velocities from the previous time step are used to calculate the currents from the canonical momenta. This method was chosen primarily for its speed and simplicity but care must be taken in applying the code when the inductive acceleration of particles in the θ direction is significant.

If boundary conditions other than A_θ or Φ equaling zero on a rectangular grid are desired, it is possible to obtain relatively arbitrary boundary conditions using the capacitive-matrix(Buneman) technique.[20] In this method a matrix is generated which is the Green's function for discrete "wall" points within the system. Then at each time step the field solver described above is used. The potential at the discrete (wall) points is obtained. By multiplying this vector potential by the invense matrix obtained previously a set of (wall) currents or changes is generated, which is used to specify the wall potential. These (wall) sources are then added to the original beam source and the field solver is used again. The result by the principle of superposition is correct inside the system and has the correct boundary condition on the "wall."

The motion of the electrons is governed by the Lorentz force

$$\frac{d(\gamma \mathbf{V})}{dt} = \frac{q}{m_0}(\mathbf{E} + \mathbf{V}\times\mathbf{B}),$$

where E and B are the total electric and magnetic field, respectively.

In component form the equations used to update the velocities and positions at each time step are

$$\gamma V_\theta = P_\theta/m_0 r - (q/m_0)A_\theta, \tag{B3}$$

$$\frac{d(\gamma V_r)}{dt} = \frac{q}{m_0}(E_r + V_\theta x B_z - V_z x B_\theta) + \frac{\gamma V_\theta^2}{r}, \tag{B4}$$

$$\frac{d(\gamma V_z)}{dt} = \frac{q}{m_0}(E_z - V_\theta x B_r + V_r x B_\theta), \tag{B5}$$

$$\frac{dr}{dt} = V_r, \tag{B6}$$

$$\frac{dz}{dt} = V_z. \tag{B7}$$

Equation (B3) is used at each timestep to compute γV_θ. Equations (B4) and (B5) are coupled. To advance these velocities a leap-frog scheme is employed. At time t all fields, positions, and V_θ are known exactly. V_r and V_z however are known at $t+1$ and the velocities will be advanced to $t+\frac{1}{2}$. Before the equations are differenced, it is convenient to rewrite the equations in terms of the relativistic momenta. Letting

$$\mathbf{U} = \gamma \mathbf{V},$$

so Eqs. (B3), (B4), and (B5) can be written as

$$U_\theta = P_\theta/m_0 r - (q/m_0)A_\theta, \tag{B3'}$$

$$\frac{dU_r}{dt} = \frac{q}{\gamma m_0}(\gamma E_r + U_\theta x B_z - U_z x B_\theta) + \frac{U_\theta^2}{\gamma r}, \tag{B4'}$$

$$\frac{dU_z}{dt} = \frac{q}{\gamma m_0}(\gamma E_z - U_\theta x B_r + U_r x B_\theta), \tag{B5'}$$

$$\frac{dr}{dt} = \frac{U_r}{\gamma}, \tag{B6'}$$

$$\frac{dz}{dt} = \frac{U_z}{\gamma}. \tag{B7'}$$

This formulation is then differenced by substituting

$$\frac{\mathbf{U}^{t+1/2} - \mathbf{U}^{t-1/2}}{\Delta t} \quad \text{for} \quad \frac{d\mathbf{U}}{dt},$$

and

$$\frac{\mathbf{U}^{t+1/2} + \mathbf{U}^{t-1/2}}{2} \quad \text{for} \quad \mathbf{U}.$$

After making these substitutions in Eq. (B4') and (B5') it is straightforward, if somewhat tedious, to solve the two coupled equations for $U_z^{t+1/2}$ and $U_r^{t+1/2}$. Since U_r and U_z are calculated at the half-timesteps while U_θ is known at the full timesteps, γ is not known at time t. This difficulty is overcome using iteration.

After advancing the velocities, the particle positions are advanced using a simple centered difference

$$r^{t+1} = r^t + \Delta t U_r/\gamma,$$

and

$$z^{t+1} = z^t + \Delta t U_z/\gamma.$$

Once all the velocities and positions are found the new current and charge densities are used to update the fields and a new time step begins.

[1]T. J. Fessenden, W. A. Atchison, D. L. Birx, R. J. Briggs, J. C. Clark, R. E. Hester, V. K. Neil, A. C. Paul, D. Rogers, Jr., and K. W. Struve, in *Proceedings of the Fourth International Topical Conference on High-Power Electron and Ion Beam Research and Technology*, Palaiseau, France, 29 June–3 July, 1981, edited by H. J. Doucet and J. M. Buzzi (CNRS, Paris, 1981), p. 813.

[2]R. Briggs, IEEE Trans. Nucl. Sci. 28, 3660 (1981).

[3]A. I. Paulovskii, D. G. Kuleshov, A. I. Gerasimov, A. P. Klementev, V. D. Kuznetsov, V. A. Tananakin, and A. D. Tarasov, Sov. Phys. Tech. Phys. 22, 218 (1977).

[4]P. Sprangle and C. A. Kapetanakos, J. Appl. Phys. 49, 1 (1978).

[5]P. Sprangle, C. A. Kapetanakos, and S. J. Marsh, see Ref. 1, p. 803.

[6]G. Barak, D. Chernin, A. Fisher, H. Ishizuka, and N. Rostoker, see Ref. 1, p. 795.

[7]H. S. Uhm and R. C. Davidson, Massachusetts Institute of Technology Plasma Fusion Center Report No. JA-81-30, 1981.

[8]D. W. Kerst, G. A. Adams, H. W. Koch, and C. S. Robinson, Rev. Sci. Inst. 21, 462 (1950).

[9]D. W. Kerst, Nature 157, 90 (1940).

[10]R. C. Davidson, *Theory of Nonneutral Plasmas* (Benjamin, New York, 1974).

[11]D. P. Chernin and P. Sprangle, Part. Accel. 12, 85 (1982).

[12]G. Schmidt, Phys. Rev. Lett. 26, 952 (1971).

[13]J. D. Lawson, *The Physics of Charged Particle Beams* (Clarendon, Oxford, 1977).

[14]P. Sprangle and C. A. Kapetanakos (submitted to Part. Accel., 1983). The drag instability is a special case of the resistive wall instability and occurs when the beam current exceeds the value given by Eq. (27).

[15]V. K. Neil, Jason Technical Report No. JSR-79-10, 1979.

[16]P. Sprangle and J. Vomvoridis, Naval Research Laboratory Report No. 4688, 1982.

[17]D. P. Chernin and P. Sprangle, Part. Accel. 12, 101 (1982).

[18]T. P. Hughes and B. B. Godfrey, Mission Research Corporation Report No. AMRC-R-354, 1982; also Report No. AMRC-R-322, 1982.

[19]C. A. Kapetanakos, P. Sprangle, and S. J. Marsh, Phys. Rev. Lett. 49, 741 (1982).

[20]J. M[illegible] and G. LaFrange, J. Comp. Phys. 23, 86 (1977).

APPENDIX C

Integer Resonances in the Modified Betatron

Particle Accelerators
1982 Vol. 12 pp. 101–106
0031-2460/82/1202-0101$06.50/0

INTEGER RESONANCES IN THE MODIFIED BETATRON*

D. CHERNIN

Berkeley Research Associates, PO Box 852, Springfield, Virginia 22150 U.S.A.

P. SPRANGLE

Plasma Theory Branch, Plasma Physics Division, Naval Research Laboratory, Washington, DC 20375 U.S.A.

(Received February 5, 1982)

The integer resonances affecting beam motion in the presence of external field imperfections in the modified betatron are studied. An upper bound is obtained on the magnitude of field error that may be tolerated. A numerical example shows that for practical parameters the resulting bound is very restrictive. The effect of longitudinal temperature and other possible stabilizing effects are discussed.

I. INTRODUCTION

In a conventional betatron, low-order resonances between particle motion and field imperfections can be avoided by restricting the beam current so that the tune shift[1] remains sufficiently small. In a modified betatron, the addition of a strong toroidal magnetic field may allow large currents to be accelerated,[2,3] but resonances become much more difficult to avoid, especially if one contemplates removing the toroidal field before the beam is extracted. This paper examines the problem of integer resonances in the modified betatron[4] and obtains a condition bounding the rate of change of the fields; when the condition is satisfied the resonances are passed through with sufficient speed so that the beam is not significantly disturbed. We consider here only errors in the fields themselves, not in field gradients, so we discuss only integer, not half-integer resonances.

In what follows, we will first consider a "cold" beam, that is, one in which there is no spread in longitudinal energy or, therefore, in circulation frequency about the machine. The effect of orbital resonances on such a cold beam will be seen to place rather severe limits on the magnitude of the tolerable field imperfections. When the effects of temperature are taken into account, however, a numerical example below will illustrate a reduction of the effect of the resonance on the motion of the beam center of mass. An explanation of this temperature effect will be given.

* Supported by the Office of Naval Research.

II. ORBITAL RESONANCES FOR A COLD BEAM

We consider a beam of circular cross section and uniform density and current profiles, as shown in Fig. 1. The torus has a major radius r_0 and minor radius a; the chamber is assumed to be perfectly conducting as far as the rapidly varying part of the self-fields is concerned. The beam radius is r_b with center located at $r = r_0 + \Delta r$, $z = \Delta z$, as shown in the figure. If we define the displacement of a particle from the design orbit $r = r_0$, $z = 0$ as $r_1 = \Delta r + \delta r$, $z_1 = \Delta z + \delta z$ then the equations of motion for r_1 and z_1 are, to first order in the displacement from the design orbit

$$\ddot{r}_1 + \frac{\dot{\gamma}_0}{\gamma_0}\dot{r}_1 + \Omega_{z0}^2(1 - n - n_s)r_1 = \frac{e\dot{B}_{\theta 0}}{2m\gamma_0 c} z_1 + \Omega_{\theta 0}\dot{z}_1 - \frac{\omega_b^2}{2\gamma_0^2}\left(1 - \frac{r_b^2}{a^2}\right)\Delta r - \frac{e}{m\gamma_0}\left[\tilde{E}_r + \beta_0\tilde{B}_z + \Omega_{z0}\int_0^t dt'\tilde{E}_\theta(t')\right] \tag{1a}$$

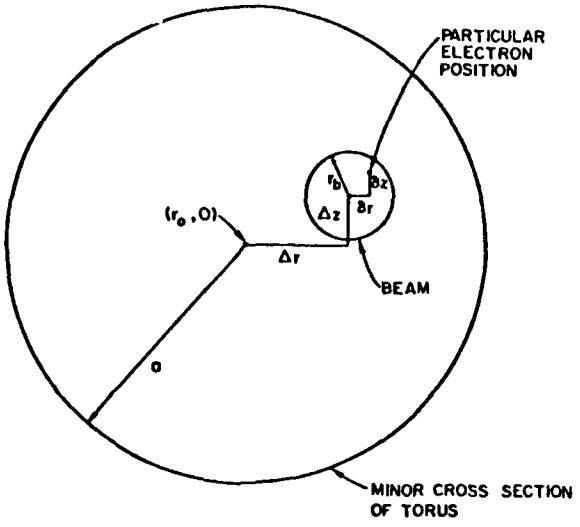

FIGURE 1 Minor cross section of modified betatron showing beam center and particle coordinates. The major radius of the device is r_0.

$$\ddot{z}_1 + \frac{\dot{\gamma}_0}{\gamma_0}\dot{z}_1 + \Omega_{z0}^2(n - n_s)z_1$$

$$= -\frac{e\dot{B}_{\theta 0}}{2m\gamma_0 c} r_1 - \Omega_{\theta 0}\dot{r}_1$$

$$-\frac{\omega_b^2}{2\gamma_0^2}\left(1 - \frac{r_b^2}{a^2}\right)\Delta z$$

$$-\frac{e}{m\gamma_0}[\tilde{E}_z - \beta_0 \tilde{B}_r], \qquad (1b)$$

where γ_0 is the particle energy on the "ideal" design orbit (in units of mc^2), $\Omega_{z0} = eB_{z0}/m\gamma_0 c$, $\Omega_{\theta 0} = eB_{\theta 0}/m\gamma_0 c$, B_{z0} is the vertical magnetic field at the design orbit, $B_{\theta 0}$ is the toroidal magnetic field, n is the betatron field index (assumed constant here), $n_s = \omega_b^2/(2\gamma_0^2\Omega_{z0}^2)$ is the self-field index, $\omega_b = (4\pi n_0 e^2/m\gamma_0)^{1/2}$ is the beam plasma frequency and e, m are the magnitude of electron charge and rest mass, and where field components with a "wiggle" on the right hand sides of (1a, b) denote the value of the field imperfection which in general will depend on the value of θ, the azimuthal position of the particle. In deriving (1a, b) we have allowed all fields to depend on time; we have therefore included the inductive poloidal electric field ($B_{\theta 0}$ terms). Also included are the effect of wall image charges and currents (r_b^2/a^2 terms), present when the beam is displaced from the center of the chamber.

We desire to have equations which describe only the motion of the beam center, $\Delta r(\theta, t)$, $\Delta z(\theta, t)$. To this end we define a distribution function f as

$$f(r, \theta, z, v_r, v_\theta, v_z, t) \equiv \sum_{\mathbf{r}^{(0)}, \mathbf{v}^{(0)}} g(\mathbf{r}^{(0)}, \mathbf{v}^{(0)})$$

$$\times \delta(r - \hat{r})\frac{\delta(\theta - \hat{\theta})}{r}\delta(z - \hat{z})\delta^{(3)}(\mathbf{v} - \hat{\mathbf{v}}), \qquad (2)$$

where $\mathbf{r}^{(0)}$ and $\mathbf{v}^{(0)}$ are particle initial conditions, $\hat{r}$, $\hat{\theta}$, $\hat{z}$, and $\hat{\mathbf{v}}$ are the solutions for the particle trajectories as functions of initial position, velocity, and time, and where $g(\mathbf{r}^{(0)}, \mathbf{v}^{(0)})$ is a weighting function. We then have that

$$\Delta r(\theta, t) = \frac{\int r\, dr\, dz\, dv (r - r_0) f}{\int r\, dr\, dz\, dv f}$$

$$= \frac{\sum g(\mathbf{r}^{(0)}, \mathbf{v}^{(0)})(\hat{r} - r_0)\delta(\theta - \hat{\theta})}{\sum g(\mathbf{r}^{(0)}, \mathbf{v}^{(0)})\delta(\theta - \hat{\theta})} \qquad (3)$$

$$\equiv \langle r_1 \rangle.$$

A similar expression holds for $\Delta z(\theta, t)$. It may be similarly shown that, for a cold beam,

$$\langle \dot{r}_1 \rangle = \left(\frac{\partial}{\partial t} + \Omega_{z0}\frac{\partial}{\partial \theta}\right)\Delta r \qquad (4)$$

$$\langle \ddot{r}_1 \rangle = \left(\frac{\partial}{\partial t} + \Omega_{z0}\frac{\partial}{\partial \theta}\right)^2 \Delta r, \qquad (5)$$

where, of course, analogous expressions hold for $\langle z_1 \rangle$, $\langle \dot{z}_1 \rangle$ and $\langle \ddot{z}_1 \rangle$. In Eqs. (4) and (5) we have assumed that all particles circulate the machine with $\dot{\hat{\theta}} = \Omega_{z0}$. This assumption will be relaxed in the next section where the effects of finite longitudinal temperature are considered.

Using this averaging procedure on Eqs. (1a, b), one obtains equations for the beam-center motion. Though these may be solved in general, the special choice $n = \frac{1}{2}$ (which is consistent with our assumption of a circular beam) simplifies the analysis. With $n = \frac{1}{2}$ and defining

$$\Delta\psi = \Delta r + i\Delta z \equiv \sum_{l=-\infty}^{\infty} \overline{\Delta\psi_l} e^{il\theta}, \qquad (6)$$

the equation for $\overline{\Delta\psi_l}$ is

$$\frac{\partial^2}{\partial t^2}\overline{\Delta\psi_l} + \left[\frac{\dot\gamma_0}{\gamma_0} + i\Omega_{\theta 0} + 2il\Omega_{z0}\right]\frac{\partial \Delta\psi_l}{\partial t} + \left[\Omega_{z0}^2\left(\frac{1}{2} - \frac{r_b^2}{a^2}n_s - l^2\right) + il\Omega_{z0}\frac{\dot\gamma_0}{\gamma_0} + i\frac{e\dot B_{\theta 0}}{2m\gamma_0 c} - l\Omega_{\theta 0}\Omega_{z0} + il\dot\Omega_{z0}\right]\overline{\Delta\psi_l} = F_l \tag{7}$$

where F_l is the l-th Fourier component of

$$-\frac{e}{m\gamma_0}\left[\tilde E_r + \beta_0\tilde B_z + i(\tilde E_z - \beta_0\tilde B_r) + \Omega_{z0}\left\langle\int_0^t dt'\tilde E_\theta(t')\right\rangle\right].$$

Equation (7) may be solved, assuming the functions multiplying derivatives of $\overline{\Delta\psi_l}$ are slowly varying over the period of a betatron oscillation:

$$\overline{\Delta\psi_l} \approx (\gamma_0\omega_0)^{-1/2}\int^t dt' e^{-i\int^{t'}dt''[\frac{1}{2}\Omega_{\theta 0} + l\Omega_{z0}]} \times\left[\frac{\gamma_0(t')}{\omega_0(t')}\right]^{1/2}\cdot\sin\left[\int_{t'}^t dt''\omega_0\right]F_l(t'), \tag{8}$$

where

$$\omega_0(t) \equiv \left[\Omega_{z0}^2\left(\frac{1}{2} - \frac{r_b^2}{a^2}n_s\right) + \frac{1}{4}\Omega_{\theta 0}^2\right]^{1/2}. \tag{9}$$

For long times (many betatron periods), the integral in (8) may be evaluated by the method of stationary phase. The points of stationary phase (resonance points) occur when

$$\Omega_l^{\pm} \equiv -\tfrac{1}{2}\Omega_{\theta 0} - l\Omega_{z0} \pm \omega_0 = 0 \tag{10}$$

for a given l. This is just the condition that the betatron frequency be l times the fundamental cyclotron frequency, Ω_{z0}. Condition (10) may also be written

$$B_{\theta 0} = -\frac{1}{l}\left(l^2 + \frac{r_b^2}{a^2}n_s - \frac{1}{2}\right)B_{z0}. \tag{11}$$

For positive $B_{\theta 0}$ and B_{z0}, Eq. (11) may be satisfied only by negative l and for such l, Eq. (10) may be satisfied only for the lower sign (fast mode resonance). Evaluating Eq. (8) then gives

$$\overline{\Delta\psi_l} \sim i\left(\frac{\pi}{2}\right)^{1/2}\left[\frac{\gamma_0(t_-)}{\gamma_0(t)\omega_0(t)\omega_0(t_-)}\right]^{1/2} \times\frac{F_l(t_-)}{|\dot\Omega_l^-(t_-)|^{1/2}}e^{i\int_{t_-}^t\Omega_l^- dt'' \pm i\pi/4}, \tag{12}$$

where t_- is the time at which $\Omega_l^- = 0$ and where the + or − sign is used in the exponent according as $\dot\Omega_l^-(t_-) > 0$ or < 0 respectively. If we neglect the possibility of cancellation due to different phases as we pass through different resonances and if we interpret F_l generically as $[-(e/m\gamma_0)\delta f_l]$ where δf_l is the l-th Fourier component of any field error, we may obtain a lower bound on $|\dot\Omega_l^-|$ by requiring

$$|\overline{\Delta\psi_l}| \ll a, \tag{13}$$

which gives

$$|\dot\Omega_l^-| \gg \frac{\pi}{2}\left[\frac{e\delta f_l}{m\gamma_0\omega_0 a}\right]^2, \tag{14}$$

which is our basic result. For γ_0 large enough that we may neglect $\dot\Omega_{z0}$ compared with $\dot\Omega_{\theta 0}$ and $r_b^2 n_s/a^2$ compared with 1/2, this constraint may be rewritten, using the relations

$$\dot\Omega_l^- = -\frac{l^2}{l^2 + 1/2}\dot\Omega_{\theta 0} \tag{15}$$

and

$$\omega_0 = \frac{l^2 + 1/2}{2|l|}\Omega_{z0}, \tag{16}$$

as

$$|\dot\Omega_{\theta 0}| \gg \frac{2\pi}{l^2 + 1/2}\left[\frac{\delta f_l}{B_{z0}}\frac{c}{a}\right]^2. \tag{17}$$

As an example, we consider the problem of passing through the $l = -1$ resonance. We consider a hypothetical experiment ($r_0 = 1$ m, $a = 10$ cm, $r_b = 1$ cm) in which γ_0 is increased linearly in time from an initial (injection) value of 7 to a final value ($t_{\text{final}} = 1$ millisecond) of 100, while simultaneously $B_{\theta 0}$ is decreased from 1.5 kG to 0. The $l = -1$ resonance will occur at $t = 627$ μsec, at which time $B_{z0} = 1120$ G, $B_{\theta 0} = 560$ G and $\gamma_0 = 65.3$. At resonance, $\dot\Omega_{\theta 0} = -6.2 \times$

10^{11} sec^{-2}. Substituting in the expression (17) we obtain an upper bound on the allowable field error

$$\frac{\delta f_{-1}}{B_{z0}} \ll 1.3 \times 10^{-4},$$

a rather severe requirement.

We conclude that, at least for the case of a cold beam, it may not be desirable to remove the toroidal field and pass through these resonances. Perhaps the toroidal field may be reduced somewhat from its initial value, assuming the high-l resonances are not too important and can be passed through easily. It may then be possible, by the use of an intentionally introduced field perturbation, to use a low-l resonance in a controlled way to extract the beam before B_θ is completely removed.

It should be noted that it is possible, at least in principle, to avoid the integer resonances altogether by raising both B_{z0} and $B_{\theta 0}$ proportionately and in such a way that condition (11) is never satisfied for any l. At the end of such an acceleration cycle, however, one will have a very large toroidal magnetic field in the device, possibly complicating the extraction process.

The above results apply to a beam all of whose particles are traveling to lowest order at the same azimuthal angular velocity. All particles are then in resonance at precisely the same moment and receive the same periodic perturbations to their orbits. In the next section we relax this assumption and examine the behavior of a beam, the particles of which possess a spread in energy.

III. EFFECT OF FINITE BEAM TEMPERATURE ON RESONANCES

To calculate the effect of beam temperature on beam behavior near a resonance, we consider an ensemble of beams, each cold and each consisting of particles traveling with a zero-order angular frequency $\dot{\theta}_0$ given by

$$\dot{\theta}_0 = \Omega_{z0} - kP, \tag{18}$$

where P is the canonical angular momentum of a particle, which is related to the difference in energy between the particle under consideration and the (reference) particle maintained at the design orbit $r = r_0$, $z = 0$ by

$$P = \frac{\Delta\gamma mc^2}{\Omega_{z0}}, \tag{19}$$

and where, in Eq. (18),

$$-k \equiv \left(\frac{1}{\gamma_0^2} - \frac{1}{1/2 - n_s}\right) \Big/ \gamma_0 m r_0^2. \tag{20}$$

For each cold beam, the relations (4) and (5) are then modified by the replacement

$$\Omega_{z0} \to \Omega_{z0} - kP, \tag{21}$$

and therefore we may obtain the solution for each cold beam by making the replacement, in Eq. (8),

$$l\Omega_{z0} \to l(\Omega_{z0} - kP). \tag{22}$$

The behavior of the actual warm beam will then be given by

$$\overline{\Delta\psi_l} \approx \left\langle (\gamma_0\omega_0)^{-1/2} \int^t dt' e^{-i\int_{t'}^{t} dt''[l\Omega_{\theta 0} + l(\Omega_{z0} - kP)]} \times \left[\frac{\gamma_0(t')}{\omega_0(t')}\right]^{1/2} \sin\left[\int_{t'}^{t} dt''\omega_0\right] F_l(t')\right\rangle_P, \tag{23}$$

where the average is defined over some normalized distribution function in P, i.e.

$$\langle\cdots\rangle_P = \int_{-\infty}^{\infty} dP G(P). \ldots \tag{24}$$

In Eq. (23) we can immediately anticipate the effect of temperature on the behavior of the beam; the entire effect is included in the phase factor, in the term kP. Such a term, when averaged over any reasonable momentum distribution, will give a reduction in amplitude of the average as the "width" of $G(P)$ is increased. Physically this means that the various particles of different energies within the beam receive, when passing through resonance, displacements in slightly different directions. The net effect on the motion of the beam center is therefore reduced. (Though our linearized treatment here necessarily includes a fixed beam size, it may in fact be the case that a warm beam will just expand

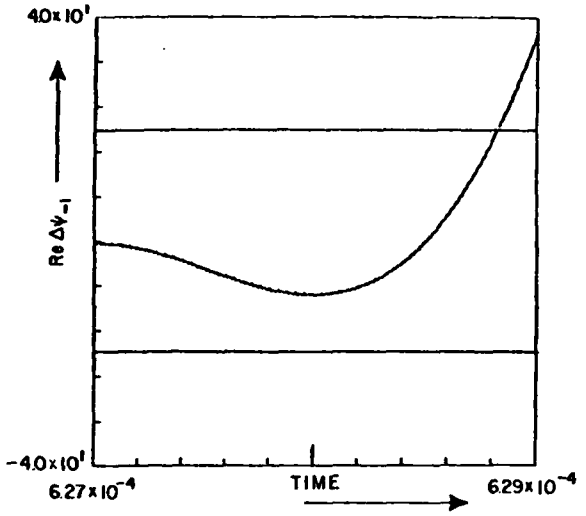

FIGURE 2 Re $(\overline{\Delta\psi_{-1}})$ vs. time for $T_L = 0$.

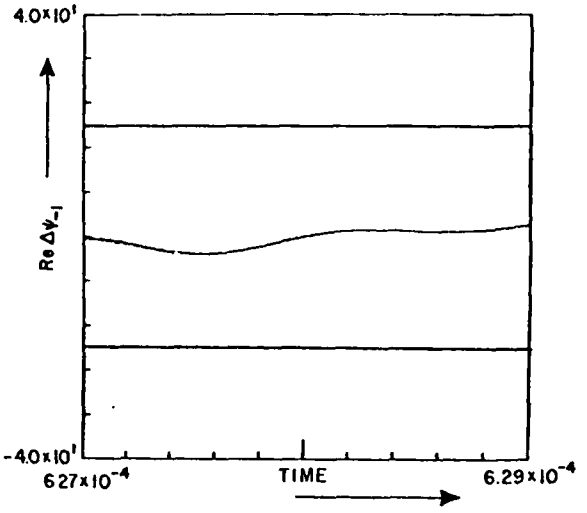

FIGURE 4 Re $(\overline{\Delta\psi_{-1}})$ vs. time for $T_L = 1.0$.

slightly while passing through resonance while the motion of the beam center remains relatively undisturbed.)

As an example, we consider a beam made up of particles having the energy distribution

$$G_E(\Delta\gamma) = \begin{cases} 1/T_L & |\Delta\gamma| < T_L/2 \\ 0 & |\Delta\gamma| > T_L/2 \end{cases}, \qquad (25)$$

where T_L is a measure of the longitudinal temperature and where $\Delta\gamma$ is related to P by Eq. (19). We consider again the hypothetical experiment described in the preceding section. For $\delta f_{-1}/B_{z0} = 5 \times 10^{-3}$ the results of a numerical evaluation of Eq. (23) are shown in Figs. 2-5, which correspond to $T_L = (0., 0.5, 1.0, 2.0)$. In each figure, the real part of $\overline{\Delta\psi_{-1}}$ in centimeters is plotted versus time in seconds. The resonance condition, Eq. (11), is satisfied at the center of the time axis. Total elapsed time is 2.1 μsec. The

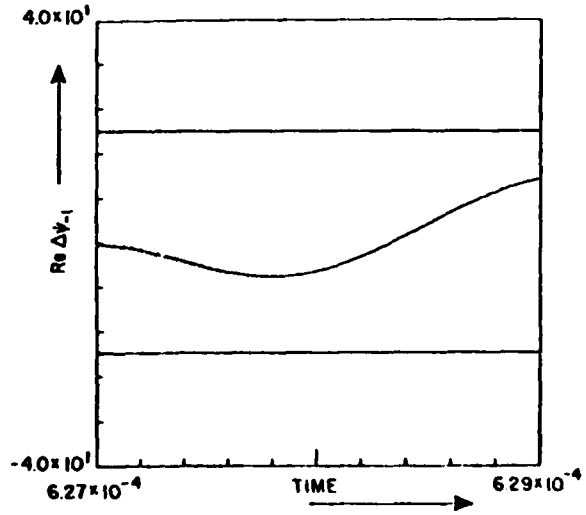

FIGURE 3 Re $(\overline{\Delta\psi_{-1}})$ vs. time for $T_L = 0.5$.

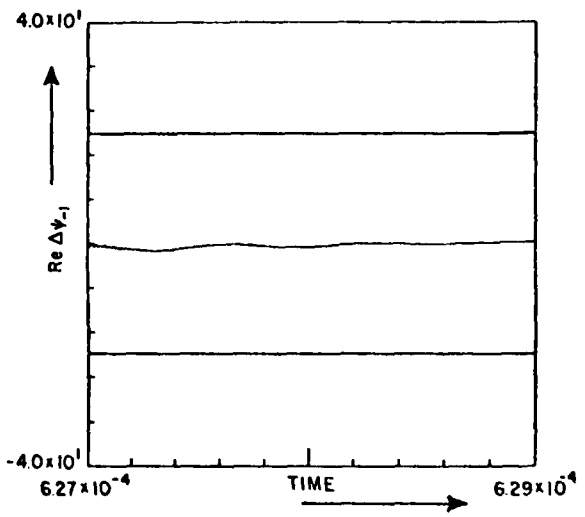

FIGURE 5 Re $(\overline{\Delta\psi_{-1}})$ vs. time for $T_L = 2.0$.

chamber diameter, $2a = 20$ cm is indicated by solid horizontal lines on each plot. We observe that for this example, $T_L = 1.0$, or a 0.5-MeV energy spread, is adequate to smooth out the effect of the resonance. This is the same order of magnitude of spread needed to damp the negative-mass/kink instability in this device[5].

IV. CONCLUSIONS

We have obtained a bound on the magnitude of field errors that can be tolerated in a modified betatron in order that certain integer resonances may be safely passed through. We have found that for practical parameters the bound is extremely restrictive. The basic difficulty stems from the fact that unless the external parameters of the system are changed very quickly, the orbits remain in or near resonance for many betatron oscillations, allowing the displacements to grow to large levels. Such a result suggests that nonlinear effects may play an important role in beam behavior near a resonance. For example, one may ask whether the radial dependence of B_θ would be sufficient to "detune" the resonance as the beam moves a finite but small distance from its equilibrium position. This possibility is receiving further study.

We have also shown that a finite longitudinal beam temperature acts to reduce the effect of the resonance on the motion of the center of the beam. The temperature spread required appears to be comparable, in a specific example, to that needed to stabilize certain microinstabilities.[5] It remains unresolved in this analysis whether the beam expands when passing through a resonance. Such behavior, of course, if severe, could be as unacceptable as large whole-beam displacement.

Should it be possible to achieve significantly lower field errors than those used in our example (0.5%), or if it is possible experimentally to detect and correct by some feedback mechanism the sudden, resonant displacement of the beam, then perhaps lower toroidal fields may be employed initially and be removed either during or following acceleration. The effects of passage through the low-l resonances may thereby be reduced to a tolerably small level.

REFERENCES

1. L. J. Laslett in "Proc. of the 1963 Summer Study on Storage Rings, Accelerators and Experimentation at Super-High Energies" BNL-7534.
2. P. Sprangle and C. A. Kapetanakos, J. Appl. Phys. *49*, 1 (1978).
3. N. Rostoker, Bull. APS. *25*, 854 (1980).
4. Laslett (ERAN-51, Jan 1970 (unpublished)) has discussed certain aspects of the resonance problem in the ERA with a toroidal field. He has derived explicit expressions for ν_r.
5. P. Sprangle and J. L. Vomvoridis, NRL Memorandum Report 4688 (to be published).

APPENDIX D

Mode Coupling in the Modified Betatron

SECURITY CLASSIFICATION OF THIS PAGE (When Data Entered)

REPORT DOCUMENTATION PAGE		READ INSTRUCTIONS BEFORE COMPLETING FORM
1. REPORT NUMBER NRL Memorandum Report 5061	2. GOVT ACCESSION NO.	3. RECIPIENT'S CATALOG NUMBER
4. TITLE (and Subtitle) MODE COUPLING IN THE MODIFIED BETATRON		5. TYPE OF REPORT & PERIOD COVERED Interim report on a continuing NRL problem. 6. PERFORMING ORG. REPORT NUMBER
7. AUTHOR(s) D. Chernin*		8. CONTRACT OR GRANT NUMBER(s)
9. PERFORMING ORGANIZATION NAME AND ADDRESS Naval Research Laboratory Washington, D.C. 20375		10. PROGRAM ELEMENT, PROJECT, TASK AREA & WORK UNIT NUMBERS 61153N; RR011-09-4E; 47-0924-B-3
11. CONTROLLING OFFICE NAME AND ADDRESS Office of Naval Research Arlington, VA 22209		12. REPORT DATE April 19, 1983 13. NUMBER OF PAGES 33
14. MONITORING AGENCY NAME & ADDRESS(if different from Controlling Office)		15. SECURITY CLASS. (of this report) UNCLASSIFIED 15a. DECLASSIFICATION/DOWNGRADING SCHEDULE

16. DISTRIBUTION STATEMENT (of this Report)

Approved for public release; distribution umlimited.

17. DISTRIBUTION STATEMENT (of the abstract entered in Block 20, if different from Report)

18. SUPPLEMENTARY NOTES

*Present address: Berkeley Research Associates, Springfield, VA 22150

This work was supported by the Office of Naval Research.

19. KEY WORDS (Continue on reverse side if necessary and identify by block number)

Modified betatron
Non-linearities
Mode-coupling
Walkinshaw resonance
Frequency shift

20. ABSTRACT (Continue on reverse side if necessary and identify by block number)

The effects of quadratic non-linearities in the single particle equations of motion on electron orbits in the modified betatron are studied. Strong coupling of the two modes of betatron oscillation is found to occur for a particular value of the ratio B_θ/B_z, unless the gradient in the field index takes a certain value. In general, in the azimuthally symmetric case, the mode coupling appears to be quite harmless. When field and/or focusing errors are present the mode coupling

(Continues)

DD FORM 1 JAN 73 1473 EDITION OF 1 NOV 65 IS OBSOLETE
S/N 0102-014-6601

SECURITY CLASSIFICATION OF THIS PAGE (When Data Entered)

20. ABSTRACT (Continued)

reduces the effect on the orbit of the $\ell = 1$ orbital resonance but does not do so sufficiently so that the $\ell = 1$ resonance could be safely passed through in a practical device.

CONTENTS

MODE COUPLING IN THE MODIFIED BETATRON

I. Introduction

For small displacements about a planar reference orbit, particle motion transverse to the toroidal field in the modified betatron may be represented as a linear superposition of two eigenmodes of motion: a "fast" mode, corresponding to gyration about the toroidal field lines and a "slow" mode, corresponding to an $\vec{F}x\vec{B}$ drift motion, where here the force $\vec{F}$ is due to the weak focusing betatron fields, space charge forces, and induced (wall image) fields. The linear theory of orbits in the modified betatron has been worked out in some detail[1-5] and will only be reviewed as needed here. In the present paper we will mainly discuss the effect of quadratic non-linearities on the motion.

Non-linear terms in the equations of motion become important to consider if: (1) displacements from the reference orbit become large, due say to the method of injection used or due to the operation of an instability of some kind, (2) strong non-linearities (e.g. large values of $\partial n/\partial r$) are present in the magnet design, or (3) the non-linear term itself contains a resonant part. In the following we will illustrate two effects of quadratic non-linearities on single particle motion, viz. the amplitude dependence of the betatron frequencies and the exchange of energy between the oscillation modes under certain conditions. These conditions turn out to be analogous to the so-called Walkinshaw resonance[6] in accelerators without a toroidal magnetic field[7-11]. We will limit ourselves here to consideration of single particle motion only, neglecting the effects of self fields; the treatment here then will only be valid for fairly large values of γ in high current devices, such that $\nu/\gamma \ll 1$, where ν is Budker's parameter.

Four sections follow. In the first we introduce some notation and sketch the derivation of the equations of motion to second order in displacements from and transverse velocities about the reference orbit, taken to be a circle in the symmetry plane. In the second section the equations of motion are solved

Manuscript approved February 15, 1983.

perturbatively and a condition for the generalized Walkinshaw resonance is obtained. Under this condition we study the behavior of the betatron oscillations, giving a numerical example as illustration. As an interesting result we find a particular value of field index gradient for which the resonance ceases to have any effect on particle motion.

In these first two sections the discussion will assume that all applied fields are azimuthally symmetric. In the presence of field perturbations other orbital resonances may occur and it is interesting to ask whether the amplitude dependence of the betatron frequencies induced by the non-linearities are sufficient to keep the oscillation amplitudes at finite, but tolerably small values. Though in general this is a difficult question we will discuss a special, simple case in the third section of this paper in which the Walkinshaw resonance coincides with both an integer and half-integer orbital resonance.

A final section summarizes these results and states some conclusions and conjectures.

II. The Equations of Motion

The geometry of the modified betatron is shown in Fig. 1. We employ standard (r,θ,z) cylindrical coordinates. The exact equations of motion, using θ in favor of time for our independent variable, are written

$$\frac{d}{d\theta}\left[r'(r'^2 + r^2 + z'^2)^{-1/2}\right] = r(r'^2 + r^2 + z'^2)^{-1/2} + \lambda^{-1}\,(rB_z - z'B_\theta) \quad (1)$$

$$\frac{d}{d\theta}\left[z'(r'^2 + r^2 + z'^2)^{-1/2}\right] = \lambda^{-1}\,(r'B_\theta - rB_r) \quad (2)$$

where $\vec{B}$ is any suitable function of position (r,θ,z), $\lambda \equiv -mc^2\beta\gamma/e$, e and m are the magnitudes of the electron charge ($e > o$) and mass, β and γ are the usual relativistic factors, c is the speed of light and a prime ($'$) denotes $d/d\theta$.

We shall assume that B_r vanishes on the plane $z = 0$ and take all fields to be independent of θ. (The assumption of azimuthal symmetry will be relaxed in Section IV, below.) We take the equilibrium orbit of a particle of relativistic factor γ_o at $r = r_o$, $z = 0$, so

$$\lambda = -\,r_o\,B_z(r_o,o). \quad (3)$$

Let us now define the normalized coordinates $x \equiv (r - r_o)/r_o$ and $y \equiv z/r_o$. The vector potential is given correctly to third order by

$$A_\theta \cong r_o B_{zo}\left[1 + \frac{1-n}{2}\,x^2 + \frac{n}{2}\,y^2 - \frac{n_2}{2}\,xy^2 + \frac{1}{6}\,(n + n_2 - 3)\,x^3\right] \quad (4)$$

where B_{zo}, n, and n_2 are constants. The corresponding fields are

$$B_r \cong -\,B_{zo}\,[n - n_2 x]y \quad (5)$$

$$B_z \cong B_{zo}\left[1 - nx + \frac{n_2}{2}x^2 + \frac{n-n_2}{2}y^2\right] \tag{6}$$

from which n_2 is identified as the second radial logarithmic derivative of B_z. The toroidal field is assumed to be given by

$$B_\theta = B_{\theta o}/(1+x) \cong B_{\theta o}(1-x + \ldots) \tag{7}$$

where $B_{\theta o}$ is the value of the toroidal field at the reference orbit, $x = y = 0$.

Using the fields (5,6,7) in the equations of motion (1,2) and keeping terms only of quadratic order gives the coupled equations:

$$x'' + (1-n)x = by' + (2n-1-\frac{n_2}{2})x^2 - (\frac{n-n_2}{2})y^2 + \frac{1}{2}(x'^2 - y'^2) \tag{8}$$

$$y'' + ny = -bx' - (2n-n_2)xy + x'y' \tag{9}$$

where $b \equiv B_{\theta o}/B_{zo}$. These equations, (8) and (9), are our starting points. In the following section we examine the behavior of an approximate solution to (8) and (9) for various values of n, n_2, and b.

III. Perturbative Solution of Equations of Motion

In general the quadratic terms in (8,9) will be small so we attempt to treat the equations perturbatively. Neglecting the non-linear terms altogether one has the solution to the linear equations:

$$\begin{pmatrix} x \\ y \end{pmatrix} = A_f \begin{pmatrix} 1 \\ \dfrac{ib\nu_f}{\nu_f^2 - n} \end{pmatrix} e^{i\nu_f\theta} + A_s \begin{pmatrix} 1 \\ \dfrac{ib\nu_s}{\nu_s^2 - n} \end{pmatrix} e^{i\nu_s\theta} + \text{c.c.} \tag{10}$$

where A_f and A_s are complex numbers depending on particle initial conditions and the frequencies are given by

$$\nu_{\substack{f \\ s}} = \left[\frac{b^2+1 \pm [(b^2+1)^2 - 4n(1-n)]^{1/2}}{2}\right]^{1/2}. \tag{11}$$

The subscripts f and s are used here and below to label the amplitudes and frequencies of the fast and slow oscillation modes. We will assume that the linear motion is stable, that is $n(1-n) > 0$.

We may calculate the correction to (10) due to the non-linear terms by inserting (10) in (8,9) and resolving. The resulting equations will be inhomogeneous with various "driving" terms at the frequencies $2\nu_f$, $2\nu_s$, 0, and $\nu_f \pm \nu_s$. Consequently, the non-linear correction to (10) will remain small unless it happens that

$$\nu_f - \nu_s = \nu_s \tag{12}$$

the condition for which, from (11), being

$$b^2 = \frac{5}{2}\,[n(1-n)]^{1/2} - 1. \tag{13}$$

In the absence of a toroidal field, (13) is satisfied for n = 0.2 or 0.8 which we identify as the Walkinshaw resonance[6], the consequences of which were first observed in cyclotrons[12]. We proceed to examine particle behavior on this resonance in the modified betatron.

On resonance conventional perturbation theory fails and one must resort to some other method. A multiple "time" scale analysis of the problem gives a solution of the form (10) in which the complex amplitudes A_f and A_s are no longer strictly constant but vary slowly with θ; they are found to obey the equations

$$\frac{dA_s}{d\theta} = i\Gamma_1(n,n_2)A_f A_s^* \tag{14}$$

$$\frac{dA_f}{d\theta} = i\Gamma_2(n,n_2)A_s^2 \tag{15}$$

where $\Gamma_{1,2}$ are two real valued functions of the field indices n and n_2,

$$\Gamma_1 = \frac{\nu_s^2 - n}{6\nu_s^3}\left[2n + 6\nu_s^2 + n_2\left(\frac{2\nu_s^2 + n}{\nu_s^2 - n}\right)\right]$$

$$= -4\left(\frac{\nu_s^2 - n}{\nu_f^2 - n}\right)\Gamma_2 \tag{16}$$

and where, on resonance, we have

$$\nu_f^2 = 4\nu_s^2 = 2(n(1-n))^{1/2}. \tag{17}$$

(An asterisk denotes complex conjugate in (14).)

The question of orbital stability on resonance is thus reduced to the

question of the behavior of the mode amplitudes in (14) and (15).

The equations (14) and (15) may be completely solved in a straightforward manner; the solution is obtained and discussed in the Appendix. To settle the stability issue, however, it is sufficient to note that there is a simple integral of motion

$$\frac{1}{2}\Gamma_1 |A_f|^2 + \frac{1}{2}\Gamma_2 |A_s|^2 \equiv D/\Gamma_1, \tag{18}$$

and consequently the motion is necessarily bounded if $\Gamma \equiv \Gamma_1 \Gamma_2 \geq 0$ which, in fact is true for all n and n_2, as follows from (16). On this resonance energy is simply exchanged back and forth between the fast and slow modes of motion.

Though we have argued that particle motion is bounded on this resonance we have not in fact specified a bound or showed that the bound is acceptable, in terms of some machine aperture. One might conjecture, from (18), that if one of $\Gamma_{1,2}$ were significantly larger than the other then transfer of energy from the more "stiff" (larger Γ coefficient) mode to the less "stiff" mode would result in increasing particle oscillation amplitude. Hence one would be concerned if, from (16), either $\nu_s^2 = n$ or $\nu_f^2 = n$. It follows from (17) and (18), however, that this can occur only for b = 0, n = .2 or .8. If n is chosen so that b is O(1) when the resonance is crossed then Γ_1 and Γ_2 are of the same order of magnitude and one expects this resonance to be quite harmless. For specific initial conditions it is possible to find a bound by calculating the turning point of a certain particle-in-a-well problem, as shown in the Appendix.

Curiously, one can render this resonance completely inoperative for any particular n by choosing n_2 so that Γ_1 and Γ_2 both vanish. From (16) and (17) this value is found to be

$$n_2 = \hat{n}_2 \equiv \frac{1}{2}\left[\frac{7n - 3 + 4[(1-n)n]^{1/2}}{1 + [(1-n)/n]^{1/2}}\right] \qquad (19)$$

Choosing this value ensures that the mode amplitudes remain constant when passing through the "exchange" resonance.

We proceed to illustrate some of these results using a simple single particle numerical orbit integration. The algorithm includes the fields (5-7) but does not use an expansion of the force or acceleration. Figures 2 and 3 show the solutions to equations (14-15) and (1-2) respectively for the case $n = 0.5$, $n_2 = \hat{n}_2 = 0.625$, $b = 0.5$. The mode amplitudes are strictly constant, no exchange occurs, and the particle orbit projection retraces itself in a stable manner over and over again. We contrast this case with that illustrated in Figures 4 and 5 for which the parameters are again $n = 0.5$ and $b = 0.5$ but now with $n_2 = 0$. Now the mode amplitudes oscillate; one rises while the other falls in order to conserve D (Eq (18)). The oscillation period, from Equation (16) in the Appendix, is 46.6 major periods for the particular initial conditions chosen. The particle orbit projection now simply (and harmlessly) rotates slowly counter-clockwise.

Our conclusion is that in the case of azimuthally symmetric fields the generalized Walkinshaw resonance is quite harmless in the modified betatron. The exchange of energy between fast and slow modes is expected to cause no major changes in the beam dimensions. When azimuthal field variations are present, however, the situation changes dramatically due to a coincidence described in the next section.

IV. A Triple Coincidence Resonance

When n = 1/2 (the case illustrated in Figures 2-5) the values of the tunes ν_f and ν_s at the exchange resonance (13) are $\nu_f = 1$, $\nu_s = 1/2$; therefore in the presence of field and focusing errors the generalized Walkinshaw resonance coincides with an integer and a half integer orbital resonance. This triple coincidence allows us to study in detail in this special case the effect of mode coupling (and the amplitude dependence of the betatron frequencies) on the orbit at an integer and half integer resonance. Though the restriction to n = 1/2 is necessary for there to be a true coincidence, if n is near but not exactly 1/2, the three resonances will be "nearby" and will occur nearly simultaneously and the analysis below should still hold in an approximate way.

At the triple coincidence resonance the mode evolution equations become

$$\frac{dA_s}{d\theta} = i\Gamma_1 A_f A_s^* + \varepsilon_1 A_s^* \tag{20}$$

$$\frac{dA_f}{d\theta} = i\Gamma_2 A_s^2 + \varepsilon_2 + \varepsilon_3 A_f^* . \tag{21}$$

The ε's in (20) and (21) are complex constants proportional to certain Fourier coefficients in expansions of the fields and their gradients; specifically, ε_1 is due to an $\ell = 1$ term in the field gradient, leading to a half integer resonance, ε_2 is due to an $\ell = 1$ term in the field, leading to an integer resonance, and ε_3 is due to an $\ell = 2$ term in the field gradient, leading to a "2-halves" integer resonance. Were they present alone (i.e. with no non-linearity) in (20) and (21) the field imperfection terms are observed to lead to the usual linear and/or exponential growth characteristic of integer and/or half integer resonances. In the presence of mode coupling the situation is much less clear. Since, as they stand, equations (20) and (21) cannot be solved analytically we

must in general resort to numerical integration. First let us comment on what we might expect to see in the solution.

The field imperfection terms in (20) and (21) act roughly speaking as source terms, pumping energy from longitudinal to transverse motion. If this energy flow continues, and if there is no mechanism to return this energy to longitudinal motion the result is disastrous -- a linear orbital resonance. Non-linearities, however, can shift the betatron frequency of the resonant particle off resonance for some finite amplitude of betatron oscillation. (The quantity $(n_2 - \hat{n}_2)$ is presumably a measure of the frequency shift induced by a given amplitude oscillation.) In practice though one can not say a priori how much frequency shift will be sufficient to terminate the growth of the resonant mode. A numerical study seems to be essential.

For a numerical example we will examine the effect of the non-linear terms in (20) and (21) on an integer resonance, that is, in the following we shall take $\epsilon_1 = \epsilon_3 = 0$. Cases have been examined numerically for various other combinations of values for the ϵ's with no major differences appearing in the results.

In Figures 6 and 7 we illustrate the mode amplitudes and orbit projection for a pure integer resonance with no mode coupling ($n_2 = \hat{n}_2 = 0.625$, $\epsilon_2 = .005$). The (resonant) fast mode amplitude grows linearly without limit; the (decoupled) slow mode stays at a fixed, small value. The particle orbit size (Figure 7) consequently grows continuously.

Turning on the mode coupling changes the behavior of the mode amplitudes dramatically but has little apparent effect on the particle orbit, which still appears to grow to intolerable size. This is illustrated in Figures 8 and 9 where we see that the mode amplitudes grow to a certain size and then turn over -- presumably a reflection of the detuning of the resonance due to the frequency shift. The "turnover", however, is at extremely large amplitudes (Recall that

the mode amplitudes are normalized to the radius of the device, r_o.), therefore the particle motion appears to be relatively unaffected, practically speaking, by changing n_2 from 5/8 to 0. This result does suggest though that by increasing $|n_2 - \hat{n}_2|$ we might reduce the resonant response to a tolerable value.

Figures 10-11, 12-13, and 14-15 show our results for $n_2 = -1.$, $-4.$, and $-10.$ respectively. We see that as $|n_2 - \hat{n}_2|$ is increased the mode turnover amplitude is reduced and the particle orbit becomes somewhat more compact, staying within the plot boundaries for significantly longer times. (Even so, the transverse orbit size is rather large, even for the largest values of $|n_2 - \hat{n}_2|$ we have tried.)

These results suggest that to stabilize the $\ell = 1$ resonance a significant non-linearity (large value of n_2) could be intentionally introduced in the betatron field. One must be careful in drawing this conclusion, however, because such a non-linearity has well known adverse effects, among them a sensitivity of the behavior of the orbit to initial conditions; that is, only some special class of particles may be confined while others are lost. Also, if n_2, which is effectively the radial derivative of n, is very large, it then becomes difficult to keep n itself within the stable range $0 \leq n \leq 1$ everywhere within the aperture. Consequently we conclude that, as a practical matter, it is best <u>not</u> to rely on non-linearities to stabilize the $\ell = 1$ resonance in the modified betatron and to design the machine with a flat radial index profile. Avoidance of this resonance as well as other low order resonances - - which then becomes the only reasonable experimental alternative - - is possible in principle by accelerating with constant b (i.e. $B_{\theta o} \propto B_{zo}$), thereby keeping the tunes fixed[5] - - except for the tune shift due to space charge, which affects the fast mode tune only very slightly for large B_θ; the slow mode tune can generally be chosen to be very small (~ .2 - .3) for all time.

V. Summary and Conclusions

We have examined the effects of mode coupling on single particle orbits in the modified betatron. We find that a generalization of the Walkinshaw (exchange) resonance can occur for any value of field index in the range $.2 \leq n \leq .8$ but that its effect on particle orbits in general is quite modest (Figures 2-5) and may be rendered completely ineffective by a special choice of field index gradient (19).

When n is near 1/2 the exchange resonance coincides with both integer and half integer resonances. An examination of orbit behavior at this triple coincidence shows that, as a practical matter, the amplitude dependent frequency shift in the betatron oscillation due to mode coupling is <u>not</u> sufficient to stabilize the $\ell = 1$ integer resonance (though presumably, as in the case of accelerators not employing toroidal fields, higher order resonances will be subject to non-linear stabilization[8]). This fact makes it advisable to allow, in the design of an experiment, for acceleration with constant or nearly constant ratio $B_{\theta o}/B_{zo}$ thereby holding the tunes approximately fixed in time.

VI. Acknowledgment

This work was supported by the Office of Naval Research.

Appendix

In this Appendix we discuss the solution to Equations (14) and (15) in the text. Writing

$$A_f = a_f \exp(i\phi_f) \qquad A_s = a_s \exp(i\phi_s) \tag{A1}$$

where $a_{f,s}$ and $\phi_{f,s}$ are real we find in a straightforward way an equation for $\rho \equiv \frac{1}{2} a_s^2$:

$$\frac{1}{2} \rho'^2 + V(\rho) = 0 \tag{A2}$$

where

$$V(\rho) = 4\Gamma\rho^3 - 4D\rho^2 + \frac{1}{2} C^2$$

$$\Gamma = \Gamma_1 \Gamma_2$$

$$C = \Gamma_1 a_f a_s^2 \cos(\phi_f - 2\phi_s) = \text{constant}$$

and the constant D is defined in the text, Eq. (18). The other quantities are given in terms of ρ by

$$a_s = (2\rho)^{1/2} \tag{A3}$$

$$\phi_s' = C/(2\rho) \tag{A4}$$

$$A_f = \frac{1}{2\rho\Gamma_1} (C - i\rho') \exp(2i\phi_s). \tag{A5}$$

These expressions hold for $\rho > 0$. If $\rho = 0$ at $\theta = 0$, say, then, from (14) and (15) $A_s \equiv 0$ and A_f remains fixed for all $\theta > 0$. The modal frequency shifts are given directly by (A4) for the slow mode and may be obtained from (A5) for the fast mode.

It may be shown that $V(\rho)$ has one negative and two positive roots. Denoting these by $\rho_{1,2,3}$ with $\rho_1 > \rho_2 > 0 > \rho_3$ we find that the exchange period (period of $\rho(\theta)$) is given by

$$\left(\frac{2}{\Gamma(\rho_1 - \rho_3)}\right)^{1/2} K(m) \qquad \text{(A6)}$$

where $m = (\rho_1 - \rho_2)/(\rho_1 - \rho_3)$ and where K is the usual complete elliptic integral.[13]

The special cases $C = 0$ and $\Gamma = 0$ lead to motion of infinite period and ρ = constant, respectively.

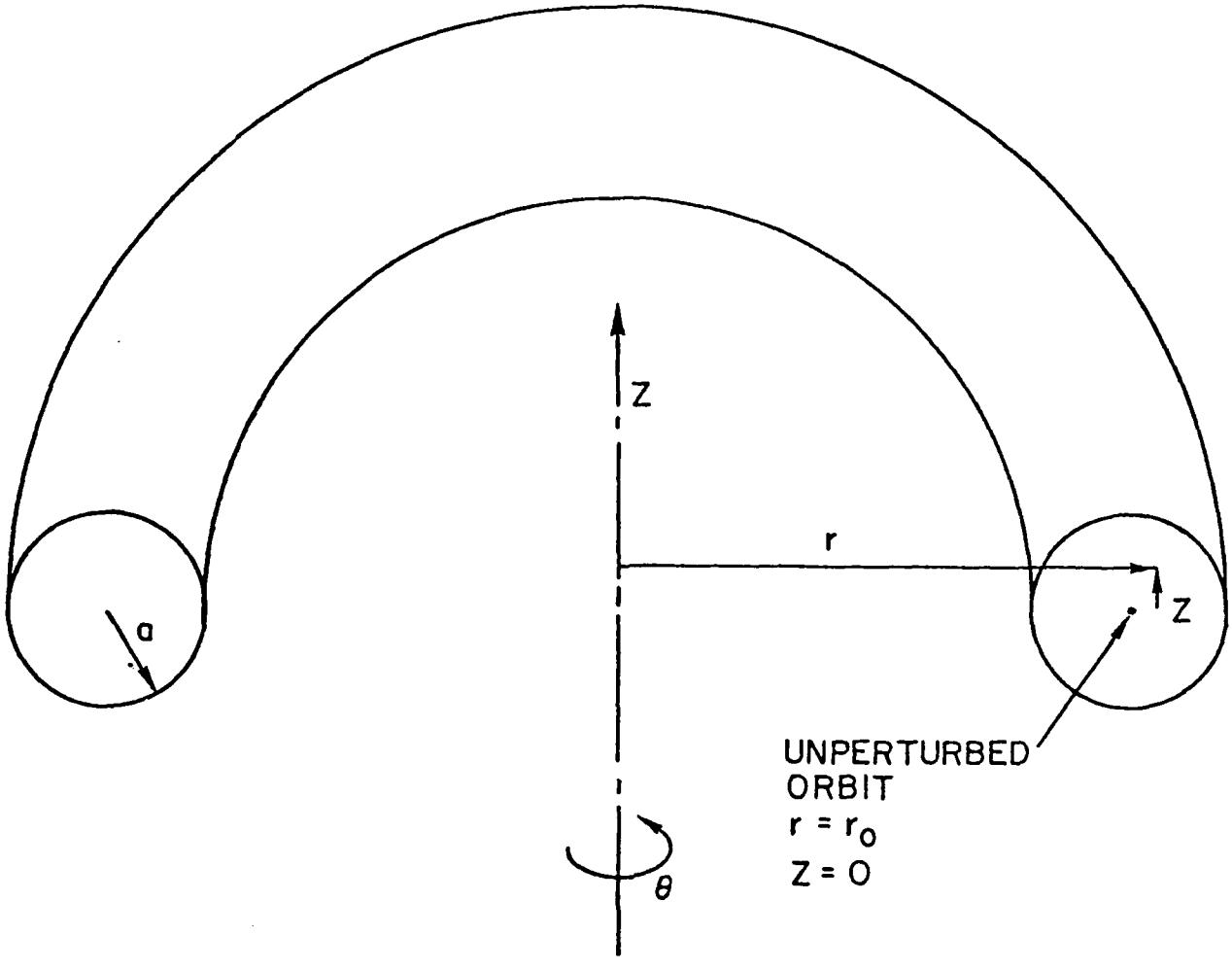

Fig. 1: Geometry of the modified betatron

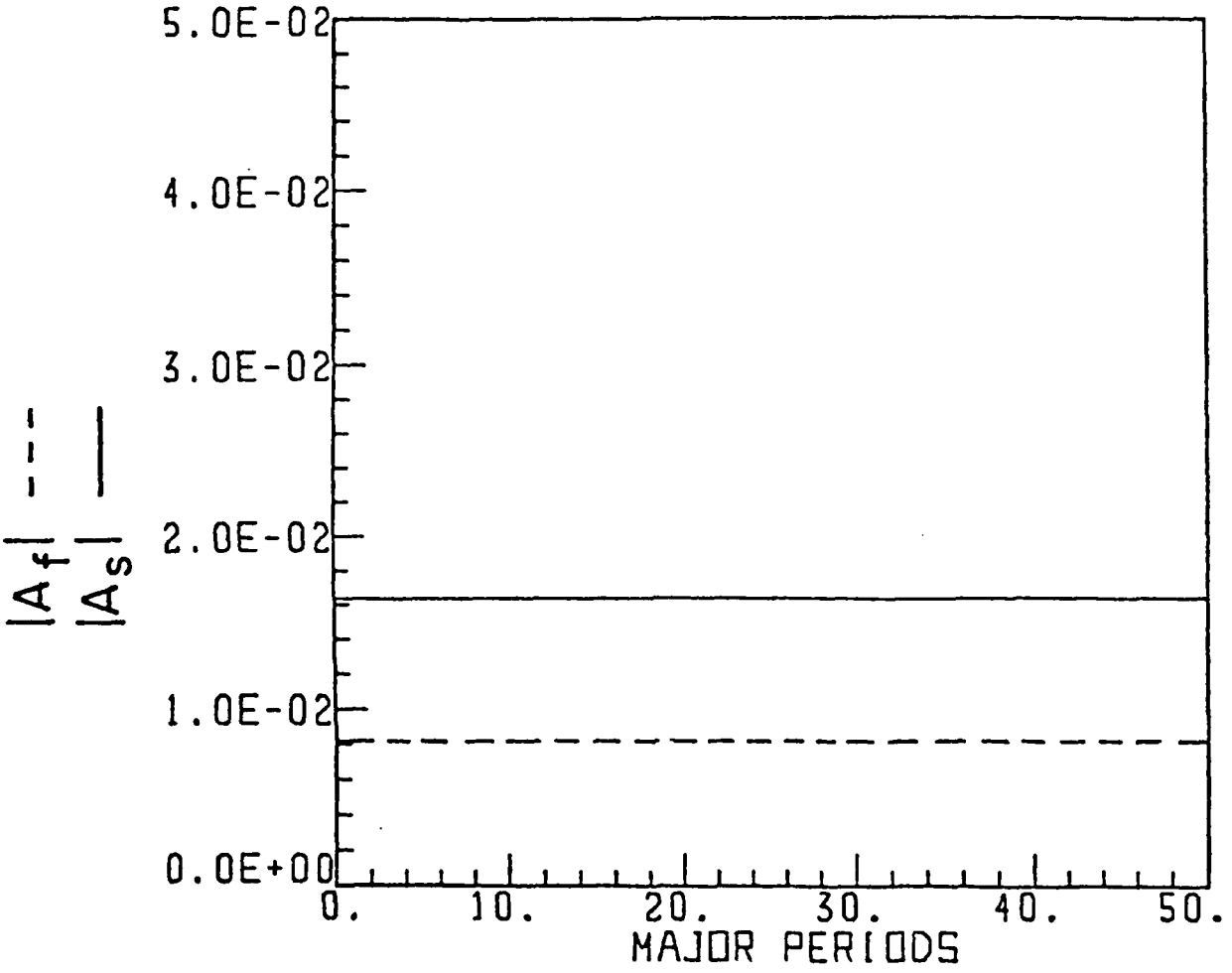

Fig. 2: $|A_f|$, $|A_s|$ vs. major periods (A major period is a change of θ by 2π.) $n = 1/2$; $n_2 = 5/8$. Initial ($\theta = 0$) values of $A_f = 5.7735 \times 10^{-3}(1 - i)$ and $A_s = 2A_f^*$ correspond to those of a particle initially at $x = y = .02$ with zero transverse velocity. The same initial values are used in all subsequent figures.

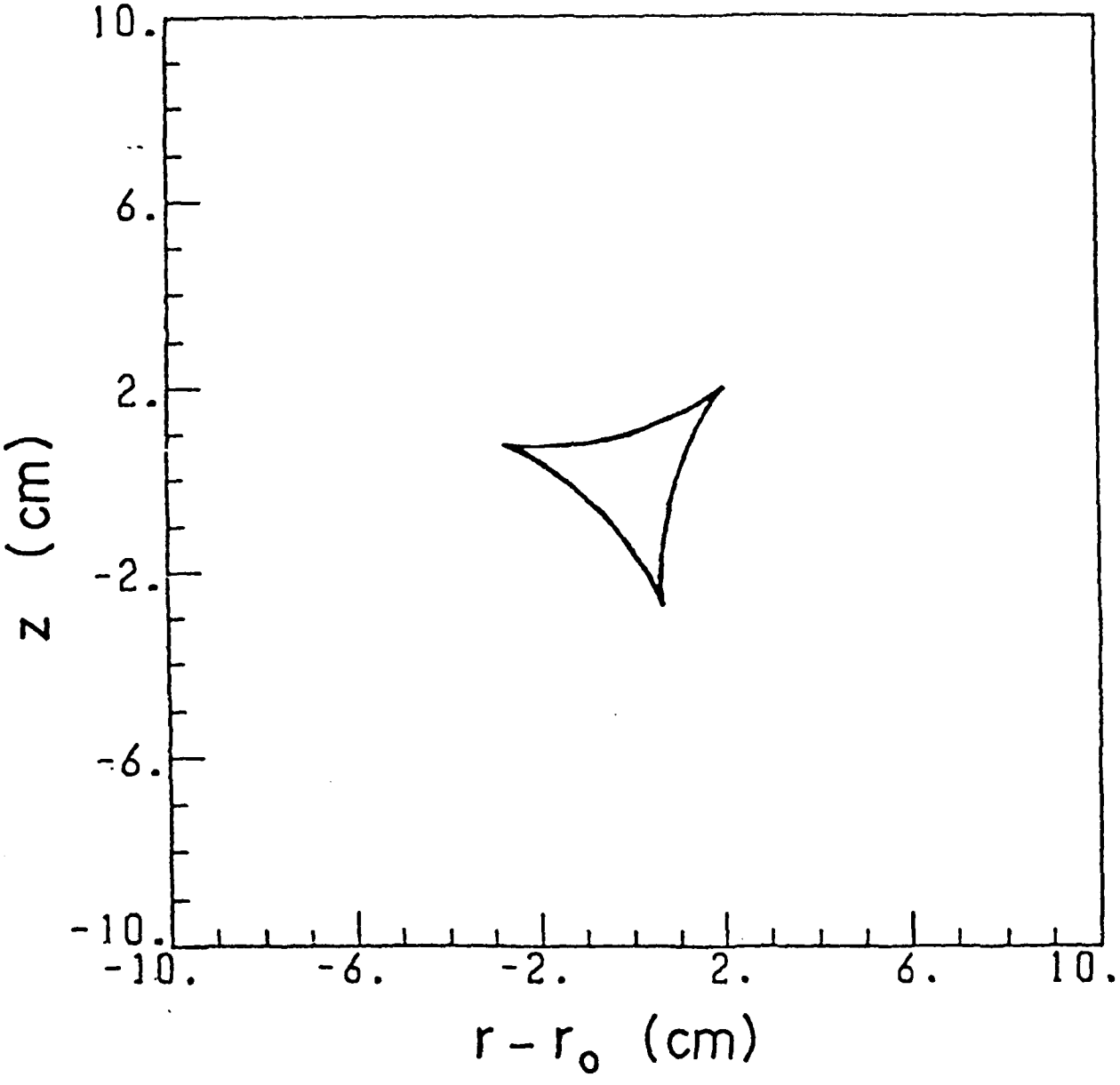

Fig. 3: z vs. $r - r_o$; $n = 1/2$; $n_2 = 5/8$. For this and subsequent figures, $r_o = 100$ cm, $B_{zo} = 118.092$ gauss, $B_{\theta o} = 1/2\ B_{zo}$, and initial values are $r - r_o = z = 2$cm, $r' = z' = 0$, $\gamma_o = 7$.

AD-A134 068 RESEARCH ON INTENSE ELECTRON BEAMS AND APPLICATIONS(U) 2/2
BERKELEY RESEARCH ASSOCIATES INC CA D CHERNIN ET AL.
AUG 83 PD-BRA-83-302R N00014-81-C-2371

UNCLASSIFIED F/G 20/7 NL

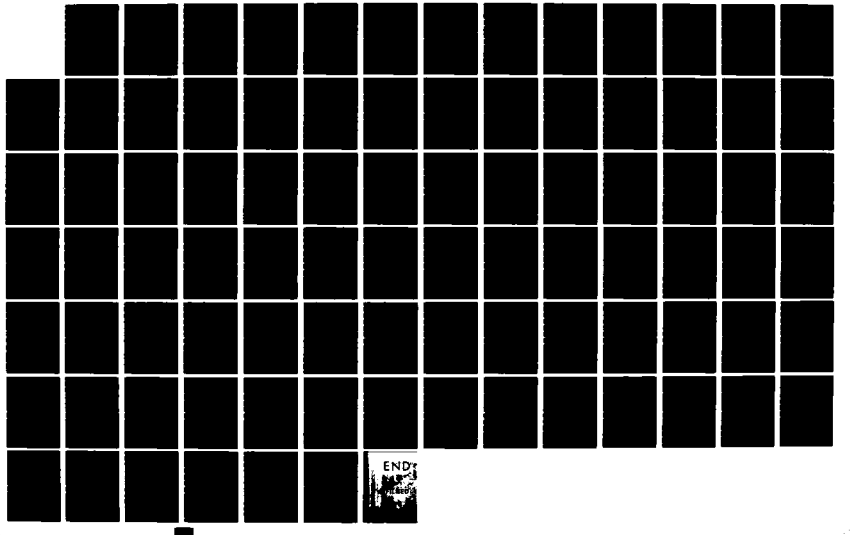

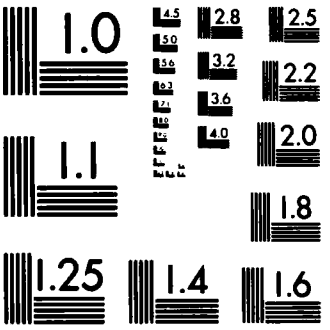

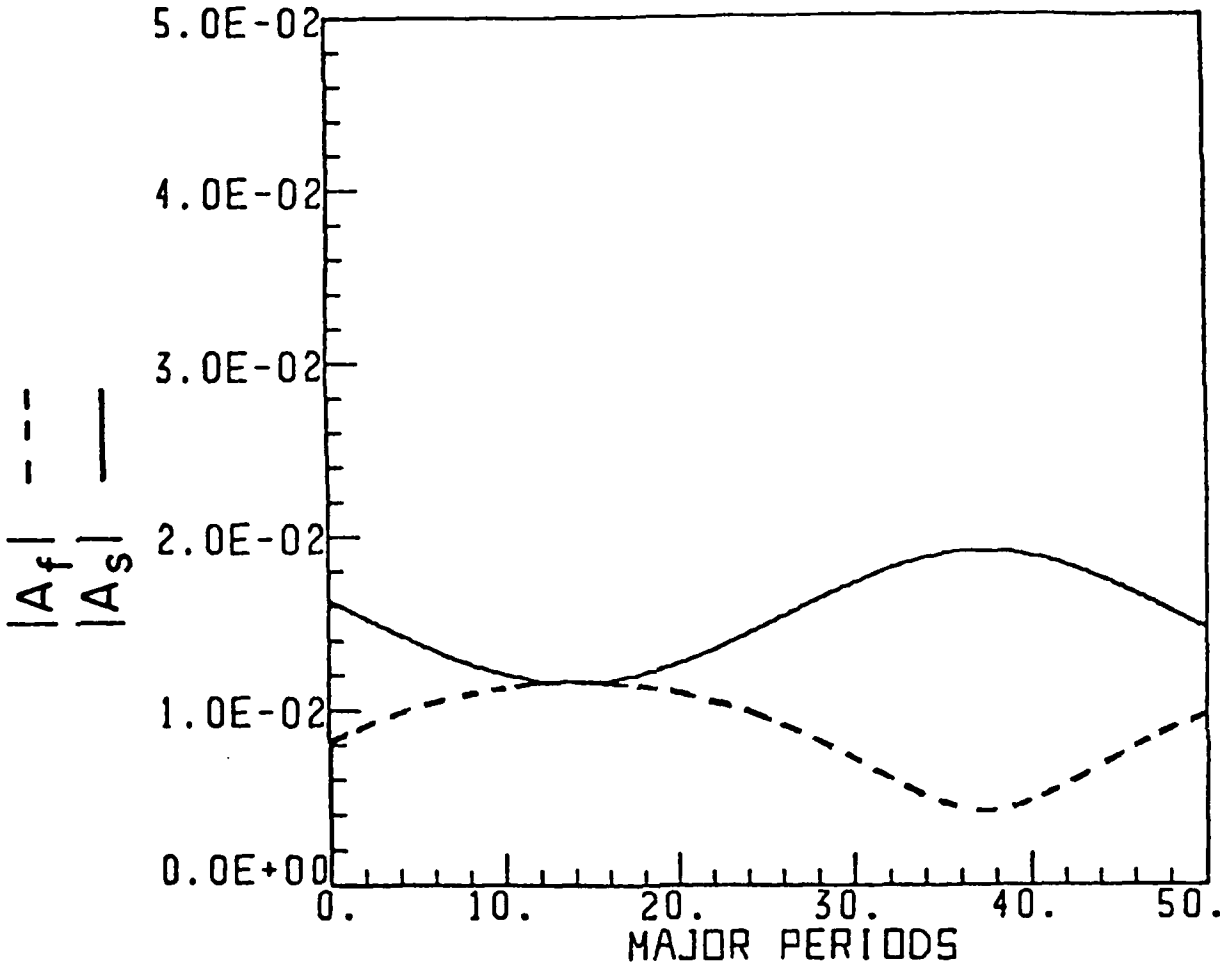

Fig. 4: $|A_f|$, $|A_s|$ vs. major periods; $n = 1/2$; $n_2 = 0$.

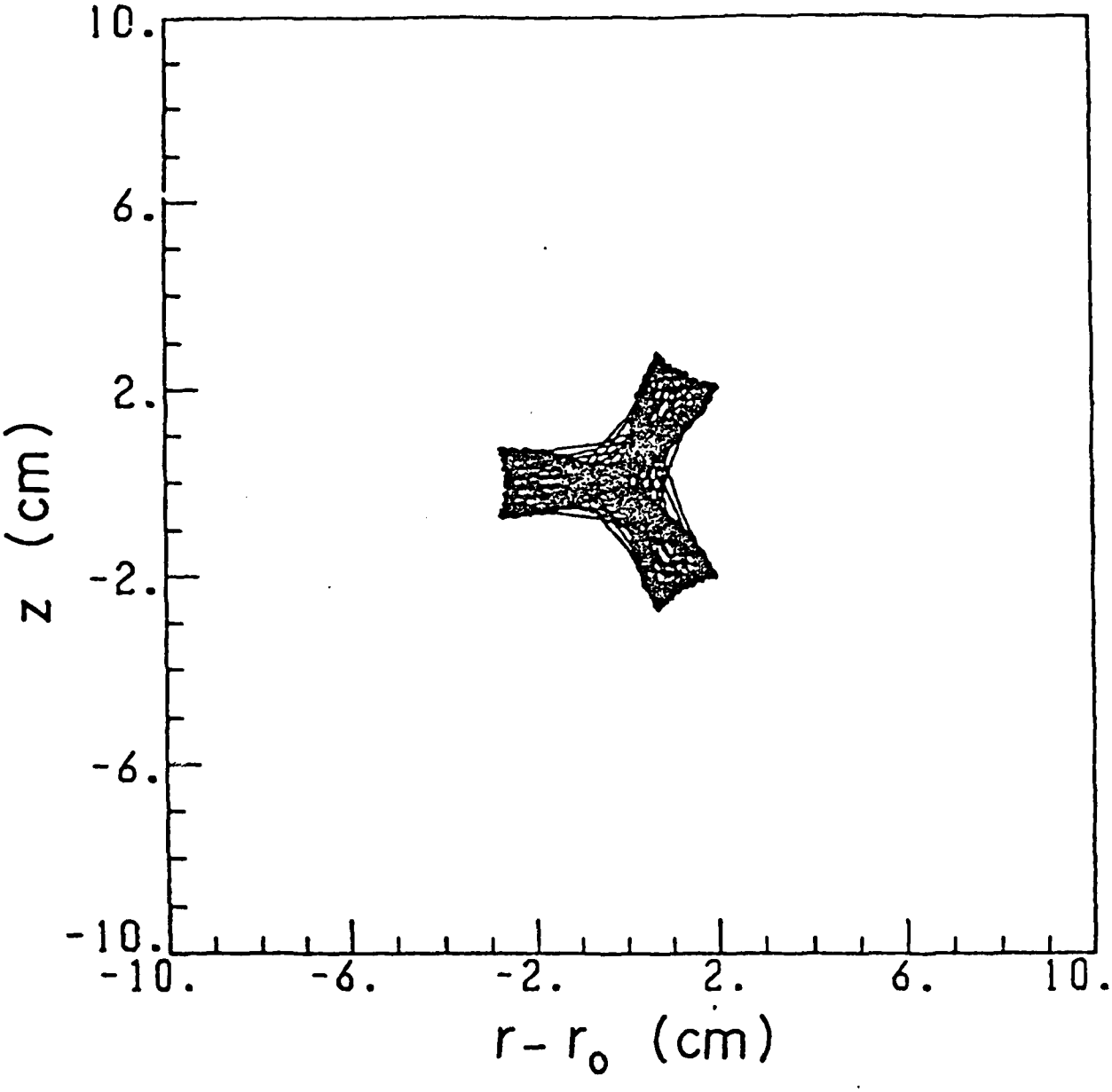

Fig. 5: z vs. $r - r_o$; $n = 1/2$; $n_2 = 0$.

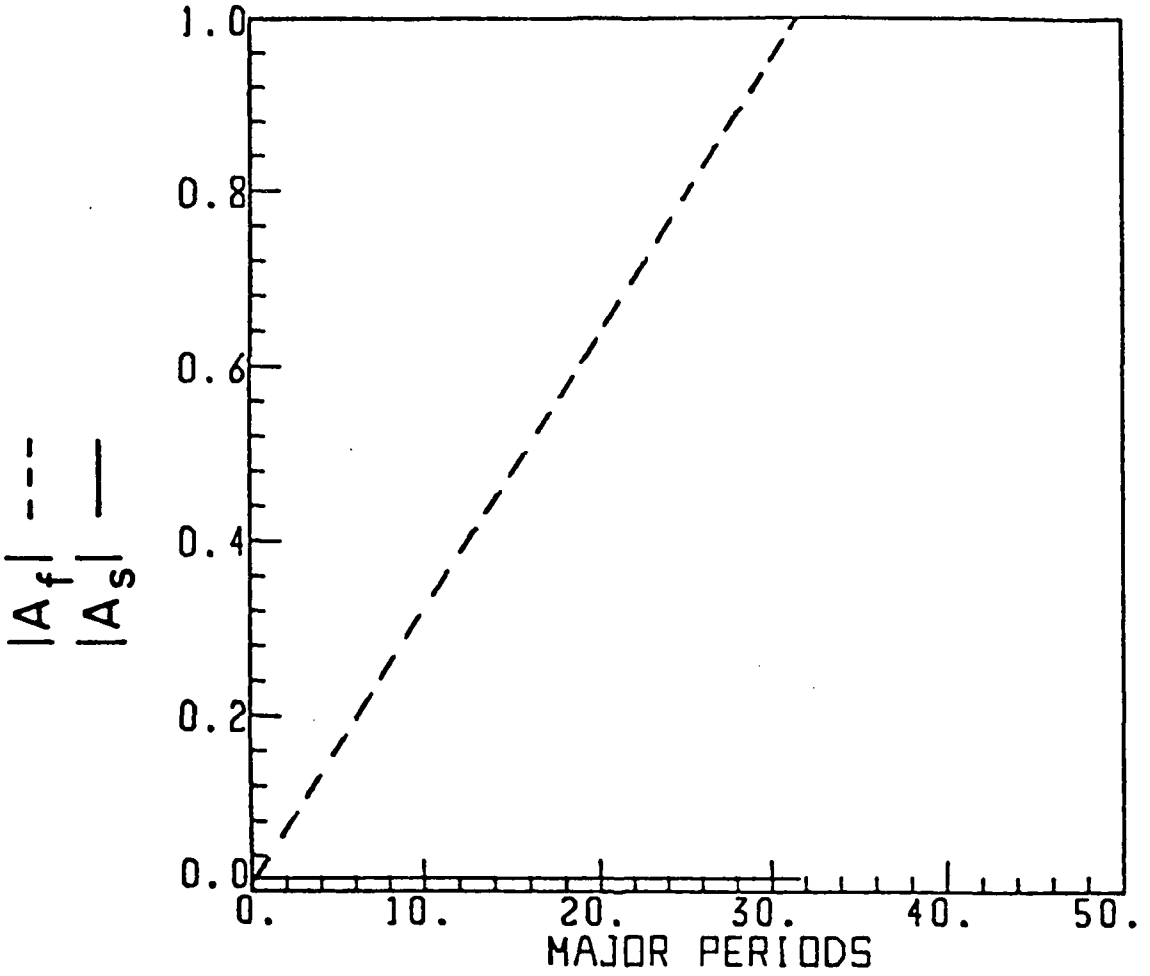

Fig. 6: $|A_f|$, $|A_s|$ vs. major periods; $n = 1/2$; $n_2 = 5/8$; $\varepsilon_1 = \varepsilon_3 = 0$; $\varepsilon_2 = 5 \times 10^{-3}$.

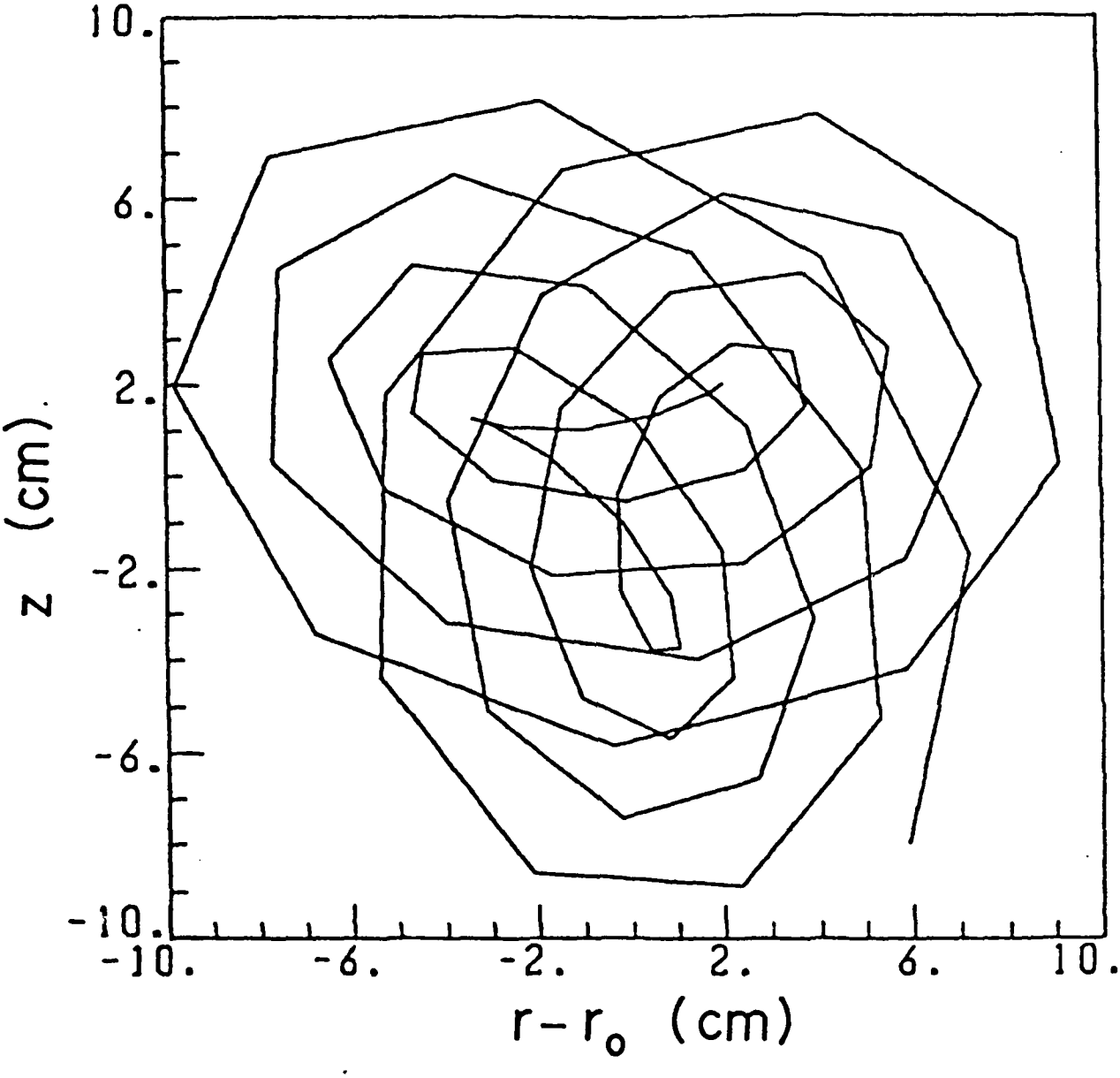

Fig. 7: z vs. $r - r_o$; $n = 1/2$; $n_2 = 5/8$; $\delta B = 0.5$ gauss in $\ell = 1$ Fourier mode. Particle leaves plot area after ~ 9 major periods.

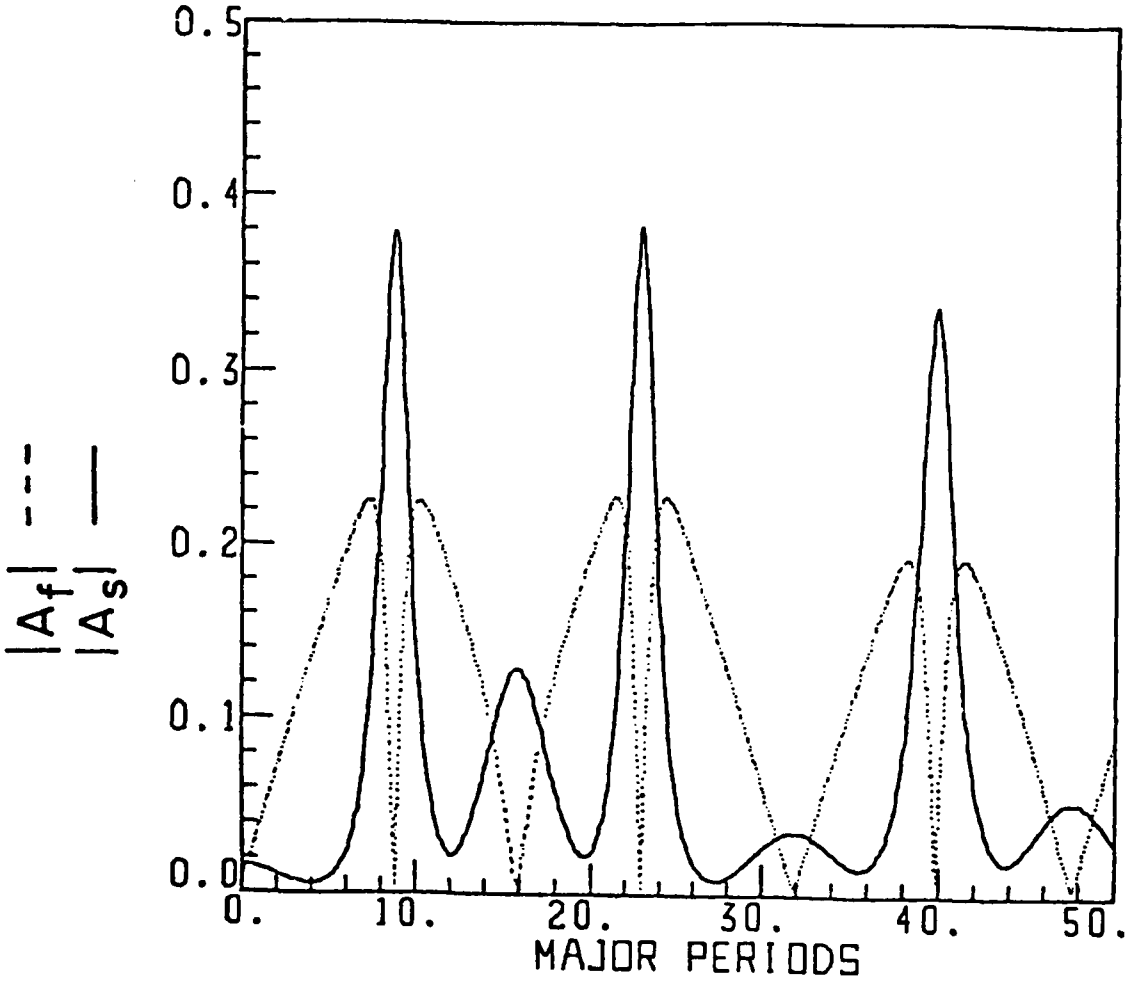

Fig. 8: $|A_f|$, $|A_s|$ vs. major periods; $n = 1/2$; $n_2 = 0$; $\varepsilon_1 = \varepsilon_3 = 0$; $\varepsilon_2 = 5 \times 10^{-3}$.

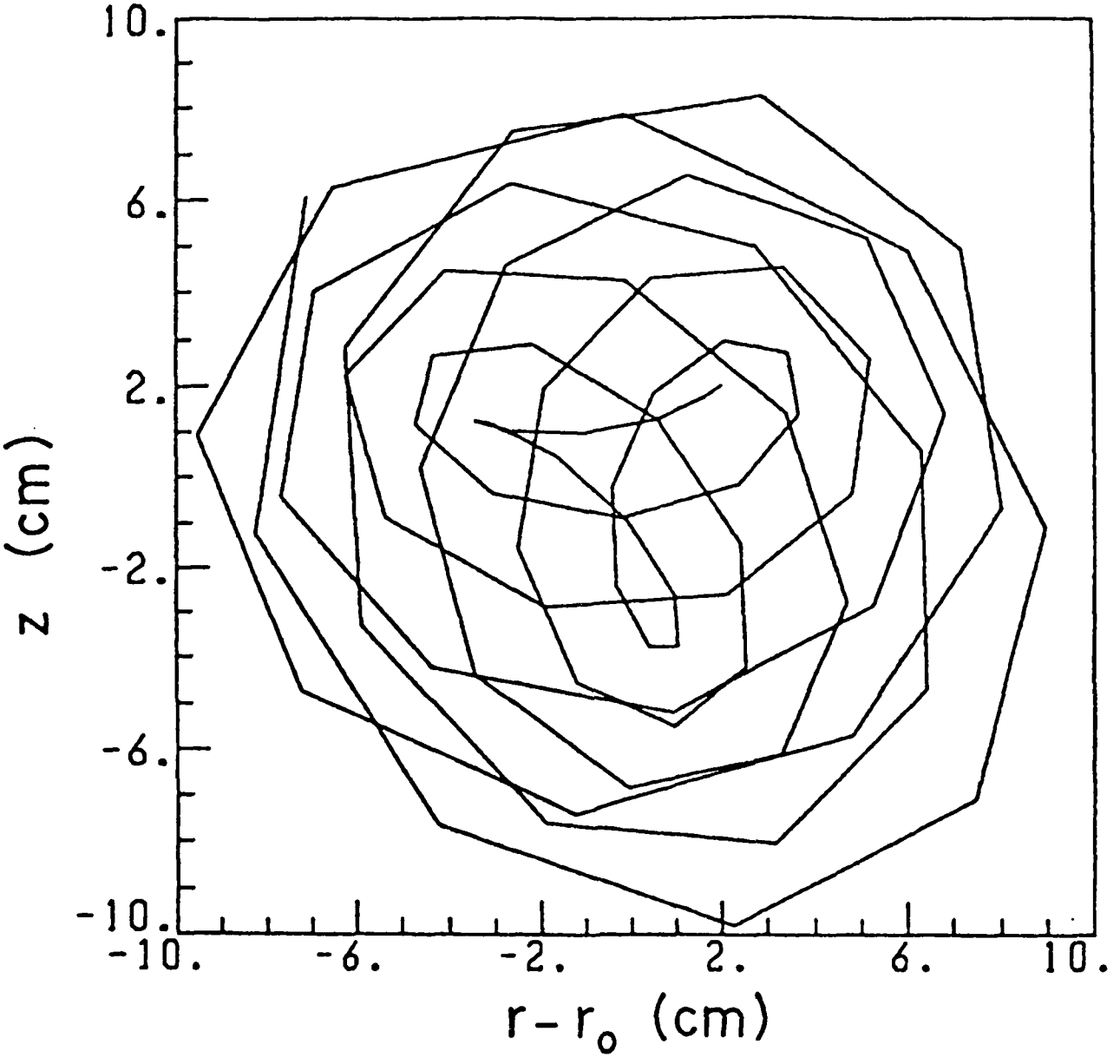

Fig. 9: z vs. $r - r_o$; $n = 1/2$; $n_2 = 0$; $\delta B = 0.5$ gauss. Particle leaves plot area after ~ 10 major periods.

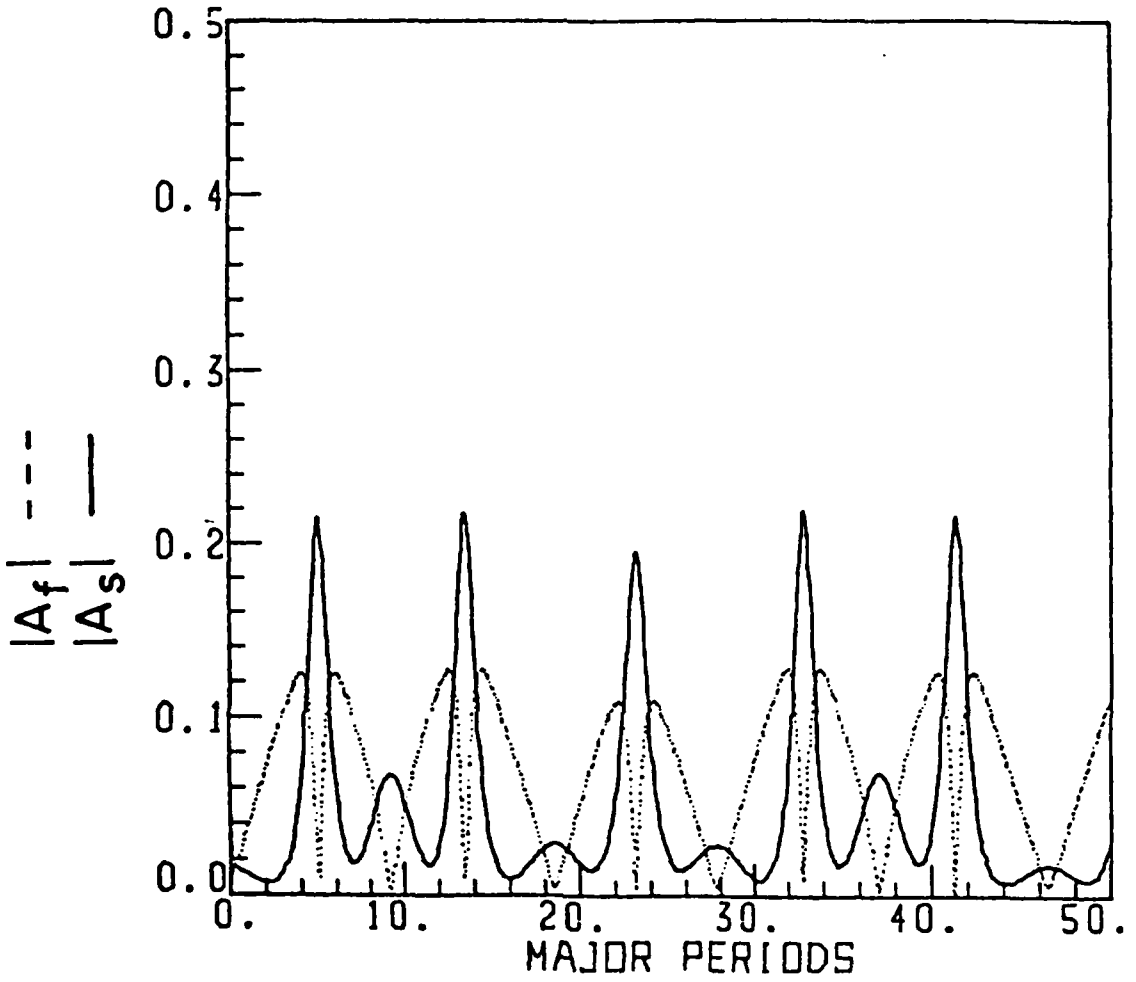

Fig. 10: $|A_f|$, $|A_s|$ vs. major periods; $n = 1/2$; $n_2 = -1$; $\varepsilon_1 = \varepsilon_3 = 0$; $\varepsilon_2 = 5 \times 10^{-3}$.

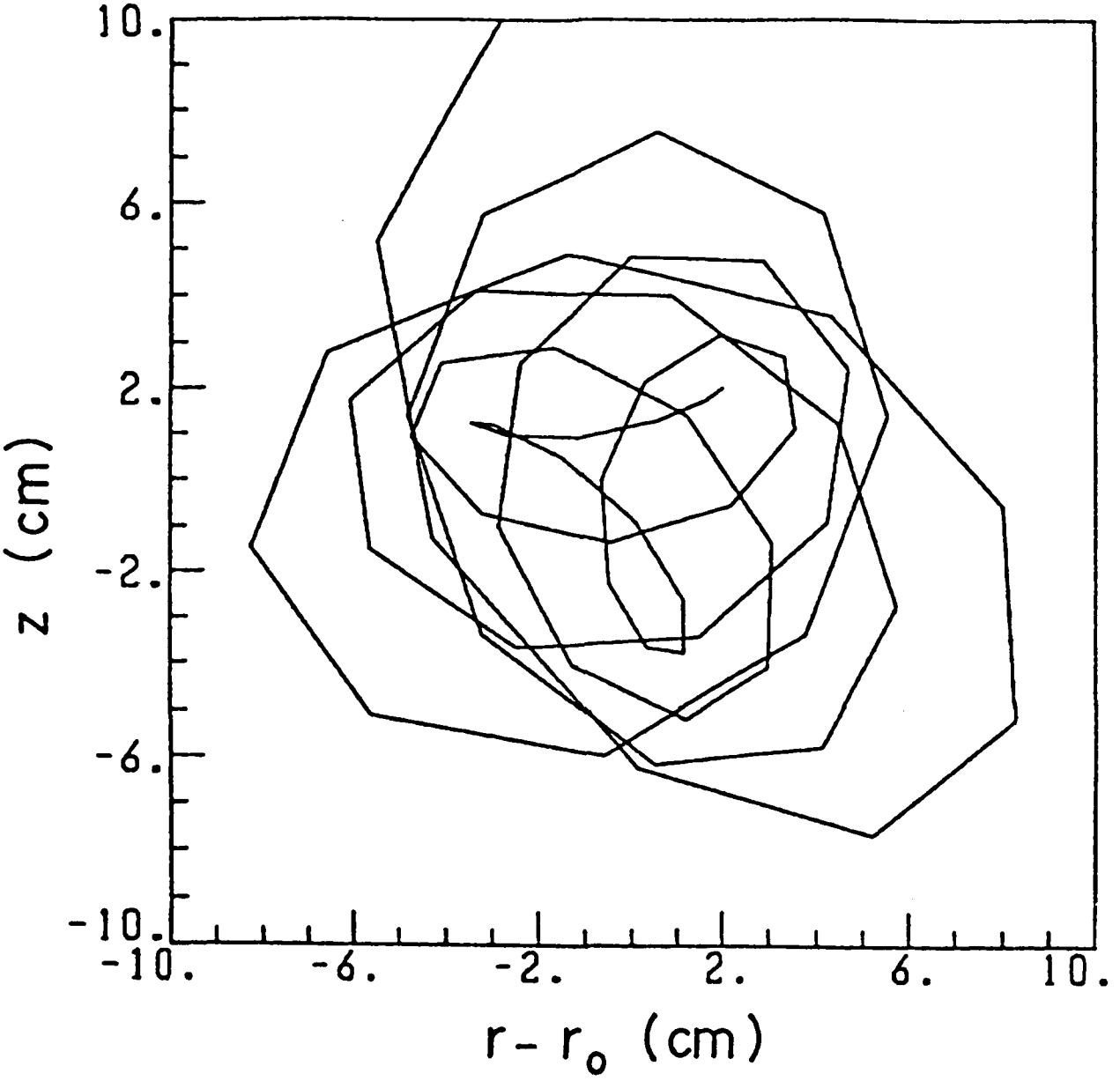

Fig. 11: z vs. $r - r_o$; $n = 1/2$; $n_2 = -1$; $\delta B = 0.5$ gauss. Particle leaves plot area after ~ 8 major periods.

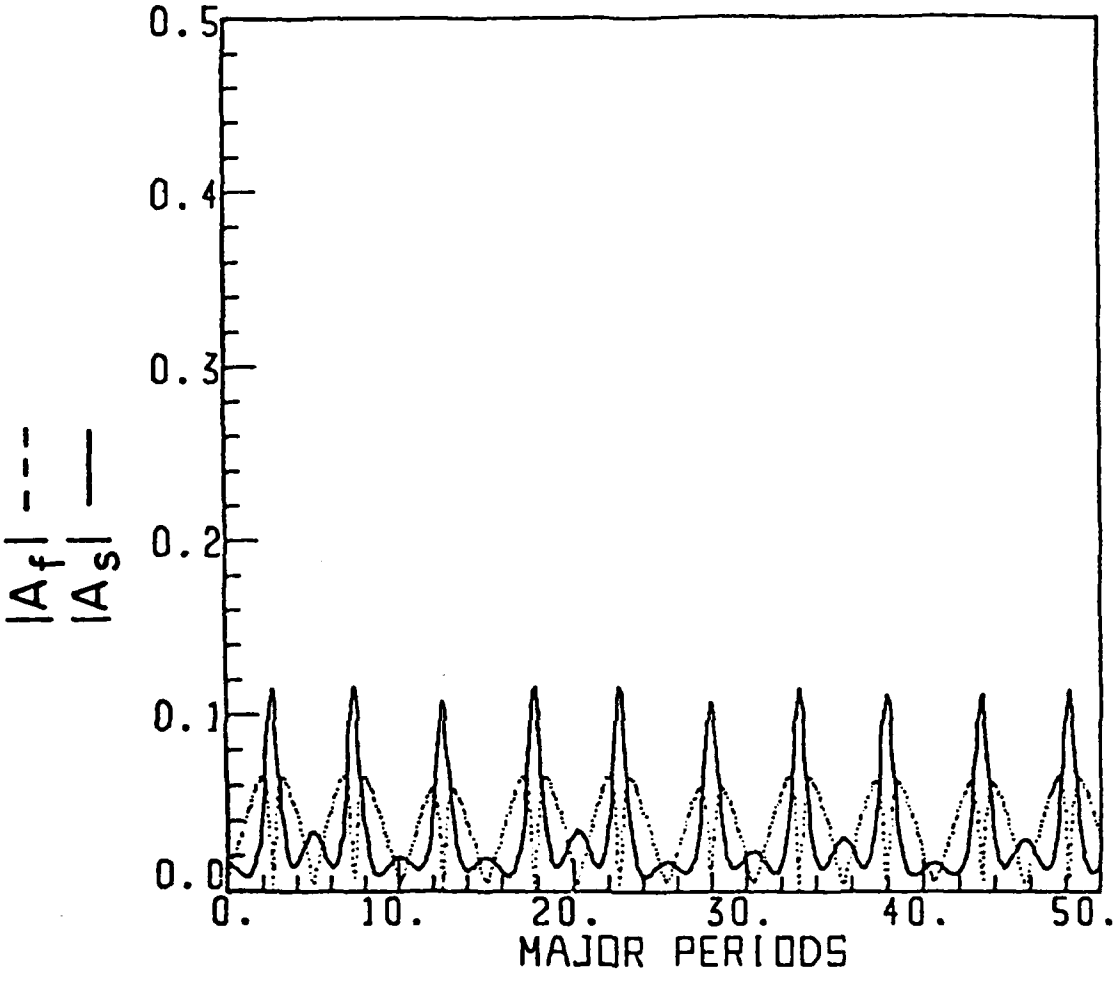

Fig. 12: $|A_f|$, $|A_s|$ vs. major periods; n = 1/2; $n_2 = -4$; $\varepsilon_1 = \varepsilon_3 = 0$; $\varepsilon_2 = 5 \times 10^{-3}$.

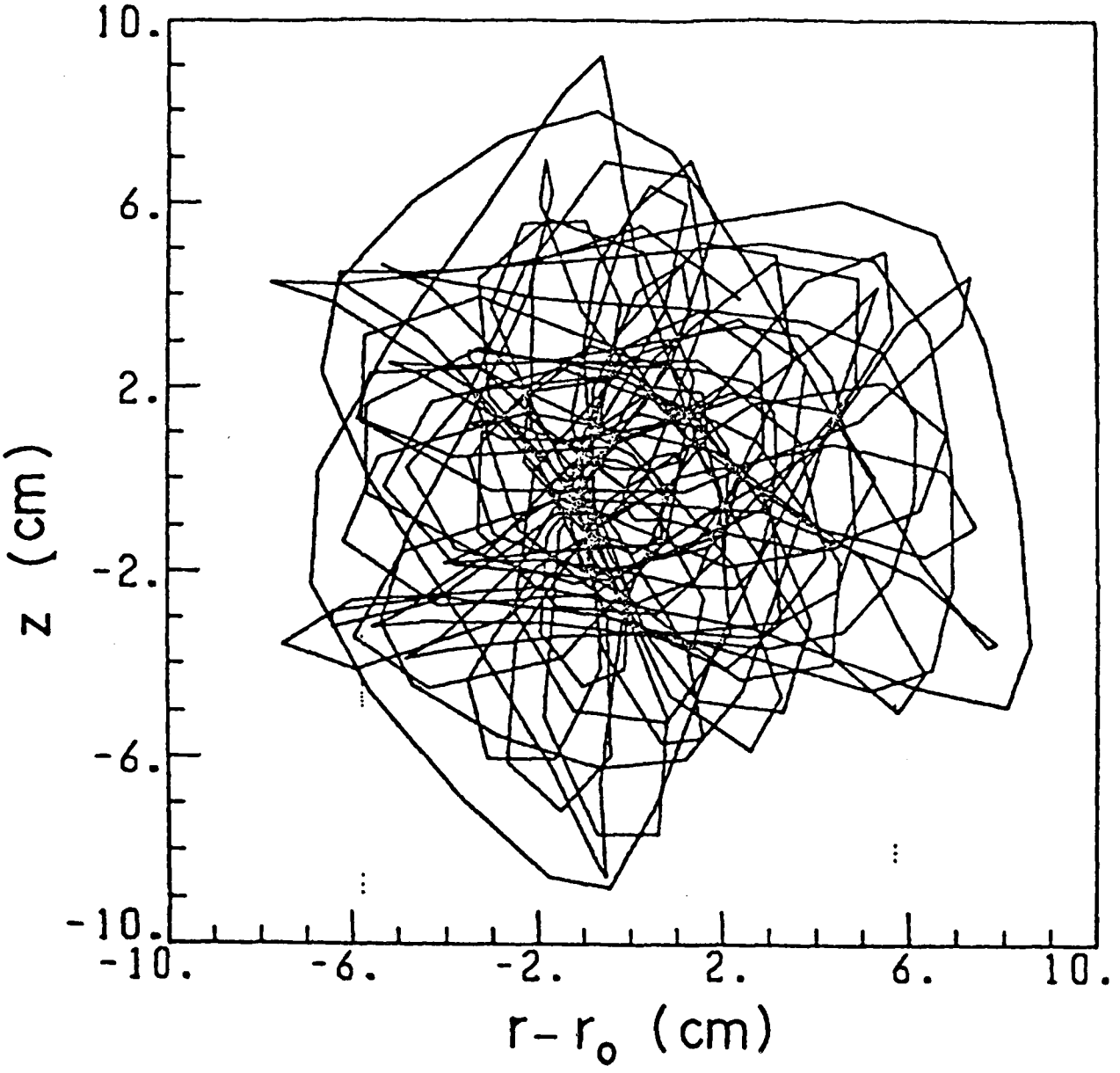

Fig. 13: z vs. $r - r_o$; $n = 1/2$; $n_2 = -4$; $\delta B = 0.5$ gauss. Particle remains in plot area for 50 major periods.

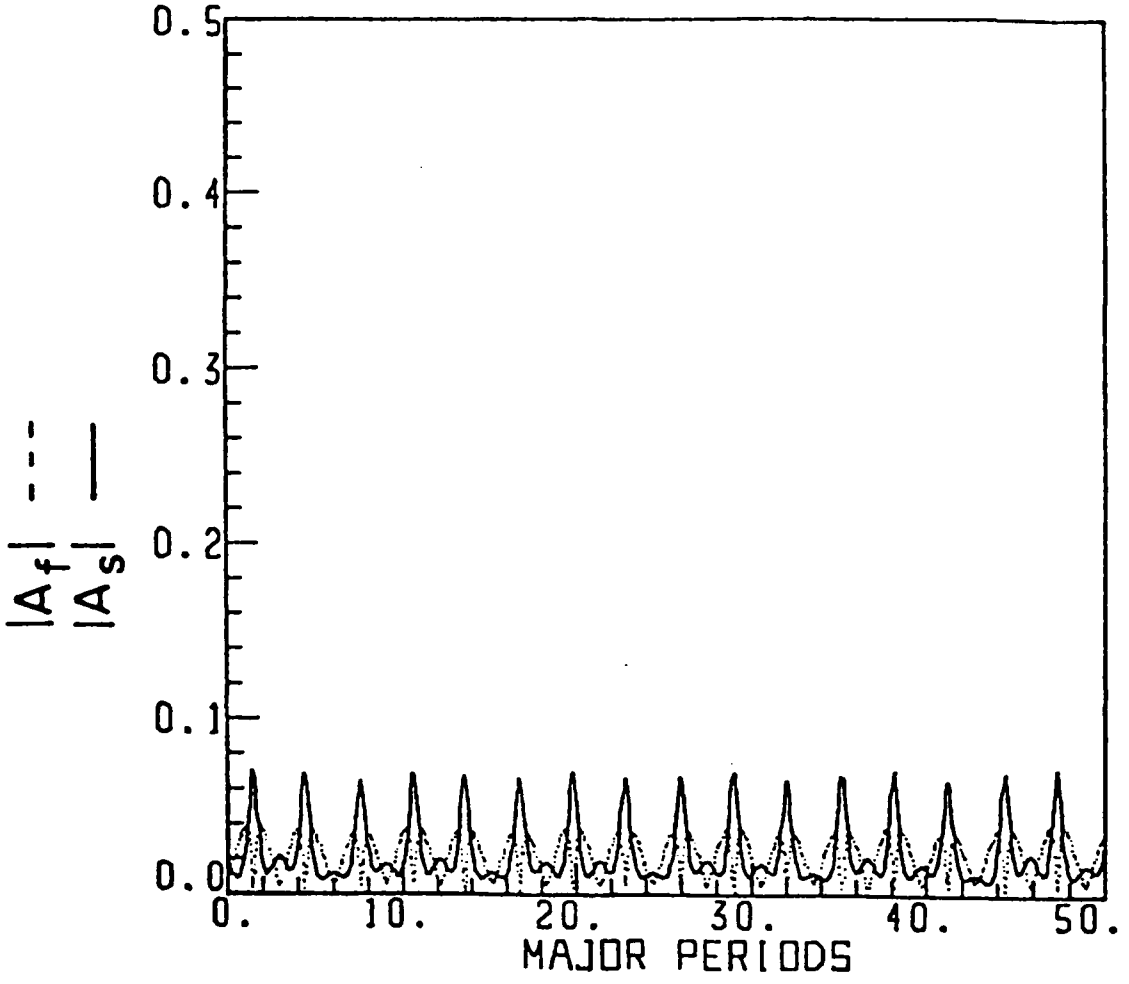

Fig. 14: $|A_f|$, $|A_s|$ vs. major periods; $n = 1/2$; $n_2 = -10$; $\varepsilon_1 = \varepsilon_3 = 0$; $\varepsilon_2 = 5 \times 10^{-3}$.

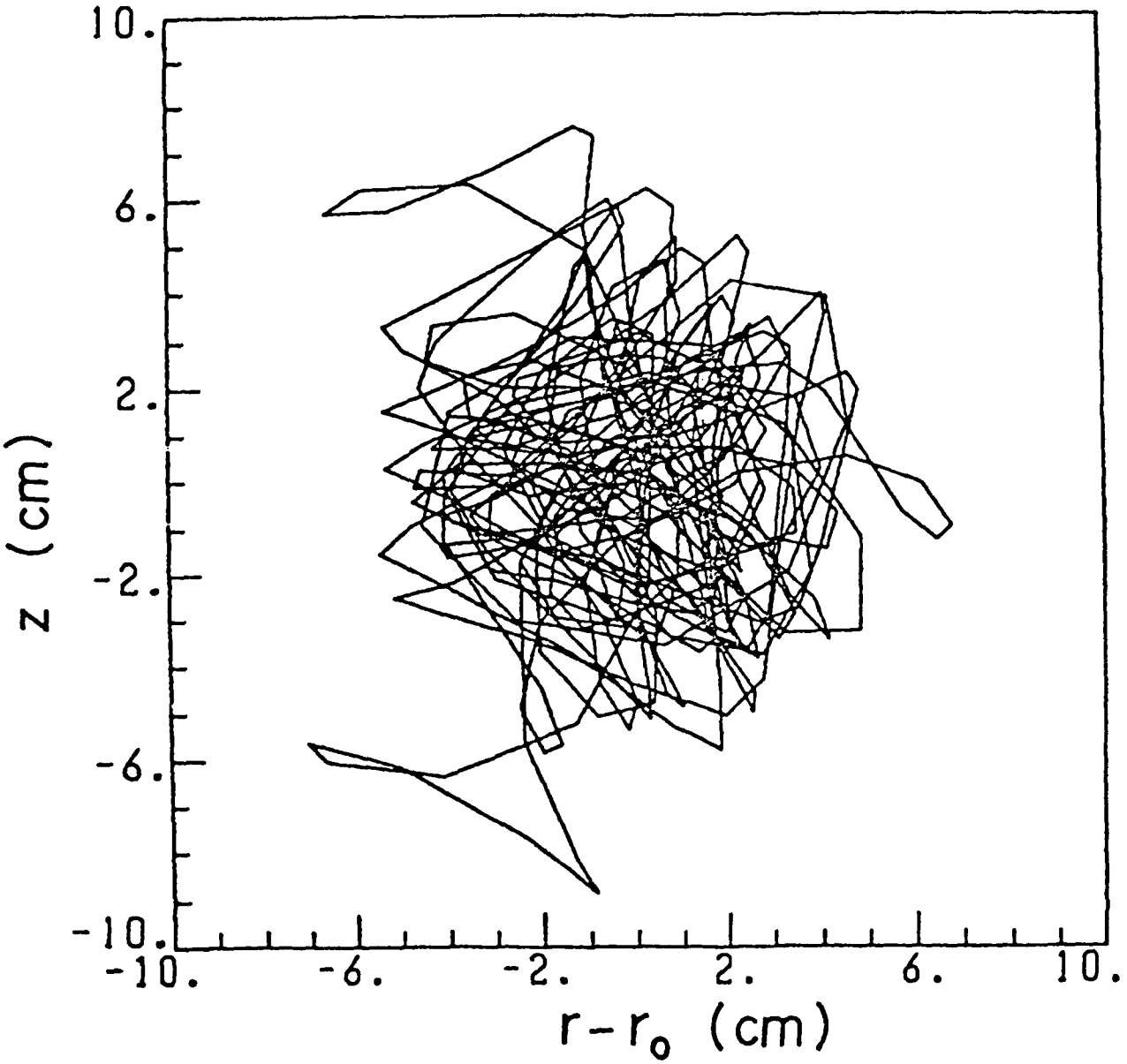

Fig. 15: z vs. $r - r_o$; $n = 1/2$; $n_2 = -10$; $\delta B = 0.5$ gauss. Particle remains in plot area for 50 major periods.

References

1. P. Sprangle and C. A. Kapetanakos, J. Appl. Phys. 49, 1 (1978).
2. N. Rostoker, Comments on Plasma Phys. 6, 91 (1980).
3. G. Barak, et al. IEEE Trans. Nucl. Sci. NS-28, 3340 (1981).
4. D. Chernin and P. Sprangle, Part. Accel. 12, 85 (1982).
5. D. Chernin and P. Sprangle, Part. Accel. 12, 101 (1982).
6. W. Walkinshaw, "A Spiral Ridged Betatron," AERE Report, Harwell (1956, unpublished).
7. Proceedings, CERN Symposium on High Energy Accelerators and Pion Physics (June, 1956) pp235ff.
8. P. A. Sturrock, Ann. Phys. 3, 113 (1958).
9. L. J. Laslett and A. M. Sessler, Rev. Sci. Instr. 32, 1235 (1961).
10. L. J. Laslett, "Growth of Axial Amplitude Associated with the Walkinshaw Resonance" ERAN-71 (March, 1970; unpublished).
11. L. J. Laslett and W. A. Perkins, Nucl. Instr. and Methods 97, 523 (1971).
12. D. C. Sewell, L. Henrich, and J. Vale, Phys. Rev. 72, 739 (1947) (abstract).
13. M. Abramowitz and I. Stegun, eds. Handbook of Mathematical Functions, Dover, New York. (Ninth printing) Equation 17.3.1.

APPENDIX E

Beam Current Limitations Due to Instabilities in Modified and Conventional Betatrons

4/13/83

Beam Current Limitations Due to Instabilities in Modified and Conventional Betatrons

P. Sprangle
Plasma Theory Branch
Naval Research Laboratory
Washington, D.C. 20375

D. Chernin
Berkeley Research Associates
Springfield, VA 22150

Abstract

Current thresholds for longitudinal and transverse instabilities are calculated for beams of specified dimensions in conventional ($B_\theta = 0$) and modified ($B_\theta \neq 0$) betatrons, using simple models for the longitudinal and transverse impedances. Self field effects of the beam are included and lead to a novel, competitive effect between the stabilization mechanism and instability growth. This competition results in a multi-valuedness in the limiting current vs beam energy spread plot, even for conventional betatrons. Accessibility of the various limiting current levels appears to depend upon the rate of beam injection. The stabilizing effects of betatron oscillations are discussed and written as the sum of three, physically interpretable contributions to an effective energy spread. We find that the presence of a strong toroidal field can significantly improve the current carrying capacity of the accelerator.

I. Introduction

The addition of a toroidal magnetic field to a conventional betatron has been shown theoretically[1-5] to increase the equilibrium current which may be confined by a factor 1/2 $(B_\theta/B_z)^2$, for large values of B_θ/B_z. In conventional accelerators without solenoidal focusing, however, beam stability considerations place the actual limit on beam current.[6-8] Therefore it becomes important to analyze the stability conditions and associated limiting currents for a given beam equilibrium in the presence of a toroidal field. In this paper we present such an analysis for both longitudinal and transverse modes.

A device in which a toroidal magnetic field is superimposed on the usual weak focusing betatron field has come to be called a "Modified Betatron". See Figure 1. A stability analysis of this accelerator necessarily must include the strong self and induced (wall image) fields of the electron beam. It is primarily the inclusion of these fields which distinguishes this work from the stability analysis performed[9] for the so-called plasma betatron in which self fields are much less important. These self field effects, however, will be seen to have a dramatic effect on the current versus energy spread scaling; namely we predict the existence of more than one stable value of current for a given beam energy spread. This somewhat surprising result will be discussed later. The

central result of this work, however, is that significantly more current may be carried by a beam in a modified betatron configuration than in a conventional betatron of the same dimensions, assuming equal beam sizes and energy spreads. In reaching this conclusion we have included not only the effects of self fields, but also the (stabilizing) effects of betatron oscillations and the (destabilizing) effects of short wavelength enhancements to the longitudinal and transverse impedances due to chamber resonances. Below we discuss the dispersion relation for arbitrary toroidal fields and currents, describe our model for the impedances, and present analytical and numerical results from the dispersion relation.

II. Discussion

A dispersion relationship for both the longitudinal and transverse modes in a modified betatron accelerator configuration has been derived.[10] Included in the derivation are: beam self field effects, induced field effects arising from wall image charges and currents as well as finite chamber wall conductivity effects. Toroidal corrections to the equilibrium beam self fields and chamber wall image fields have been neglected. The longitudinal and transverse impedances, which characterize the beam environment, are incorporated in a phenomenological way in the short wavelength limit. The dispersion relation,

therefore, treats disturbances of all wavelengths, including wavelengths much longer or shorter than the chamber minor radius.

The short wavelength model for the impedances contains effects associated with propagating chamber modes. These effects can significantly affect the instability growth rates. With the inclusion of the short wavelength contributions to the impedances a realistic estimate for the current limitations due to the various instabilities can be obtained for the modified betatron configuration and compared to those of a conventional betatron. To perform a meaningful comparison we will choose identical parameters for the two types of betatrons, i.e., same geometry, injection energy, field index, etc. The only difference of course will be that the modified betatron configuration will include a toroidal magnetic field.

The dispersion relation[10] for the longitudinal and transverse modes of a cold beam may be written

$$1 = \frac{\tilde{\omega}_{\parallel}^2}{\Delta\tilde{\omega}_{\ell}^2}\left\{\frac{1}{\gamma^2} + \frac{(\Delta\tilde{\omega}_{\ell}^2 - \tilde{\omega}_{\perp}^2)}{(\Delta\tilde{\omega}_{\ell}^2 - \tilde{\omega}_{\perp}^2)^2 - b^2\Delta\tilde{\omega}_{\ell}^2}\right\}, \qquad (1)$$

where $\Delta\tilde{\omega}_{\ell} = (\omega - \ell\omega_c)/\omega_c$, ω is the complex mode frequency, $\ell = 1,2,3,\ldots$ is the longitudinal (toroidal) harmonic mode number, $\omega_c = \Omega_z/\gamma$ is the electron rotation

frequency, $\Omega_z = |e|B_z/m_o c$ is the non-relativistic cyclotron frequency, $\gamma = (1 - v_o^2/c^2)^{-1/2}$, v_o is the longitudinal (toroidal) beam velocity, $\tilde{\omega}_\parallel^2 = -2i\ell^2 (\nu/\gamma)(Z_\parallel/\ell Z_o)$, ν is Budker's parameter($\nu = I[A]/17 \times 10^3$), $Z_\parallel = Z_\parallel(\omega)$ is the total effective longitudinal impedance, $Z_o = 4\pi/c$ ($Z_o = 377\ \Omega$ in MKS units), $\tilde{\omega}_\perp^2 = 1/2 - 2(\nu/\gamma^3)(r_o/r_b)^2 - 2i(\nu/\gamma)(r_o Z_\perp/Z_o)$, r_o is the major electron beam radius, r_b is the minor electron beam radius, $Z_\perp = Z_\perp(\omega)$ is the total effective transverse impedance, $b = B_\theta/B_z$ and B_θ is the toroidal magnetic field. In (1) finite amplitude betatron oscillations were neglected, the external field index was taken to be 1/2 and the electron beam was assumed to be mono-energetic, highly relativistic ($v_o \approx c$) and circular in cross section.

III. Approximate Representation of Impedances

In our model the longitudinal impedance $Z_\parallel(\omega)$ is taken to consist of three terms

$$Z_\parallel = Z_{\parallel,s} + Z_{\parallel,\sigma} + Z_{\parallel,r} \qquad (2)$$

The first term in (2) is the long wavelength space charge shielding contribution associated with a smooth infinitely conducting chamber and is given by

$$Z_{\parallel,s} = \ell Z_o (i/2\gamma_w^2)(1 + 2 \ell n\, a/r_b), \qquad (2a)$$

where γ_w is the relativistic factor corresponding to the wave phase velocity and a is the minor radius of the toroidal chamber. Due to the $1/\gamma_w^2$ factor this impedance term is typically quite small; it may even change sign.

The part of the longitudinal impedance due to the resistive nature of the chamber wall, in the long wavelength regime, is

$$Z_{\parallel,\sigma} = \ell Z_o (1 - i)\, \delta/2a. \qquad (2b)$$

where $\delta = c\,(2\pi\sigma|\omega|)^{-1/2}$ is the skin depth and σ is the wall conductivity. It has been assumed in (2b) that the skin depth is small compared to the thickness of the chamber wall.

Finally, the last term in (2) represents the resonance contribution to the total longitudinal impedance and arises from the fact that the chamber can support propagating waves. To obtain the exact form for $Z_{\parallel,r}$ would require a rather involved analysis of the beam-chamber structure and is beyond the goals of the present paper. We will, therefore, simply represent this contribution by the phenomenological expression[11]

$$Z_{\parallel,r} = R_o \frac{\omega}{\omega_r} \left(\frac{\omega/\omega_r - i\, Q(1 - (\omega/\omega_r)^2)}{(\omega/\omega_r)^2 + Q^2(1 - (\omega/\omega_r)^2)^2}\right), \qquad (2c)$$

where R_o defines the chamber shunt impedance, $\omega_r \approx 2.4\ c/a$ is the cutoff frequency of the lowest order chamber mode, and Q is the quality factor associated with the chamber. The chamber shunt impedance, R_o, can be estimated by noting that near a resonant frequency $\omega = \omega_r$ the longitudinal impedance is roughly equal to the free space impedance

$$Z_{f.s.} \approx \frac{Z_o}{2} (\sqrt{3} - i)\, \ell^{1/3}. \qquad (3)$$

It follows, therefore, that $R_o \approx Z_o\, \ell_r^{1/3}$ where ℓ_r is the toroidal mode number associated with the resonant frequency, i.e., $\ell_r = \omega_r/\omega_c$.

The expression for the total transverse impedance $Z_\perp(\omega)$ is also written as the sum of three contributions

$$Z_\perp = Z_{\perp,s} + Z_{\perp,\sigma} + Z_{\perp,r}. \qquad (4)$$

The long wavelength space charge part of the impedance, for a smooth infinitely conducting chamber, is

$$Z_{\perp,s} = i\, r_o Z_o (1/r_b^2 - 1/a^2)/\gamma^2. \qquad (4a)$$

The second term is the long wavelength contribution due to the resistive nature of the wall and is given by

$$Z_{\perp,\sigma} = r_o Z_o (1 - i)\, \delta/a^3. \qquad (4b)$$

Chamber resonances contribute to the transverse impedance a part which we will represent by the form[11]

$$Z_{\perp,r} = \frac{2r_o}{\ell a^2}\, Z_{\parallel,r}, \qquad (4c)$$

where $Z_{\parallel,r}$ is defined in (2c).

In the present work we will not be concerned with resistive wall effects which lead, in conventional acclerators, to well known longitudinal and transverse instabilities[6] having, however, comparatively slow growth rates. Equations (2b) and (4b) are included here only for reference purposes.

We remark that with the impedances as defined above the dispersion relation is virtually independent of the beam minor radius, r_b, except for the weak

logarithmic dependence in (2a). This is reasonable if we think of the dynamics involved in the various instabilities, that is, if we consider that it is the beam centroid which moves transversely, even in the "longitudinal" or negative mass instability in which beam bunching occurs as the beam centroid moves in or out radially. Motion of the beam centroid is affected by the externally applied fields, including those due to wall image charges and currents; these fields, unlike beam self fields which are carried along transversely by the moving beam, do not depend on the minor radius of the beam.

IV. Stability Condition and Limiting Current

To obtain the limiting current, based on stability requirements, for the modified and conventional betatron a stability criterion is needed. If the distribution in particle rotation frequencies is Lorentzian in shape the criterion for stability is simply

$$\Gamma \leq \ell |\Delta\Omega|, \tag{5}$$

where Γ is the growth rate in the absence of a frequency spread and $\Delta\Omega$ is the half width of the frequency spread on the beam. It should be noted that the

large tails associated with a Lorentzian distribution make the criterion in (5) somewhat less stringent than would be the case if a more realistic choice of frequency distribution were used. However, the use of a more realistic distribution of particle frequencies would result in a considerably more involved stability criterion. Since we are interested here mainly in making a comparison of the limiting currents of the modified and conventional betatrons, consistent use of a Lorentzian for both devices should serve our purpose.

Both an intrinsic longitudinal energy spread on the beam electrons as well as finite amplitude betatron oscillations will produce a spread in rotation frequencies. Solving the particle orbit equations correct to second order in the betatron oscillation amplitude, with self-field effects and intrinsic energy spread effects included, the average spread in the beam's rotation frequency is found to be given by

$$|\Delta\Omega| = |\Delta\Omega|_{\Delta E} + |\Delta\Omega|_{B}, \tag{6}$$

where

$$|\Delta\Omega|_{\Delta E} = \frac{1}{2}\,\omega_c\,|\alpha|(\Delta E/E) \tag{6a}$$

$$|\Delta\Omega|_B = \omega_c (r_b/2r_o)^2 |b^2/2 - n_s - 3/2|, \qquad (6b)$$

with $\alpha = (1/2 - n_s)^{-1} - \gamma^{-2}$. The two terms on the right hand side of (6) are due to an intrinsic energy spread and to finite amplitude betatron oscillations, respectively. In (6a) the fractional intrinsic energy spread is denoted by $\Delta E/E$ where $E = \gamma m_o c^2$ is the beam particle energy, ($\gamma \gg 1$) and $n_s = 2(\nu/\gamma^3)(r_o/r_b)^2$ is the field index associated with the beam's self fields. In obtaining (6a,b) we assumed a circular beam cross section and an external field index of 1/2. Note that it is here, in the relation between $\Delta E/E$ and $\Delta\Omega$, that self fields play an important role.

By utilizing the beam envelope equation, the frequency spread term $|\Delta\Omega|_B$ can be expressed in a more illuminating form. The condition for a matched beam, i.e. non-oscillating minor beam radius, is[12]

$$\frac{1}{4} b^2 = n_s - 1/2 + (r_o \varepsilon_n)^2/(r_b^2 \gamma)^2, \qquad (7)$$

where ε_n is the normalized transverse beam emittance as measured in the Larmor frame. Substituting (7) into (6b) gives

$$|\Delta\Omega|_B = \frac{\omega_c}{\gamma^2} |(\epsilon_N/r_b)^2/2 - \frac{5}{8} (r_b/r_o)^2\gamma^2 + \nu/2\gamma| \qquad (8)$$

In (8), the first term in brackets is the familiar longitudinal energy spread due to emittance, the second term is a toroidal correction to the first, while the last term is the energy spread associated with the electrostatic potential drop across the beam. Both contributions to the total frequency spread, $|\Delta\Omega|_{\Delta E}$ and $|\Delta\Omega|_B$, are proportional to the various energy spreads. The two different proportionality factors, $|\alpha|$ in the case of $|\Delta\Omega|_{\Delta E}$ and γ^{-2} in the case of $|\Delta\Omega|_B$, arise because the intrinsic particle energy spread produces a rotational frequency spread primarily by changing the particle's radial position whereas the various energy spreads contributing to $|\Delta\Omega|_B$ merely result in a longitudinal velocity spread. Hence the various contributions to the longitudinal energy spread contribute differently to the frequency spread.

The desired stability criterion is obtained by substituting (6) into (5) and becomes

$$\Gamma \leq \ell\omega_c \left[\frac{1}{2} |\alpha|(\Delta E/E) + |(\epsilon_n/r_b)^2/2 - \frac{5}{8} (r_b/r_o)^2\gamma^2 + \nu/2\gamma|/\gamma^2\right] \qquad (9)$$

Given the intrinsic energy spread, beam radius and emittance, the criterion in

(9) implies a limiting beam current which if exceeded will result in instability. As a simple illustration we will first consider the negative mass mode in a low current conventional betatron, i.e., $B_\theta = 0$, $n_s \ll 1/2$. From (1), the dispersion relation for the negative mass instability is $\Delta\tilde{\omega}_\ell^2 = -\omega_\parallel^2/\omega_\perp^2$ $\approx 4i\ell^2(\nu/\gamma)(Z_\parallel(\omega)/\ell Z_o)$, where we have assumed that $|\Delta\tilde{\omega}_\ell| \ll |\tilde{\omega}_\perp| \approx 1/\sqrt{2}$. Approximating $Z_\parallel(\omega)$ by $Z_\parallel(\ell\omega_c)$ we find that the growth rate is $\Gamma = 2\ell\omega_c(\nu/\gamma)^{1/2}\,|(Z_\parallel(\ell\omega_c))|^{1/2}/(\ell Z_o)^{1/2}$. Using (9) and neglecting the betatron oscillations we recover the well known negative mass stability condition

$$\frac{\nu}{\gamma} \leq \frac{\ell Z_o}{|Z_\parallel(\ell\omega_c)|}\left(\frac{\Delta E}{E}\right)^2. \qquad (10)$$

In obtaining (10) we have assumed that the real and imaginary parts of $Z_\parallel$ are approximately equal.

Next we consider the full dispersion relation (1) for arbitrary b. Here and below we will continue to neglect the effect of betatron oscillations on the stability of the beam. The effect is generally small and, due to the b^2 dependence in (6b), it favors the modified betatron. Therefore, neglect of the betatron oscillations is conservative when comparing the modified and conventional betatrons.

If we may continue to approximate $Z_{\parallel,r}(\omega)$ by $Z_{\parallel,r}(\ell\omega_c)$ and if we set $\delta = 0$ then (1) is in general a sixth order (fourth order, if $b = 0$) polynomial. By neglecting resistive wall effects we are assuming that these are negligible for the negative mass branch of the dispersion relation in which we will be interested here. Of the six roots, two pair correspond to transverse modes (a pair being a forward and backward wave, essentially) and one pair to the longitudinal mode.

For a given set of parameters, we have found the roots numerically, for a large range of ℓ; a maximum value of Γ/ℓ is then found and substituted into the stability criterion from which a value of $\Delta E/E$ is computed. An important point to note is that the toroidal field has more of a stabilizing effect on the high ℓ modes than on the low ℓ modes; consequently, as b is increased the behavior of the impedance for <u>small</u> ℓ tends to determine the maximum Γ/ℓ and therefore the limiting current.

Typical results are illustrated in Figures 2 and 3. Here we plot the beam current vs the Lorentzian full width energy spread required for stable motion for $b = 0, 5, 10, 20$, $r_o/a = 6$, $a/r_b = 3$, $R_o/Z_o = 4$, and $Q = 10$. Figures 2 and 3 are plotted for $\gamma = 3$ and 6 respectively. The dashed lines are plots of

$$\frac{\Delta E}{E} = |1 - 2n_s| \frac{r_b}{r_o} \qquad (11)$$

For consistency we must be to the left of these lines. This restriction may be understood by considering the displacement of a particle from the center of the beam:

$$\frac{\delta r}{r_o} = \frac{\delta E/E}{\frac{1}{2} - n_s} + \text{betatron oscillations}$$

where δE is the difference between the particular particle energy and the average energy of the particles in the beam. It follows that

$$\frac{r_b}{r_o} \geq \left|\frac{\Delta E/E}{1-2n_s}\right| \qquad (12)$$

where ΔE is the full width of the distribution.

The effects of the self fields, as represented by n_s in (6a) and (11) are immediately evident in the plots of Figures 2 and 3. If n_s were zero then the dashed boundary lines would be a single vertical line and the curves would be monotonic. As it is, the effect of the self fields is basically traceable to the increasing (as n_s increases toward 1/2) then decreasing (as n_s increases beyond 1/2) factor $|\alpha|$. The multi-valuedness of the curves may then be understood as follows (Refer to Figure 4.): For very small currents (Branch I, in Figure 4)

the cold beam growth rate is small and an increasing function of current. The self field index, n_s, is negligible compared to 1/2 and the energy spread required for stability is an increasing function of current. This is the regime in which virtually all conventional accelerators operate. As the current is further increased, however, a second branch becomes accessible, shown as Branch II, in Figure 4: While the cold beam growth rate continues to increase with increasing current, the intrinsic energy spread stabilization mechanism becomes more effective due to the increase in $|\alpha|$ until, near $n_s \lesssim 1/2$ a very small energy spread results in a large spread in angular velocity; the instability is therefore easily stabilized. More simply said, we have stability on the low current branch (Branch I) because the growth rate is small and on the high current branch (Branch II) because the stability mechanism is strong.

There is a third branch which appears in the example of Figure 2 above $n_s = 1/2$ ($I > 316$ A) for $b = 10$ and 20 and is illustrated as Branch III in Figure 4. This region is accessible only in the modified betatron since we are constrained in the conventional betatron by the equilibrium condition $n_s < 1/2$. For $b = 5$ in the example shown in Figure 2 the stable points fall to the right of the dashed line and so are not shown. As the current is increased beyound 316 A the growth rate increases and the stability mechanism becomes less effective

as $|\alpha|$ decreases. Consequently as the current is increased beyond this point the required energy spread increases monotonically. This is illustrated by the third branch in the figure.

Finally we comment on the accessibility of the various branches available for small energy spreads. If beam injection proceeds slowly, over many growth times, say, it appears that only the lowest branch is accessible; attempting to add more current will drive the system unstable. If however current can be introduced into the accelerator more rapidly, the higher current branches may become accessible. Only a carefully designed experiment can test this speculation. For $b = 5$ and 10 for the parameters of Figure 2 typical growth times are ~ 3 particle circulation periods so that high current injection on this time scale is a practical experimental possibility. The third branch in Figure 2 is clearly the most promising for very high current operation.

V. Conclusions

We have shown that the addition of a toroidal magnetic field to a conventional betatron may significantly improve the current carrying capacity of the betatron by controlling the collective instabilities which limit the current. The calculation has included self field effects and a simple, though realistic model for the longitudinal and transverse impedances. The stabilizing effects of

betatron oscillations, which have been shown to include the effects of emittance, toroidal geometry, and energy shear due to the electrostatic potential drop across the beam, become stronger as the toroidal field is increased, given a fixed beam radius. Inclusion of self field effects in the stability criterion (6) has been shown to lead to a multi-valuedness in the current vs energy spread plot which has been interpreted as the result of the competition between the growth and stabilization mechanisms. Accessibility of the high current branches may depend on the duration of the injection process.

VI. Acknowledgments

We have profitted from discussions with C. A. Kapetanakos and E. P. Lee and wish to thank V. K. Neil for helpful comments. This work was supported by the Office of Naval Research.

References

1. A. G. Bonch-Osmolovskii, G. V. Dolbilov, I. N. Ivanov, E. A. Perelstein, V. P. Sarantsev, O. I. Yarkova; JINR Report P9-4135 Dubna (USSR), 1968 (Unpublished).

2. P. Sprangle and C. A. Kapetanakos, J. Appl. Phys. 49, 1 (1978).

3. N. Rostoker, Comments on Plasma Phys. 6, 91 (1980).

4. D. Chernin and P. Sprangle, Particle Accelerators 12, 85 (1982).

5. G. Barak and N. Rostoker, Phys. Fluids 26, 856 (1983).

6. V. K. Neil and A. M. Sessler, Rev. Sci. Instr. 36, 429 (1965).

7. L. J. Laslett, V. K. Neil, and A. M. Sessler, Rev. Sci. Instr. 36, 436 (1965).

8. E. P. Lee, A. Faltens, L. J. Laslett, and L. Smith, paper presented at Tenth Particle Accelerator Conference; Santa Fe, NM (1983) (to be published in IEEE Trans. Nucl. Sci.).

9. R. W. Landau, Phys. Fluids 11, 205 (1968).

10. P. Sprangle and J. L. Vomvoridis, NRL Memorandum Report 4688 (1982).

11. C. Pellegrini, in Physics of High Energy Particle Accelerators (Fermilab Summer School, 1981), R. A. Carrigan, F. R. Huson, and M. Month, eds. pp 77ff.

12. See, e.g. J. D. Lawson, The Physics of Charged Particle Beams, Oxford University Press, (1977) Eq (4.37).

Figure Captions

Figure 1. Modified Betatron configuration.

Figure 2. Instability threshold current vs energy spread for b = 0, 5, and 10. The beam and chamber parameters are $r_o/a = 6$, $a/r_b = 3$, $\gamma = 3$, $R_o/Z_o = 4$, $Q = 10$.

Figure 3. Same as Fig. 2 except $\gamma = 6$.

Figure 4. Sample plot of limiting current vs energy spread, illustrating the three possible branches.

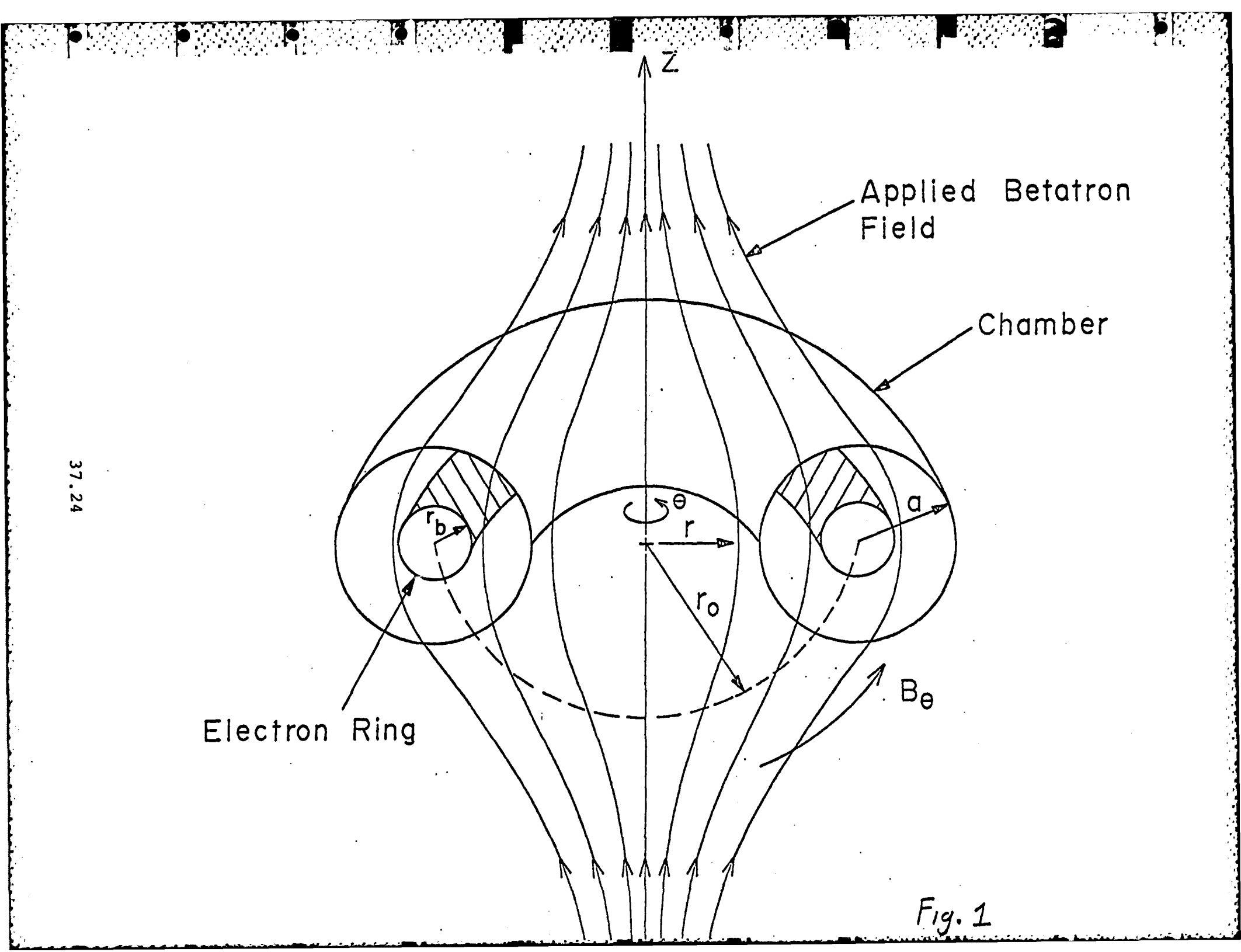

Fig. 1

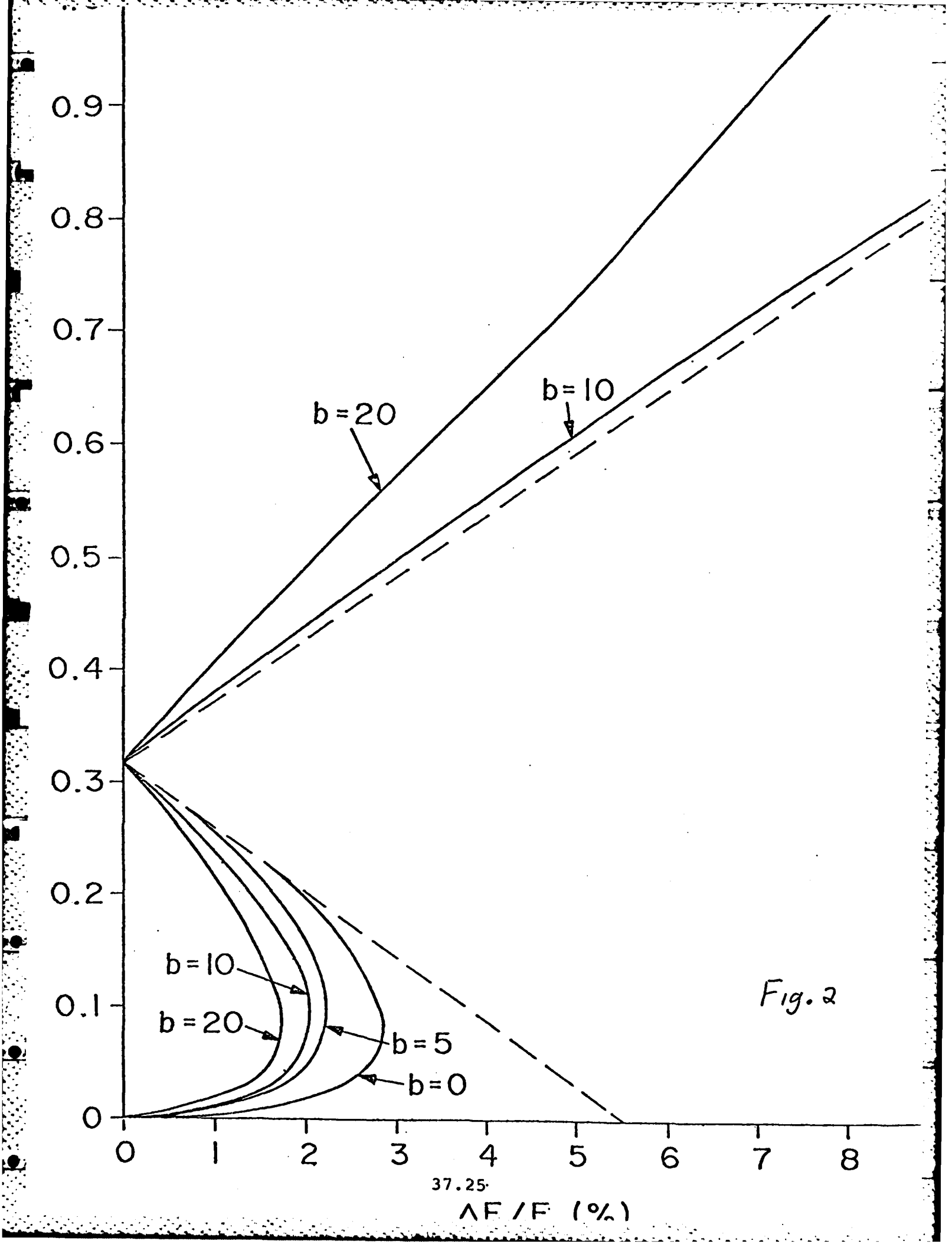
0.9
0.8
0.7
0.6
0.5
0.4
0.3
0.2
0.1
0
b=20
b=10
b=10
b=20
b=5
b=0
0
1
2
3
4
5
6
7
8
37.25
ΔF/F (%)

Fig. 2

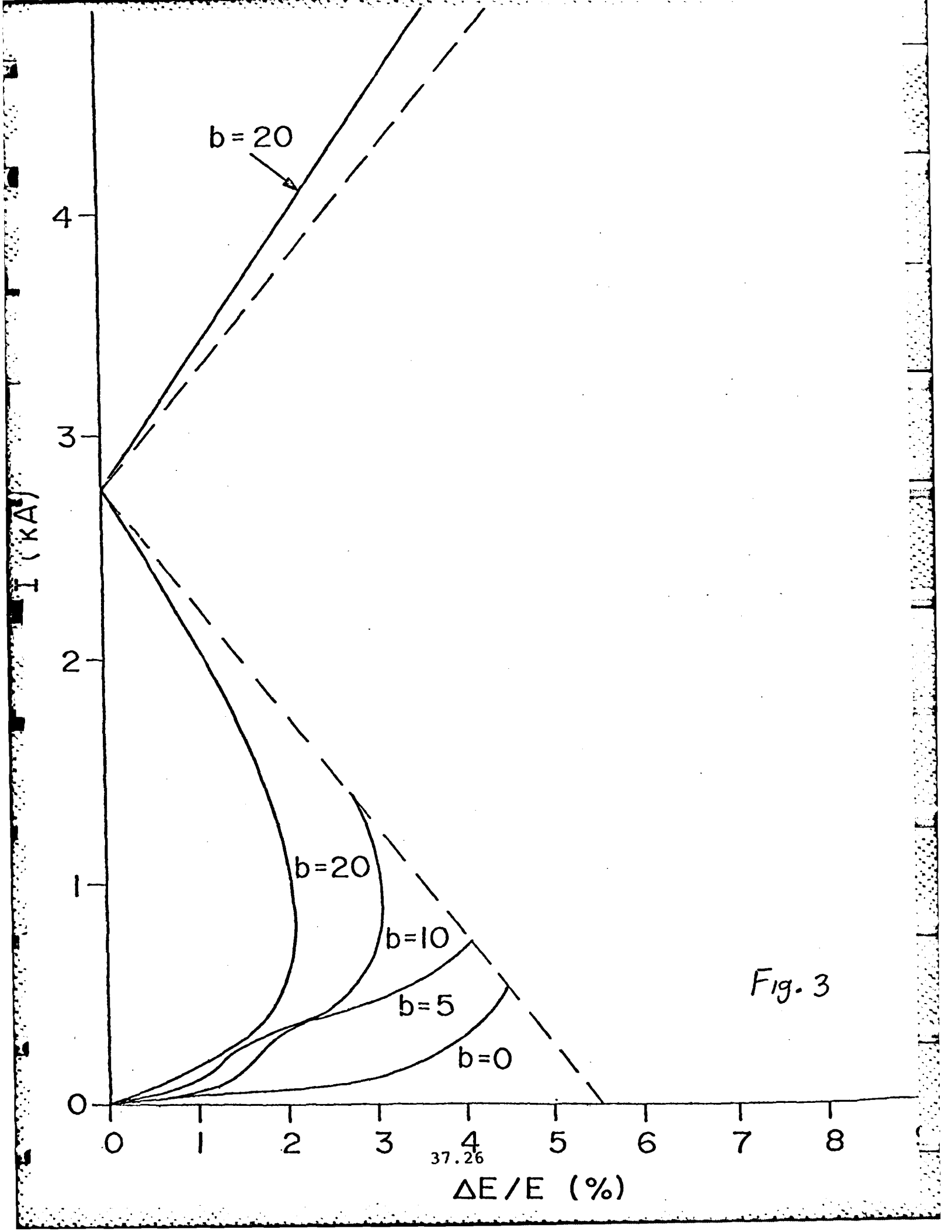

Fig. 3

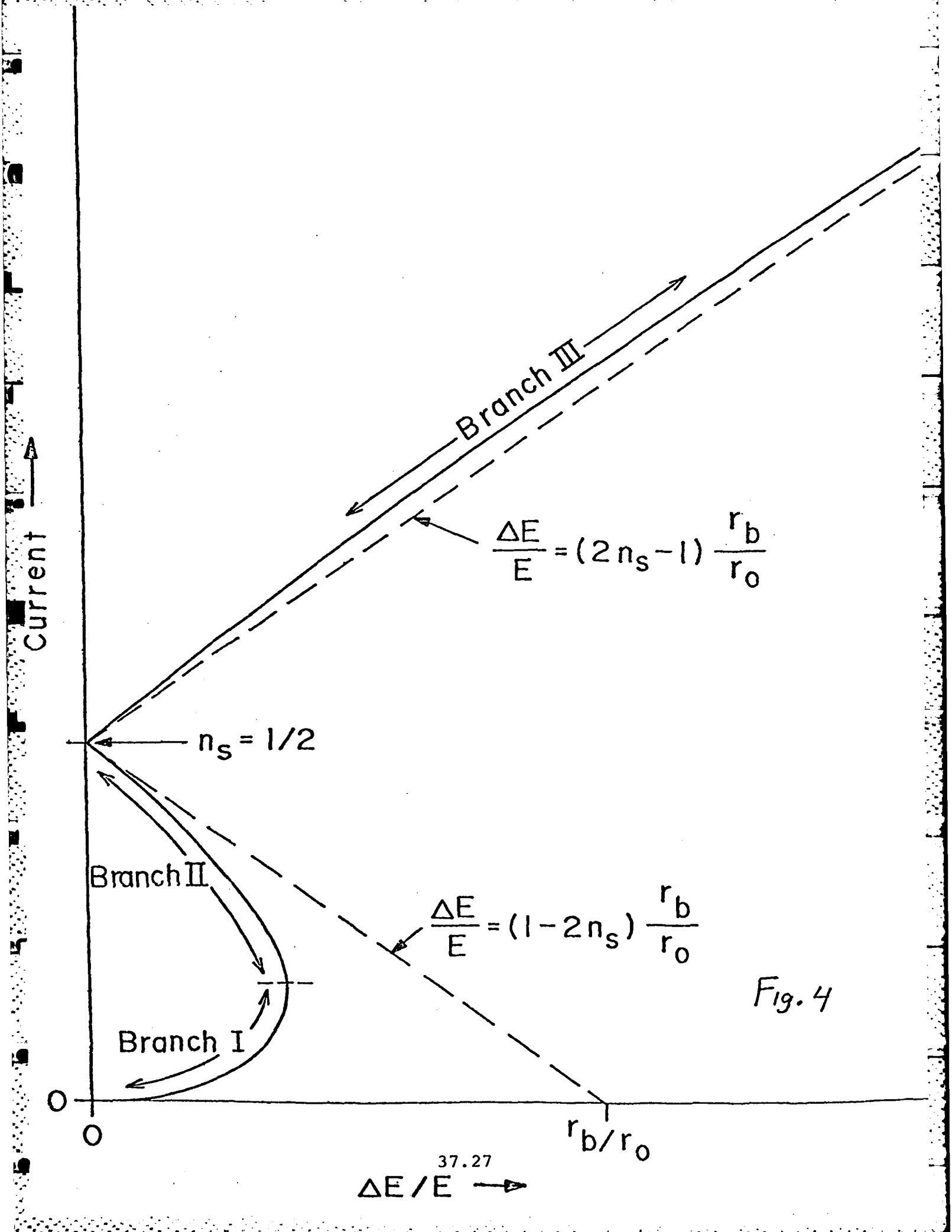
Current
Branch III
$\frac{\Delta E}{E} = (2n_s - 1)\frac{r_b}{r_o}$
$n_s = 1/2$
Branch II
$\frac{\Delta E}{E} = (1 - 2n_s)\frac{r_b}{r_o}$
Branch I
0
0
r_b/r_o
$\Delta E/E$

Fig. 4

APPENDIX F

High-Current Betatron with Stellerator Fields

High-Current Betatron with Stellarator Fields

C. W. Roberson
Office of Naval Research, Arlington, Virginia 22217

and

A. Mondelli
Science Applications, Inc., McLean, Virginia 22102

and

D. Chernin
Berkeley Research Associates, Springfield, Virginia 22150

(Received 2 November 1982)

By adding an $l=2$ stellarator field to a betatron accelerator, a new configuration is obtained which is capable of accelerating multikiloamp beams and which will tolerate a large (more than 50%) mismatch between the particle energy and the vertical magnetic field. The additional field is a twisted quadrupole which acts as a strong-focusing system. This device has been analyzed both analytically and numerically.

PACS numbers: 52.75.Di, 29.20.Fj

Conventional betatrons[1,2] are current limited at injection. Recently, efforts have been made to extend the current-carrying capability of the betatron. For example, the plasma betatron[3] employs a toroidal magnetic field in the direction of the particle orbit to contain the plasma. Current interest is focused on high-current nonneutral electron acceleration in modified betatrons.[4-6]

By adding a stellarator field to a cyclic accelerator, a strong-focusing system[7] is obtained which can sustain high currents and large mismatch between particle energy and vertical field. The energy bandwidth relaxes the design requirements for the injector and the magnetic field system. Unlike fixed-field alternating-gradient betatrons,[8] the stellarator-betatron (or stellatron) includes a strong toroidal field to confine very high currents. Figure 1 shows a sketch of the stellatron configuration.

We have quantitatively studied the stellatron configuration. Our studies have consisted of numerical and single-particle orbit calculations, as well as analytical linearized orbit theory, including the beam self-fields.

We may study the behavior of an intense electron beam in the stellatron quantitatively by considering small departures from a "reference orbit," a circle located at the null point in the quadrupole field, at $r=r_0$, $z=0$. Here and below we use a cylindrical (r,θ,z) coordinate system with origin at the center of the torus's major cross section. Quantities evaluated at the reference orbit will carry a subscript 0 below; departures from this orbit will carry a subscript 1. The twisted quadrupole field, of period $2\pi/m$, then is written as

$$B_r \cong kB_z(-r_1 \sin m\theta + z_1 \cos m\theta),$$
$$B_z \cong kB_z(r_1 \cos m\theta + z_1 \sin m\theta), \quad B_\theta \cong B_{\theta 0}, \tag{1}$$

where $k, B_z, B_{\theta 0}$ are constants, and the betatron field is

$$B_r \cong -nB_{z0}z_1/r_0, \quad B_z \cong B_{z0}[1-n(r_1/r_0)], \tag{2}$$

where B_{z0} is the vertical field at the reference orbit and n is the usual field index.

We consider the motion of an electron located within a beam whose center is located at $r=r_0+\Delta r$, $z=\Delta z$; the electron's position is $r=r_0+\Delta r+\delta r \equiv r_0+r_1$, $z=\Delta z+\delta z \equiv z_1$. Using a cylindrical approximation for the beam self-fields, we

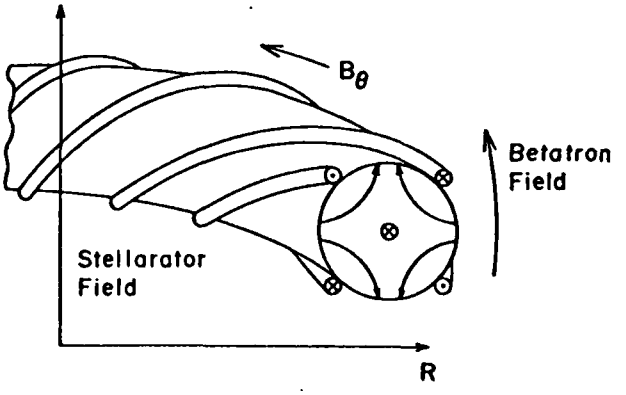

FIG. 1. Stellatron configuration.

find

$$\ddot{r}_1+\Omega_{s0}^2(1-n+\mu\cos m\theta)r_1-\frac{1}{2}\frac{\omega_b^2}{\gamma_0^2}\left(\delta r+\frac{r_b^2}{a^2}\Delta r\right)=\frac{\gamma_1 c^2}{\gamma_0 r_0}-(\mu\Omega_{s0}^2\sin m\theta)z_1+\Omega_{\theta 0}\dot{z}_1), \tag{3a}$$

$$\ddot{z}_1+\Omega_{s0}^2(n-\mu\cos m\theta)z_1-\frac{1}{2}\frac{\omega_b^2}{\gamma_0^2}\left(\delta z+\frac{r_b^2}{a^2}\Delta z\right)=-(\mu\Omega_{s0}^2\sin m\theta)r_1-\Omega_{\theta 0}\dot{r}_1, \tag{3b}$$

$$\dot{\theta}_1=-(r_1/r_0)\Omega_{s0}, \tag{3c}$$

where $\Omega_{s0}=eB_{s0}/m\gamma_0 c$, γ_0 is the relativistic factor for the reference orbit, $\omega_b^2=4\pi n_0 e^2/m\gamma_0$, n_0 is the beam number density, r_b is the minor radius of the beam, a is the minor radius of the (perfectly conducting) chamber, and $\mu=kr_0B_s/B_{s0}$.

By performing a formal ensemble average of (3a)–(3c) one may find equations governing single-particle motion and that of the beam centroid. Details will be published elsewhere. By changing the independent variable from t to θ, and making the transformation $\xi=(r_1+iZ_1)/r_0=\psi\exp(im\theta/2)$, one obtains an equation for ψ which may be solved in the special case, $n=\frac{1}{2}$, with the following results.

Particle motion is oscillatory (under certain conditions; see below) about a center located at

$$\frac{\delta r}{r_0}=\frac{\Delta-\langle\Delta\rangle}{\bar{n}_b+\mu^2(m^2+mb-\bar{n}_b)^{-1}}, \tag{4}$$

where $\bar{n}_b=\frac{1}{2}-n_s$, $n_s=\omega_b^2/2\gamma_0^2\Omega_{s0}^2$, $b=B_{\theta 0}/B_{s0}$, $\Delta=\gamma_1/\beta_0^2\gamma_0$, and angular brackets denote an ensemble average. There are five characterisitc oscillation frequencies, $m\Omega_{s0}$ and $(m/2\pm\nu_s)\Omega_{s0}$, where

$$\nu_s^2=\hat{n}+\tfrac{1}{4}\hat{m}^2\pm(\hat{n}\hat{m}^2+\mu^2)^{1/2} \tag{5}$$

with $\hat{n}=\bar{n}_b+\frac{1}{4}b^2$, $\hat{m}=m+b$. These frequencies are real when the system is located within the regions of the plane of Fig. 2 marked "stable." We remark that for low-current beams ($n_0\to 0$) the stability condition reduces to

$$|\tfrac{1}{2}m^2+mb-1|>|2\mu|. \tag{6}$$

The "most" stable configuration results when the field lines are twisted clockwise ($m>0$) when viewed in the direction of $B_\theta\hat{\theta}$, i.e., in the same sense as electron gyration about B_θ.

Similarly, the motion of the beam center is itself oscillatory about a center located at

$$\frac{\Delta r}{r_0}=\frac{\langle\Delta\rangle}{\bar{n}_b+\mu^2(m^2+mb-\bar{n}_b)^{-1}}, \tag{7}$$

where $\bar{n}_b=\frac{1}{2}-(r_b^2/a^2)n_s$, with characteristic frequencies as in (5), under the replacement $n_s\to(r_b^2/a^2)n_s$.

Two important features of the solution are worth pointing out. First, stable motion is possible throughout an injection-acceleration cycle. This has been checked for many possible time histories. A typical trajectory in the stability plane is shown in Fig. 2. The unstable region on the left of the diagram would not be entered in this case even if the acceleration were continued; "u" never changes sign in this case.

The second important feature of the solution pertains to the energy bandwidth of this machine. We note that the radial shift (7) of the orbit of a mismatched beam is, as expected, much smaller than that in a weak focusing ($\mu=0$) device. (μ can easily exceed 100–200 in designs we have considered.) The stellatron's large energy bandwidth has very helpful consequences for injector and magnetic field design tolerances.

The introduction of *fixed* toroidal and helical fields to the betatron causes the betatron wavelengths to depend on energy, resulting in resonant instabilities driven by field errors during acceleration. If the toroidal field is sufficiently large, the betatron wavelengths will be insensitive to beam current. Such instabilities may be avoided by holding all the fields in constant ratio during acceleration. Alternatively, the effect of the

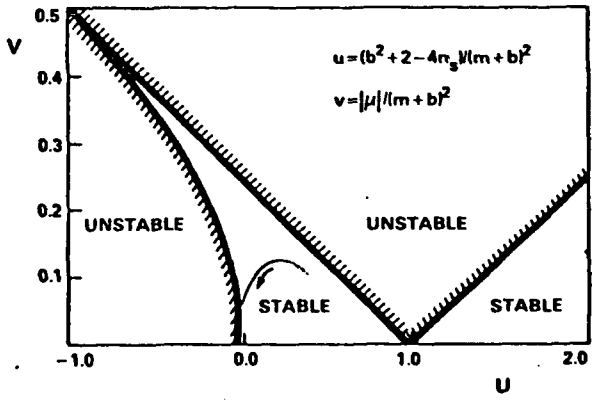

FIG. 2. Stellatron stability plane ($n=\frac{1}{2}$). The dotted line is the trajectory of an experiment with $I=10$ kA, $B_{\theta 0}=5$ kG, $\epsilon_l\equiv 2\mu/mb=1$, $m=20$, $r_0=1$ m, while B_{s0} is raised from 118 to 1700 G, corresponding to an increase in energy from ~3.5 to 50 MeV.

instabilities may be minimized if the energy gain per revolution is large enough to pass rapidly through each resonance.

A single-particle code, which integrates the relativistic equations of motion for an electron in an applied magnetic field, has been utilized to study certain nonlinear aspects of the stellatron configuration. Unlike the analytical analysis of the preceding paragraphs, this analysis does not employ a paraxial approximation for the electron motion and does not use an expansion in the particle displacement from a reference orbit. Also, the applied field in this analysis includes toroidal corrections to first order in the inverse aspect ratio.

The total magnetic field utilized by the code may be expressed as $\vec{B}=\vec{B}_b+\vec{B}_s$, where $\vec{B}_b$ is the conventional betatron field, given by Eq. (2), and $\vec{B}_s$ is the stellarator field, given by $\vec{B}_s=\nabla\Phi_s$, in terms of the magnetic scalar potential, Φ_s, which may be expressed as $\Phi_s{}^{(0)}+\Phi_s{}^{(1)}$, where

$$\Phi_s{}^{(0)}(\rho,\varphi,s)=B_{\theta 0}\{s+(\epsilon_l/\alpha)I_l(x)\sin[l(\varphi-\alpha s)]\}.$$

Here, $x=l\alpha\rho$, $\alpha=2\pi/L$, L is the helix pitch length, and I_l represents the modified Bessel function. The coordinates (ρ,φ,s) form a local cylindrical system centered on the minor axis, where $s=R_0\theta$ is distance measured along the minor axis for toroidal angle θ, and (ρ,φ) are polar coordinates in the plane transverse to the minor axis at s. The toroidal correction, $\varphi_s{}^{(1)}$, is given to first order in the inverse aspect ratio by Danilkin.[9] All calculations have been performed for $l=2$. The variables μ and m, which describe the helical field in the previous analytical analysis, are given by $\mu=\epsilon mb/2$ and $m=2\alpha R_0$ for $l=2$.

This model has been utilized to investigate the single-particle bandwidth of the stellatron. As ϵ_l increases, the allowed mismatch in the stellatron becomes too large to be correctly modeled by the linearized theory. Figure 3 shows the results from both models for bandwidth versus ϵ_l. These calculations assume a torus having a 1-m

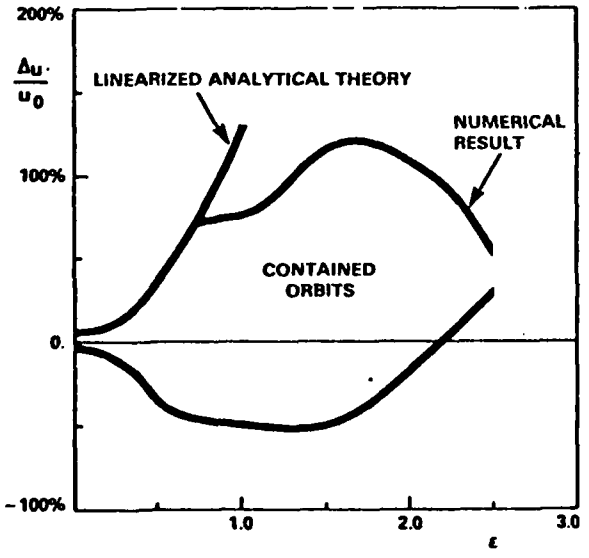

FIG. 3. Stellatron single-particle bandwidth. The bandwidth $\Delta u/u_0$, where $u=\gamma\beta$, is plotted against $\epsilon_l \equiv 2\mu/mb$. The accelerator is matched at $\gamma=7$ with $B_{s0}=118$ G, and $B_{00}=1$ kG.

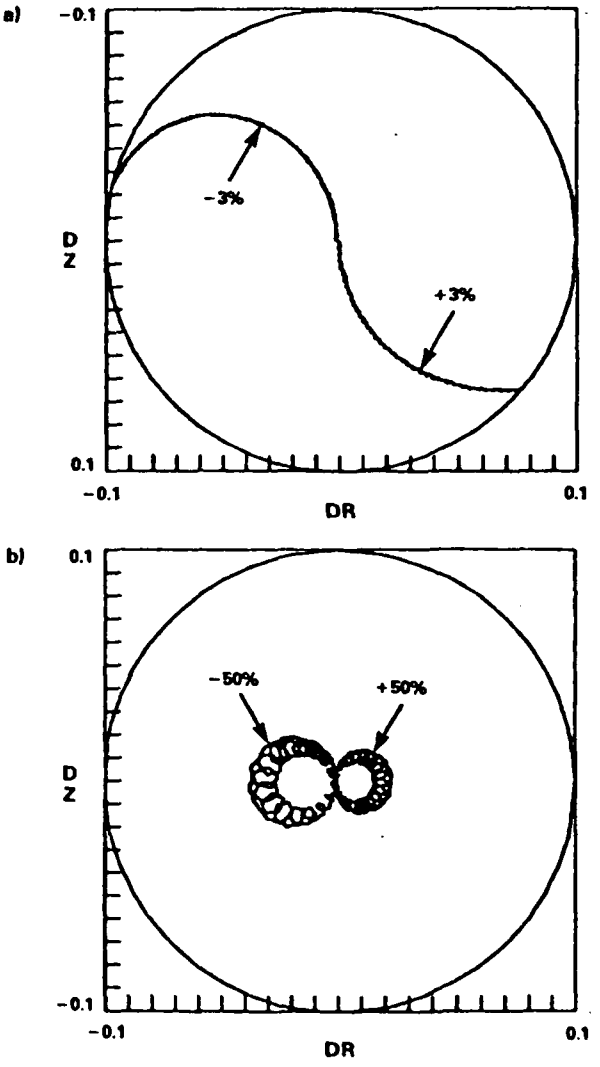

FIG. 4. Single-particle orbits. (a) Without the helical field components ($\epsilon_l \equiv 0$), $\Delta u/u_0=\pm 3\%$; (b) stellatron orbit with $\epsilon_l=\frac{1}{2}$, $\Delta u/u_0=\pm 50\%$.

major radius and a 10-cm minor radius. A test electron is launched tangent to the minor axis with relativistic momentum $u=\gamma\beta$, which differs from the matched momentum, u_0, by varying amounts, Δu. The figure shows $\Delta u/u_0$ against ϵ_l, and represents the maximum $|\Delta u/u_0|$ for which the test orbit remained confined in the device. Mismatch in excess of 50% can be tolerated for these parameters.

Figure 4(b) shows typical stellatron orbits, projected on the minor cross section, for $B_{\theta 0}=5$ kG, $\epsilon_l=\frac{1}{2}$ for $\pm 50\%$ mismatch. The betatron field is again 118 G with $n=\frac{1}{2}$. Without the helical field contribution, Fig. 4(a) shows that as little as $\pm 3\%$ mismatch is not tolerable.

The superposition of twisted quadrupole, toroidal, and conventional betatron magnetic fields appears to offer significant practical advantages for the confinement and acceleration of large electron currents (tens of kiloamperes) to moderate energies (hundreds of megaelectronvolts). Foremost among these advantages is the greatly improved energy bandwidth over that of a weak-focusing device. The large bandwidth of the stellatron relaxes the requirements for monoenergetic injection, for a uniform (within a few percent) magnetic field configuration, and for a rigid mechanical design. Injection should not be any more difficult than for other high-current accelerator concepts, and is facilitated by the externally applied rotational transform of the stellerator field. The orbits should remain stable from injection up to the highest energies achievable by conventional inductive acceleration.

It is a pleasure to acknowledge numerous discussions with members of the Naval Research Laboratory Special Focus Program "Advanced Accelerators." This work was supported by the Naval Research Laboratory.

---

[1]D. W. Kerst, Phys. Rev. 58, 841 (1940).

[2]D. W. Kerst, G. D. Adams, H. W. Koch, and C. S. Robinson, Phys. Rev. 78, 297 (1950).

[3]L. A. Ferrari and K. C. Rogers, Phys. Fluids 10, 1319 (1967).

[4]P. Sprangle and C. A. Kapetanakos, J. Appl. Phys. 49, 1 (1978).

[5]N. Rostoker, Comments Plasma Phys. Controlled Fusion 6, 91 (1980).

[6]P. Sprangle, C. A. Kapetanakos, and S. J. Marsh, in Proceedings of the International Topical Conference on High-Power Electron and Ion Beam Research and Technology, Palaiseau, France, 1981 (unpublished), p. 803.

[7]A. A. Mondelli and C. W. Roberson, NRL Memorandum Report No. 5008, 1982 (unpublished).

[8]K. R. Symon, D. W. Kerst, L. W. Jones, L. J. Laslett, and K. M. Terwilliger, Phys. Rev. 103, 1837 (1956).

[9]I. S. Danilkin, in *Stellarators, Proceedings of the P. N. Lebedev Physics Institute*, edited by D. V. Skobel'tsyn (Consultants Bureau, New York, 1974), Vol. 65, p. 61ff.

APPENDIX G

A Bumpy Torus Betatron

A BUMPY TORUS BETATRON

D. Chernin
Berkeley Research Associates
Springfield, Virginia 22150

A. Mondelli
Science Applications, Inc.
McLean, Virginia 22102

C. Roberson
Office of Naval Research
Arlington, Virginia 22217

ABSTRACT

The combination of a bumpy torus field and a conventional betatron field leads to an interesting strongly-focused, high-current accelerator configuration. We discuss the single particle orbital stability question and show that the strong-focusing in this accelerator can easily lead to greater than 20% bandwidth in allowed mismatch between the vertical magnetic field and the average beam particle energy.

Conventional betatrons[1] are current-limited due to the space charge at injection. Until recently, the approach to multi-kiloampere betatrons has concentrated exclusively on overcoming this space charge limit. High current conventional betatrons[2] employ high-energy injectors, while modified betatrons[3,4] employ a toroidal magnetic field to prevent space charge blow-up. In both of these cases however, a mismatch between the injection energy and vertical field of a few percent will cause the beam to hit the wall. The maximum allowed error in the vertical field is typically on the order of a few gauss. Recently it was shown[5] that the combination of an $\ell = 2$ stellarator and betatron field results in a strong focusing high-current betatron or, "stellatron," with a large energy bandwidth. Such a configuration has the advantages of relaxing the vertical field and injector tolerances. In addition, the strong focusing introduces a threshold for the negative mass instability, so that this instability does not operate at injection. In this note we report analytical and numerical results on the bandwidth and stability of an alternative strong-focusing scheme, namely, a combination "bumpy torus" and betatron field, corresponding to the $\ell = 0$ stellatron.

The bumpy-torus betatron field consists of a superposition of an $\ell = 0$ stellarator field and the field of a conventional betatron. Near the minor axis at $r = r_o$, $z = 0$, this field has the form

$$B_r = -nyB_{zo} + \frac{1}{2}\,\delta B_\theta\, mx \sin m\theta$$

$$B_\theta = B_{\theta o}\left(1 + \frac{\delta B_\theta}{B_{\theta o}} \cos m\theta\right) \qquad (1)$$

$$B_z = B_{zo}(1 - nx) + \frac{1}{2}\,\delta B_\theta\, my \sin m\theta$$

where $x \equiv (r-r_o)/r_o$, $y \equiv z/r_o$, θ is the azimuthal angle, n is the vertical field index, and m is the number of bumpy-torus field periods around the torus. B_{zo}, $B_{\theta o}$, and δB_θ are constants.

In the paraxial approximation, the equation for particle motion is, for $n = \frac{1}{2}$,

$$\frac{d^2\psi}{d\phi^2} + \frac{1}{m^2}\left[2 - 4n_s + b^2\,(1 + \varepsilon\cos 2\phi)^2\right]\psi = \frac{4}{m^2}\,\frac{\delta p}{p_o}\, e^{\frac{ib}{2m}(2\phi + \varepsilon \sin 2\phi)}, \qquad (2)$$

where $\phi \equiv m\theta/2$, $\psi \equiv (x+iy)\exp\left[(i/2)\int b(1 - \varepsilon\cos m\theta)\,d\theta\right]$, $b \equiv B_{\theta o}/B_{zo}$, $\varepsilon \equiv \delta B_\theta/B_{\theta o}$, p_o is the momentum of a particle which would circulate on the minor axis, δp is the "momentum error," and the self-fields are included via $n_s \equiv \omega_b^2/\left(2\gamma_o^2\,\Omega_{zo}^2\right)$ where ω_b, Ω_{zo} are the beam plasma frequency and the vertical-field cyclotron frequency, respectively.

Eq.(2) is a Hill equation, which has characteristic bands of stability, as shown in Figure 1. The shaded regions in the figure are unstable portions of the plane, ε vs. b/m, for the case $n_s = 30$ and $m = 30$. The intersections of the unstable regions with the abscissa are given by

$$\left(b^2 + 2 - 4n_s\right)/m^2 = q^2, \text{ where } q = 0, 1, 2, \ldots.$$

As we increase B_z to accelerate the electrons, we typically would not wish to increase B_θ. The result is that the operating point of the accelerator will tend to move from right to left in Figure 1. Consequently, the accelerator should be run in the left-most stable band to avoid crossing unstable bands. These considerations require m>b at injection and force the use of a large number of field periods in the design of the strong-focusing system.

The left-most unstable band, corresponding to q = 0, is due to beam space-charge and rapidly disappears during acceleration since the self-field index, n_s, is proportional to γ^{-3}, where γ is the relativistic factor. The left-most stable band, therefore, becomes broader during acceleration.

In conventional betatrons, resonances are avoided by increasing γ and the accelerating field in synchronism. The introduction of non-synchronous fields, as in the modified betatron and the stellatron, makes the betatron wavelengths energy-dependent, which can lead to the crossing of resonant instabilities driven by field errors during acceleration. As in all strong-focusing devices, the occurence of orbital resonances plays an important role in the operation of the bumpy-torus betatron. Using the Floquet solutions to (2) it is possible to obtain a condition for the integer resonances, when space-charge effects may be neglected:

$$\psi_1(\pi) = \cos\left[\pi\left(\frac{b+2n}{m}\right)\right] \tag{3}$$

where $\psi_1(\phi)$ is the solution to (2) with $\delta P \equiv 0$ satisfying $\psi_1(o) = 1$, $\psi_1'(o) = 0$ where n is an integer, the Fourier component number of the dipole field error. Equation (3) provides the basis for numerical calculation of contours in the stability plane where (3) is satisfied for a given n; an example is given in Figure 2.

If all the fields cannot be made synchronous with the particle energy, the effect of resonant instabilities could be minimized by making the energy gain per pass large.

Finally, we consider the question of containment of beams whose average momentum is not matched to the vertical betatron field, i.e. the question of the momentum compaction of this configuration. Figure 3 shows the allowed mismatch, $\Delta P/P_0$, plotted against $\varepsilon \equiv \delta B_\theta/B_\theta$ for $B_{\theta o} = 2kG$, $B_{zo} = 118G$, $n = \frac{1}{2}$, $r_o = 100cm$ and $m = 30$. This plot is generated numerically by launching particles on the minor axis along the toroidal direction with various amounts of mismatch. The figure shows the largest mismatch for which the calculated orbits are contained in a 10 cm minor radius chamber. Containment of particles with a mismatch of $\pm 20\%$ is obtained for $\varepsilon \simeq 0.2$.

In conclusion, we find the spatially alternating transverse magnetic field associated with a bumpy-torus provides an alternating field gradient on the minor axis, which leads to a potentially interesting strongly-focused accelerator configuration. This new accelerator is seen to have a region

of stable orbits, and to have a significant bandwidth in allowed mismatch between the vertical magnetic field and the particle momentum.

This work was supported by the Naval Research Laboratory. We wish to acknowledge discussions with members of the Advanced Accelerator Project at NRL.

References

1. See, e.g. D.W. Kerst, Handbuch der Physik, XLIV, 13 (1959).

2. E. Lee et al, Proc. 1983 Particle Accelerator Conference (to be published).

3. P. Sprangle and C.A. Kapetanakos, J. Appl. Phys. 49. 1 (1978).

4. N. Rostoker, Comm. Plasma Phys. 6, 91 (1980).

5. C. Roberson, A. Mondelli, and D. Chernin, Phys. Rev. Lett. 50, 507 (1983).

LIST OF FIGURES

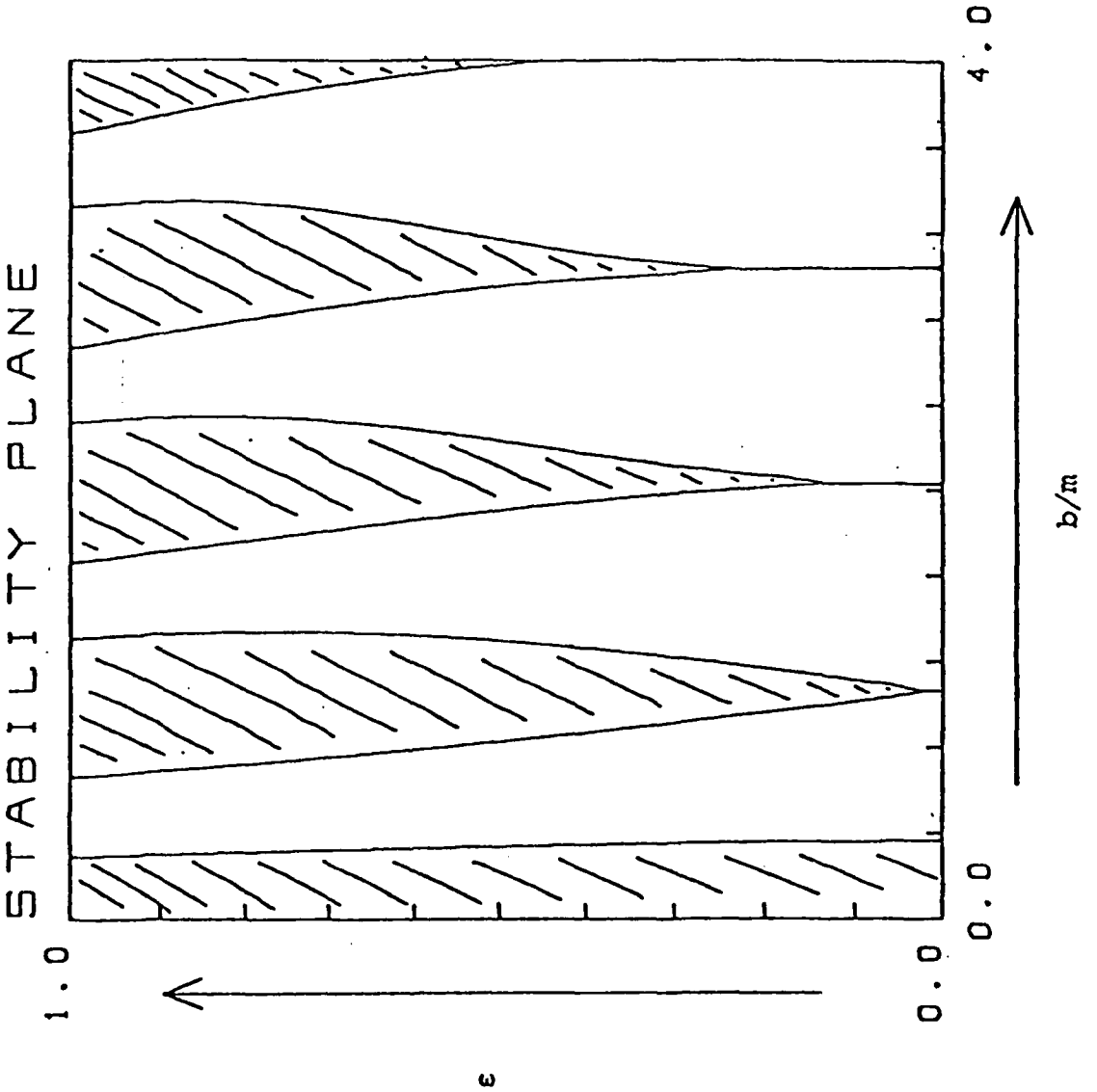
STABILITY PLANE
1.0
0.0
ω
0.0
4.0
b/m

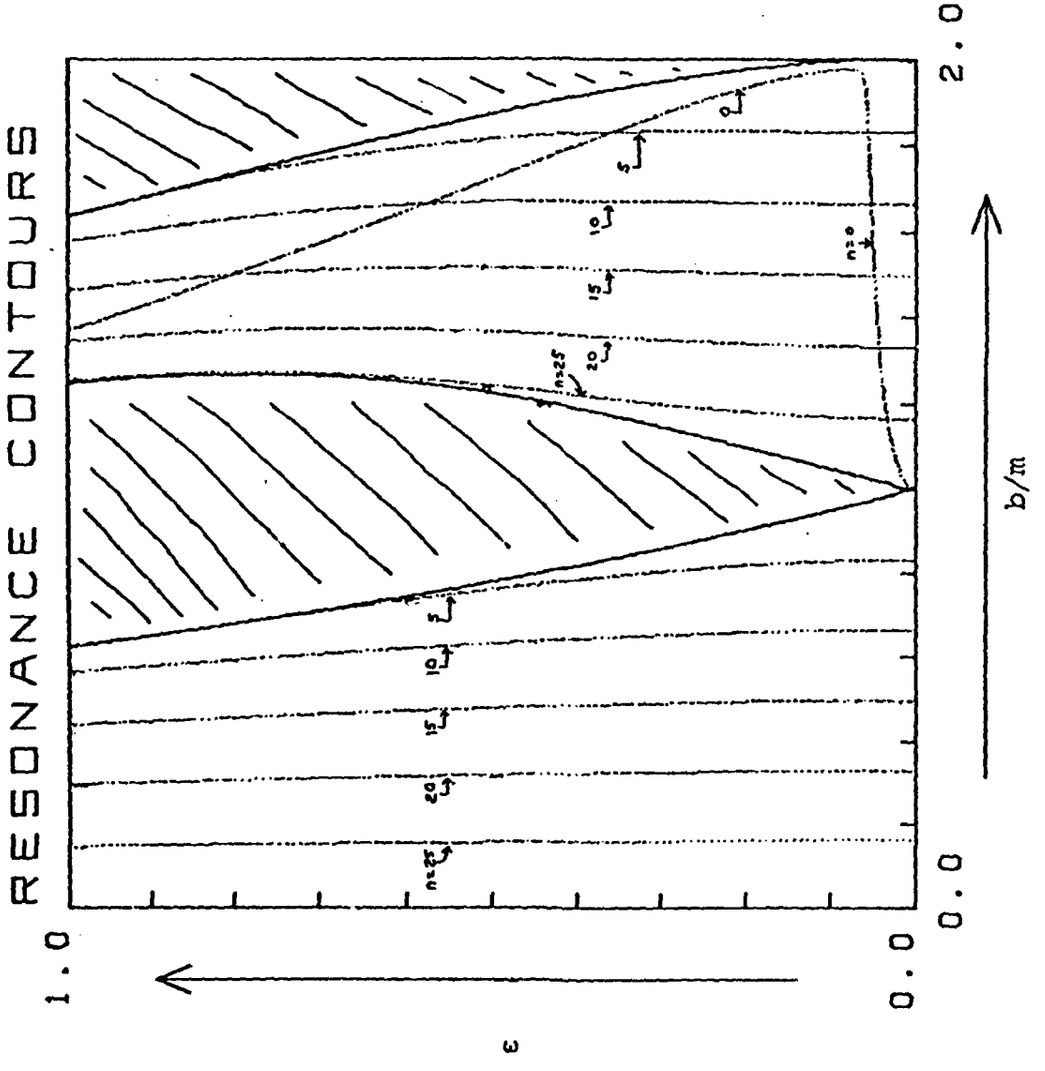
RESONANCE CONTOURS
1.0
0.0
0.0
2.0
b/m
ε
n=0
5
10
15
20
n=25

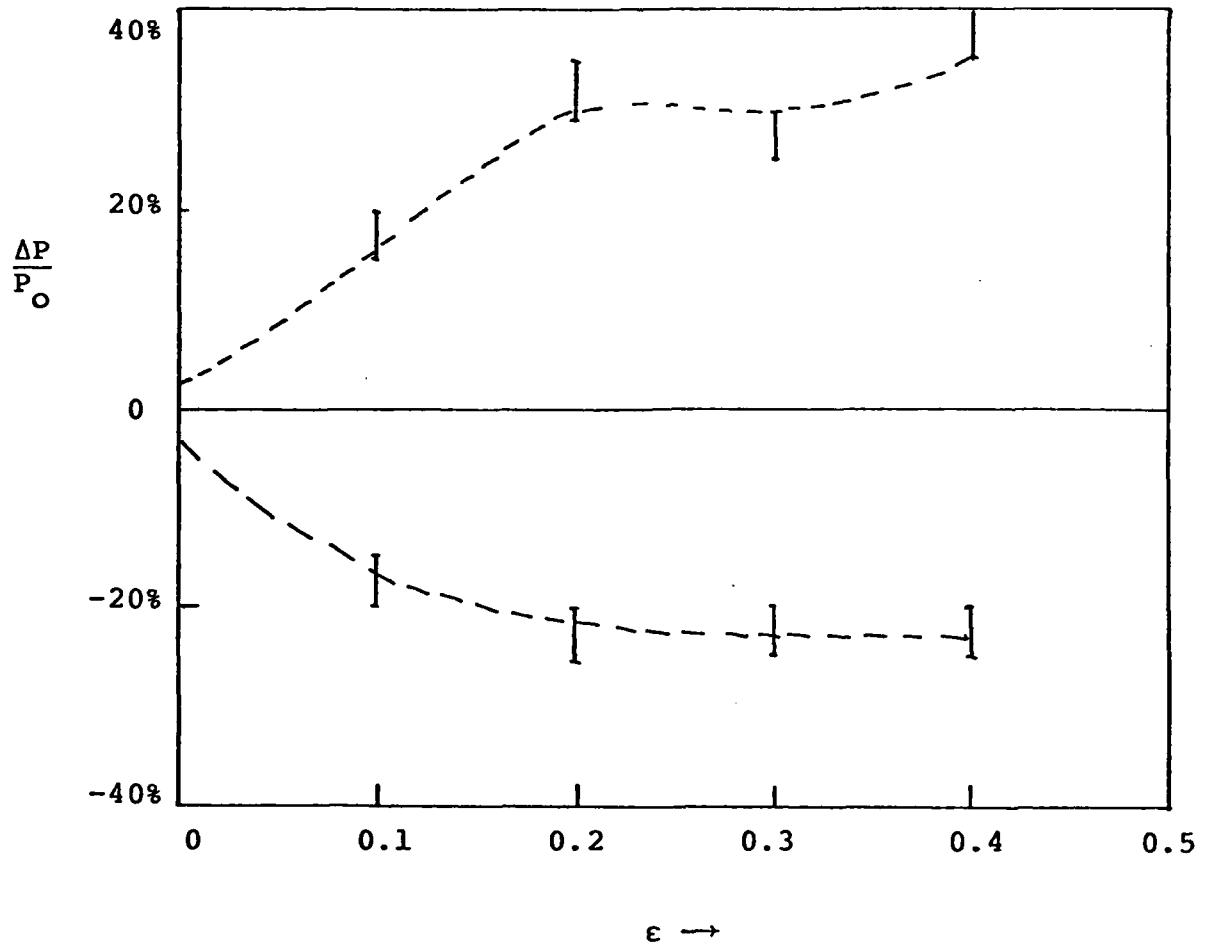
40%
20%
0
-20%
-40%
$\frac{\Delta P}{P_o}$
0
0.1
0.2
0.3
0.4
0.5
ε →

APPENDIX AA

Program LBE

This program uses the IMSL subroutine DVERK to integrate the linearized equations of motion for either the beam centroid or for individual particles within a beam in a modified betatron.

Input Data File[1]: FORØØ2.DAT

IFLAG, IFLAG 1 : IFLAG = Ø: beam center equations

= 1: particle equations

IFLAG 1 = Ø: use nonlinear image fields (IFLAG = Ø, only)

= 1: use linear image fields only (IFLAG = Ø, only)

$r-r_o$, $\dot{r}$, z, $\dot{z}$: Initial values for position and velocity

DPTH : $\frac{1}{mr_oc} \langle \delta p_\theta \rangle$ for IFLAG = Ø

: $\frac{1}{mr_oc} [\delta p_\theta - \langle \delta p_\theta \rangle]$ for IFLAG = 1

r_o, a, n : Chamber major, minor radii, field index

I, r_b : Current (kA)[2], beam minor radius

AE, AB : Dimensionless correction quantities added to ℓ_E and ℓ_B, respectively. (Logarithms appearing in toroidal correction terms.) ($\ell_E = \ell n(a/r_b) + AE$; $\ell_B = \ell n(a/r_b) + 1 + AB$)

Dτ, KMAX, KPT, TOL: Dimensionless time step[3], total number of steps, output file writing frequency[4], integration error parameter

B_{zi}, B_{zf}, t_{acc} : Initial, final vertical field values; acceleration time[5]

$B_{\theta i}$, $B_{\theta f}$, $t_{B\theta}$: Initial, final toroidal field values; time for change of B_θ[5]

Notes: [1]All quantities in cgs units unless otherwise specified.

[2]If I is entered as a negative number, the density used in calculating n_s is $(|I|/17)/\pi r_b^2 r_o$, as for positive I, but all toroidal corrections to coefficients are set to zero.

[3]Time step = $D\tau/(eB_{\theta i}/m\gamma_i c)$.

[4]e.g. If KPT = 2, output is written (to file FORØØ3.DAT) every other time step.

[5]A linear variation in time is used.

Output Data File: FORØØ3.DAT

Binary File

At successive times:

$$t,\ r-r_o,\ z,\ \gamma,\ \omega_x^2/\Omega_{\theta o}^2,\ \omega_y^2/\Omega_{\theta o}^2$$

```
00020   0001            PROGRAM LBE
00040   0002            INCLUDE 'LBECM.FOR'
00060   0012            COMPLEX*16 ZW
00080   0013            XIMW=0.D0
00100   0014            REWIND 3
00120   0015            CALL INPUT
00140   0016            WRITE(6,5)
00160   0017    5       FORMAT(' INITIAL VALUES (T=0):')
00180   0018            WRITE(6,6)BZI,BTHI,GMA
00200   0019    6       FORMAT(' BZ=',1PD12.3,4X,'BTHETA=',1PD12.3,4X,'GAMMA=',
00220   0020        *   1PD12.3)
00240   0021            CALL OUTPUT
00260   0022            DO10 K=1,KMAX
00280   0023            CALL STEP
00300   0024            CALL COEF(OM,OMDT,WX2,WY2,TAU/WSCALE)
00320   0025            IF(WX2*WY2.GT.0.D0)GOTO8
00340   0026            OM2=OM*OM
00360   0027            W2=WX2+WY2+OM2
00380   0028            ZW=W2-DSQRT(W2*W2-4.D0*WX2*WY2)
00400   0029            ZW=CDSQRT(ZW/2.D0)
00420   0030            XIMW=XIMW+DIMAG(ZW)*DTAU/WSCALE
00440   0031    8       CONTINUE
00460   0032            IF(MOD(K,KPT).NE.0)GOTO10
00480   0033            CALL OUTPUT
00500   0034    10      CONTINUE
00520   0035            ENDFILE 3
00530   0036            TD=TAU/WSCALE
00540   0037            WRITE(6,15)TD
00560   0038    15      FORMAT(' FINAL VALUES (t=' 1PD12.3,'):')
00580   0039            BZ=BZI+BZDT*TD
00600   0040            BTH=BTHI+BTHDT*TD
00620   0041            WRITE(6,6)BZ,BTH,GMA
00640   0042            PRINT20,XIMW
00660   0043    20      FORMAT(/,5X,' THE INTEGRAL OF IM(W)= ',1PD10.3,/)
00680   0044            STOP
00700   0045            END
```

40.2

```
00720   0001    C
00740   0002            SUBROUTINE INPUT
00760   0003            INCLUDE 'LBECM.FOR'
00780   0013            DATA CC/24*0.D0/,IND/1/,EOMC/1.7588D7/
00800   0014            DIMENSION G(4)
00820   0015            REWIND 2
00840   0016            READ(2,*)IFLAG,IFLAG1
00860   0017            READ(2,*) (G(I),I=1,4)
00880   0018            TAU=0.D0
00900   0019            READ(2,*)DPTH
00920   0020            READ(2,*)R0,A,EN
00940   0021            READ(2,*)CURR,RB
00960   0022            XNU=CURR/17.045
00980   0023            RB2=RB*RB
01000   0024            DEN=XNU/(RB2*8.8527D-13)
01020   0025            IF(DEN.GE.0.D0)GOTO5
01040   0026            DEN=-DEN
01060   0027            XNU=0.D0
01080   0028    5       CONTINUE
01100   0029            ELK=RB2/(4*A*A)
01120   0030            ELN=DLOG(A/RB)
01130   0031            READ(2,*)AE,AB
01140   0032            ELE=ELN+ELK+AE
01160   0033            ELB=ELN+1-ELK+AB
01180   0034            FACTR=(RB/A)**2
01200   0035            IF(IFLAG.EQ.1)FACTR=1.D0
01220   0036            FACTR=FACTR*1.5913D9*DEN
01240   0037            READ(2,*)DTAU,KMAX,KPT,TOL
01260   0038            READ(2,*)BZI,BZF,TAC
01280   0039            BZDT=(BZF-BZI)/TAC
01300   0040            READ(2,*)BTHI,BTHF,TBTH
01320   0041            DBTH=BTHF-BTHI
01340   0042            CALL GAMMA(GMAI,BZI,XNU,ELE,ELB,R0)
01360   0043            GMA=GMAI
01380   0044            WSCALE=ABS(EOMC*BTHI/GMAI)
01400   0045            WS2=WSCALE**2
01420   0046            SGMA=DSQRT(GMAI)
01440   0047            F(1)=SGMA*g(1)
01460   0048            F(3)=SGMA*G(3)
01480   0049            F(2)=(GMADT*G1/(2*SGMA)+SGMA*G(2))/WSCALE
01500   0050            F(4)=(GMADT*G1/(2*SGMA)+SGMA*G(2))/WSCALE
01520   0051            DTIME=DTAU/WSCALE
01540   0052            PRINT10,DTIME
01560   0053    10      FORMAT(5X,'TIME STEP FOR THIS PROBLEM IS ',1PD12.3)
01580   0054            RETURN
01600   0055            END
```

```
0162@   0001     C
0164@   0002           SUBROUTINE STEP
0166@   0003           INCLUDE 'LBECM.FOR'
0168@   0013           DIMENSION W(4,9)
0170@   0014           EXTERNAL FDOT
0172@   0015           TAU1=TAU+DTAU
0174@   0016           CALL DVERK(4,FDOT,TAU,F,TAU1,TOL,IND,CC,4,W,IER)
0176@   0017           IF(IND.LT.0.OR.IER.GT.0)GOTO20
0178@   0018           GOTO30
0180@   0019     20    PRINT 25,IND,IER,(CC(J),J=1,24)
0182@   0020     25    FORMAT(//,5X,'***ERROR CONDITION---SUBROUTINE DVERK*
0184@   0021          1  **',/,10X,'IND=',I3,3X,'IER=',I3,/,10X,'CC=',/,
0186@   0022          2  8(15X,1P3D11.3,/))
0188@   0023           STOP
0190@   0024     30    RETURN
0192@   0025           END
```

PROGRAM SECTIONS

	Name	Bytes	Attributes
0	$CODE	123	PIC CON REL LCL SHR EXE RD NOWRT LONG
1	$PDATA	98	PIC CON REL LCL SHR NOEXE RD NOWRT LONG
2	$LOCAL	352	PIC CON REL LCL NOSHR NOEXE RD WRT QUAD
3	C0	8	PIC OVR REL GBL SHR NOEXE RD WRT LONG
4	C1	48	PIC OVR REL GBL SHR NOEXE RD WRT LONG
5	C2	24	PIC OVR REL GBL SHR NOEXE RD WRT LONG
6	C3	40	PIC OVR REL GBL SHR NOEXE RD WRT LONG
7	C4	236	PIC OVR REL GBL SHR NOEXE RD WRT LONG
8	C5	24	PIC OVR REL GBL SHR NOEXE RD WRT LONG
9	C6	24	PIC OVR REL GBL SHR NOEXE RD WRT LONG
10	C7	16	PIC OVR REL GBL SHR NOEXE RD WRT LONG
	Total Space Allocated	993	

ENTRY POINTS

Address	Type	Name
0-00000000		STEP

VARIABLES

Address	Type	Name	Address	Type	Name	Address	Type	Name	Address	Type	Name
5-00000008	R*8	A	9-00000000	R*8	BTHI	4-00000020	R*8	BZI	9-00000008	R*8	DBTH
6-00000018	R*8	DPTH	7-00000000	R*8	DTAU	8-00000010	R*8	DTIME	10-00000008	R*8	ELB
10-00000000	R*8	ELE	5-00000010	R*8	EN	6-00000010	R*8	FACTR	8-00000000	R*8	GMA
8-00000008	R*8	GMADT	2-00000128	I*4	IER	3-00000000	I*4	IFLAG	3-00000004	I*4	IFLAG1
7-000000E8	I*4	IND	2-0000012C	I*4	J	7-00000018	I*4	KMAX	7-0000001C	I*4	KPT
5-00000000	R*8	R0	6-00000008	R*8	RB	4-00000028	R*8	TAU	2-00000120	R*8	TAU1
9-00000010	R*8	TBTH	6-00000020	R*8	TEMPT	7-000000E0	R*8	TOL	7-00000010	R*8	WS2

```
01940     0001     C
01960     0002           SUBROUTINE FDOT(N,TAUD,F,DFDT)
01980     0003           IMPLICIT REAL*8(A-H,O-R,T-Z)
02000     0004           COMMON/C0/IFLAG
02020     0005           COMMON/C3/XNU,RB,FACTR,DPTH,TEMPT
02040     0006           COMMON/C4/DTAU,WSCALE,WS2,KMAX,CC(24),TOL,IND
02060     0007           DIMENSION F(N),DFDT(N)
02080     0008           CALL COEF(OM,OMDT,WX2,WY2,TAUD/WSCALE)
02100     0009           DFDT(1)=F(2)
02120     0010           DFDT(2)=OM*F(4)/WSCALE+0.5*OMDT*F(3)/WS2-WX2*F(1)/WS2
02140     0011         1 +TEMPT/WS2
02160     0012           DFDT(3)=F(4)
02180     0013           DFDT(4)=-OM*F(2)/WSCALE-0.5*OMDT*F(1)/WS2-WY2*F(3)/WS2
02200     0014           RETURN
02220     0015           END
```

PROGRAM SECTIONS

	Name	Bytes	Attributes
0	$CODE	187	PIC CON REL LCL SHR EXE RD NOWRT LONG
2	$LOCAL	136	PIC CON REL LCL NOSHR NOEXE RD WRT QUAD
3	C0	4	PIC OVR REL GBL SHR NOEXE RD WRT LONG
4	C3	40	PIC OVR REL GBL SHR NOEXE RD WRT LONG
5	C4	232	PIC OVR REL GBL SHR NOEXE RD WRT LONG
	Total Space Allocated	599	

40.5

ENTRY POINTS

Address	Type	Name
0-00000000		FDOT

VARIABLES

Address	Type	Name	Address	Type	Name	Address	Type	Name	Address	Type	Name
4-00000018	R*8	DPTH	5-00000000	R*8	DTAU	4-00000010	R*8	FACTR	3-00000000	I*4	IFLAG
5-000000E4	I*4	IND	5-00000018	I*4	KMAX	AP-00000004@	I*4	N	2-00000000	R*8	OM
2-00000008	R*8	OMDT	4-00000008	R*8	RB	AP-00000008@	R*8	TAUD	4-00000020	R*8	TEMPT
5-000000DC	R*8	TOL	5-00000010	R*8	WS2	5-00000008	R*8	WSCALE	2-00000010	R*8	WX2
2-00000018	R*8	WY2	4-00000000	R*8	XNU						

ARRAYS

Address	Type	Name	Bytes	Dimensions
5-0000001C	R*8	CC	192	(24)
AP-00000010@	R*8	DFDT	**	(*)
AP-0000000C@	R*8	F	**	(*)

```
 02240     0001     C
 02260     0002           SUBROUTINE COEF(OM,OMDT,WX2,WY2,TD)
 02280     0003           INCLUDE 'LBECM.FOR'
 02300     0013           DATA EOMC/1.7588D7/,C/2.9979D10/
 02320     0014           BZ=BZI+BZDT*TD
 02340     0015           GMADT2=0.D0
 02360     0016           CALL GAMMA(GMA,BZ,XNU,ELE,ELB,R0)
 02380     0017           BZ2=BZ+BZDT*DTIME
 02400     0018           CALL GAMMA(GMA2,BZ2,XNU,ELE,ELB,R0)
 02420     0019           GMADT=(GMA2-GMA)/DTIME
 02440     0020           OMZ=EOMC*BZ/GMA
 02460     0021           AA=OMZ*R0/C
 02480     0022           OMG2=0.5*GMADT2/GMA-0.25*((GMADT/GMA)**2)
 02500     0023           XNUG=XNU/GMA
 02520     0024           ELEA=ELE/(AA**2)
 02540     0025           BTHDT=DBTH/TBTH
 02560     0026           BTH=BTHI+BTHDT*TD
 02580     0027           OM=EOMC*BTH/GMA
 02600     0028           OMDT=EOMC*(BTHDT/GMA-BTH*GMADT/(GMA*GMA))
 02620     0029           ENST=EN*(1.D0-XNUG*(ELEA+ELB))
 02640     0030           ENSLFF=FACTR/((GMA**3)*(OMZ**2))
 02660     0031           IF((IFLAG.EQ.0).AND.(IFLAG1.EQ.0))
 02680     0032          1  ENSLFF=ENSLFF/(1.D0-(F(1)**2+F(3)**2)/(GMA*A*A))
 02700     0033           S=2.D0+DFLOAT(IFLAG)
 02720     0034           WX2=OMZ*OMZ*(1.D0-ENST-ENSLFF-XNUG*(S*ELEA+2.D0
 02740     0035          1  *ELB))-OMG2
 02760     0036           WY2=OMZ*OMZ*(ENST-ENSLFF)-OMG2
 02780     0037           CORR=XNUG*((1.D0+1.D0/(GMA**2))*ELEA+ELB)
 02800     0038           TEMPT=OMZ*C*DPTH*(1.D0-CORR)/GMA
 02820     0039           RETURN
 02840     0040           END
```

40.6

```
02860   0001    C
02880   0002            SUBROUTINE OUTPUT
02900   0003            INCLUDE 'LBECM.FOR'
02920   0013            DATA IN/0/
02940   0014            T=TAU/WSCALE
02960   0015            ST=T
02980   0016            CALL COEF(OM,OMDT,WX2,WY2,T)
03000   0017            OM2=OM*OM
03020   0018            SX2=WX2/OM2
03040   0019            SY2=WY2/OM2
03060   0020            SG=GMA
03080   0021            IF(WX2*WY2)10,20,20
03100   0022    10      CONTINUE
03120   0023            IF(IN)50,30,50
03140   0024    30      IN=1
03160   0025            PRINT35,ST,SG
03180   0026    35      FORMAT(/,5X,'SPACE CHARGE INSTABILITY ONSET AT T=',
03200   0027         1  D10.3,/,40X,'GAMMA=',F8.3)
03220   0028            GOTO50
03240   0029    20      IF(IN)50,50,40
03260   0030    40      IN=0
03280   0031            PRINT45,ST,SG
03300   0032    45      FORMAT(/,5X,'SPACE CHARGE INSTABILITY TURN OFF AT T=',
03320   0033         1  D10.3,/,40X,'GAMMA=',F8.3)
03340   0034    50      CONTINUE
03360   0035            FG=DSQRT(GMA)
03380   0036            SDR=F(1)/FG
03400   0037            SDZ=F(3)/FG
03420   0038            WRITE(3)ST,SDR,SDZ,SG,SX2,SY2
03440   0039            RETURN
03460   0040            END
```

```
03480   0001     C
03500   0002           SUBROUTINE GAMMA(SGMA,BZ,XNU,ELE,ELB,R0)
03520   0003           IMPLICIT REAL*8(A-H,O-R,T-Z)
03540   0004           DATA EOMC/1.75887D7/,C/2.9979D10/
03560   0005           CN=EOMC*R0*BZ/C
03580   0006           GM0=DSQRT(1+CN**2)
03600   0007           ALH=CN/GM0
03620   0008           CN2=CN*CN
03640   0009           SGMA=GM0-XNU*(ELE+CN2/(1+CN2)*ELB)
03660   0010           RETURN
03680   0011           END
```

PROGRAM SECTIONS

	Name	Bytes	Attributes
0	$CODE	84	PIC CON REL LCL SHR EXE RD NOWRT LONG
2	$LOCAL	48	PIC CON REL LCL NOSHR NOEXE RD WRT QUAD
	Total Space Allocated	132	

ENTRY POINTS

Address	Type	Name
0-00000000		GAMMA

VARIABLES

Address	Type	Name	Address	Type	Name	Address	Type	Name	Address	Type	Name
2-00000020	R*8	ALH	AP-00000008@	R*8	BZ	2-00000008	R*8	C	2-00000010	R*8	CN
2-00000028	R*8	CN2	AP-00000014@	R*8	ELB	AP-00000010@	R*8	ELE	2-00000000	R*8	EOMC
2-00000018	R*8	GM0	AP-00000018@	R*8	R0	AP-00000004@	R*4	SGMA	AP-0000000C@	R*8	XNU

FUNCTIONS AND SUBROUTINES REFERENCED

Type	Name
R*8	MTH$DSQRT

COMMAND QUALIFIERS

```
  FORTRAN /LIS LBE

  /CHECK=(NOBOUNDS,OVERFLOW,NOUNDERFLOW)
  /DEBUG=(NOSYMBOLS,TRACEBACK)
  /STANDARD=(NOSYNTAX,NOSOURCE_FORM)
  /SHOW=(NOPREPROCESSOR,NOINCLUDE,MAP)
  /F77  /NOG_FLOATING  /I4  /OPTIMIZE  /WARNINGS  /NOD_LINES  /NOCROSS_REFERENCE  /NOMACHINE_CODE  /CONTINUATIONS=19
```

```
100           IMPLICIT REAL*8(A-H,O-R,T-Z)
150           COMMON/C0/IFLAG,IFLAG1
200           COMMON/C1/F(4),BZI,TAU
300           COMMON/C2/R0,A,EN
400           COMMON/C3/XNU,RB,FACTR,DPTH,TEMPT
500           COMMON/C4/DTAU,WSCALE,WS2,KMAX,KPT,CC(24),TOL,IND
600           COMMON/C5/GMA,GMADT,DTIME
700           COMMON/C6/BTHI,DBTH,TBTH
800           COMMON/C7/ELE,ELB
```

APPENDIX BB

Program BTRAK

This program uses the IMSL subroutine DVERK to integrate the single particle equations of motion in various accelerator field configurations.

Input Data File[1]: FORØ25.DAT

r_o	:	Major radius
B_{zo}, n, n_2, n_3	:	Vertical magnetic field and field indices at r_o[2]
$B_{\phi o}$	:	Toroidal field at r_o
KSTEL	:	(Ø,1) = (no,yes) stellarator field present
μ,m	:	(if KSTEL = 1, for stellarator field[3])
Model	:	Field error model[4]: 0 = No field error 1 = Cylindrical limit ($r_o \to \infty$) 2 = (r,z) cylindrical coordinates
δB, m, ℓ	:	Model = 1
δB, α, λr_o, m, NZ	:	Model = 2
Dτ, KTOT, TOL, MXOUT	:	Dimensionless step size[5], total number of steps, integrator error control, max number of points written to output file.
δr, δz, ϕ	:	Initial values
$(\delta r)_{max}$, $(\delta z)_{max}$	:	If $\lvert\delta r\rvert > \delta r_{max}$ or $\lvert\delta z\rvert > \delta z_{max}$ during calculation, program is halted.
γ, f_r, f_z	:	$\gamma_{initial}$, $f_r \equiv \beta_r/\beta$, $f_z \equiv \beta_z/\beta$ initial values.

Notes: [1]All quantities in cgs units

[2]$$B_z = B_{zo}\left(1 - nx + \frac{1}{2}n_2x^2 + \frac{1}{2}(n-n_2)y^2 + n_3x^3/6 - \frac{1}{2}(n+n_2+n_3)xy^2\right)$$

$$x = (r-r_o)/r_o;\quad y = z/r_o$$

[3]$$B_r = B_{zo}\mu[-x\,\sin m\phi + y\,\cos m\phi]$$

$$B_z = B_{zo}\mu[x\,\cos m\phi + y\,\sin m\phi]$$

[4]Model 1:

$$\left.\begin{aligned} B_r &= \delta B\,\mathrm{Im}[(k\delta r + ik\delta z)^{\ell-1}e^{im\phi}] \\ B_\phi &= \delta B\tfrac{1}{\ell}\mathrm{Re}[(k\delta r + ik\delta z)^{\ell}e^{im\phi}] \\ B_z &= \delta B\,\mathrm{Re}[(k\delta r + ik\delta z)^{\ell-1}e^{im\phi}] \end{aligned}\right\} \quad \text{if } \ell \neq 0$$

$$\left.\begin{aligned} B_r &= \tfrac{1}{2}\delta B k\delta r\,\sin m\phi \\ B_\phi &= \delta B\,\cos m\phi \\ B_z &= \tfrac{1}{2}\delta B k\delta z\,\sin m\phi \end{aligned}\right\} \quad \text{if } \ell = 0$$

where $k \equiv m/r_o$.

Model 2:

$$B_r = \frac{\delta B}{\lambda r_o}\,[\alpha + 2\beta x]\,z(\lambda z)\sin m\phi$$

$$B_\phi = \frac{\delta B}{\lambda r_o}\,m\,[1 + \alpha x + \beta x^2]\,z(\lambda z)\cos m\phi$$

$$B_z = \delta B[1 + \alpha x + \beta x^2]\,z'(\lambda z)\sin m\phi$$

where $x = (r-r_o)/r_o$

$$\beta = \tfrac{1}{2}(m^2 - \alpha - (\lambda r_o)^2)$$

$z(\lambda z) = \sinh(\lambda z)$ NZ = 1

$z(\lambda z) = \cosh(\lambda z)$ NZ $\neq$ 1

[5]$dt = t^* d\tau$ where $t^* = 2\pi/\max(\Omega_{zo}, \Omega_{\theta o})$.

BTRAK OUTPUT FILE

FORØ26.DAT

Binary File

At successive times:

$r-r_o$, $\phi/2\pi$, z, β_r, $1-\beta_\phi$, β_z, γ, t

```
0001  0001            PROGRAM BTRAK
0002  0002      C     LINK BTRAK+STEPPER+'IMSL'
0003  0003            IMPLICIT REAL*8(A-H,O-R,T-Z)
0004  0004            DIMENSION YI(6),W(6,9)
0005  0005            COMMON/CONTROL/DTAU,TSTAR,CTSTAR,FF,KTOT,TOL,MXOUT
0006  0006            COMMON/GMA/GMMN,GMMX
0007  0007            EXTERNAL FDOT,OUTPT
0008  0008            CALL INPUT(YI)
0009  0009            CALL STEPPER(6,YI,0.D0,DTAU,KTOT,TOL,W,FDOT,OUTPT,MXOUT)
0010  0010            PRINT10,GMMN,GMMX
0011  0011      10    FORMAT(' RANGE OF GAMMA:',/,2X,1P2D30.16,/)
0012  0012            STOP
0013  0013            END
```

PROGRAM SECTIONS

	Name	Bytes	Attributes
0	$CODE	80	PIC CON REL LCL SHR EXE RD NOWRT LONG
1	$PDATA	42	PIC CON REL LCL SHR NOEXE RD NOWRT QUAD
2	$LOCAL	532	PIC CON REL LCL NOSHR NOEXE RD WRT QUAD
3	CONTROL	48	PIC OVR REL GBL SHR NOEXE RD WRT LONG
4	GMA	16	PIC OVR REL GBL SHR NOEXE RD WRT LONG
	Total Space Allocated	718	

41.3

ENTRY POINTS

Address	Type	Name
0-00000000		BTRAK

VARIABLES

Address	Type	Name	Address	Type	Name	Address	Type	Name	Address	Type	Name
3-00000010	R*8	CTSTAR	3-00000000	R*8	DTAU	3-00000018	R*8	FF	4-00000000	R*8	GMMN
4-00000008	R*8	GMMX	3-00000020	I*4	KTOT	3-0000002C	I*4	MXOUT	3-00000024	R*8	TOL
3-00000008	R*8	TSTAR									

ARRAYS

Address	Type	Name	Bytes	Dimensions
2-00000030	R*8	W	432	(6, 9)
2-00000000	R*8	YI	48	(6)

```
0001              SUBROUTINE INPUT(YI)
0002              INCLUDE 'BTRAKCOM.FOR'
0018              DIMENSION YI(6)
0019              READ(25,*)RØ
0020              READ(25,*)BZØ,EN,EN2,EN3
0021              ENSM=EN+EN2+EN3
0022              READ(25,*)BPHØ
0023              READ(25,*)KSTEL
0024              IF(KSTEL.EQ.Ø)GOTO5
0025              READ(25,*)XMU,MSTEL
0026              Q=XMU*BZØ
0027     5        CONTINUE
0028              READ(25,*)MODEL
0029              GOTO(1ØØ,1Ø,2Ø)(MODEL+1)
0030     1Ø       CONTINUE
0031     C
0032     C        MODEL 1: CYLINDRICAL LIMIT OF TORUS
0033     C
0034              READ(25,*)DELB,M,L
0035              GOTO1ØØ
0036     2Ø       CONTINUE
0037     C
0038     C        MODEL 2: CYLINDRICAL COORDINATES
0039     C
0040              READ(25,*)DELB,AA,ELAMRØ,M,NZ
0041              BA=Ø.5DØ*(M*M-ELAMRØ**2-AA)
0042     1ØØ      CONTINUE
0043              READ(25,*)DTAU,KTOT,TOL,MXOUT
0044              W=EOMC*BZØ*RØ/C
0045              G=DSQRT(1.DØ+W*W)
0046              OMZ=DABS(EOMC*BZØ/G)
0047              OMPH=DABS(EOMC*BPHØ/G)
0048              TSTAR=TPI/DMAX1(OMZ,OMPH)
0049              DT=DTAU*TSTAR
0050              CTSTAR=C*TSTAR
0051              FF=-EOMC*TSTAR
0052              PRINT11Ø,DT
0053     11Ø      FORMAT(//,' TIME STEP FOR THIS PROBLEM=',1PD1Ø.2,/)
0054              READ(25,*)DELR,DELZ,PHIØ
0055              READ(25,*)STPR.STPZ
0056              READ(25,*)GMA,FR,FZ
0057              GMMN=GMA
0058              GMMX=GMA
0059              YI(1)=RØ+DELR
0060              YI(2)=PHIØ
0061              YI(3)=DELZ
0062              BETA=DSQRT(1.DØ-1.DØ/(GMA**2))
0063              U=BETA*GMA
0064              FP=DSQRT(1.DØ-FR**2-FZ**2)
0065              YI(4)=FR*U
0066              YI(5)=FP*U
0067              YI(6)=FZ*U
0068              PRINT2ØØ,(YI(J),J=1,6),GMA
0069     2ØØ      FORMAT(' INITIAL VALUES(R,PHI,Z,UR,UPHI,UZ):',/,
0070          1   6(1X,1PD15.8,/),' GAMMA=',1PD3Ø.16,/)
0071              RETURN
0072              END
```

```
      SUBROUTINE FDOT(N,T,Y,YDOT)
      IMPLICIT REAL*8(A-H,O-R,T-Z)
      COMMON/CONTROL/DTAU,TSTAR,CTSTAR,FF,KTOT,TOL,MXOUT
      DIMENSION Y(6),YDOT(6),X(3),F(6)
      DO10 K=1,3
   10 X(K)=Y(K)
      CALL AFIELDS(X,T,F)
      R=Y(1)
      UR=Y(4)
      UP=Y(5)
      UZ=Y(6)
      G=DSQRT(UR**2+UP**2+UZ**2+1.D0)
      D=CTSTAR/G
      OMN=D/R
      YDOT(1)=D*UR
      YDOT(2)=OMN*UP
      YDOT(3)=D*UZ
      YDOT(4)=(UP**2)*OMN+F(1)+(UP*F(6)-UZ*F(5))/G
      YDOT(5)=-UR*UP*OMN+F(2)+(UZ*F(4)-UR*F(6))/G
      YDOT(6)=F(3)+(UR*F(5)-UP*F(4))/G
      RETURN
      END
```

41.5

PROGRAM SECTIONS

	Name	Bytes	Attributes								
0	$CODE	257	PIC	CON	REL	LCL	SHR	EXE	RD	NOWRT	LONG
2	$LOCAL	196	PIC	CON	REL	LCL	NOSHR	NOEXE	RD	WRT	QUAD
3	CONTROL	48	PIC	OVR	REL	GBL	SHR	NOEXE	RD	WRT	LONG
	Total Space Allocated	501									

ENTRY POINTS

Address	Type	Name
0-00000000		FDOT

VARIABLES

Address	Type	Name	Address	Type	Name	Address	Type	Name	Address	Type	Name
3-00000010	R*8	CTSTAR	2-00000070	R*8	D	3-00000000	R*8	DTAU	3-00000018	R*8	FF
2-00000068	R*8	G	2-00000080	I*4	K	3-00000020	I*4	KTOT	3-0000002C	I*4	MXOUT
AP-00000004@	I*4	N	2-00000078	R*8	OMN	2-00000048	R*8	R	AP-00000008@	R*8	T
3-00000024	R*8	TOL	3-00000008	R*8	TSTAR	2-00000058	R*8	UP	2-00000050	R*8	UR
2-00000060	R*8	UZ									

```
0930  0001            SUBROUTINE AFIELDS(X,T,F)
0940  0002            INCLUDE'BTRAKCOM.FOR'
0950  0018            DIMENSION X(3),F(6)
0960  0019            COMPLEX*16 ZZ1,ZZ2,ZZ3,ZZI
0970  0020            DATA ZZI/(0.D0,1.D0)/
0980  0021            R=X(1)
0990  0022            P=DMOD(X(2),TPI)
1000  0023            Z=X(3)
1010  0024            TT=T*TSTAR
1020  0025            XN=(R-R0)/R0
1030  0026            YN=Z/R0
1040  0027            XN2=XN*XN
1050  0028            YN2=YN*YN
1060  0029      C     BETATRON FIELDS
1070  0030            BRB=-BZ0*YN*(EN-EN2*XN-0.5D0*EN3*XN2+ENSM*YN2/6.D0)
1080  0031            BPB=BPH0/(1.D0+XN)
1090  0032            BZB=BZ0*(1.D0-EN*XN+0.5D0*EN2*XN2+0.5D0*(EN-EN2)*YN2
1100  0033           1+EN3*XN2*XN/6.D0-0.5D0*ENSM*XN*YN2)
1110  0034            BRS=0.D0
1120  0035            BPS=0.D0
1130  0036            BZS=0.D0
1140  0037            IF(KSTEL.EQ.0)GOTO5
1150  0038      C     STELLARATOR FIELDS
1160  0039            DC=DCOS(MSTEL*P)
1170  0040            DS=DSIN(MSTEL*P)
1180  0041            BRS=Q*(YN*DC-XN*DS)
1190  0042            BPS=0.D0
1200  0043            BZS=Q*(XN*DC+YN*DS)
1210  0044      5     CONTINUE
1220  0045            BRE=0.D0
1230  0046            BPE=0.D0
1240  0047            BZE=0.D0
1250  0048            GOTO(100,10,20)(MODEL+1)
1260  0049      10    CONTINUE
1270  0050      C     MODEL1
1280  0051            FK=DFLOAT(M)/R0
1290  0052            ZZ1=CDEXP(ZZI*M*P)
1300  0053            IF(L.EQ.0)GOTO15
1310  0054            ZZ2=((R-R0)+ZZI*Z)*FK
1320  0055            ZZ3=ZZ2**(L-1)
1330  0056            BRE=DELB*DIMAG(ZZ3*ZZ1)
1340  0057            BZE=DELB*DREAL(ZZ3*ZZ1)
1350  0058            BPE=DELB*(R0/(DFLOAT(L)*R))*DREAL(ZZ3*ZZ2*ZZ1)
1360  0059            GOTO100
1370  0060      15    CONTINUE
1380  0061            Q=0.5D0*DELB*DIMAG(ZZ1)*FK
1390  0062            BRE=Q*(R-R0)
1400  0063            BZE=Q*Z
1410  0064            BPE=DELB*(R0/R)*DREAL(ZZ1)
1420  0065            GOTO100
1430  0066      20    CONTINUE
1440  0067      C     MODEL 2
1450  0068            DS=DSINH(ELAMR0*YN)
1460  0069            DC=DCOSH(ELAMR0*YN)
1470  0070            IF(NZ.EQ.1)GOTO40
1480  0071            FZ=DC
1490  0072            FZ1=DS
```

```
1500    0073          GOTO50
1510    0074    40    FZ=DS
1520    0075          FZ1=DC
1530    0076    50    CONTINUE
1540    0077          FR=1.D0+AA*XN+BA*XN*XN
1550    0078          FR1=AA+2.D0*BA*XN
1560    0079          DSN=DSIN(M*P)
1570    0080          DCN=DCOS(M*P)
1580    0081          BRE=DELB*FR1*FZ*DSN/ELAMR0
1590    0082          BPE=DELB*M*FR*FZ*DCN*R0/(ELAMR0*R)
1600    0083          BZE=DELB*FR*FZ1*DSN
1610    0084    100   CONTINUE
1620    0085          F(1)=0.D0
1630    0086          F(2)=0.D0
1640    0087          F(3)=0.D0
1650    0088          F(4)=FF*(BRB+BRS+BRE)
1660    0089          F(5)=FF*(BPB+BPS+BPE)
1670    0090          F(6)=FF*(BZB+BZS+BZE)
1680    0091          RETURN
1690    0092          END
```

PROGRAM SECTIONS

	Name	Bytes	Attributes
0	$CODE	1173	PIC CON REL LCL SHR EXE RD NOWRT LONG
2	$LOCAL	384	PIC CON REL LCL NOSHR NOEXE RD WRT QUAD
3	C1	8	PIC OVR REL GBL SHR NOEXE RD WRT LONG
4	C2	40	PIC OVR REL GBL SHR NOEXE RD WRT LONG
5	C3	8	PIC OVR REL GBL SHR NOEXE RD WRT LONG
6	C4	4	PIC OVR REL GBL SHR NOEXE RD WRT LONG
7	C5	16	PIC OVR REL GBL SHR NOEXE RD WRT LONG
8	C6	28	PIC OVR REL GBL SHR NOEXE RD WRT LONG
9	STEL	16	PIC OVR REL GBL SHR NOEXE RD WRT LONG
10	CONTROL	48	PIC OVR REL GBL SHR NOEXE RD WRT LONG
11	GMA	16	PIC OVR REL GBL SHR NOEXE RD WRT LONG
12	QUIT	8	PIC OVR REL GBL SHR NOEXE RD WRT LONG
	Total Space Allocated	1749	

ENTRY POINTS

Address	Type	Name
0-00000000		AFIELDS

```
17000  0001            SUBROUTINE OUTPT(Y,T)
17100  0002            INCLUDE'BTRAKCOM.FOR'
17200  0018            DIMENSION Y(6),S(8)
17300  0019            S(1)=Y(1)-R0
17400  0020            S(2)=Y(2)/TPI
17500  0021            S(3)=Y(3)
17600  0022            G=DSQRT(1.D0+Y(4)**2+Y(5)**2+Y(6)**2)
17700  0023            S(4)=Y(4)/G
17800  0024            S(5)=1.D0-Y(5)/G
17900  0025            S(6)=Y(6)/G
18000  0026            S(7)=G
18100  0027            S(8)=T*TSTAR
18200  0028            WRITE(26) (S(J),J=1,8)
18300  0029            IF(G.LT.GMMN)GMMN=G
18400  0030            IF(G.GT.GMMX)GMMX=G
18500  0031            IF((ABS(S(1)).GE.STPR).OR.(ABS(S(3)).GE.STPZ))GOTO10
18600  0032            GOTO20
18700  0033    10      CONTINUE
18800  0034            WRITE(6,12) S(8)
18900  0035    12      FORMAT(/,' PARTICLE HITS WALL AT T= ',1PE10.3,/)
19000  0036            STOP
19100  0037    20      RETURN
19200  0038            END
```

PROGRAM SECTIONS

	Name	Bytes	Attributes
0	$CODE	280	PIC CON REL LCL SHR EXE RD NOWRT LONG
1	$PDATA	36	PIC CON REL LCL SHR NOEXE RD NOWRT LONG
2	$LOCAL	100	PIC CON REL LCL NOSHR NOEXE RD WRT QUAD
3	C1	8	PIC OVR REL GBL SHR NOEXE RD WRT LONG
4	C2	40	PIC OVR REL GBL SHR NOEXE RD WRT LONG
5	C3	8	PIC OVR REL GBL SHR NOEXE RD WRT LONG
6	C4	4	PIC OVR REL GBL SHR NOEXE RD WRT LONG
7	C5	16	PIC OVR REL GBL SHR NOEXE RD WRT LONG
8	C6	28	PIC OVR REL GBL SHR NOEXE RD WRT LONG
9	STEL	16	PIC OVR REL GBL SHR NOEXE RD WRT LONG
10	CONTROL	48	PIC OVR REL GBL SHR NOEXE RD WRT LONG
11	GMA	16	PIC OVR REL GBL SHR NOEXE RD WRT LONG
12	QUIT	8	PIC OVR REL GBL SHR NOEXE RD WRT LONG
	Total Space Allocated	608	

ENTRY POINTS

Address	Type	Name
0-00000000		OUTPT

```
      IMPLICIT REAL*8(A-H,O-R,T-Z)
      COMMON/C1/RØ
      COMMON/C2/BZØ,EN,EN2,EN3,ENSM
      COMMON/C3/BPHØ
      COMMON/C4/MODEL
      COMMON/C5/DELB,M,L
      COMMON/C6/AA,BA,ELAMRØ,NZ
      COMMON/STEL/KSTEL,Q,MSTEL
      COMMON/CONTROL/DTAU,TSTAR,CTSTAR,FF,KTOT,TOL,MXOUT
      COMMON/GMA/GMMN,GMMX
      COMMON/QUIT/STPR,STPZ
      DATA EOMC/1.7588D7/
      DATA C/2.9979D1Ø/
      DATA TPI/6.2831853Ø7DØ/
```

APPENDIX CC

Program TUNES

This program checks for resonances of the form

$$n_+\nu_+ + n_-\nu_- = P$$

where $\nu_\pm$ are the tunes of the fast and slow modes and $n_\pm$, P are integers. The program checks those $n_\pm$ satisfying $|n_+| + |n_-| \leq 3$ and for $P \leq P_{max}$ where P_{max} is input.

Input Data File[1]: FORØ55.DAT

IFLAG : (o,1) = (beam, particle) motion

r_o, a, r_b : Chamber major, minor radii, beam minor radius

I : Current (kA)

AE, AB : Toroidal corrections: $\ell_E = \ell n(a/r_b) + AE$;

$\ell_B = \ell n(a/r_b) + 1 + AB$

B_{zi}, B_{zf}, n: Initial, final vertical field values[2], field index.

$B_{\theta i}$, $B_{\theta f}$: Initial, final toroidal field values[2].

P_{max} : Maximum value of P to be checked.

Notes: [1]All quantities in cgs units, unless otherwise specified.

[2]Linear variation in time used. (T: 0 - 1)

Interactively Generated Plots

(Uses JAYCOR plotting routine)

Response to plot option? request:

0: No plot (Stop)

1: ν_+, ν_- plane, showing resonance lines

2: ν_+ vs time

3: ν_- vs time

4: γ vs time

Output File: FORØ57.DAT

: List of resonances crossed, with values of ν_+, ν_-, T, γ, B_z, and B_θ at crossing.

```
      PROGRAM TUNES
C     LINK IS: LINK TUNES+'SPLOT'+'JPLOT'
      INCLUDE 'TUNECOM.FOR'
      READ(55,*)IFLAG
      READ(55,*)RØ,A,RB
      RN=(1-IFLAG)*A+IFLAG*RB
      READ(55,*)CUR
      XNU=CUR/17.Ø45
      READ(55,*)AE,AB
      ELE=DLOG(A/RB)+AE
      ELB=ELE-AE+1.DØ+AB
      READ(55,*)BZI,BZF,EN
      DBZ=BZF-BZI
      READ(55,*)BTHI,BTHF
      DBTH=BTHF-BTHI
      READ(55,*)PMAX
      IF(IFLAG.EQ.Ø)WRITE(57,1)
      IF(IFLAG.EQ.1)WRITE(57,2)
1     FORMAT(' BEAM MOTION')
2     FORMAT(' PARTICLE MOTION')
      WRITE(57,3)RØ,CUR,A,EN,RB,PMAX
3     FORMAT(/,' MAJOR RADIUS= ',F7.2,' CM',5X,'I= ',F7.2,' KA'
     * ,/,' MINOR RADIUS= ',F7.2,' CM',5X,'N= ',F6.3,/,
     * '  BEAM RADIUS= ',F7.2,' CM',5X,'PMAX= ',I2,//,
     * '    NF NS P',6X,'NU+',7X,'NU-',7X,'TIME',
     * 5X,'GAMMA',6X,'BZ',8X,'BTHETA',/)
      DT=1.D-3
      T=Ø.
      M=Ø
      ISTEP=1
2Ø    CALL TUNE
      IF(VF*VS.EQ.Ø.DØ)GOTO25
      CALL JKPSET(JKP1)
      T=T+DT
      ISTEP=ISTEP+1
      GOTO5Ø
25    T=T+DT
      ISTEP=ISTEP+1
      IF(ISTEP.GT.1ØØ1)GOTO1ØØ
      GOTO2Ø
5Ø    CONTINUE
      CALL TUNE
      IF(VF*VS.EQ.Ø.DØ)GOTO75
      CALL JKPSET(JKP2)
      CALL JKPCOM(JKP1,JKP2)
75    CONTINUE
      T=T+DT
      ISTEP=ISTEP+1
      IF(ISTEP.GT.1ØØ1)GOTO1ØØ
      GOTO5Ø
1ØØ   CALL PLOTS
      STOP
      END
```

```
0540 0001              SUBROUTINE TUNE
0550 0002              INCLUDE 'TUNECOM.FOR'
0560 0019              BZ=BZI+T*DBZ
0570 0020              BTH=BTHI+T*DBTH
0580 0021              B=BTH/BZ
0590 0022              F=5.8668D-4*R0*BZ
0600 0023              F2=F*F
0610 0024              GMA0=DSQRT(1.D0+F2)
0620 0025              GMA1=-XNU*(ELE+(F2/(1.D0+F2))*ELB)
0630 0026              GMA=GMA0+GMA1
0640 0027              XNUG=XNU/GMA
0650 0028              ENSX=2.D0*XNUG*((R0/RN)**2)/F2
0660 0029              AA2=F2/(GMA*GMA)
0670 0030              ELEA=ELE/AA2
0680 0031              E=1.D0-XNUG*(ELEA+ELB)
0690 0032              ENST=EN*E
0700 0033              EL=((2+IFLAG)*ELEA+2.D0*ELB)*XNUG
0710 0034              WX2=1.D0-ENST-ENSX-EL
0720 0035              WY2=ENST-ENSX
0730 0036              Z1=WX2+WY2+B**2
0740 0037              Z2=Z1**2-4.D0*WX2*WY2
0750 0038              Z3=CDSQRT(Z2)
0760 0039              ZF=CDSQRT((Z1+Z3)/2.D0)
0770 0040              ZS=CDSQRT((Z1-Z3)/2.D0)
0780 0041              VF=DREAL(ZF)/E
0790 0042              VS=DREAL(ZS)/E
0800 0043              IF(MOD(ISTEP,2).EQ.0)GOTO10
0810 0044              KP=(ISTEP+1)/2
0820 0045              SVFR(KP)=VF
0830 0046              SVFI(KP)=DIMAG(ZF)/E
0840 0047              SVSR(KP)=VS
0850 0048              SVSI(KP)=DIMAG(ZS)/E
0860 0049              SGMA(KP)=GMA
0870 0050              STM(KP)=T
0880 0051     10       RETURN
0890 0052              END
```

```
00000     0001            SUBROUTINE JKPSET(JKP1)
00100     0002            INCLUDE 'TUNECOM.FOR'
00200     0019            DO10 P=0,PMAX
00300     0020            P1=P+1
00400     0021            DO20 N=1,13
00500     0022            IF(P.EQ.0.AND.(N.LE.6.OR.N.EQ.10))GOTO20
00600     0023            IF((N.EQ.2.OR.N.EQ.3).AND.MOD(P,K(N)).EQ.0)GOTO20
00700     0024            IF((N.EQ.5.OR.N.EQ.6).AND.MOD(P,J(N)).EQ.0)GOTO20
00800     0025            X=J(N)*VS+K(N)*VF-P
00900     0026            IF(X.LE.0.D0)JKP1(N,P1)=-1
10000     0027            IF(X.GT.0.D0)JKP1(N,P1)=1
10100     0028    20      CONTINUE
10200     0029    10      CONTINUE
10300     0030            RETURN
10400     0031            END
```

PROGRAM SECTIONS

	Name	Bytes	Attributes
0	SCODE	218	PIC CON REL LCL SHR EXE RD NOWRT LONG
2	SLOCAL	668	PIC CON REL LCL NOSHR NOEXE RD WRT QUAD
3	C0	4	PIC OVR REL GBL SHR NOEXE RD WRT LONG
4	C1	56	PIC OVR REL GBL SHR NOEXE RD WRT LONG
5	C2	4	PIC OVR REL GBL SHR NOEXE RD WRT LONG
6	C3	40	PIC OVR REL GBL SHR NOEXE RD WRT LONG
7	C4	24	PIC OVR REL GBL SHR NOEXE RD WRT LONG
8	C5	28	PIC OVR REL GBL SHR NOEXE RD WRT LONG
9	PLOT1	12024	PIC OVR REL GBL SHR NOEXE RD WRT LONG
10	PLOT2	1204	PIC OVR REL GBL SHR NOEXE RD WRT LONG
	Total Space Allocated	1427	

42.4

E..TRY POINTS

Address	Type	Name
0-00000000		JKPSET

VARIABLES

Address	Type	Name	Address	Type	Name	Address	Type	Name	Address	Type	Name
4-00000008	R*8	A	7-00000008	R*8	BTH	6-00000018	R*8	BTHI	7-00000000	R*8	BZ
6-00000000	R*8	BZI	6-00000020	R*8	DBTH	6-00000008	R*8	DBZ	4-00000030	R*8	ELB
4-00000028	R*8	ELE	6-00000010	R*8	EN	7-00000010	R*8	GMA	3-00000000	I*4	IFLAG
8-00000018	I*4	ISTEP	10-00000000	I*4	M	2-00000280	I*4	N	2-00000278	I*4	P
2-0000027C	R*4	P1	5-00000000	I*4	PMAX	4-00000000	R*8	R0	4-00000010	R*8	RB
4-00000018	R*8	RN	8-00000010	R*8	T	8-00000000	R*8	VF	8-00000008	R*8	VS
2-00000270	R*8	X	4-00000020	R*8	XNU						

```
10500   0001            SUBROUTINE JKPCOM(JKP1,JKP2)
10600   0002            INCLUDE 'TUNECOM.FOR'
10700   0019            DO10 P=0,PMAX
10800   0020            P1=P+1
10900   0021            DO20 N=1,13
11000   0022            IF(P.EQ.0.AND.(N.LE.6.OR.N.EQ.10))GOTO20
11100   0023            IF((N.EQ.2.OR.N.EQ.3).AND.MOD(P,K'[illegible]).EQ.0)GOTO20
11200   0024            IF((N.EQ.5.OR.N.EQ.6).AND.MOD(P,J[illegible]).EQ.0)GOTO20
11300   0025            IF(JKP1(N,P1)*JKP2(N,P1))22,20,20
11400   0026     22     WRITE(57,100)K(N),J(N),P,VF,VS,T,GMA,BZ,BTH
11500   0027     100    FORMAT(1X,3I3,4F10.3,2F11.3)
11600   0028            M=M+1
11700   0029            MRES(M,1)=K(N)
11800   0030            MRES(M,2)=J(N)
11900   0031            MRES(M,3)=P
12000   0032            JKP1(N,P1)=JKP2(N,P1)
12100   0033     20     CONTINUE
12200   0034     10     CONTINUE
12300   0035            RETURN
12400   0036            END
```

PROGRAM SECTIONS

	Name	Bytes	Attributes
0	$CODE	357	PIC CON REL LCL SHR EXE RD NOWRT LONG
1	$PDATA	17	PIC CON REL LCL SHR NOEXE RD NOWRT LONG
2	$LOCAL	160	PIC CON REL LCL NOSHR NOEXE RD WRT LONG
3	C0	4	PIC OVR REL GBL SHR NOEXE RD WRT LONG
4	C1	56	PIC OVR REL GBL SHR NOEXE RD WRT LONG
5	C2	4	PIC OVR REL GBL SHR NOEXE RD WRT LONG
6	C3	40	PIC OVR REL GBL SHR NOEXE RD WRT LONG
7	C4	24	PIC OVR REL GBL SHR NOEXE RD WRT LONG
8	C5	28	PIC OVR REL GBL SHR NOEXE RD WRT LONG
9	PLOT1	12024	PIC OVR REL GBL SHR NOEXE RD WRT LONG
10	PLOT2	1204	PIC OVR REL GBL SHR NOEXE RD WRT LONG
	Total Space Allocated	13918	

ENTRY POINTS

Address	Type	Name
0-00000000		JKPCOM

VARIABLES

Address	Type	Name	Address	Type	Name	Address	Type	Name	Address	Type	Name
4-00000008	R*8	A	7-00000008	R*8	BTH	6-00000018	R*8	BTHI	7-00000000	R*8	BZ
6-00000000	R*8	BZI	6-00000020	R*8	DBTH	6-00000008	R*8	DBZ	4-00000030	R*8	ELB
4-00000028	R*8	ELE	6-00000010	R*8	EN	7-00000010	R*8	GMA	3-00000000	I*4	IFLAG

```
12500   0001            SUBROUTINE PLOTS
12600   0002            DIMENSION XPLOT(501),YPLOT(501),XL(2),YL(2)
12700   0003            CHARACTER*19 IT1(2)
12800   0004            CHARACTER*13 IT2(2)
12900   0005            CHARACTER*5 LBL(4)
13000   0006            CHARACTER*1 NO
13100   0007            COMMON/C0/IFLAG
13200   0008            COMMON/PLOT1/VFR(501),VFI(501),VSR(501),VSI(501),
13300   0009          * GMA(501),TM(501)
13400   0010            COMMON/PLOT2/M,MRES(100,3)
13500   0011            DATA VFMAX,VFMIN,VSMAX,VSMIN,GMAX,GMIN/6*0./
13600   0012            DATA IT1/'  BEAM RESONANCES  ','PARTICLE RESONANCES'/
13700   0013            DATA IT2/'  BEAM TUNE  ','PARTICLE TUNE'/
13800   0014            DATA LBL/' NU+ ',' NU- ','TIME ','GAMMA'/
13900   0015            DATA NO/' '/
14000   0016            IF=0
14100   0017    1       PRINT10
14200   0018    10      FORMAT(/,' PLOT OPTION ?',$)
14300   0019            READ(5,*)IPLOT
14400   0020            IF(IPLOT.LE.0)RETURN
14500   0021            IF=IF+1
14600   0022            IF(IF.GT.1)GOTO25
14700   0023            DO20 J=1,501
14800   0024            VFMAX=AMAX1(VFR(J),VFI(J),VFMAX)
14900   0025            VFMIN=AMIN1(VFR(J),VFI(J),VFMIN)
15000   0026            VSMAX=AMAX1(VSR(J),VSI(J),VSMAX)
15100   0027            VSMIN=AMIN1(VSR(J),VSI(J),VSMIN)
15200   0028            GMAX=AMAX1(GMA(J),GMAX)
15300   0029            GMIN=AMIN1(GMA(J),GMIN)
15400   0030    20      CONTINUE
15500   0031    25      GOTO(100,200,300,400)(IPLOT)
15600   0032    100     CONTINUE
15700   0033    C       PLOT NU+ - NU- PLANE,SHOWING RESONANCE LINES.
15800   0034            WRITE(5,110)VFMIN,VFMAX,VSMIN,VSMAX
15900   0035    110     FORMAT(/,' RANGES OF NU+,NU- ARE: ',2F8.4,/,24X,2F8.4,/,
16000   0036          * ' ENTER PLOT RANGE(MIN,MAX) FOR NU+: ',$)
16100   0037            READ(5,*)YMIN,YMAX
16200   0038            WRITE(5,112)
16300   0039    112     FORMAT(' ENTER PLOT RANGE(MIN,MAX) FOR NU-: ',$)
16400   0040            READ(5,*)XMIN,XMAX
16500   0041    C       PLOT RESONANCE  LINES
16600   0042            IF(M.EQ.0)GOTO169
16700   0043            DO120 MM=1,M
16800   0044            NF=MRES(MM,1)
16900   0045            NS=MRES(MM,2)
17000   0046            P=MRES(MM,3)
17100   0047            IF(NF.EQ.0)GOTO140
17200   0048            AOB=FLOAT(NS)/FLOAT(NF)
17300   0049            IF(NS.NE.0)COA=P/FLOAT(NS)
17400   0050            COB=P/FLOAT(NF)
17500   0051            YMX=COB-AOB*XMAX
17600   0052            YMN=COB-AOB*XMIN
17700   0053            L=0
17800   0054            IF((YMN.LE.YMIN).AND.(YMX.GE.YMIN).AND.(YMX.LE.YMAX))L=1
17900   0055            IF(((YMN.LE.YMIN).AND.(YMX.GE.YMAX)).OR.
18000   0056          * ((YMN.GE.YMAX).AND.(YMX.LE.YMIN)))L=2
18100   0057            IF((YMN.LE.YMAX).AND.(YMN.GE.YMIN).AND.(YMX.LE.YMIN))L=3
```

```
18200  0058            IF((YMN.LE.YMAX).AND.(YMN.GE.YMIN).AND.(YMX.LE.YMAX)
18300  0059         1  .AND.(YMX.GE.YMIN))L=4
18400  0060            IF((YMN.LE.YMAX).AND.(YMN.GE.YMIN).AND.(YMX.GE.YMAX))L=5
18500  0061            IF((YMN.GE.YMAX).AND.(YMX.LE.YMAX).AND.(YMX.GE.YMIN))L=6
18600  0062            IF((NS.EQ.0).AND.(YMX.LE.YMAX).AND.(YMX.GE.YMIN))L=4
18700  0063            GOTO(120,121,121,122,122,122,123)(L+1)
18800  0064     121    XL(1)=COA-YMIN/AOB
18900  0065            YL(1)=YMIN
19000  0066            GOTO(224,223)L
19100  0067     122    XL(1)=XMIN
19200  0068            YL(1)=YMN
19300  0069            GOTO(221,224,223)(L-2)
19400  0070     123    XL(1)=COA-YMAX/AOB
19500  0071            YL(1)=YMAX
19600  0072            GOTO224
19700  0073     221    XL(2)=COA-YMIN/AOB
19800  0074            YL(2)=YMIN
19900  0075            GOTO150
20000  0076     223    XL(2)=COA-YMAX/AOB
20100  0077            YL(2)=YMAX
20200  0078            GOTO150
20300  0079     224    XL(2)=XMAX
20400  0080            YL(2)=YMX
20500  0081            GOTO150
20600  0082     140    CONTINUE
20700  0083     C      VERTICAL LINE
20800  0084            COA=P/FLOAT(NS)
20900  0085            IF((COA.GE.XMAX).OR.(COA.LE.XMIN))GOTO120
21000  0086            YL(1)=YMAX
21100  0087            YL(2)=YMIN
21200  0088            XL(1)=COA
21300  0089            XL(2)=XL(1)
21400  0090     150    CONTINUE
21500  0091            LT=2
21600  0092            IF(NF*NS.GE.0)LT=1
21700  0093            CALL PLOT(XL,YL,2,1,LT,NO,NO,0,25,5,XMAX,XMIN,NO,
21800  0094         1  0,25,5,YMAX,YMIN,NO)
21900  0095     120    CONTINUE
22000  0096     C      PLOTS OF RESONANCE LINES COMPLETED
22100  0097     C      PLOT EXPERIMENTAL TRAJECTORY
22200  0098     169    CONTINUE
22300  0099            JJ=0
22400  0100            DO170 J=1,501
22500  0101            IF((VFR(J).GT.YMAX).OR.(VFR(J).LT.YMIN)
22600  0102         1  .OR.(VSR(J).GT.XMAX).OR.(VSR(J).LT.XMIN))GOTO170
22700  0103            JJ=JJ+1
22800  0104            XPLOT(JJ)=VSR(J)
22900  0105            YPLOT(JJ)=VFR(J)
23000  0106     170    CONTINUE
23100  0107            CALL PLOT(XPLOT,YPLOT,JJ,0,3,NO,IT1(IFLAG+1),0,25,5,XMAX,
23200  0108         1  XMIN,LBL(2),0,25,5,YMAX,YMIN,LBL(1))
23300  0109            GOTO1
23400  0110     200    CONTINUE
23500  0111     C      PLOT NU+ VS TIME
23600  0112            WRITE(5,250)LBL(1),VFMIN,VFMAX
23700  0113     250    FORMAT(/,' RANGE OF ',A5,': ',2F8.3,/,
23800  0114         1  ' ENTER AXIS LIMITS(MIN,MAX): ',$)
```

```
23900   0115              READ(5,*)YMIN,YMAX
24000   0116              CALL PLOT(TM,VFR,501,1,1,NO,NO,0,25,5,1.,0.,NO,
24100   0117          1   0,25,5,YMAX,YMIN,NO)
24200   0118              CALL PLOT(TM,VFI,501,0,2,NO,IT2(IFLAG+1),0,25,5,1.,0.
24300   0119          1   ,LBL(3),0,25,5,YMAX,YMIN,LBL(1))
24400   0120              GOTO1
24500   0121    300       CONTINUE
24600   0122    C         PLOT NU- VS TIME
24700   0123              WRITE(5,250)LBL(2),VSMIN,VSMAX
24800   0124              READ(5,*)YMIN,YMAX
24900   0125              CALL PLOT(TM,VSR,501,1,1,NO,NO,0,25,5,1.,0.,
25000   0126          1   NO,0,25,5,YMAX,YMIN,NO)
25100   0127              CALL PLOT(TM,VSI,501,0,2,NO,IT2(IFLAG+1),0,25,5,
25200   0128          1   1.,0.,LBL(3),0,25,5,YMAX,YMIN,LBL(2))
25300   0129              GOTO1
25400   0130    400       CONTINUE
25500   0131    C         PLOT GAMMA VS TIME
25600   0132              WRITE(5,250)LBL(4),GMIN,GMAX
25700   0133              READ(5,*)YMIN,YMAX
25800   0134              CALL PLOT(TM,GMA,501,0,1,NO,NO,0,25,5,1.,0.,LBL(3),
25900   0135          1   0,25,5,YMAX,YMIN,LBL(4))
26000   0136              GOTO1
26100   0137              END
```

42.8

PROGRAM SECTIONS

	Name	Bytes	Attributes
0	$CODE	1467	PIC CON REL LCL SHR EXE RD NOWRT LONG
1	$PDATA	234	PIC CON REL LCL SHR NOEXE RD NOWRT LONG
2	$LOCAL	4840	PIC CON REL LCL NOSHR NOEXE RD WRT LONG
3	C0	4	PIC OVR REL GBL SHR NOEXE RD WRT LONG
4	PLOT1	12024	PIC OVR REL GBL SHR NOEXE RD WRT LONG
5	PLOT2	1204	PIC OVR REL GBL SHR NOEXE RD WRT LONG
	Total Space Allocated	19773	

ENTRY POINTS

Address	Type	Name
0-00000000		PLOTS

VARIABLES

Address	Type	Name	Address	Type	Name	Address	Type	Name	Address	Type	Name
2-00001054	R*4	AOB	2-00001058	R*4	COA	2-0000105C	R*4	COB	2-00001020	R*4	GMAX
2-00001024	R*4	GMIN	2-00001028	I*4	IF	3-00000000	I*4	IFLAG	2-0000102C	I*4	IPLOT
2-00001030	I*4	J	2-00001070	I*4	JJ	2-00001068	I*4	L	2-0000106C	I*4	LT
5-00000000	I*4	M	2-00001044	I*4	MM	2-00001048	I*4	NF	2-0000100C	CHAR	NO
2-0000104C	I*4	NS	2-00001050	R*4	P	2-00001010	R*4	VFMAX	2-00001014	R*4	VFMIN

```
C     SUBROUTINE FOR PROGRAM ONE
      IMPLICIT REAL*8(A-H,O,Q,K,T-Y)
      IMPLICIT COMPLEX*16(Z)
      INTEGER P,PMAX
      DIMENSION JKP1(13,10),JKP2(13,10), J(13), K(13)
      COMMON/C0/IFLAG
      COMMON/C1/R0,A,RB,RN,XNU,ELE,ELB
      COMMON/C2/PMAX
      COMMON/C3/BZI,DBZ,EN,BTHI,DBTH
      COMMON/C4/BZ,BTH,GMA
      COMMON/C5/VF,VS,T,ISTEP
      COMMON/PLOT1/SVFR(501),SVFI(501),SVSR(501),SVSI(501),
     * SGMA(501),STM(501)
      COMMON/PLOT2/M,MRES(100,3)
      DATA J/0,0,0,1,2,3,1,-1,-1,2,1,2,-2/
      DATA K/1,2,3,0,0,0,1,1,2,-1,2,1,1/
```